Life cycle monitoring of composite aircraft components with structural health monitoring technologies

By

Valentin Buchinger

Thesis submitted in part fulfilment of the requirements for the degree of Doctor of Philosophy of Imperial College London

Department of Aeronautics
Faculty of Engineering
Imperial College London
2022

Declaration of Originality

I hereby confirm that the work presented in this thesis is my own. All else is appropriately referenced.

Copyright Declaration

”Nothing in life is to be feared, it is only to be understood. Now is the time to understand more, so that we may fear less.”

\- Marie Curie

Acknowledgements

Foremost, I am deeply grateful having had Prof. Zahra Sharif-Khodaei as my supervisor. Her tireless support, patience, and invaluable advice was incremental in shaping this thesis and making me a better researcher. For these reasons, I am forever thankful and indebted to her. I would also like to take this opportunity to once more congratulate her on the promotion to Full Professor in July 2022.

Funding for this research came from the Department of Aeronautics. This enabled me to fully focus on my work and I am immensely thankful for having had that support.

I am thankful to my family for shaping my educational journey. My wonderful and loving wife Aditya who supported me the entire time with her always positive outlook on life and believing in me in times I was unsure. And to our little star.

As a mostly experimental researcher, I would like to thank the entire technical support staff of the Department of Aeronautics for their help with manufacturing of components and setting up of experiments. In particular, I owe gratitude to Gary Senior, Jonathan Cole, Joseph Meggyesi, Keith Wolstenholme, Mark Grant, Franco Giammaria, Roland Hutchins and Frank Gommer.

I want to also thank other members of staff in the Department of Aeronautics for making my journey through Imperial so much easier and enjoyable. My thanks go to Clodagh Li, Lisa Kelly, Ravinder Panesar, Sian Haynes, Ela Sapinska-Elise, Magda Homa. For their continued academic input I want to thank Prof. Ferri Aliabadi, Prof. Paul Robinson, Prof. Lorenzo Iannucci, Dr Levis Errikos, Dr Siti Ros Shamsuddin, Prof. Koon-Yang Lee, Dr Omar Bacarreza Nogales and Dr Nigel MacCarthy.

For his continued guidance and unwavering support in my academic development, I thank Prof. Dipl.Ing. Dr.techn. Roland Hinterhölzl.

Lastly, I want to dedicate a big part of this PhD to my friends close and far. At Imperial I have been able to meet some truly amazing characters and shared many laughs and late nights at the Union. I'd like to mention in particular Nan, Llewellyn, Dimitrios, Florian, Francisco, Aldy, Massimiliano, Haolin, Fatih, Samet, Sina, Ilias, Fatemeh, Dimitris, Filipo, Feifei and Yingwu, Sonal, Hwei-Linn, Angus, Ruby, Jochen, Grace, Benita, Dong, Yuhang, Fanzeng, Ali, Alireza, Abdullah, Shapol, Alex, Rui, Danielle, Tianyi, Mengke and many more.

Abstract

Life cycle monitoring could considerably improve the economy and sustainability of composite aircraft components. Knowledge about the quality of a component and its structural health allows thorough exploitation of it's useful life and offers opportunity for optimization.

Current life cycle monitoring efforts can be split in two main fields 1) process monitoring and 2) structural health monitoring with little overlap between them. This work aims to propose an integral monitoring approach, enabling entire life monitoring with the same sensor. First, the state of the art of both composite manufacturing as well as structural health monitoring technologies is presented. Piezoelectric sensors have been ruled out for further investigation due their brittleness.

Fiber optical sensors and electrical property-based methods are further investigated. Distributed fiber optic sensors have been successfully used in composite manufacturing trials. Two processes were demonstrated: vacuum assisted resin transfer molding and resin infusion under flexible tooling. Due to their flexibility, optical fibers can survive the loads occurring during manufacturing and deliver valuable insights. It is shown for the first time numerically and experimentally, that fiber bed compaction levels and volume fractions can be calculated from the optical frequency shift measured by the optical fiber sensors. The same sensor was used for subsequent structural health monitoring. This proves that the gap between process monitoring and structural health monitoring can be closed with mutual benefits in both areas.

The final chapter presents a novel electrical property-based sensing technique. The sensors are highly flexible and manufactured with a robot-based 3D-printing method. They are shown to reliably work as strain sensors and crack detectors.

This work presents a thorough investigation of available and novel sensing technologies for process monitoring and structural health monitoring settings. The results obtained could pave the way to more efficient aircraft structures.

Contents

List of Figures

List of Tables

Glossary

AE	Acoustic emission
AWG	Arbitrary waveform generator
BVID	Barely visible impact damage
CBM	Condition based maintenance
CFRP	Carbon fiber reinforced plastic
CTE	Coefficient of thermal expansion
DAQ	Data acquisition unit
DoC	Degree of cure
DMF	Dimethylformamide
EFS	Etched fiber sensor
EMI	Electromechanical impedance
FBG	Fiber Bragg grating
FOS	Fiber optical sensor
GFRP	Glass fiber reinforced plastic
IDE	Interdigital electrode
IMPS	In-mold pressure sensor
MRO	Maintenance repair and overhaul
NDT	Non destructive testing, also known as non destructive inspection (NDI) and non destructive evaluation (NDE)
OBR	Optical backscattering reflectometry
OEM	Original equipment manufacturer, like Boeing, Rolls-Royce but also used for raw material manufacturer of resin and prepreg etc.

OHT	Open hole tension (a type of tensile test specimen)
PE	Piezoelectric element (e.g. transducer)
PM	Process monitoring
PMC	Polymer matrix composite
Prepreg	Reinforcement fibers preimpregnated with polymeric matrix
PVDF	Polyvinylidene fluoride
PZT	Lead zirconate titanate
RIFT	Resin infusion under flexible tooling
SHERLOC	SHERLOC is part of the Clean Sky 2 airframe innovative technology demonstrator (ITD), the High Versatility Cost Efficient (HVCE) technology stream, and the work package B-4.3 more affordable composite fuselage.
SHM	Structural health monitoring
TC	Thermocouple
TFBG	Tilted fiber Bragg grating
Tg	Glass transition temperature
THF	Tetrahydrofuran
ToA	Time of arrival
ToF	Time of flight
TPPU	Thermoplastic polyester-polyurethane
TRL	Technical readiness level
UGW	Ultrasonic guided waves
VaRTM	Vacuum assisted resin transfer molding

Chapter 1

Introduction

1.1 Motivation

Air transport has in recent decades become a necessity for many people, and yet only about 20% of the world's population has ever taken a flight in their life. In addition, with the promise of so-called flying cars the aviation industry finds itself in a gold rush moment. All of the above occurs in a time of a climate emergency. Globally the emissions of harmful greenhouse gases like carbon dioxide need to be reduced at unprecedented levels.

Air travel has seen a lot of scrutiny for its large environmental footprint. It is therefore paramount to ensure that the projected growth potential of this important sector is accompanied by the introduction of technology and materials that deliver a revolutionary new way of flying. This revolution can in part come from replacing heavy, metallic structures and components with ones made from much lighter composite materials consisting of fibers and polymers. Such replacement efforts have begun a few decades ago already and have peaked with the most recent generation of long haul aircraft like the Boeing 787 and Airbus A350. Those aircraft models each have a share of more than 50% of their structural weight being made up of composites [1].

Such a transition, as is usual in aerospace applications, was one of careful iteration to ensure safety standards are met or exceeded with this relatively new material class. Initially only few non-critical metallic components were replaced. Over the years a steadily increasing composite part count fueled by higher confidence was observed. This trend has led to the use of composites for safety and visually critical structures. For such applications, a rigorous inspection regime is required in order to ensure the longevity of said components.

Non destructive testing (NDT) techniques, initially developed for medical purposes or metals have proven to work well for composites. Some examples are ultrasonic inspection, X-Ray and computer tomography [2]. A major downside of such technologies is the need for removal of the component from the aircraft leading to longer service intervals and losses for the aircraft operators [2].

The process of inspection, if necessary repair and re-certification to a safety standard is required, usually falls within the scope of a maintenance repair and overhaul (MRO) facility. A MRO-provider is certified and allowed to perform checks and mending work on aircraft components that have been indicated for inspection by the relevant maintenance manual [3]. These facilities are either located at airports to perform work on the aircraft itself or have dedicated sites to deal with the disassembled components. An indication for MRO attention can be either the fact that a certain amount of flight-hours have been completed or through visual inspection by the airport ground-crew or the pilot. The latter requires any potential damage to be found only through visual means [3].

It is widely accepted that certain defects, caused by an impact cannot be found through visual inspection by human eyesight alone [2]. Such a damage is known as a barely visible impact damage (BVID) and accounted for during the aircraft design stage to cause no safety concern [3].

> **Guidance by the Federal Aviation Administration.** The document AC 20-107B [3] authored by the Federal Aviation Administration (FAA) outlines general composite structure design guidelines. It takes into consideration the unique benefits and challenges that are inherent to composites as a building material.
>
> It highlights the different levels of assurance that are applicable at the different levels in a composite manufacturing and supply chain. The basic principle is that certified material from certified sources, will lead to an airworthy product when manufactured in a certified facility following a process that is tightly controlled. From thereon a procedure for inspection and maintenance is in place to cover any deviations or damages that may occur in the life of a component.
>
> Five distinct damage categories are introduced with corresponding recommended course of action. **Category 1** describes allowable damages that stem from either manufacturing or in service. Damage that falls under this category is undetectable using prescribed inspection methods and has been taken into consideration during design and testing for ultimate load capability. This category includes BVID.
>
> **Category 2** damages are readily detectable within the regular intervals or through directed inspection. An aircraft retains its limit load capability despite having suffered a damage within this category. Any Category 2 damage may not grow significantly.
>
> **Category 3** damages can be detected reliably without the need for special skills or training. This includes ground personnel, ramp operatives or cabin personnel. Such damage requires immediate intervention, however, flight performance may not be impaired significantly.
>
> **Category 4 and 5** damages represent severe scenarios requiring immediate action and full flight performance is not available. Any design needs to have reasonably high resistance to such an

occurrence.

Such a regime has worked well for metallic aircraft over many decades owing to the metal's ductile nature and tendency for damages not to grow quickly. This means that when a certain damage is smaller than the BVID threshold and therefore impossible to find, this particular damage will not grow beyond the threshold limits until the next visual check is due [3]. For metallic components this works well as the actual damage size is the same as is visually detectable. For composites such a methodology has proven difficult in practice. This is due to the fact that damages in composite structures are visually much smaller than they are further beneath the surface [2]. A composite damage of only a few millimeters on the surface could easily be several 10 mm across at a deeper ply level. This invalidates the need to know the exact damage size and to assure slow damage growth. Therefore in practice, a composite structure needs to be checked in a specialised MRO facility with NDT more often than a metallic one.

To address this problem structural health monitoring (SHM) techniques have been developed. SHM utilizes NDT methods to ensure the state of structural integrity is known throughout the life of a component. It can be used to aid in scheduled aircraft service work, or be used as a basis for condition based maintenance (CBM) [4]. MROs can use SHM data to ascertain damage presence, location or severity. CBM, however, is widely viewed as the future of aircraft maintenance. The notion of CBM suggests to perform checks and repairs only when a specific predictive condition has been met. This condition can be a damage index of any suitable description as long as it accurately and conservatively serves as an early warning.

Having a good understanding of the current state and being able to predict future failure is arguably a valuable asset in itself. However, when considering the additional potential for weight savings due to the reduction of uncertainties at the design stage the benefits of SHM are self evident.

Composites are also inherently more expensive than legacy materials. The major cost drivers are expensive raw materials, the need for tight processing parameter control, complicated and long supply-chains, costly cold storage requirements, large single purpose machinery needs (e.g. autoclaves) and a high level of employee training among others [3]. Given all of that, it becomes obvious as to why low scrap rates are important for manufacturers. To ensure this, a solid process control mechanism is required. Being that many composite manufacturing steps are very sensitive to slight changes in the environment, it is common practice in a modern production facility to monitor and control environmental conditions like temperature, pressure and humidity with fine temporal granularity. In additional to that, oftentimes specific processing calls for additional controls. Some non-exhaustive examples are heat-treatment, curing or press-molding.

Process monitoring (PM) tools mean the sensor based augmentation of production processes to ensure that selected parameters are within limits and if coupled with a predictive software and/or decision making logic can inform the outcome of that process. For composites the most simplistic form of such a tool can be thermocouples measuring the part temperature and comparing it to the cure cycle prescribed by the original equipment manufacturer (OEM). A cycle within limits promises a component complying to specification and good mechanical performance. However, only the temperature readings alone cannot paint the whole picture. They give no indication on important factors like consolidation, fiber volume fraction or true degree of cure. For such performance indicators typically a second set of sensors is required or they can only be verified after the component is irreversibly cured. It would be desirable to get a clear picture of the state of the component as soon as possible in order for the manufacturer to enact changes and salvage the part. This sentiment is similar to the one used in SHM and CBM. In this work we therefore strive to find a monitoring solution that is capable of capturing as many aspects as possible.

Should any detrimental processing condition remain undetected during manufacturing, implications on the life of a composite component can be expected. As with below-threshold BVID such potential occurrences are considered in the design stages [3]. This again leads to inefficiencies and over-engineered structures. It is evident that a good understanding of the state of expensive and critical composite structures is important and can offer benefits along the entire value chain.

Lastly, the question arises whether it is possible to enable an entire life monitoring solution that works both for SHM and PM. We therefore formulate the following:

Hypothesis: *There exists a technology that can monitor both the manufacturing stages as well as the useful life of aerospace composite structures.*

1.2 Aims and objectives

In order to prove or disprove the hypothesis laid out, a set of aims and corresponding objectives is presented below. In this thesis that list is methodically worked through. The results will build a convincing case and contribute substantially to the understanding of how SHM technologies can be used to aid part manufacturing.

- **Aim 1:** Identify what SHM technologies have potential for PM
  - *Objective 1:* Identify important processing parameters for composite manufacturing that need to be monitored.

  - *Objective 2:* Perform an extensive literature search for established SHM technologies being used in a PM setting.

  - *Objective 3:* Present case studies of successful, integral PM and SHM implementations.

- **Aim 2:** Demonstrate PM capabilities of pre-selected technologies theoretically and in a realistic manufacturing environment.
  - *Objective 1:* Experimentally verify pre-selected technologies in a realistic manufacturing environment.
  - *Objective 2:* Consider sensor integration and protection strategies.
  - *Objective 3:* Perform a down-selection to a single technology.
- **Aim 3:** Develop an appropriate PM-SHM technique for a novel use case.
  - *Objective 1:* Show numerically the sensor's working principle.
  - *Objective 2:* Develop in-house sensor manufacturing route for chosen technology.
  - *Objective 3:* Develop a PM-SHM solution for two prototypes, representative of complex aeronautical structures.
- **Aim 4:** Proposal of a novel monitoring technique that considers the learnings made and extends PM capabilities.
  - *Objective 1:* Develop a sensor profile with desired mechanical and monitoring properties.
  - *Objective 2:* Develop in-house sensor manufacturing route for the chosen technology.
  - *Objective 3:* Demonstrate the novel technology in PM and SHM settings.

1.3 Overview

1.3.1 Outline of the thesis

This thesis is structured into seven chapters which encompasses the entirety of the work undertaken in this research and structures the information.

- Chapter 2: Theoretical background

- Chapter 3: Technology demonstrator - SHERLOC panel
- Chapter 4: Development of process monitoring techniques: technology down-selection
- Chapter 5: Deployment of an integrated PM and SHM system for a GFRP plate
- Chapter 6: Integrated PM and SHM applied to representative aerospace components
- Chapter 7: Development of novel sensing elements for integrated PM and SHM
- Chapter 8: Conclusion and future research

1.3.2 Contributions

The work presented herein builds upon the below publications:

- Valentin Buchinger & Zahra Sharif Khodaei (2021) *"Vacuum assisted resin transfer molding process monitoring by means of distributed fibre-optic sensors: a numerical and experimental study"*, Advanced Composite Materials, DOI: 10.1080/09243046.2021.2001910
- Valentin Buchinger & Zahra Sharif Khodaei (2022) *"OFDR-based integral Process Monitoring and SHM system for Composites manufactured by Resin Infusion under Flexible Tooling"*, 10th European Workshop on Structural Health Monitoring, EWSHM 2022, 1, pp 360–368
- Valentin Buchinger & Zahra Sharif Khodaei, *"Use of OBR for PM and SHM of complex structures"*, (in preparation)
- Valentin Buchinger & Zahra Sharif Khodaei & M.H. Aliabadi, *"Development of 3D-printed Flexible Devices for Strain Sensing and Damage Detection"*, 20th International conference on Fracture and Damage Mechanics FDM 2022 (awaiting publication)

Chapter 2

Theoretical background

This chapter reviews in a structured way the available literature covering aspects around composite manufacturing processes, SHM and PM technologies. It will give a general, non-exhaustive overview of the available solutions. However, the technologies pre-selected for further study are discussed in great detail in chapter 4. SHM for composite components has been studied heavily over the last decades. This has led to researchers proposing a wide variety of different sensors and interrogation techniques. Innovative materials and production processes have been coupled with computer-based evaluation algorithms and produced encouraging results. Typically, SHM sensors are secondarily bonded to the component they monitor [5, 6]. This means most manufacturing steps have been completed. However, an earlier integration can be desirable in certain cases. This work tries to explore the feasibility of established SHM sensor systems being used for PM (Figure 2.1). The knowledge about the process parameters under which a specific component was made is not only valuable for the manufacturer, but also for the operator. The process steps in scope are: layup, compaction, fiber wet-out and curing. Those are deemed as the most critical and cost intensive steps. Once the challenge of integrating the sensors into the structure has been solved, they can be operated as originally envisioned. Any further manufacturing related damages during e.g. drilling, routing or assembly may then be detected as if the part was already in service. PM may enable more efficient manufacturing processes due to reduced material wastage and improved component quality. This is important when considering the incurred weight penalty of a SHM implementation.

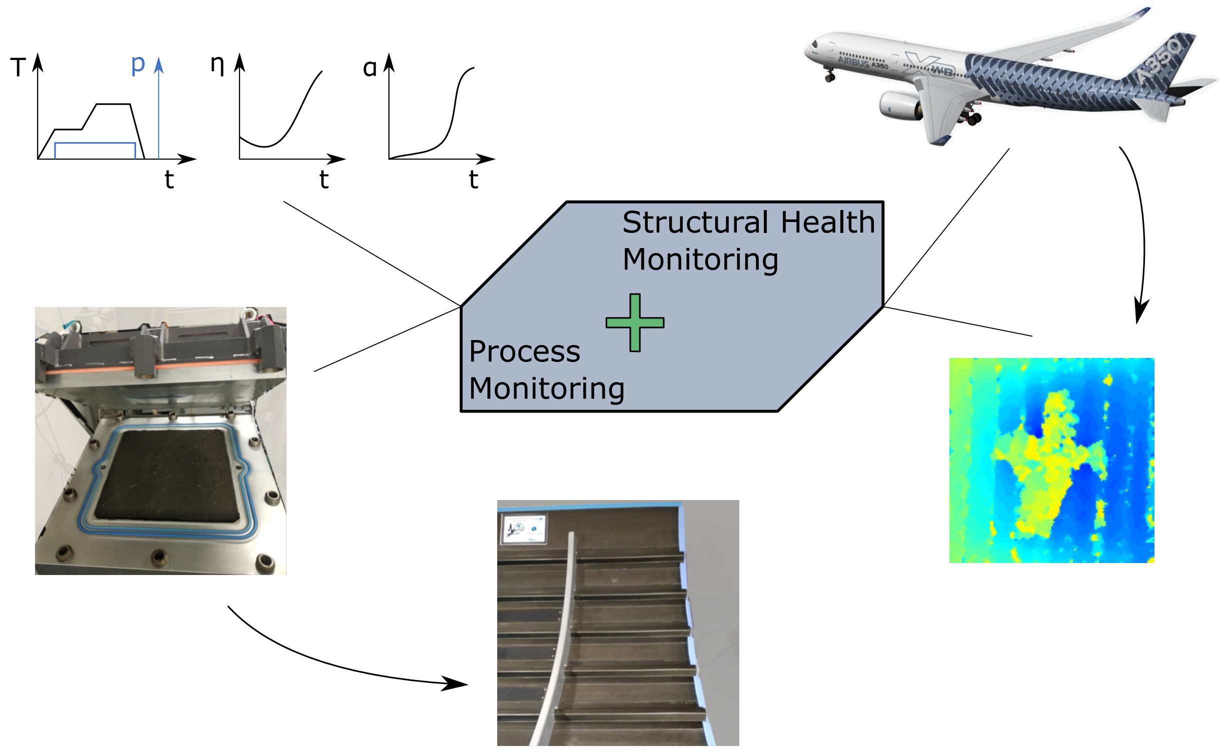

Figure 2.1: Combination of process- and structural health monitoring

Any SHM system needs to be tailored and designed specifically for an engineering structure. The system must be suitable for the structure's material and geometrical features and complexities. Different composite manufacturing processes can cause different types of defects in the structure, which in time can lead to damage initiation and progression. Therefore, it is essential for the engineer to first consider what are the expected types and characteristics of damages that can occur due to the manufacturing and in service application of the structure under investigation. The SHM technologies and methodologies will then be developed, tailored and validated for the specific structure and demonstrated in service conditions. Therefore it is important to present different manufacturing technologies and investigate their part manufacturing quality and assessment techniques, in order to select the most appropriate SHM technology for PM as well as for in-service diagnosis.

One limitation of SHM technologies that is not within the scope of this work is to develop a technology that competes against or replaces established NDT methods. The spatial resolution of such techniques can only be matched by a very dense sensing network, thereby nullifying the benefits of SHM with regards to achieving weight savings.

Dong and Kim [7] analysed the cost effectiveness of SHM for a metallic fuselage aircraft and found that it had the potential to reduce the maintenance cost by \$5 M per aircraft over its lifetime. The costs caused through the additional weight was \$50 M for same time frame. This clearly shows a need for further research

in the field of SHM before it will be applied on a large scale. They mentioned, however, that for an aircraft using composite materials design with SHM in mind, a monetary benefit might be realised easier [7]. A sensor system that can be integrated and operate during manufacturing should therefore be able to incur profits even faster.
Motivated by the vision of an aircraft that is cheaper to operate and offers improved safety, the available literature dealing with integrated PM and SHM was studied and is presented in this section.

2.1 Polymer matrix composite manufacturing

Polymer matrix composites (PMC) as referred to within this work is the mixture of an advanced polymer with continuous fiber reinforcement. Significant R&D activity has led to the creation of a multitude of available materials. The author has selected systems that have demonstrated potential of being applied to near future aircraft programs due to their increasing maturity.

2.1.1 Thermosets - materials and processes

Thermoset polymers have been used for polymer matrix composites for many decades already and have a significant market share. They typically are processed using manual lay-up of individual layers. The pressure to manufacture components at high rates and low cost has led to the development of new manufacturing methods and increased levels of automation [2]. This work focuses mainly on those relatively new processes due to the increasing demand of the aerospace industry to apply them for future programs or even replace current designs [8].

2.1.1.1 Resin infusion

Loos [9] has published a summary and comparison of the most widely used resin infusion processes. They are characterised by the fact that the reinforcement textile (dry preform) and polymer resin are combined in the mold. This is in contrary to the prepreg process, where the fibers are already wetted with resin when they are laid into the mold.
Resin infusion processes can be further classified into resin transfer molding (RTM), vacuum assisted resin transfer molding (VaRTM) and resin film infusion. In Figure 2.2 the processes are shown schematically. There also exists an array of other patented, slightly modified resin infusion processes. The underpinning principles, however, are similar. Due to that fact, the high degree of repeatability and its potential for

automation, the RTM process is described in more detail in the following section.

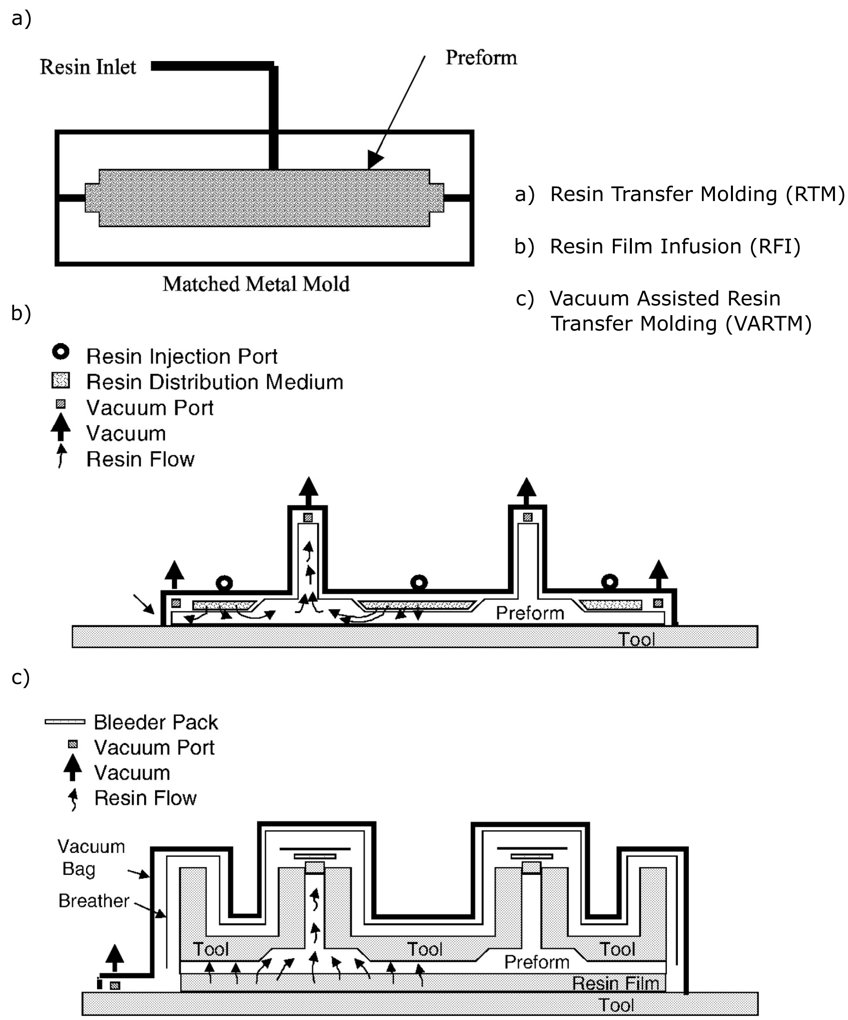

Figure 2.2: Schematic depiction of different resin infusion processes: a) RTM, b) VaRTM and c) RFI. Reprinted, with permission, from www.tandfonline.com [9], p. 100-102

2.1.1.2 Resin transfer molding

RTM has received considerable attention by several high-performance industries like: aircraft manufacturing, automotive, marine, sports and leisure. It has proven to be capable of producing good laminate qualities and lends itself to a high degree of automation [10].

The process consists of three main phases: 1) mold preparation, preform placement and closure (dependent on the pressures this may require a hydraulic press), 2) injection of a mixed and heated thermoset resin into the mold, thereby wetting the reinforcement and 3) component cure and part removal.

For RTM typically, matched metallic molds are used. This provides for a good surface finish and a high degree of thickness control. The merits of the RTM process have been summarised by Loos ([9], p. 101) to be:

- near net-shape molded parts possible
- short cycle time
- close dimensional tolerances achievable
- void-free, structural quality parts possible
- low pressure and temperature process
- closed mold process reduced volatile emissions
- smooth surface finish on both sides of the part (class A surface possible)
- cores, ribs, and inserts can be encapsulated into the part

Given the many advantages this process has to offer over classical hand layup, it is predicted that this technique is going to find more and more applications and it is therefore considered in this work.

2.1.1.3 Filament winding

Filament winding is especially suited for axially symmetric components, like pressure vessels (Figure 2.3). The process involves a rotating mold that is wrapped with pre-impregnated reinforcement tapes or fiber tows at different defined angles. This allows for a high degree of automation.

Whilst the focus on axially symmetric geometries seems to greatly restrict its application, filament-wound pressure vessels are a big market for composites materials [11]. Given the sensitive applications those components are operated in, SHM has become an important field to consider and there is considerable amount of published research available [12–15]. One such example is the SMART layer [13] which allows for SHM sensors to be embedded into composites (Acellent Technologies Inc.) whilst they are being manufactured (red tapes in Figure 2.3).

Figure 2.3: SMART layers and embedding in composite: Courtesy Acellent Technologies Inc., www.acellent.com [13], p. 225

2.1.1.4 Automated fiber placement

Automated fiber placement (AFP) is a highly automated prepreg based layup process using robot- or gantry-based (Figure 2.4) machines equipped with a heating, consolidation and cutting unit (placement head). A variation of this process exists for dry fibers (automated dry fiber placement [16]). Such machines can replace hand layup for flat and mildly curved components. When considering the implementation of a SHM system into the manufacturing process the ability of the sensor and cabling to survive the handling is a major concern. Important factors to consider are the radius of the consolidation roller (typically in the order of 70 mm [17]), applied consolidation pressures and temperatures (dependent on matrix polymers). The sensor's conformability to the component curvature is also important not to cause extensive reinforcement waviness. Generally speaking, an suitable sensor for these manufacturing processes allows for a relatively high degree of bending and is not susceptible to lateral compression.

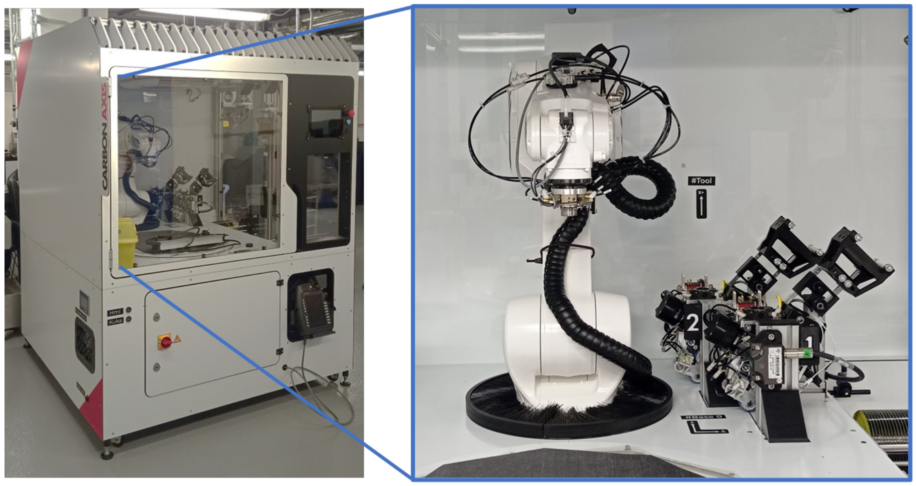

Figure 2.4: A robot-based automated fiber placement machine by Carbon Axis at Imperial College London.

2.1.1.5 Automated tape laying

Automated tape laying (ATL) [18] can be compared with AFP in terms of required machinery, but at a larger scale. This process, however, only works for mostly flat sections as it lays down much wider prepreg tapes. It requires a secondary process step for curved components to shape the uncured composite layers. Comparable with AFP are the challenges to overcome when considering SHM-integration. The requirement for the sensor to survive secondary heat forming, adds further complexity.

2.1.2 Thermoplastics - materials and processes

PMCs based on thermoplastic resins have found wide applications in various fields. It was only until recently that they have also found application for aircraft control surfaces (e.g. Gulfstream 650 rudder [19]) and thereby demonstrating their maturity. Due to their favourable mechanical properties [20] and their good recyclability [20,21], thermoplastic composites are being considered for an array of possible applications [20]. In addition to AFP and ATL, which are also viable processing routes for thermoplastic "prepregs" (Figure 2.5), some other manufacturing process are to be considered when assessing their suitability for SHM integration. Those processing routes are: 'press consolidation' and 'heat forming/stamp forming' and are described in some detail below.

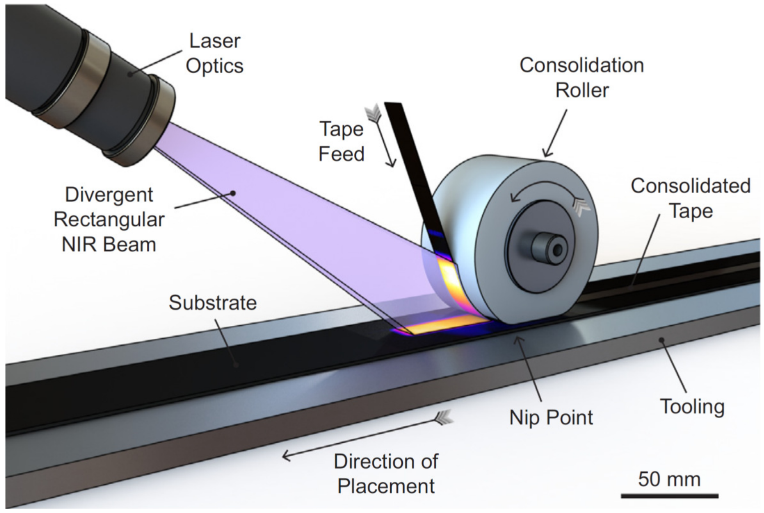

Figure 2.5: Automated tape laying of thermoplastic prepregs indicating the involved main components. *Reprinted from Composites: Part A, 78, C. M. Stokes-Griffin, P. Compston, The effect of processing temperature and placement rate on the short beam strength of carbon fiber-PEEK manufactured using a laser tape placement process, 274-283, ©2015 with permission from Elsevier.*

2.1.2.1 Press consolidation

Since thermoplastic polymers are comprised of long macromolecular chains, their viscosity is some orders or magnitude greater than that of unreacted thermosets. One possible way of forcing the polymer to migrate into the intra-tow fiber spaces is to bring it into powder form [22]. Once dispersion is achieved, a consolidation cycle above melting temperature is performed to drive out gases and impregnate the fiber bed properly (Figure 2.6). The result of this is a pre-impregnated single ply that can be stacked at different angles like with thermoset prepregs. For fusion between layers, an additional consolidation cycle is required. Due to the high viscosity, high temperatures and pressures are again required to make the polymer resin flow. Typically, this is carried out in a heated platen press [23]. Those relatively harsh conditions need to be considered when selecting a SHM system that shall also be used for PM.

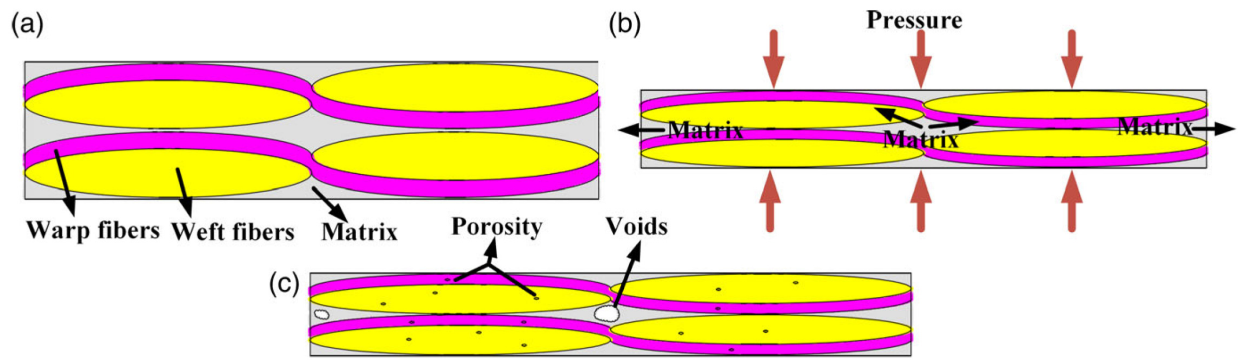

Figure 2.6: Thermoforming process stages for thermoplastic prepreg laminates: (a) pre-heating stage, (b) holding pressure stage, (c) cooling stage. [22] p. 8. *Reprinted with permission from John Wiley and Sons. © 2019 Society of Plastics Engineers.*

2.1.2.2 Heat forming/stamp forming

As described above, thermoplastic composites tend to be processed in the form of sheets or blanks. To bring them into the shape of an enginering part, a subsequent process step is required. This process again involves the application of heat and considerably high pressures. The process steps involved are depicted in Figure 2.7.

Naturally, the bending and shaping of a blank made up of multiple layers, leads to relative movement of those blanks and inter-layer shear. A sensor system being embedded into such a blank would have to be able to withstand the forces exerted on it during the forming process.

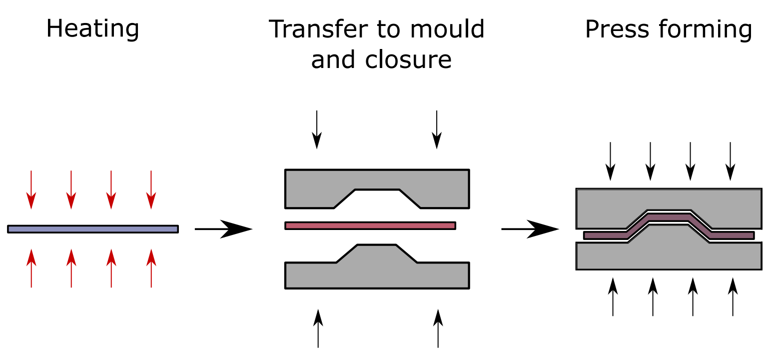

Figure 2.7: Process steps involved in press forming of thermoplastic prepregs.

2.1.3 Manufacturing defects typically encountered

Despite the great differences in chemical composition, physical properties and manufacturing processes employed between thermoset and thermoplastic PMCs, the main concern for a component manufacturer is the avoidance of defects. The main defects that occur do not vary greatly between the systems and can be summarised to be:

- Fiber volume fraction variabilities affecting the general mechanical properties
- Reinforcement wet-out [24]
- Presence of voids/porosities [22, 25]
- Consolidation (bond/fusion between layers) [26, 27]
- Correct thermal processing [26]
- Residual stresses [25]
- Mechanical damages may be detected via the SHM route and are not in scope for the production PM schemes highlighted

2.1.4 Benefits of integrated PM

Defects cannot be tackled or avoided only by monitoring the manufacturing process. It is important to first understand the root cause of a specific defect and then finding the relationship this measured physical parameter has with the defect. Based on the sensor reading an optimisation scheme can be performed to improve the process and the product [28]. It is therefore imperative to understand what process factors need to be captured by a successful manufacturing monitoring system:

- Temperature (tool and material [10, 12, 23, 26, 29–32])
- Pressure (in-mold, consolidation [15, 17, 22, 23, 26, 28, 33, 34])
- Resin viscosity [29, 35, 36]
- Resin flow and flow front uniformity [10, 24, 28, 35, 37–41]

The following review of sensing techniques has been collated with those parameters in mind. It shall also be mentioned that it only covers sensors and monitoring techniques that currently also find broad application in SHM. This was done to ensure that a component needs only be equipped with one system that can capture the entire product life.

2.2 SHM: background, state of the art and technologies used

This section provides a brief overview of SHM concepts and the technologies used. It will also shed light on current trends and the state of the art.

SHM finds application across several disciplines, including: civil, mechanical, aerospace, oil & gas and marine engineering. The common goal is the understanding of the state of structural degradation of critical or valuable infrastructure. Given the wide range of applications a large amount of technologies has been developed to meet the specific requirements of each use-case. Despite this plethora of SHM solutions, some general features are found in all of them. These are:

- One or more **sensors** form the physical interface between the monitored item and the rest of the SHM system. Many different sensor types have been shown to provide useful insights and the development of new sensing technologies is a very active research field within the SHM community. The most important ones are highlighted in section 2.3.

- **Data acquisition unit (DAQ):** The DAQ enables and receives the sensor's measurements. Most sensors require some form of energy supply (electric, optical, etc.) for them to function. Since the DAQ is usually the only device physically interacting with the sensor, the energy supply function is served by the DAQ. The input energy is then transformed by the sensor's interaction with the monitored item and sent back in altered form to the DAQ. This can be in the form of voltage changes or a change in the optical spectrum to name two examples. These changes are registered and digitized by the DAQ unit to allow the digital data to be processed further.

- **Data processing unit:** Data processing can be performed 'online' or 'offline'. Online data processing refers to real time data manipulation and interpretation to allow some form of decision making. For offline data processing, the data created by the SHM system needs to be stored in order to be accessed at a later time. In both cases, data processing is usually done computationally in order to produce insights that are human-readable. This can for example be a damage index, remaining useful life indicators or an alarm trigger.

Whilst the DAQ and data processing units are usually fairly standard devices, the sensors' working principles are less trivial and require further introduction. For that purpose two commonly used methods are described further: 1) strain-based methods and 2) ultrasonic guided waves-based methods.

2.2.1 Strain-based methods using FOS

Strains in a structure are the result of loading. These loads can be mechanical or caused by the environment (temperature, humidity, atmospheric conditions, etc.). The stiffness of a structure is the material parameter that defines how much a structure strains as a function of the applied load. In pristine conditions, a structure will deform the same way, every time a non-damaging load is applied. However, once a damage is introduced that has an effect on the structure's stiffness, the deformation and strains will deviate from the known, pristine state (Figure 2.8). Such a deviation indicates the presence of damage and forms the basis of a strain-based SHM system.

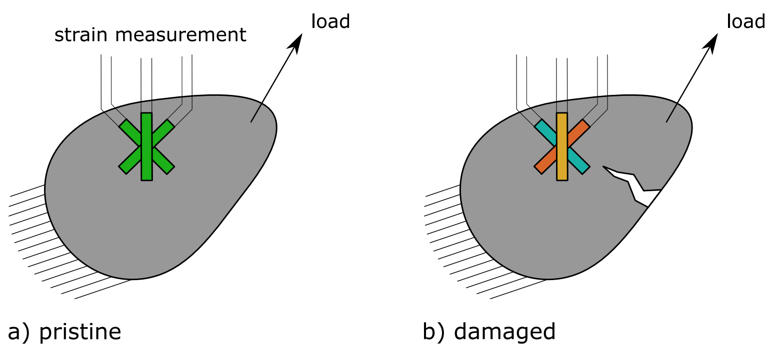

Figure 2.8: Strain-based SHM concept, a) pristine structure and b) damaged structure with a qualitative illustration of changes to the strain field.

For this method, strain sensors are required in the critical areas in order to capture these potentially occurring differences. The most common type of strain sensors are foil strain gauges. They possess great sensitivity and, given their small footprint, can be installed precisely wherever they might be required. Foil strain gauges are produced at large scale and are used in both academic and industrial applications. The labour-intensive application process and required electrical wiring make them undesirable for a SHM system that captures many data points on a large structure, like an aircraft.

Fiber optical sensors (FOS) also find application for strain sensing applications. Since their application is still very much in early stages and mostly limited to academic research, the following section gives an insight into the working principle of two selected technologies: 1) fiber Bragg gratings (FBG) and 2) optical backscattering reflectometry (OBR).

FOS for strain measurements are a relatively new development with FBGs emerging in the late 1970s [42] and OBR first described by Froggatt and Moore [43] in 1998. In both cases, standard telecommunication-grade optical fibers form the backbone of the technology. In this section, the working principles of those measurement techniques are described.

2.2.1.1 Fiber Bragg gratings - background

FBGs are artificially created, periodic changes to the optical fiber core's refractive index. They are manufactured by lateral exposure of the fiber with a laser (Figure 2.9). The wavelength of the writing laser needs to be chosen such that it interferes with a certain dopant within the fiber's core [42]. This interference causes the core to heat-up and change its morphology. The change in the core's morphology causes its reflective index to be slightly different to the surrounding material, which leads to reflections. These reflective regions in turn act as filters, reflecting back a narrow and specific wavelength (Figure 2.10).

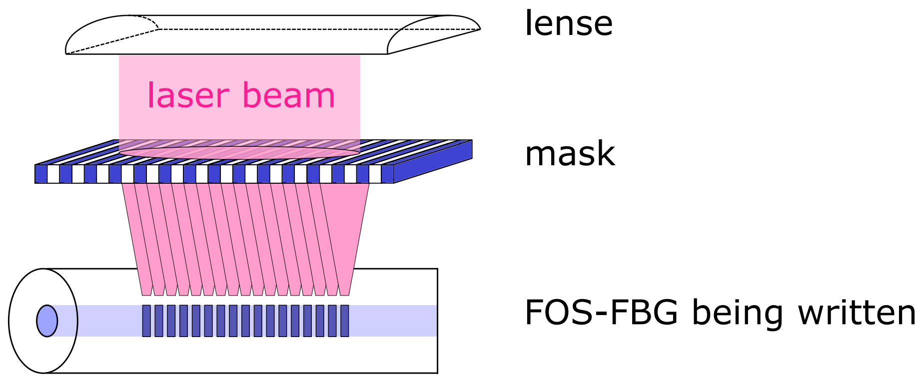

Figure 2.9: Writing of FOS-FBG sensors into an optical fiber.

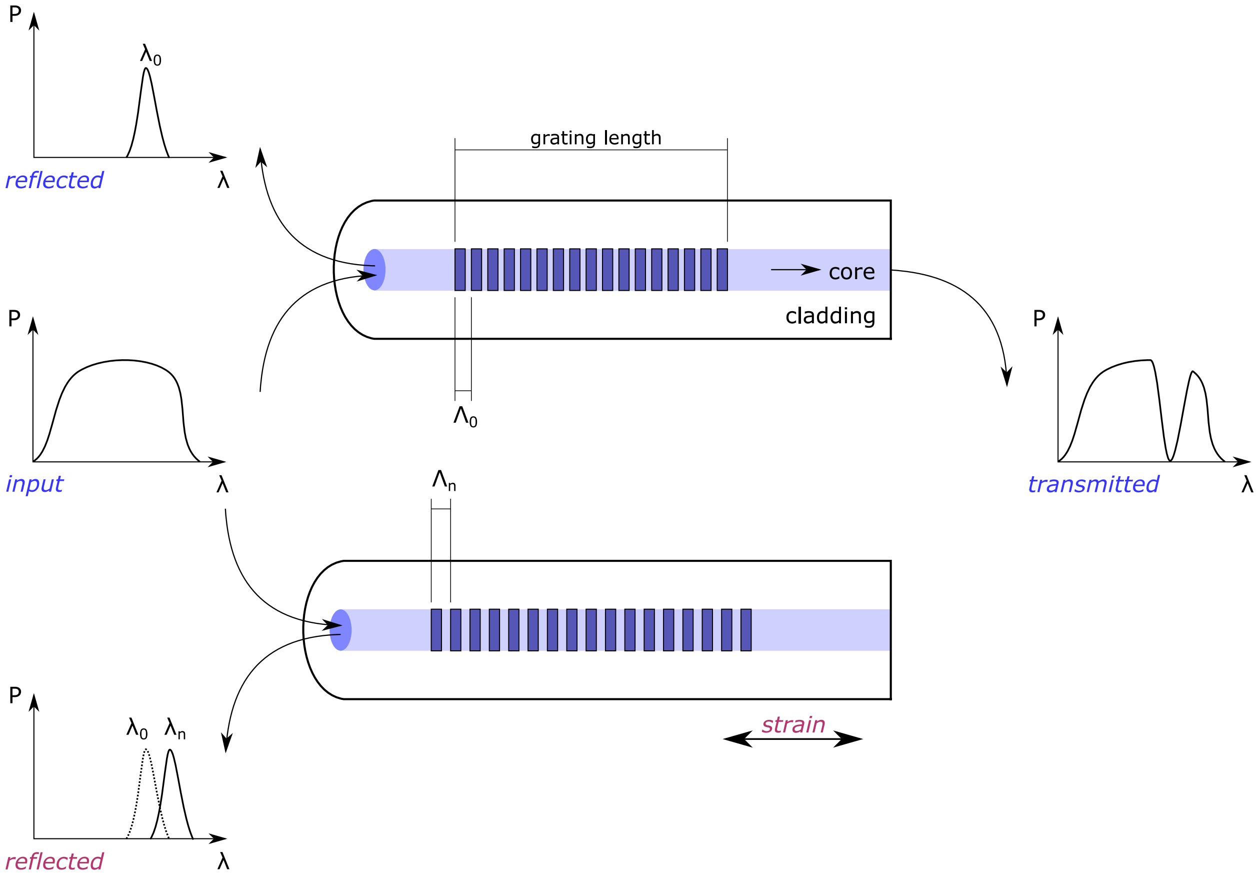

Figure 2.10: Working principle of FOS-FBG sensors.

When considering the reflected power spectrum in Figure 2.10 one can notice the peak at wavelength λ_0. The wavelength at which this peak occurs is called the Bragg-wavelength and is specific to the current periodicity Λ of the grating (see Equation 2.1). The grating length defines the sensitive area of the FBG and its reflectivity bandwidth [44]. It typically ranges in the order of 10 mm. When the fiber is strained mechanically or through environmental influence, Λ_0 takes on a new value Λ_n and so does the reflected part of the optical spectrum. The physical change in periodicity therefore causes λ_0 to become λ_n.

$$\lambda_B = 2n_{eff}\Lambda \tag{2.1}$$

Tracking these changes allows the measurement of strain, temperature (Equation 2.2 [44]) and other physical parameters over the length of the FBG's grating. Additionally, since the Bragg-wavelength can be controlled during FBG manufacture several FBGs with each one having a unique Bragg-wavelength, can be written into the same fiber allowing multi-point measurements.

It is important to note that any physical parameter measured with an FBG (be that strain, temperature, etc.) requires that parameter to be computed from the shift of the Bragg-wavelength via pre-determined calibration factors (Equation 2.3 and 2.4 [44]).

Where $\Delta\lambda_B$ is the shift in Bragg-wavelength, n_{eff} is the effective refractive index, Λ is the periodicity of the grating, P_{11} and P_{12} are strain-optic coefficients, ε is the applied strain, α is the coefficient of thermal expansion and T the temperature, it follows that:

$$\Delta\lambda_B = 2n_{eff}\Lambda\left(\left\{1-\left(\frac{n_{eff}^2}{2}\right)[P_{12}-\nu(P_{11}+P_{12})]\right\}\varepsilon+\left[\alpha+\frac{\frac{dn_{eff}}{dT}}{n_{eff}}\right]\Delta T\right) \tag{2.2}$$

which, by inserting the relevant material parameters, can be simplified to

$$\frac{1}{\lambda_B}\frac{\delta\lambda_B}{\delta\varepsilon} = 0.78\times10^{-6}\ \ \mu\varepsilon^{-1} \tag{2.3}$$

for pure strain dependence and

$$\frac{1}{\lambda_B}\frac{\delta\lambda_B}{\delta T} = 6.67\times10^{-6}\ \ {}^{\circ}C^{-1} \tag{2.4}$$

for pure temperature dependence.

To enable strain and/or temperature measurements with FOS-FBG, an interrogation system is required (see Figure 2.11). Such a system typically consists of a laser light source (broadband or tunable) and a photo detector at the minimum. Depending on whether the reflected or transmitted spectrum shall be analyzed, the position of the photo detector in relation to the FOS-FBG has to be adjusted. Whilst it can be positioned in-line for transmission measurements, the detector needs to be connected through a circulator to the FOS-FBG arm. The circulator allows a split between the incoming laser light and the reflected one ensuring that only the portion of interest reaches the photo detector.

Such a system is capable of acquiring data with several 10 MHz bandwidth. It is possible to multiplex several FOS-FBG onto a single optical fiber. This yields a spatial resolution as low as a few hundred microns [45–47], limited by the minimum physical length of a single grating. The maximum number of gratings on a single fiber are determined by the need for sufficient wavelength separation of individual gratings and can reach up to a few thousand FBGs on a single fiber [45, 46].

In addition to the above, FOS-FBGs may also be interrogated using an OBR setup. This is particularly common for ultra short FBG lengths [45, 46]. Refer to section 2.2.1.2 for further details about that interrogation method.

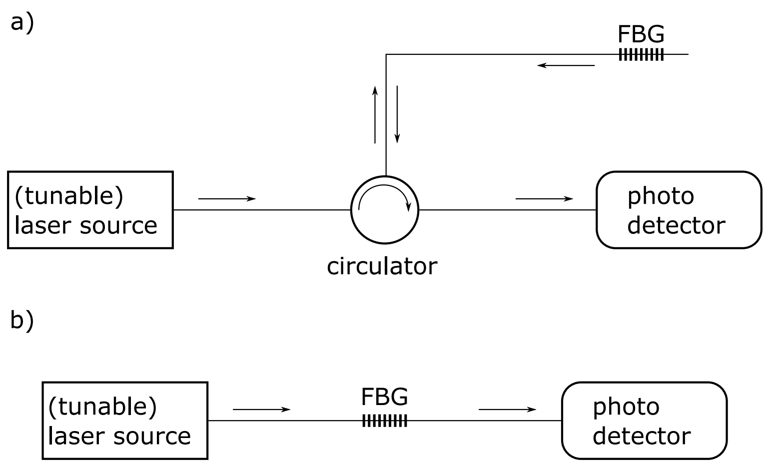

Figure 2.11: Principle of FOS-FBG interrogation with a) the reflected spectrum and b) the transmitted spectrum being analyzed.

2.2.1.2 Optical backscattering reflectometry - background

OBR in a way similarly to FBG-technology, also is based on stationary reflective regions within an optical fiber (Figure 2.12). For OBR, however, these regions are not created artificially, but rather they are present naturally within the fiber core. Also, their periodicity is not fixed but randomly distributed. As such, they are not wavelength-specific and a swept laser input is used for interrogation.

For a strain-/temperature- or pressure-measurement to be enabled, the current position of reflections is compared to a stored reference state. This is done through the calculation of correlation strengths for individual peaks and determining how far they have shifted. This wavelength shift (expressed as optical frequency shift and reported in GHz) is the native unit of measurement, which can be translated into strains or temperatures through known calibration values.

These calibration factors can be derived through carefully designed experimental setups in which a state of pure uni-axial strain is required. For this factor to be used to compute the strain within a component, the strain transfer conditions need to be known and considered as well. Throughout this work, in most cases the native unit of the OBR measurement system was plotted and reported. This has three main reasons: Firstly, uni-axial strain could in most experiments not be guaranteed or a multi-axial response was deliberately initiated. Secondly, when embedding the FOS-OBR inside a composite panel the strain transfer is difficult to establish and/or a separate calibration would be required to consider any existing pre-load.

Thirdly, as in all cases presented within this work the change in the absolute value of the obtained frequency shift is related to an external load (temperature, pressure, etc.) there is no added value in translating the native unit first to another calibrated unit. For these reasons, the author decided to report in most cases the native OBR unit of measurement.

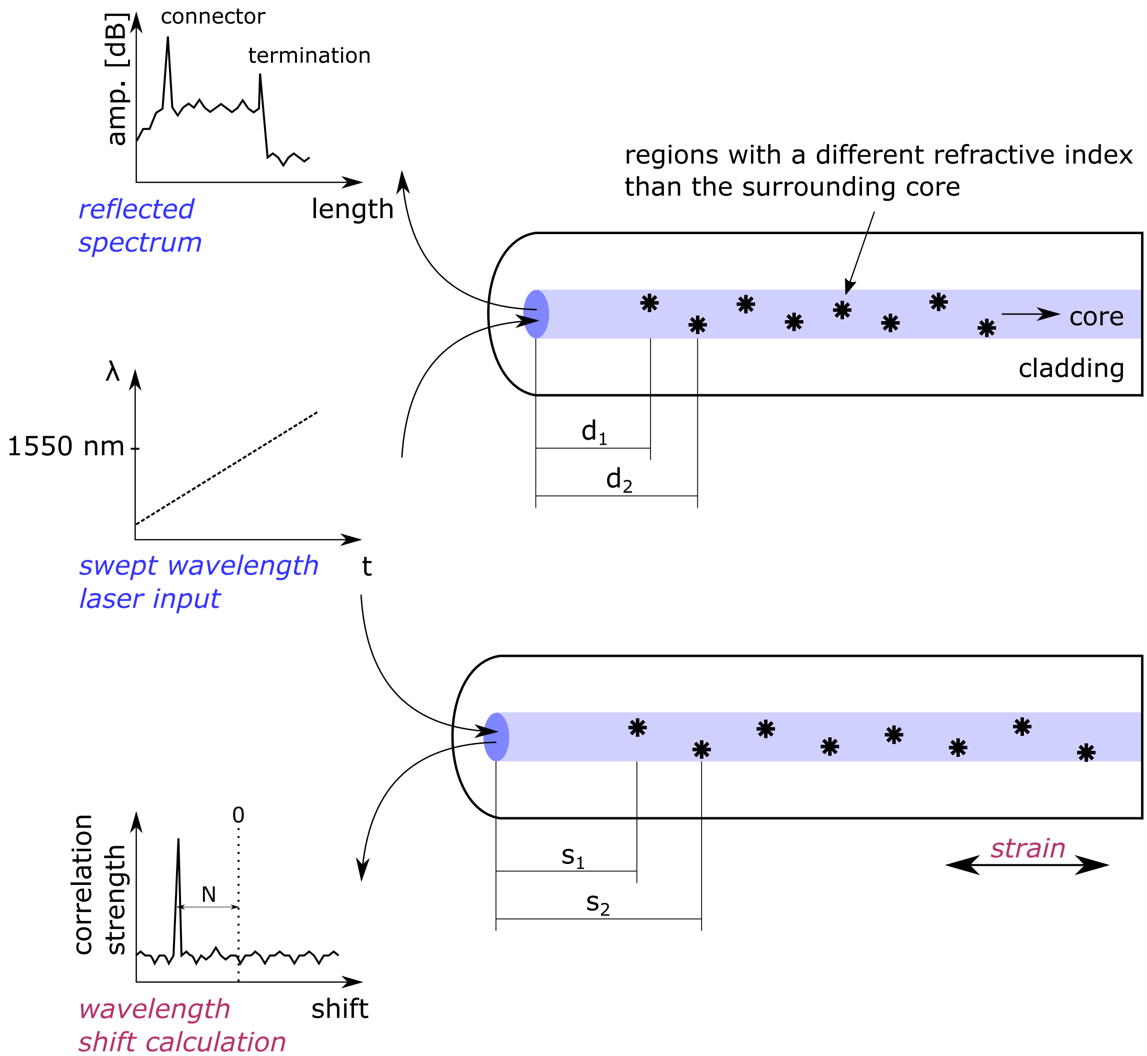

Figure 2.12: Working principle of FOS-OBR sensors.

Since the reflective regions within a FOS-OBR are distributed in the whole fiber, the entire length of the FOS is sensitive to external influences. The FOS can be thought of as a chain with individual gauge regions stringed together. For each gauge region a single shift value is calculated (Figure 2.13). An individual gauge region can be as short as 0.65 mm [48].

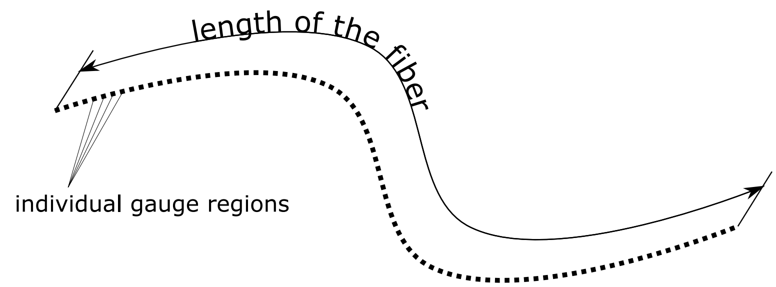

Figure 2.13: Gauge regions of a FOS-OBR on a optical fiber.

Depending on the overall length of the fiber, several thousand individual gauge regions are possible. This enables the data collection of spatially very dense sensor networks. However, one downside with this technology is the large amount of data that needs to be processed (peak matching for every gauge region) which significantly impacts the acquisition rate that is achievable. Currently, the maximum measurement rate possible is 250 Hz [48].

To enable strain and/or temperature measurements with FOS-OBR, an interrogation system is required (see Figure 2.14). Such a system consists of a tunable laser light source, the sensor (also called device under testing) and a photo detector. Since OBR is an interferometer based technique, there is the need for a reference fiber. Having this reference interfere with the sensor signal allows the determination of shift patterns. From these patterns the optical frequency shift is computed.

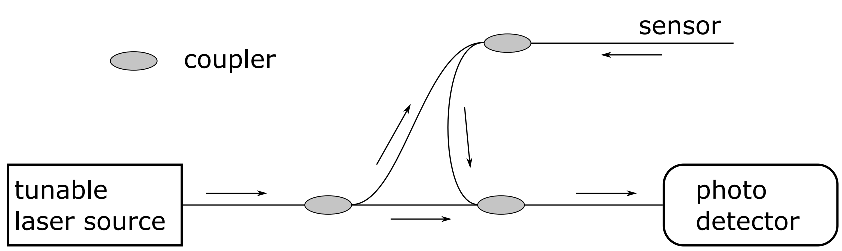

Figure 2.14: Principle of FOS-OBR interrogation.

The following two paragraphs are based on a publication by Buchinger and Sharif-Khodaei [49].

The optical frequency shift fraction $\frac{\delta u}{u}$ is analogous to the wavelength shift fraction $\frac{\delta \lambda}{\lambda}$ of a FOS-FBG, which can be calculated when considering the three dimensional strain sensitivity of a SM fiber. It can be derived by exploring the strain-optic properties of SM optical fibers [50]. A detailed study reporting the strain-optic coefficients $p11$ and $p12$ has been performed by Bertholds and Daendliker [51]. These coefficients establish a relationship between the strains present in the fiber and its optical properties. Voet [52] has proven the applicability of the reported values for Germanium-doped fibers, which is the fiber type used in the present work.

The effect of multi axial strains on the differences in the refractive index that are picked up by the FOS-OBR is calculated by Equation 2.5.

$$\frac{\delta u}{u} = \frac{\delta\lambda}{\lambda} = \delta\varepsilon_{11} - \frac{1}{2}n^2\left[p_{11}\delta\varepsilon_{22} + p_{12}(\delta\varepsilon_{11} + \delta\varepsilon_{33})\right] \tag{2.5}$$

where $\Delta\varepsilon_n$ are the 3D-strain components, $p11 = 0.113$, $p12 = 0.252$ are the strain-optic coefficients following [51] and $n = 1.4459$ is the Refractive Index [52].

Given the commonality of the mathematical relationships for FOS-OBR and FOS-FBG the simplified formulations introduced earlier (Equation 2.3 and 2.4) also apply here and can be used to describe single-source physical changes experienced by the fiber.

2.2.2 Lamb wave - based methods

Lamb waves are a type of ultrasonic guided waves (UGW) that occur in thin plates with frequencies above 20 kHz [53]. They have been named after and described by Horace Lamb [54]. Two fundamental wave modes exist: 1) symmetrical and 2) anti-symmetrical modes. They can be best visualized when considering a plate with thickness $2f$ in a x, y plane with the y direction being perpendicular to the plate's medial x plane (Figure 2.15).

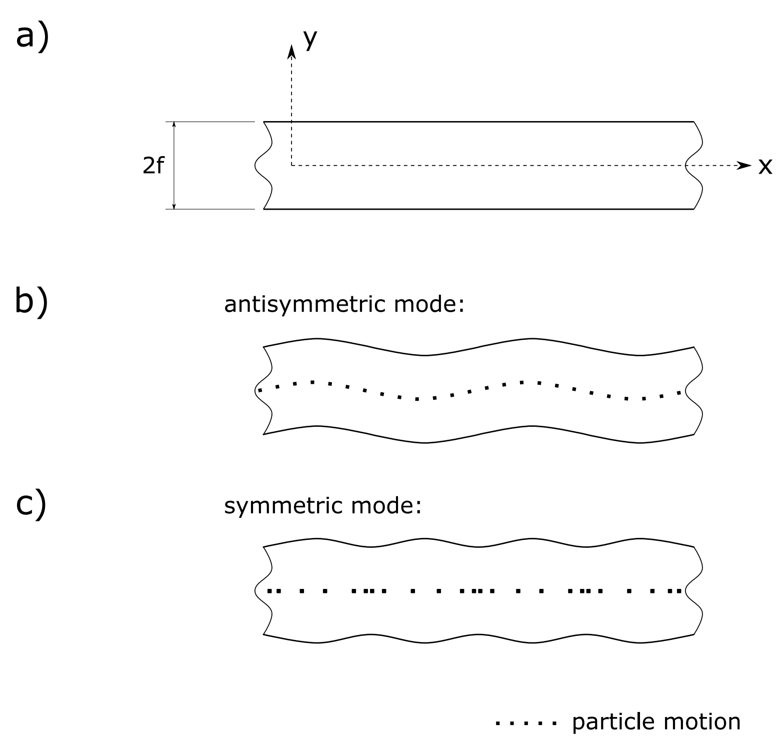

Figure 2.15: Elastic waves in plates a) description of generalized plate b) antisymmetric wave modes with transversal particle motion c) symmetric wave modes with longitudinal particle motion.

As these waves propagate through the plate, they cause transient strain fields which can be picked up by strain-sensitive sensors. The propagation velocity of symmetric and antisymmetric waves are different and can be calculated by Equations (2.6) and (2.7) where μ, ν and ρ are the shear modulus, Poisson's ratio and density respectively [53]. Velocities in the order of 2-10 kilometers per second for CFRP plates interrogated between 20 to 500 kHz are to be expected [55]. The displacements a Lamb wave typically causes within a CFRP plate are in the order of nanometers [56]. This means that sensors need to be capable of acquisition bandwidths in the MHz-range and sensitivies in sub-nanometer scale in order to detect Lamb waves.

$$c_{sym} = \sqrt{\frac{2\mu(1-\nu)}{\rho(1-2\nu)}} \tag{2.6}$$

$$c_{anti} = \sqrt{\frac{\mu}{\rho}} \tag{2.7}$$

Lamb waves can be selectively coupled into plates through targeted actuation, for example by employing piezoelectric transducers. Once actuated, Lamb waves travel relatively far without suffering from severe dampening or other losses.

2.2.3 Piezoelectric transducers

Transducers in this work refer to devices made from piezoelectric materials. Such devices are used to impart mechanical strains into a structure or inversely, pick up these strains. The piezoelectric material exhibits a means of translating mechanical strains into electric signals or vice versa (the piezoelectric effect and its opposite, the inverse piezoelectric effect) [57]. For this reason they are ideally suited as transducers.

2.2.3.1 Working principle of piezoelectric transducers

In this section their working principles are briefly described. First, by inspecting their constitutive equations (Equation 2.8 and 2.9 [58]).

$$S_{ij} = s^E_{ijkl}T_{kl} + d_{kij}E_k + \delta_{ij}\alpha^E_i\theta \tag{2.8}$$

$$D_i = d_{ikl}T_{kl} + \varepsilon^T_{ik}E_k + \tilde{D}_i\theta \tag{2.9}$$

With:

- S_{ij} = strain
- T_{kl} = stress

- D_i = electric displacement
- E_k = electric field
- θ = temperature
- s^E_{ijkl} = compliance measured at zero electric field
- d_{kij} = electric/mechanical coupling factors
- $\tilde{D}_i$ = electric displacement temperature coefficient
- ε^T_{ik} = electric permittivity measured at zero stress
- α_i = coefficient of thermal expansion
- δ_{ij} is the Kronecker delta (δ_{ij} is 1 if $i = j$, otherwise its zero)
- Superscripts E, T, D signify that the accompanied parameter was measured at zero E, T or D respectively.

These equations provide the mutual relationship between mechanical and electrical parameters. They are also known as the *Actuation Equations* and describe the strain produced at the transducer as a function of the applied stress, electrical field and temperature (Equation 2.8) [57]. Equation 2.9 predicts the required charge per unit area to drive the transducer to the state given by the acting loads (stress, electric field and temperature).

When using the transducers in a sensing function (reading the electrical field produced) the constitutive equations take the form of the *Sensing Equations* (Equation 2.10 and 2.11) [57].

$$S_{ij} = s^D_{ijkl}T_{kl} + g_{kij}D_k + \delta_{ij}\alpha^D_i\theta \tag{2.10}$$

$$E_i = -g_{ikl}T_{kl} + \beta^T_{ik}D_k + \tilde{E}_i\theta \tag{2.11}$$

With:

- $g_{ikl}T_{kl}$ = piezoelectric voltage coefficient (electric field as a function of applied stress)
- β^T_{ik} = impermittivity coefficient
- $\tilde{E}_i$ = pyroelectric coefficient (electric field as a function of applied temperature)

Equation 2.10 and 2.11 allow the selection of a suitable transducer to obtain a certain voltage as a function of the parameters to be monitored [57].

The exploitation of both the actuating and sensing properties of piezoelectric elements (PE) is the back-bone of many SHM techniques and the basic principle is summarized in Figure 2.16. The PE, here shown in the typical wafer form, experiences strains from vibrations or UGWs within the structure and electric signals are measured for analysis (piezoelectric effect) or the inverse piezoelectric effect is used to impart vibrations or UGWs into the structure.

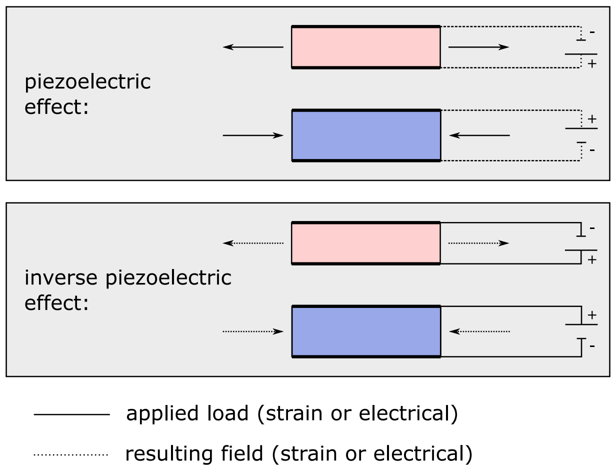

Figure 2.16: The piezoelectric effect and inverse piezoelectric effect.

2.2.3.2 Piezoelectric materials used for SHM

Several materials exhibit piezoelectric behavior, however, only two are introduced in this section as they are most relevant for SHM systems. The most widely used material for making PEs is lead zirconate titanate (PZT). PZT is a perovskite ceramic material and characterized by relatively high electric/mechanical coupling factors, meaning they are able to induce larger strains or deliver higher amplitude signals [57]. However, since they are ceramic in nature they are very brittle and rather difficult to handle.

In opposition to that are piezoelectric polymers, like polyvinylidene flouride (PVDF). PVDF shows significantly higher degrees of flexibility and conformability. This flexibility, however, comes at the cost of lower piezoelectric properties.

Both of these materials do not exhibit strong piezoelectric properties in their natural form. During manufacturing, the orientation of internal domains is random and in equilibrium (Figure 2.17). A secondary step is required to achieve a re-orientation of the piezoelectric domains. This process step is called poling and is achieved by applying strong electric fields and/or temperature [59].

When poling is performed as shown in Figure 2.17 along the thickness direction, the electric/mechanical coupling factors (d_{kij}) along the poling direction become more pronounced. Poling through thickness is most common for wafer-like PEs and leads to high values of d_{33}, d_{13} and d_{23}. This is necessary in order to receive high amplitude measurement signals and to be able to induce UGWs effectively.

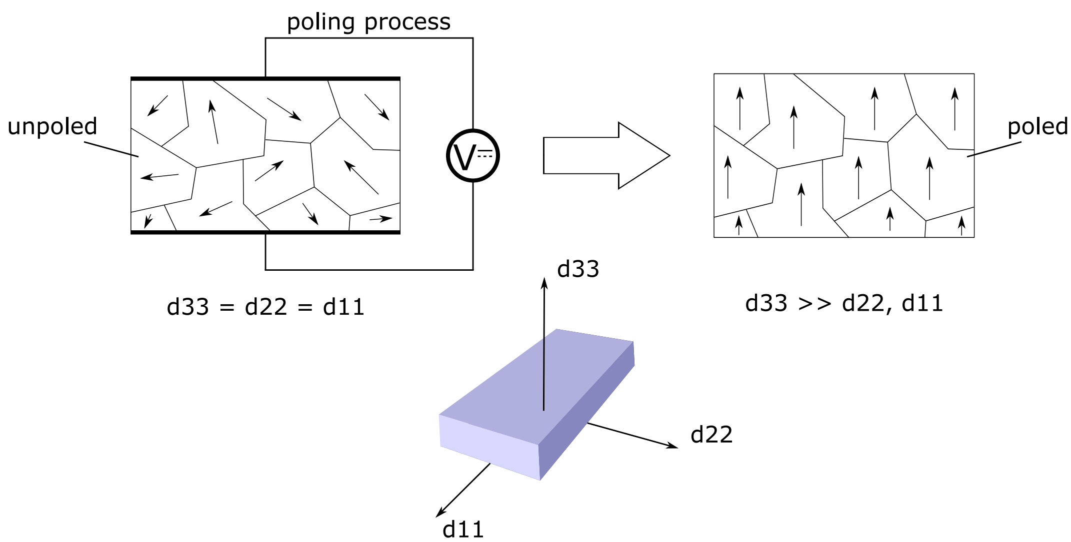

Figure 2.17: Piezoelectric material's poling process and associated piezoelectric coefficients.

2.3 SHM technologies for advanced composites

Intensive research over the last decades has brought to existence a wealth of available SHM techniques and sensors. Among the most utilised are FOS and PE. Those are also the techniques considered to have achieved the highest levels of maturity [60, 61]. Sensors, able to detect changes to electrical properties (e.g. resistance [62–64] and impedance [65–68]) and especially designs employing interdigital electrodes offer a wide range of possible usages [67]. They give room for optimised layouts and highly specialised applications. Together with the relative ease at which they can be manufactured [67] interdigital electrodes are attractive to research and industrial applications alike. This work covers all three of the above-mentioned technologies. It reviews and compares them based on their potential to serve as SHM and manufacturing monitoring sensing systems. In the following section operating mechanisms, merits and limitations shall be briefly summarised.

2.3.1 Piezoelectric transducer-based sensing

PE transducers find extensive use in SHM systems for both, active and passive sensing. Their merits are low weight, small footprint and broad frequency spectra they can operate in. Most commonly they are used to induce UGW (active) [53] or for acoustic emission (AE, passive) sensing [69].

PE elements, most commonly made of PZT, are typically bonded [5] to the structure they monitor. They may, however, also be embedded as is the case with the SMART layers developed by Acellent Technologies

Inc. (see Figure 2.3). UGWs, notably Lamb waves, are guided by the surfaces of plate-like structures [53] and are able to travel great distances without much attenuation [55]. The waves interact with defects and the resulting reflections or changes to the wave mode and losses can be picked up by either the transducer, that generated them, in sensing mode or by a separate sensor. By comparing the readings to a baseline, it is possible to determine whether there is damage present or not. Algorithms may then be used to determine the damage location [53]. When a PZT is sensing passively, the acoustic wave is generated by an external perturbation (e.g. impact) and its existence and propagation is monitored [69]. One notable development in terms of sensor geometries are piezoelectric fibers (Figure 2.18) [70]. The production of such fibers in reasonable sizes (15 cm) is becoming viable and they are reportedly able to conform to tight radii without the risk of being damaged [71]. An integration into composite parts and manufacturing processes would therefore be relatively easy.

There exists a vast amount of studied applications, modelling approaches and evaluation algorithms making PEs interesting candidates for near future composite aircraft designs [60].

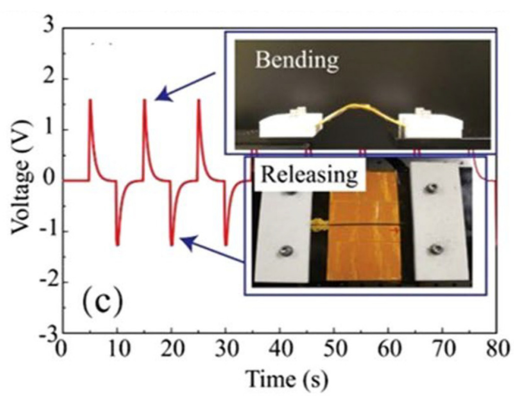

Figure 2.18: A piezoelectric fiber used as a bending sensor [71] p. 7.
Reprinted under the Creative Commons CC BY license applied to the original work.

2.3.2 Fiber optics based sensing

FOS can be used for SHM in two ways: 1) strain measurement, e.g. in [72–74] and 2) damage detection [75, 76]. Those techniques have different levels of technical readiness levels (TRL), namely TRL8 and TRL5 respectively [77].

A FOS can be either bonded to the structure or embedded into the laminate (Figure 2.19). In either way, the load is introduced into the sensor by shear [24]. Damage detection is done indirectly by measuring the impact a certain detrimental condition has on the strain field in the vicinity of the fiber as a FOS can typically only measure strains. The way a structure deforms upon an external stimulate with a damage present, is compared with the way it was acting in a pristine way [77]. Since a damage is expected to have an influence on stiffness, a defect can be detected by noticing a difference between pristine and damaged states. A delamination present under the FOS leads to local strains being formed. These can be measured evaluating the strain in the FOS. This method, however, requires the optical fibers being distributed very densely [77].

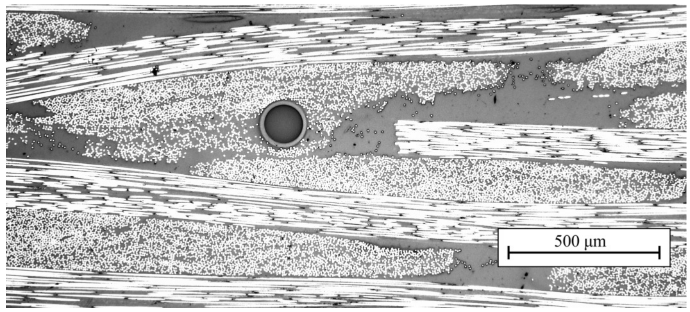

Figure 2.19: A FOS embedded inside a composite laminate.

2.3.3 Electrical properties-based

Strain gauges are the most widely known devices that relate changes in electrical properties to a state of material loading. The sensors described herein, however, are more recent developments that aim at giving more insights into the extent of damage and position – a functionality that could only be achieved by a very dense strain gauge network. This type of sensor also possesses great potential for PM.

Electrical conductivity is of great importance to enable measurements. This can be done either by e.g. introducing metallic conductors [62, 64–67], by modifying the polymer matrix [63, 78, 79] or by applying a PZT sensor [68]. Changes to the material's internal structure (mechanical damage, chemical reactions or material orientation) affect the way an electric current is transported (affecting resistance or impedance). Such differences are picked up by the sensor (Figure 2.20) and translated into a signal output.

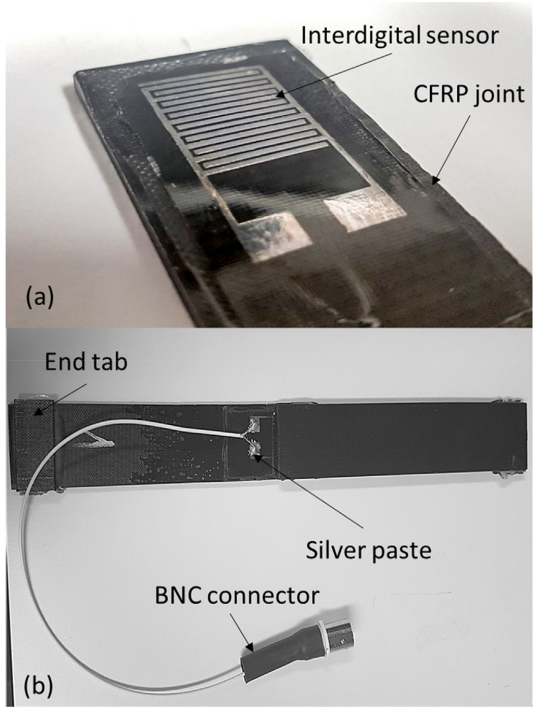

Figure 2.20: Inkjet-printed interdigital electrode sensor [67] p. 559.
Reprinted from: Composite Structures, 211, D. G. Bekas, Z. Sharif-Khodaei, D. Baltzis, M. H. Ferri Aliabadi and A. S. Paipetis, Quality assessment and damage detection in nanomodified adhesively-bonded composite joints using inkjet-printed interdigital sensors, pages: 557-563 ©2019, with permission from Elsevier.

2.4 SHM sensors in process monitoring

This section is structured in the order of the process steps involved in the formation of a fiber reinforced polymer. PM techniques are suggested for all those stages. The order is: fiber wetting, consolidation, change of polymeric properties (gelation and vitrification for thermosets during curing; melting and crystallisation for thermoplastics during heating [26]) and finally cool down to room or service temperature.

2.4.1 Fiber wetting and flow front detection

Bringing the reinforcing fibers in intimate contact with the polymeric matrix is considered as the first step in the process. This is typically done by bringing the resin into a state of low viscosity. This can be achieved by either using unreacted monomer mixtures or by melting. The low viscosity resin travels through the reinforcement and wets it out. For the monitoring of a resin infusion process it is imperative to know the location of the resin front and whether the entire part is soaked as this is important for part quality. It also marks the end of the infusion and the curing process can begin.

Yildiz et al. noticed the arrival of the resin front during an RTM experiment by a sudden drop in the Bragg wavelength on their FOS. To verify their results, they utilised a Fresnel reflection refractometer in which a clear step change could be identified when the FBG was dipped into resin. By using multiple FBGs they were able to detect how the flow front moves through the fiber bed [38]. Such a trend has also been observed by other researchers [25]. Besides the location of a flow front, its flow direction can also be monitored using FOS. Wong et al. [41] used chirped long period grating (LPG) FOS (see Figure 2.21) successfully to study the direction resin is covering the FOS during the flow of resin down a plastic pipe.

To be able to use FOS for PM, a strategy for a stable connection between the sensor and an acquisition unit needs to be defined. One possible method to achieve a safe fiber ingress and egress is to use a thin hypodermic tube for the protection of the fiber [79].

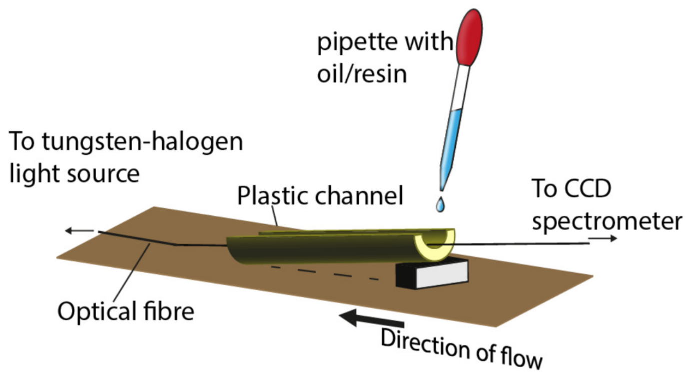

Figure 2.21: Resin flow direction measurement using LPG sensors [41], p. 6608.
©2017 IEEE.

Piezoelectric sensors may as well be used for the detection of a resin front. Using a transfer function, one can relate the input voltage with the electrical potential decrease over the wafer as resin moves across it. The flow front can then be predicted by using the percentage of coverage of the surface with resin [80] as input. The resin injection and curing act as a perturbation on the resonant response. It basically changes the boundary conditions in which the piezoelectric element operates i.e. clamped vs. free condition of the sensor. This problem can also be treated analytically – the corresponding formulae have been presented by Wang et al. [80].

Liebers et al. used PEs directly bonded to the manufacturing mold in both pulse-echo and transmission mode. They were successful in detecting the arrival of the resin flow front. This has been successfully demonstrated for autoclave infusion [28], which is remarkable given the harsh process conditions.

Electrical properties-based sensors have also been successful in monitoring the flow front and degree of saturation [35, 40]. Gueroult et al. [35] have used two strip-electrodes and were able to relate the changes in resistance to the arriving flow front and void formation. Analytical solutions obtained from the liquid's flow properties have shown satisfactory agreement in terms of percentage of voidage. This technique, however, requires the infusion resin to be conductive.

One possible approach to equip the composite with electrical conductivity even in the through thickness direction, is to coat the reinforcing fibers (Figure 2.22) with graphene [40]. In addition to flow monitoring such a property has also been shown to be useful in estimating vacuum pressure. After the manufacturing is completed, the conductive properties of the composite part may be utilised for SHM [40].

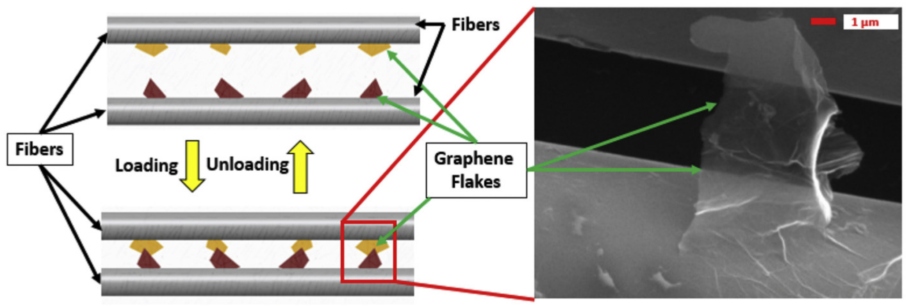

Figure 2.22: Graphene flakes used as a PM tool with additional SHM capability [40] p. 109.
Reprinted from: Composites Science and Technology, 148, M. A. Ali, R. Umer, K. A. Khan, Y. A. Samad, K. Liao, W. Cantwell, Graphene coated piezo-resistive fabrics for liquid composite molding process monitoring, pages: 106-114, ©2017, with permission from Elsevier.

2.4.2 Consolidation

Consolidation was described in more detail for thermoplastic composites (section 2.1.2.1). It also plays a vital role for thermoset composites aiming at the same targets, namely: force resin flow, drive out air and make intimate contact between layers. FBGs have been studied for consolidation monitoring for filament winding as part of an entire-life monitoring approach [12]. It was noticed that every layer laid up could be clearly identified by a step in the strain readings with the step becoming less prominent as the thickness grew. Such an approach may be utilised to monitor the consolidation pressure applied to the composite stack, which is an important parameter during this process phase.

Pressure sensing using a FBG sensor has already been proposed for composite manufacturing almost 20 years ago by Hao et al. [81]. They proposed using a standard FBG oriented at 90 degrees to the adjacent fibers. The pressure imposed by the reinforcing fibers on the FBG leads to the grating length to vary. This variation would then be correlated to the pressure acting on the composite. Advances in femtosecond laser technology has in the meantime, however, enabled the development of birefringent fibers with intricate nano-structures (Figure 2.23), like the butterfly structure used by Huang and colleagues at VUB Brussels [82,83]. They have successfully demonstrated a sensor that is capable of measuring pressures up to 1400 bar at temperatures up to 290 degrees Celsius [82]. Multiplexing such a pressure sensor with an etched fiber sensor (EFS) for cure and flow monitoring and multiple FBGs for strain measurements could lead to the creation of a single optical

fiber able to capture a vast array of process parameters with a single sensor. Whilst such high pressures are not relevant for composite processes it indicates the advances made in optical fiber manufacture.
Other fiber-optical pressure sensing techniques include diaphragm capped fibers [84] and encapsulated cavities [85], both based on Fabry-Perot configurations. Their pressure sensitivities are reported to lie between 0 to 0.6 bar [84] and 0 to 690 bar [85] respectively, with high degrees of linearity.

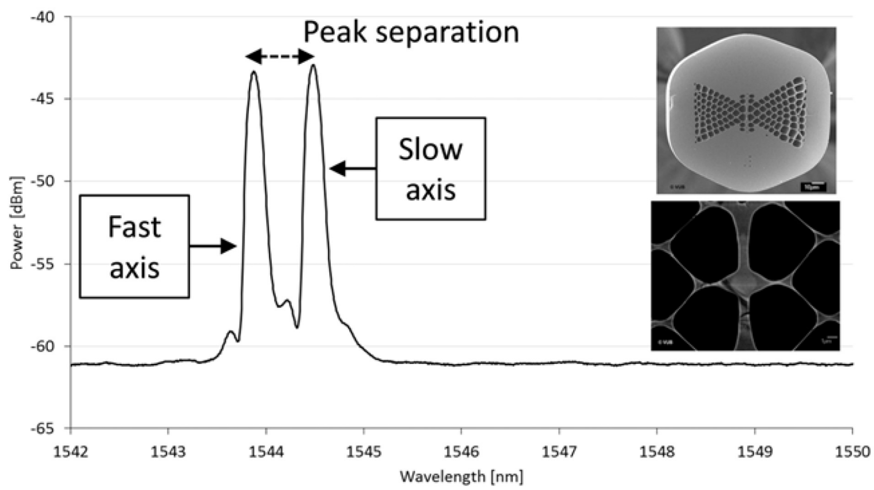

Figure 2.23: FBG written into a birefringent optical fiber [82] p. 17941.

The effect of hydrostatic pressure on a piezoelectric wafer was studied and a linear relationship was found. The pressure can be modelled as an additional capacitance in the representative Butterworth-van-Dyke circuit [86]. A direct approach to measure consolidation was presented by Liebers et al. [28]. The development of thickness as the fiber bed wets out and swells can be measured using ultrasonic sensors. The effect pressurisation had on the thickness could also be effectively demonstrated. Given a defined number of plies, the knowledge of the laminate thickness after infusion, essentially becomes a measure for the fiber volume fraction.
A tool-mounted manufacturing monitoring system utilising piezoceramic elements in bulk-wave propagation mode is described by Liebers et al. [87]. They have tested different piezoceramic thicknesses and developed an optimised bonding and acoustic coupling method to ensure good signal transfer into the mold. A comparison with established ultrasonic transducers has shown that the piezoceramic elements bonded with this new process offer an increased sensitivity at lower cost. Their system is capable of operating for processes that offer both single-sided access (pulse-echo), as well as double-sided (transmission) with no significant loss in sensitivity to cure progress. To overcome the issue of calibration a novel method is suggested by which

the piezoelement is mounted to a rheometer. The rheometer captures the evolution of viscosity during resin cure. This information can finally be coupled with the information gathered by the ultrasonic sensor and calibration can be performed [87].

2.4.3 Change of polymeric properties

2.4.3.1 FOS-based monitoring

The application of heat to a polymer leads to changes to their mechanical properties, chemical structure and ultimately, the polymer's state of matter. This is true for both thermosets and thermoplastics. Uncured thermoset materials undergo a curing reaction, which in addition to changes in mechanical properties, leads to differences in the refractive index [38]. Yildiz et al. characterised this behaviour using a Fresnel reflection refractometer and were able to relate the degree of cure (DoC) with the changing refractive properties of curing resin [38]. Other optical fiber based sensors that have been shown to be sensitive to resin cure include long period grating sensors and tilted FBG [25]. The results obtained by these methods were also compared with impedance spectroscopy and DSC cure monitoring and good agreement between the methods has been found [25]. A technique to adjust the sensitivity of an EFS by looping the fiber to increase the amount of light being "lost" in the exposed area has been described in literature [24, 79]. This is said to increase the impact of changes to the refractive index [79] and the sensitivity can be adjusted by altering the bend radius [24]. Such a highly specialised device can also easily be integrated into a fiber, already carrying other FOS [24].

2.4.3.2 PE-based monitoring

Whilst FOS focus on the change in optical properties of a polymer, piezoelectric sensors aim at the transition mechanical properties undergo during a curing or heating cycle – namely from liquid to solid for thermosets, or from solid to liquid for thermoplastics. Due to its importance as an indicator for this transition, viscosity development has been modelled frequently. Kanazawa and Gordon [88] developed a model (Equation 2.12) based on first principles for the impact of the viscosity of a liquid on the fundamental frequency of a piezoelectric element (Figure 2.24). The dampened liquid is considered rigidly bound to one face of the transducer and is driven by the same. The nature of this transfer can be related to the properties of the liquid. Inflicted shear velocities die off at a certain distance away from the transducer. If the liquid's viscosity rises, this distance increases and leads to more weight being driven by the transducer. This, in turn, is reflected by a shift in the fundamental frequency (Equation 2.12 [88]).

$$\Delta f = -f_0^{\frac{3}{2}} (\frac{\eta_L \rho_L}{\pi \mu_Q \rho_Q})^{\frac{1}{2}} \tag{2.12}$$

where f_0 is the oscillation frequency of the free (dry) crystal, η_L and ρ_l are the absolute viscosity and density of the liquid, respectively and μ_Q and ρ_Q are the elastic modulus and density of the quartz.

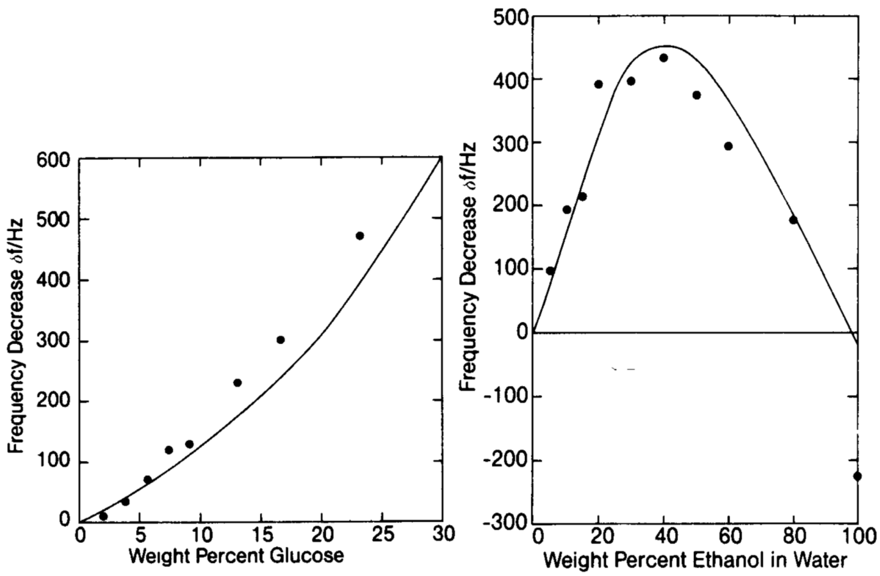

Figure 2.24: Effect of different liquid concentrations and viscosities on the resonance frequency of oscillators [88] p. 104.
Reprinted from: Analytica Chimica Acta, 175, K.K. Kanazawa, J. G. II Gordon, The Oscillation Frequency of a Quartz Resonator in Contact with a Liquid, 99-105, ©1985, with permission from Elsevier.

Wang et al. also concluded that viscosity monitoring is possible with piezoelectric wafers. Their analytical solutions show that the electrical properties will change based on changes to the liquid [89]. Their developed model is based on energy transfer from the transducer to the liquid (mass-damper-spring representation) and shows good sensitivity to viscosity up until gelation where it tends to infinity. Experiments confirmed the applicability of the model and justified the decision to eliminate all factors but viscosity in the analytical description. It was also noticed that the resonance frequency changed as the cure progresses, which can be understood taking into consideration the previously described dependence after Kanazawa and Gordon [88]. Actuating at the resonance frequency is important in order to achieve maximum excitation.

Viscosity can also be inferred using a piezoelectric transducer and evaluating its impact on electric impedance. It was found that the sensors are sensitive to both viscosity and temperature. The mixed response, however, could be mathematically decoupled into a real part and an imaginary part and effectively isolate the two influencing factors [80]. In addition to this observation, Wang et al. attributed changes in the resin to a shift in the maxima and minima of the transfer function (affecting the resonance and anti-resonance frequency of the wafer) through which they relate input and output voltage [80].

Besides the described changes in viscosity, mechanical properties of a thermoset can be related to the DoC as well. Since acoustic properties of a material in turn are strongly related to mechanical properties an indirect relationship between the DoC and acoustic properties could be drawn. Ghodhbani et al. [36] attempted to show this relationship through their analytical and experimental works. First, they used a Cole-Cole model applied to study wave propagation in cured resin. This model was based on a power law using ultrasonic velocities at different temperatures they obtained from experimental measurements. In addition to that, it is based on the knowledge that at temperatures below the glass transition temperature (Tg) no chain movements occur (only vibrations and rotations of bonds) whereas above the Tg material is rubbery and less elastic. The ultrasonic velocity is reduced. Their model allows for analytical treatment of the problem. An elastic constant is used for representation of the change in mechanical properties in the model. This constant was correlated to the DoC from a polymer concentration model and leads to a link being established between the phenomenological properties of the experiments and the elastic properties which in turn affect the ultrasonic properties [36].

The change in ultrasonic velocities as a measure for the progressing resin cure state (Figure 2.25) has also been captured by piezoelectric elements [28, 90]. Following the depicted trends for sound velocity and attenuation with time, three distinct areas can be identified: 1) an initial plateau in sound velocity is attributed to a the time before any curing reaction occurs 2) a steep rise at around 25 minutes whilst gelation occurs (viscosity rises drastically) and 3) vitrification, i.e. the saturation stage where the curing reaction slows down due to a lack of available cross-linking points and highly limited chain mobility [90].

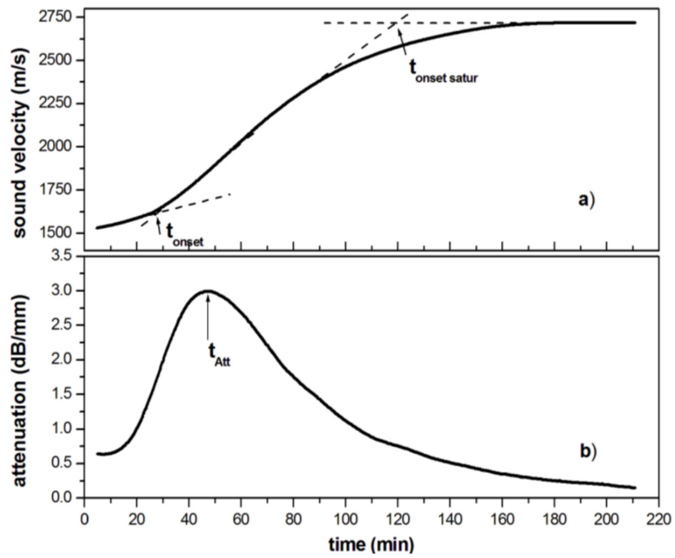

Figure 2.25: Degree of cure monitoring using piezo elements [90], p. 3790.
Reproduced under the open access Creative Common CC BY license applied to the referenced original article.

Once the material has attained a certain rigidity (e.g. sufficiently progressed gelation of a curing thermoset) the PZT can be used for wave propagation analysis. A combination of a PZT for guided wave actuation and a FBG for detection was successfully used for real time cure monitoring after gelation including vitrification [91]. This allows to track the DoC even for very high viscosities.

Whilst most thermoset curing temperatures are in the range of 120 to 180 °C, thermoplastic composites need to be processed at temperatures reaching up to 600 °C [26]. It is therefore important to consider the resistance to high temperatures of a sensor. Piezoelectric systems are limited by their Curie temperature as polarisation is lost above that. The maximum useable temperature for PZTs typically lies between 250 °C and 300 °C [92]. This renders PZTs not useable for thermoplastics. However, several high-temperature capable piezoelectric materials, some proven to work as SHM transducers, are described in literature [93–95]. A creative way of dealing with this issue, is to perform polarisation during molding making use of the temperature applied, or once the part has been cooled down to room temperature [96]. When utilising PZTs at higher temperatures it is also important to consider, that some properties are affected by thermal dependence (Figure 2.26). As an example the permittivity increases by 75% for PIC255 ceramic and roughly 180% for PIC155 ceramic over a temperature window -40 to 150 °C [97].

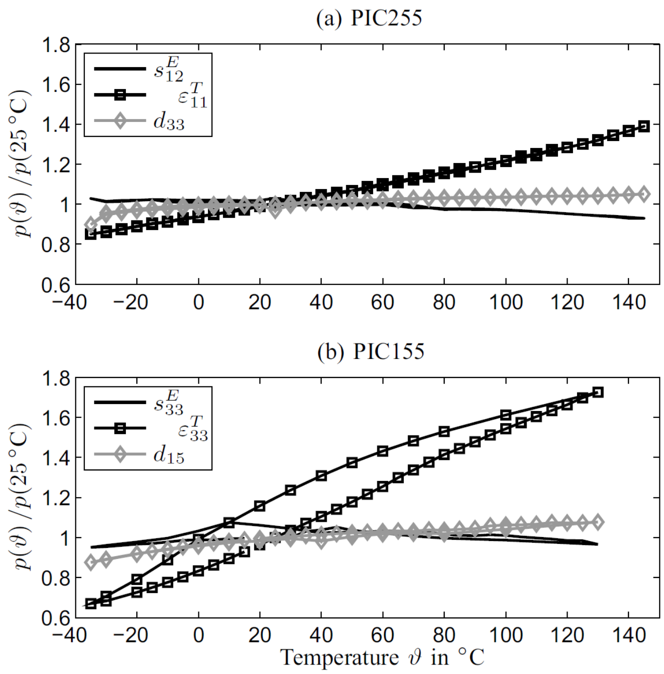

Figure 2.26: Temperature dependence of piezoelectric properties of PIC155 and PIC255 [97], p. 186
©2013 IEEE. Reprinted, with permission, from S. J. Rupitsch, J. Ilg and R. Lerch, Inverse scheme to identify the temperature dependence of electromechanical coupling factors for piezoceramics, 2013 Joint IEEE International Symposium on Applications of Ferroelectric and Workshop on Piezoresponse Force Microscopy (ISAF/PFM), February 2014

2.4.3.3 FOS-based monitoring

FOS have been used to either directly measure or infer changes within the polymeric matrix in several different ways. An important feature of every thermoset curing cycle is a reliable estimate for the DoC at a given time. Fresnel reflection refractometers at the fiber end were often used [16, 98–100] and shown to be on par with DSC [98] results. Such capability is derived from the interaction of the curing resin with the fiber end. This interaction causes Fresnel reflections traveling back the fiber towards the detector and the power of that light propagating backwards, is proportional to the refractive index of the resin. Since that index changes throughout the cure, so does the reflected power. TFBG [41] and LPG sensors [101, 102] also have been shown to be sensitive to the refractive index of the resin and therefore are able to work well as DoC sensors.

Chehura et al. [103] used FBGs written into birefringent optical fiber to successfully track the transverse strain development during progressing cure. They compared those results with DSC measurements and were able to use them as a DoC indicator.

Finally, simpler temperature measurements can also be exploited to infer the degree of cure of a thermoset resin. This is state of the art in the composite manufacturing industry and is done by thermocouples. Given the high sensitivity to temperature, FOS make for ideal temperature monitoring tools. Chehura et al. [104]

evaluated different fibers and FBG architectures for their temperature sensitivity. However, FOS are also sensitive to mechanical strains in addition to temperature and it therefore is important to differentiate the source of the changes observed.

A few solutions exist to achieve a good discrimination of factors. One of them is exploiting different temperature sensitivities of the core and cladding modes (Figure 2.27) of TFBGs has been proposed as a promising solution [105, 106]. Other researchers have shown that by only exposing a part of the sensitive region of FBGs to loading and leaving the rest unloaded allows the discrimination of external loads and temperatures [107, 108] as well.

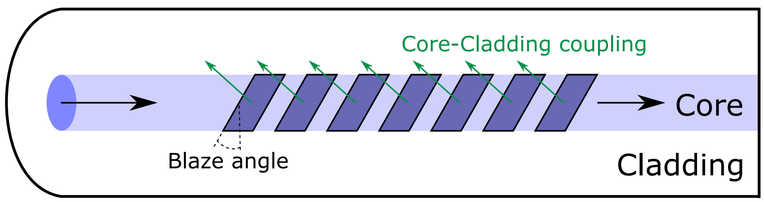

Figure 2.27: Tilted fiber Bragg grating (TFBG) working principle showing the core modes and cladding modes. Cladding modes are coupled through the gratings in the core oriented at a given blaze angle.

2.4.4 Post cure and service life monitoring

As highlighted earlier there may be several reasons to subject a component to elevated temperatures during a manufacturing process. After curing at elevated temperatures is completed the components are cooled down to room temperature/service temperature. Hernandez-Moreno et al. [12] have found a significant difference in the strain readings of an FBG fitted to a pressure vessel upon heating (i.e. starting the curing reaction) and subsequent cooling. This difference indicates that in fact curing has occurred. Whilst this is a rather basic method, it gives a clear indicator for a change in materials' properties [12].

Building upon this observation, the cause for this phenomenon becomes obvious considering the large differences in the coefficient of thermal expansion (CTE) between reinforcement and matrix, with residual strains as the result [109]. In L- or U-shaped parts (Figure 2.28) residual stresses may even cause angular mismatch [110]. Such detrimental behaviour is termed spring-in or spring-out depending on the direction. Considerable attempts to capture these straining effects have been made using SHM technologies for both thermoplastic and thermoset composites by FOS [12, 24, 79, 99, 102, 103, 109–115].

FOS are being strained by the structure via shear [24] in a similar way as the reinforcement fibers are strained. In order to understand the effectiveness of such an integral strain measurement, tensile test specimen may be produced and the results compared with those of conventional strain gauges [24, 72, 79]. Good agreement has been found between the two methods [24, 72, 100] even for a multiplexed fiber [79].

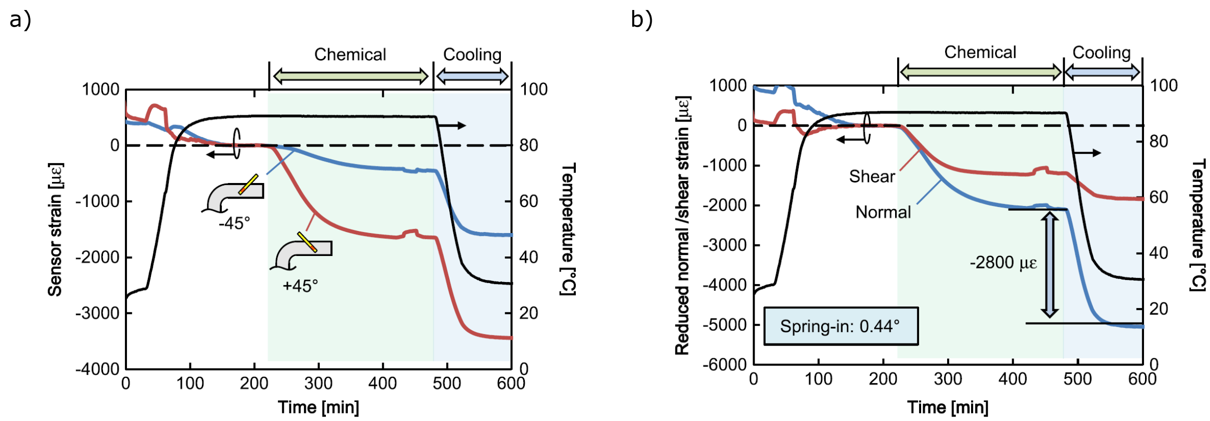

Figure 2.28: Capturing different sources for residual strains in a thermoset L-section using a FOS. a) shows the strains captured by the FOS and b) the component strains derived from the FOS strains. [110], p. 242 *Reprinted from Composites: Part A, 103, K. Takagaki, S. Minakuchi, N. Takeda, Process-induced strain and distortion in curved composites. Part I: Development of fiber-optic strain monitoring technique and analytical methods, pages: 236-251, ©2017, with permission from Elsevier.*

2.4.5 Integral PM and SHM solutions - case studies

Motivated by the idea of using only one sensor system for both PM and SHM, some research, although limited, is already available trying to close this gap. Two examples are given in the following section, one for thermoset- and one for thermoplastic based composites.

2.4.5.1 Pressure, temperature and DoC measurements for RTM

Scheerer et al. [30] have developed and validated an integral sensor that combines a PE element with a PT100 temperature sensor. The PE is applied during the RTM process (Figure 2.29) and functions as a process and cure monitoring system [10]. Once the part is completed, the PE may be interrogated for active damage detection or used as passive AE receptors. They were successful in detecting the resin flow front and captured changes to the curing resin by measuring the admittance. An increase of the resonance frequency of 6-8 kHz has also been noted [10]. Whilst validating the ability of this sensor to detect impact damages, the importance of temperature compensation was highlighted. Since at every PE location there is a co-located PT100 temperature sensor, the baseline could be corrected successfully and a reasonably good damage detection and localisation ability was established for both AE and active sensing [10].

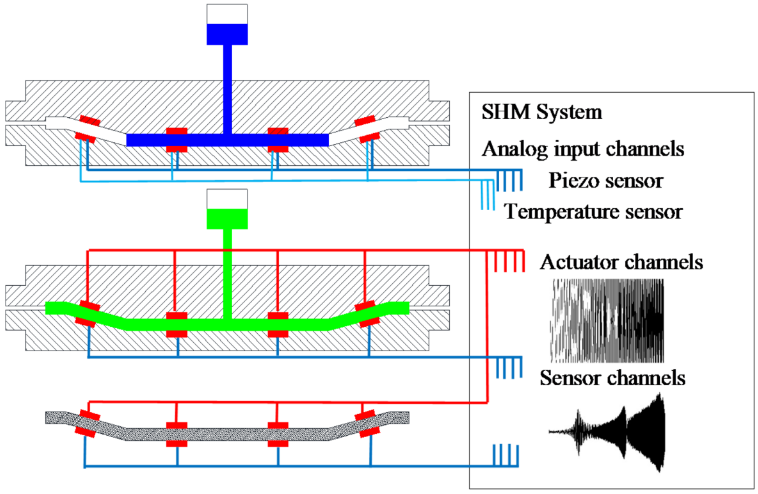

Figure 2.29: Integral PM system with SHM [10] p. 7.
Reprinted under the Creative Commons CC BY NC license applied to the original work.

2.4.5.2 Automated layup of thermoplastic sheets with PE integration

Hufenbach et al. [96] published the description of an innovative high volume lay-up and hot pressing production process for active thermoplastic composites (Figure 2.30). Whilst active composites are not to be confused with composites fitted with sensors, the developed strategy may easily be adapted for an automated senor application. It also offers solutions to inherent concerns in terms of processing conditions, sensor wiring and piezoelectric polarisation.

The piezoceramic module is able to sustain temperatures up to 430 °C and pressures of 4 bar ([96], p. 5) and the entire process is automated. Since the high temperatures exerted during hot pressing are detrimental to the chosen piezoelectric properties (above the PE's Curie temperature, upon which depolarization would occur), a polarisation cycle is performed after the completion of manufacture. After this step a fully functional SHM system is in place, fully embedded within the composite.

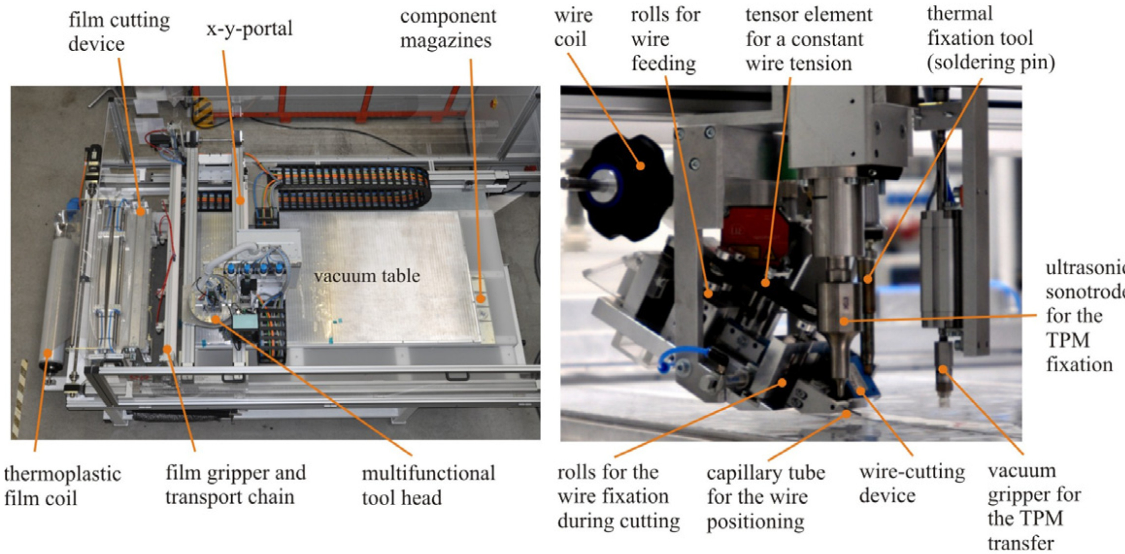

Figure 2.30: Automated unit developed for the application of piezoelectric active modules [96] p. 4. *Reprinted from Smart Materials and Structures, 23, W. A. Hufenbach, N. Modler, A. Winkler, J. Ilg, S. J. Rupitsch, Fiber-reinforced composite structures based on thermoplastic matrices with embedded piezoceramic modules, 1-10, ©2014, DOI: 10.1088/0964-1726/23/2/025011 © IOP Publishing. Reproduced with permission. All rights reserved .*

2.5 Suitability matrices

To summarize the findings of the above sections, two suitability matrices are presented (Table 2.1 and 2.2). They give an overview of what composites processing parameters certain technologies are able to monitor. In addition they give an insight into how likely they are to survive the loads that act on them during these processes.

Table 2.1: Suitability of different monitoring technologies for parameter monitoring

	SHM potential	Temp.	Press.	Visco.	Resin	Vf	Resid. stress	Voids	Com-paction
PZT	++	o	+	++	++	+	-	o	+
PVDF	+	o	+	+	++	+	-	o	+
FOS	+	++	++	-	++	-	++	−	o
EFS	-	o	−	++	++	-	-	o	+
Electrical	o	+	+	++	++	+	-	o	++

++ very suitable, + suitable, o possible, - rather not suitable, - - unsuitable

Table 2.2: Suitability of different monitoring technologies for composite processes

	RTM	VaRTM	RFI	Filament Winding	AFP	ATL	Press	Stamp forming	Welding
PZT	++	++	++	-	−	−	+	−	+
PVDF	++	++	++	+	+	+	+	+	+
FOS	++	++	++	++	+	+	-	-	+
EFS	++	++	++	++	+	+	-	-	+
Electrical	++	++	++	o	o	o	+	+	+

++ very suitable, + suitable, o possible, - rather not suitable, - - unsuitable

2.6 Conclusions

SHM has the potential to considerably improve the economical utilisation of composite components. Significant amount of research in recent decades has led to the development of many different sensing technologies. In about the same time the way manufacturers produce composite parts has changed as well. Highly automated processes have the potential to widely replace manual layup.

For a successful implementation of SHM, it will therefore be necessary to consider constraints related to part manufacturing. A clever design could offer the unique opportunity to use the highly capable sensors to improve the part quality and process. Ways of exploiting this symbiosis are highlighted in this work. Since it will not be possible to solve all current issues with one single sensor type and architecture it is imperative to know what merits and downsides the different technologies possess. The information provided herein was selected with the vision to equip the reader with a thorough overview and the ability to find the right technologies for the desired application.

FOS have already been used for both manufacturing monitoring and SHM for many years now. Fibers can be surface-treated or nano-structured in order to make them selectively more sensitive. In addition to that, the fact that fibers with different functionalities can be spliced together offers the possibility to add several different sensor types on a single fiber. Besides convenience this allows the reduction of ingress and egress locations to a minimum. Those carry a significant risk of fiber breakage for all processes where an entirely closed mold is used. Whilst their relative ease of integration and signal processing makes them very appealing candidates, their ability to detect and locate damage is limited. However, they do allow to assess the overall condition of a structure.

A more detailed information about the location and severity of a damage may be retrieved from piezoelectric transducers, with the largest share attributed to PZTs. The most widely utilised modes of operation are

AE and Lamb-wave propagation analysis. Acoustic properties of a part are strongly related to the local mechanical properties. They strongly affect the way acoustic waves move through a part, get absorbed or are reflected. Should a damage occur, the mechanical properties are altered. Such changes can be detected by a piezoelectric sensor. The main difference between AE and Lamb-wave propagation is the way the acoustic wave is generated. Whilst for AE an external perturbation is necessary Lamb-waves are deliberately generated by a piezoelectric transducer. This can be done by the sensor itself or a pair of sensors – one acting as the actuator and the other as the sensor. For both AE and Lamb-waves the detection of the incoming acoustic waves is achieved by exploiting the piezoelectric effect.

The displacement imparted on the sensor is turned into an electronic signal which is then evaluated. For manufacturing and PM the ultrasonic waves may be used to measure the viscosity of a resin, shear modulus and after gelation the wave propagation. As already mentioned there is a great interdependence between acoustic and mechanical properties of a material. During the formation of a composite, the modulus increases by at least one order of magnitude (fiber reinforcement of a polymer). This offers a wide scope for the exploitation of acoustic wave propagation for PM.

The third branch of sensor technology evaluated herein are electrical properties-based sensors. They offer a wide variety of measuring principles and sensor designs. As such they are highly suitable for PM but their ability to detect and locate damage is limited.

To sum up, there is a great wealth of technologies and areas of research that are involved in solving the challenge of implementing SHM sensors into the manufacturing- and service environment of advanced composite components. There remain, however, some challenges still to be resolved. The knowledge of advantages a specific technique offers and how the disadvantages can be overcome by skillful combination of different sensor types is essential.

The following chapter 3 will aid greatly in better understanding the merit of certain discussed SHM methods in a representative application.

Chapter 3

Technology demonstrator - SHERLOC panel

The objective of this chapter is to demonstrate the ability of some of the most popular sensor technologies, for SHM application, before assessing their capabilities in PM. To this aim, some pre-selected techniques were tested on a representative aeronautical structure. A range of experiments were carried out on a realistic composite aircraft fuselage demonstrator with PE, FOS-FBG and FOS-OBR. The composite fuselage demonstrator is part of a CleanSky2 research project, SHERLOC, where different SHM techniques are being tested at an industrial level. The work presented in this chapter was complimentary to the project objectives. The main goal is to build an understanding for the main SHM concepts these sensors are able to support, on a complex structure (large scale, curved, anisotropic) which is representative of a real aeronautical subcomponent. Building on this knowledge in the following chapters will allow for an informed decision-making when deciding the most suitable sensor type for integrated PM and SHM.

3.1 Description of the panel

The panel was manufactured as part of the ongoing research project, SHERLOC, and has a size of roughly 2.5 x 6 m (made by one of the project partners, FIDAMC in Spain). It has been manufactured and inspected to aerospace standards and consists of a CFRP skin with varying thickness ranging between 2 to 6 mm. The skin is stiffened with omega stiffeners that were co-bonded. The frames are made from aluminium and have been installed on the panel using fasteners. See Figure 3.1 for an image showing the configuration in more detail.

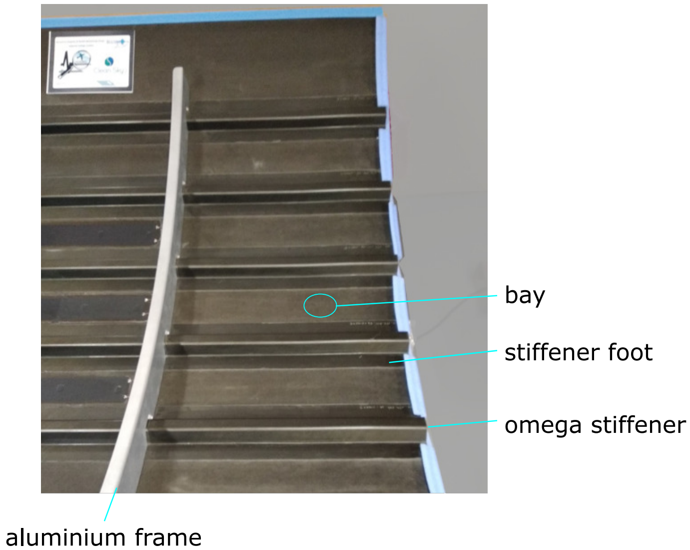

Figure 3.1: Technology demonstrator fuselage panel

3.2 Sensor application

Since the panel has been already manufactured, all sensing elements had to be applied to the structure through secondary bonding operations. For that purpose a thermoplastic hot-melt adhesive (Collano 36.004, Collano AG Switzerland) was used. This is a special type of adhesive which uses the melting of the thermoplastic matrix to initiate a bond between elements. In previous works this thermoplastic adhesive has been shown to work well [5, 116].

In a first step the adhesive which is in the form of a film and has no adhesion at room temperature needs to be put in place. On top of that film, the sensing elements are placed and fixed using a pressure sensitive tape. In a final step a vacuum bagging enclosing a heating blanket (GMI Aero, Anita EZ - 2 Zone Hot Bonder) is constructed. This ensures that bonding pressure can be applied and the heating blanket melts the adhesive film. A short bonding cycle made up of a quick ramp up from room temperature to 135°C, a holding phase of 15 minutes followed by free cool down back to room temperature ensures a solid mechanical connection of the sensor to the structure (Figure 3.2).

In total three different types of devices were installed on the panel. They were: 5 meters of distributed FOS (Fibercore Ltd. SM1500(9/125)P, terminated with a LC/APC connector on one end and 150 mm of spliced on core-less termination fiber (Thorlabs, Inc.) on the other), three optical fibers with five FOS-FBG each on them (FemtoFiberTec GmbH, Fibercore Ltd. SM1250BI(9.8/125)P, Polyimide coated, Femtosecond laser written, terminated at both ends with a FC/APC connector) and two PZTs (PI Ceramic GmbH, DuraAct Patch Transducer). See Figure 3.2 for installation details. Both types of FOS were co-located within 10 mm

of each other to objectively assess their individual strengths and weaknesses under comparable conditions. The FOS-FBG each had five gratings written at 1540, 1545, 1550, 1555 and 1560 nm with a physical distance of 50 mm between the centre of each grating. The gratings had a width of 8 mm. One entire unit cell of the fuselage demonstrator was sensurized meaning that one bay and the adjacent feet of the omega stiffener was monitored between two frame elements. This is a reasonable scenario both in terms of expected spatial resolution of the sensors and practicality for a potential OEM use case.
The above described setup was then step subjected to a range of different scenarios designed to produce insights into the aptitude of each technology. They were:

- Temperature monitoring of the structure using both types of FOS
- Passive impact detection using both types of FOS
- Active sensing using a PZT-FBG pitch-catch hybrid approach

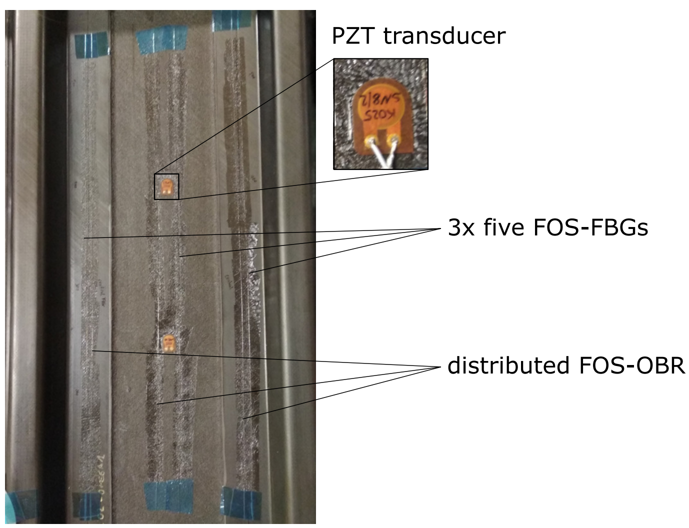

Figure 3.2: PZT, FBG and distributed FOS sensors bonded on the SHERLOC panel

3.3 Sensor interrogation

Having three different types of sensors installed, requires bespoke interrogation systems capable of acquiring signals from these sensors. All FOS-FBG and piezoelectric based systems were connected to a custom built optic and piezoelectric hybrid system developed by Lambinet [117]. It consits of a tunable laser source, optical circulator, optical switch, photodetector and a filter for FOS-FBG interrogation combined through LabVIEW interfaces with an arbitrary wave generator, switch and a digitizer for the handling of piezoelectric actuation and sensing. This highly integrated system allows for up to 60 MS/s bandwith FOS-FBG and

piezoelectric hybrid measurements. By only using the individual components through customized LabVIEW implementations the systems can also be used individually as required.
An ODiSI B Interrogator (by Luna Inc., Blacksburg, VA, United States) is employed to obtain the Rayleigh backscattering signature of the FOS-OBR.

3.4 FOS temperature monitoring

Mechanical properties of any material are strongly related to temperature. This is particularly true for polymeric materials and is important to consider when employing UGWs for SHM. The changes in the propagation properties of UGWs caused by temperature alone need to be understood and compensated for in order to not mistake these changes for structural degradation. To help with such temperature compensation during PZT-based active sensing [118, 119], in this paragraph the capability to monitor the component temperature with FOS is demonstrated. The temperature gradient necessary to perform the measurements was created by a hot air gun. The distributed FOS was bonded to the panel using a thermoplastic adhesive as described earlier. For reference, two K-type thermocouples (TC) were taped to the surface, as close to the fiber as possible and measurements were performed with a National Instruments™ CompactDAQ system.
The frequency shift dataset (ref. section 2.2.1.2) presented in Figure 3.3 is averaged over the entire bonded FOS-OBR fiber and is split in three parts. For heat application a heat gun (Bosch GHG 660 LCD) was used. The first part covers heat application from the concave face of the panel (i.e. the interior of the aircraft). Here the magnitude and overall shape of the peak are very similar and a high degree of resolution is evident. The second part shows the cooling and stabilization at room temperature before commencing a heating cycle from the convex face (i.e. the aircraft's exterior). The gaps between the three parts in the FOS-OBR data are due to the fact that measurements were triggered manually through the ODiSI B software. During external heat application a significant amplitude divergence in frequency shift in comparison to the TC readings can be observed. Whilst the overall shape is again very well preserved, the amplitude of the frequency shift excursion is higher than the one on the TCs.
This observation can be explained by the fact that the distributed FOS was in fact bonded to the panel whilst the TC is only taped to the surface. The temperature gradient experienced by the sensors differs between the outer face, which is directly hit by the hot air stream, and the one where the TC readings are taken. Since the fiber is attached to the component it is affected by the thermal expansion the structure experiences, the fiber is able to deliver a very accurate estimation of the temperature within the component. This is opposed to the surface mounted TC which can only pick up heat that is transported through the thickness of the structure. As such the aptitude of the FOS-based temperature monitoring approach was demonstrated successfully.

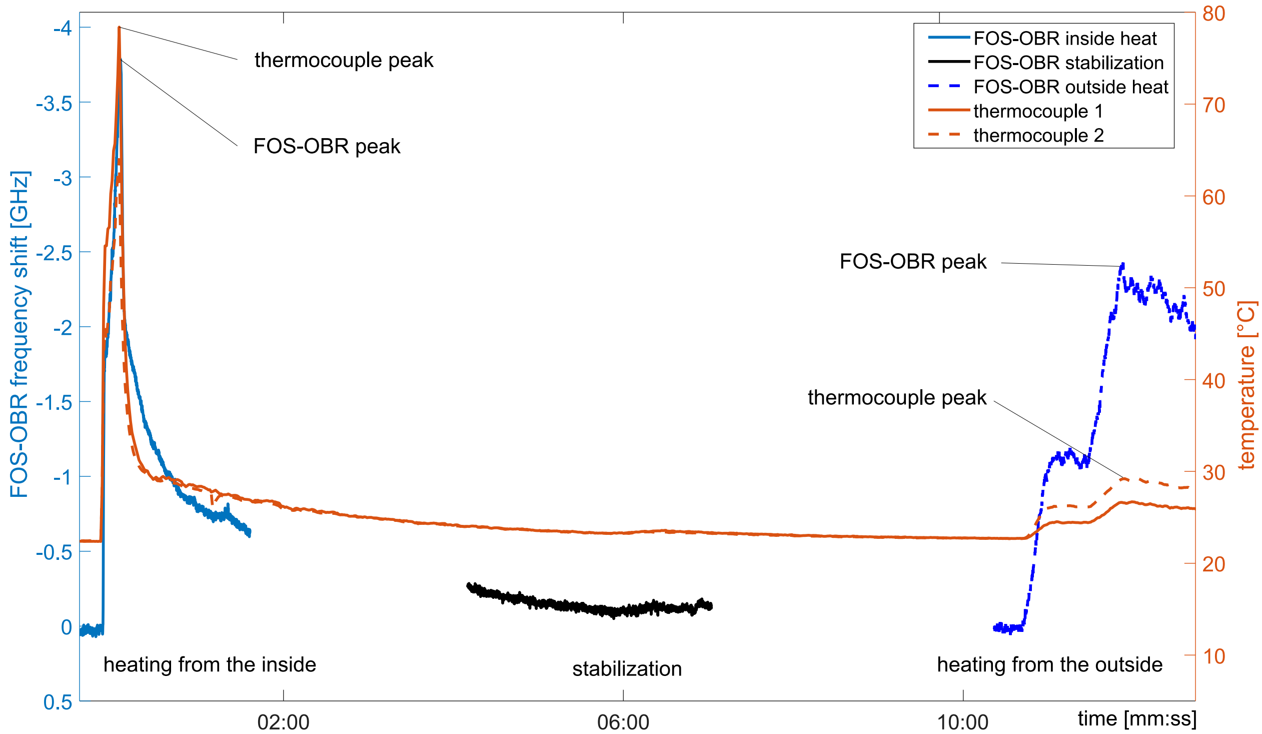

Figure 3.3: Measurement indicating the temperature sensitivity of the distributed FOS-OBR system in comparison with TCs

3.5 FOS passive sensing

Passive sensing in the field of SHM means a technique for which no agent controlled actuation of the structure is required. Potential damage events themselves cause the necessary perturbations to the structure to trigger a measurement and the resulting data is analysed to characterize the event. Typical features of interest are: severity of the potential damage event and location.

3.5.1 Impact method characterization

For FOS passive sensing in this work, the SHERLOC composite structure is impacted with a Modally Tuned® impact hammer (by PCB ® Piezotronics, NY USA). Such impact experiments are carried out to simulate either in-service events like hail and bird strike or on-ground events like collisions with ground handling equipment and tool drop during MRO activities. The Modally Tuned® impact hammer ensures high levels of reproducibility and captures the force-response by means of an in-built load cell. The force response is used to estimate the amount of energy introduced into the structure.

These impacts were monitored using two different FOS monitoring techniques: 1) FBG, see Figure 3.4 and

2) distributed FOS. This allows for the comparison between those techniques and will give an indication on what features of the impact event can be captured with each technology.

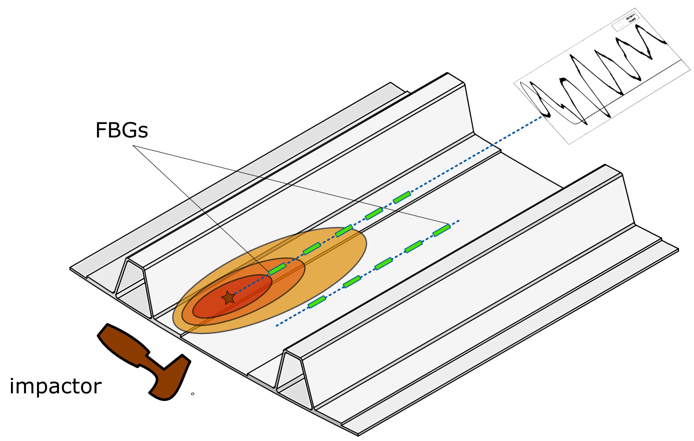

Figure 3.4: Concept of passive impact detection using FBGs and an impactor

To understand the effect such impacts have at different locations on the SHERLOC panel, a comparison was made. All impacts were performed with a Modally Tuned® impact hammer and the load cell signal was acquired. As can be seen in Figure 3.5 three distinct regions exist on the SHERLOC panel: 1) the foot area of the stringer 2) the transition from the foot to the bay and 3) the bay area. Each distinct area was hit with the hammer several times at sub-critical loads for the SHERLOC panel. Sub-critical in this context means non-damaging which was verified using a DOLPHICAM (dolphitech UK, Cambridge, UK) ultrasonic scanning device.

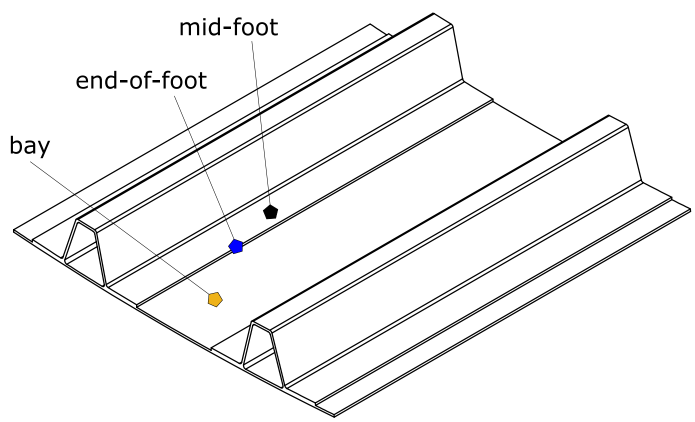

Figure 3.5: Representation of a repeatable unit on the SHERLOC panel with the impact locations: bay, end-of-foot and mid-foot indicated

From the results it is clearly visible how the local stiffness affects the response obtained by the hammer's load cell (Figure 3.6). Since the thickness of the panel varies greatly between the skin section (bay) and the foot of the stiffener (ref. Figure 3.5) so does the local stiffness. The major differences in the signal are the length of the impact event, load increase and decrease gradients as well as the overall shape of the signal. This information may be useful when interpreting the results obtained by the FOS later on as it gives a good indication as to where the impact occurred on the structure and may aid with impact event localization.

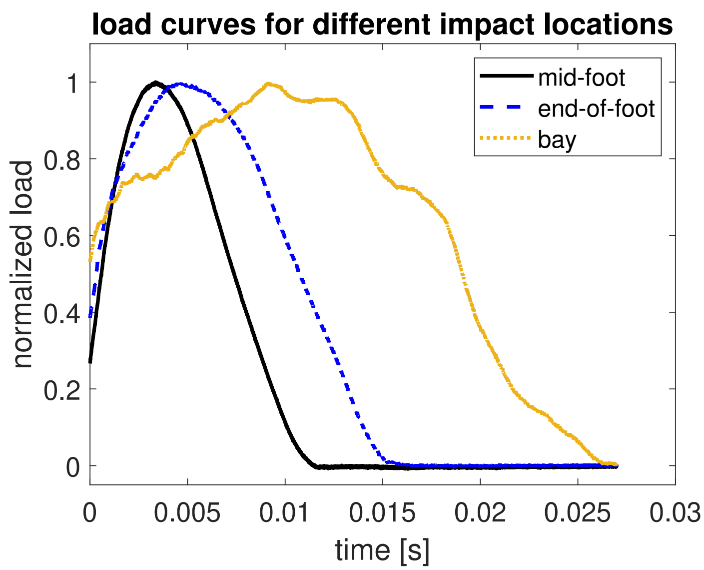

Figure 3.6: Comparison of the load signal upon impacting different locations on the SHERLOC panel

Analyzing the load cell data further and taking into consideration the results from multiple impact events at the same location (Figure 3.7), two main observations can be made: 1) each location has a unique impact morphology and 2) the load vs. time curves display a very high degree of repeatability. In order to compare the signals, despite slightly varying amplitudes (15 individual impacts were performed at the same location) an amplitude normalization was performed. The results reveal a high degree of match between the individual load curves. Whilst Figure 3.7 only shows one location, similar levels of repeatability were also observed on the other positions.

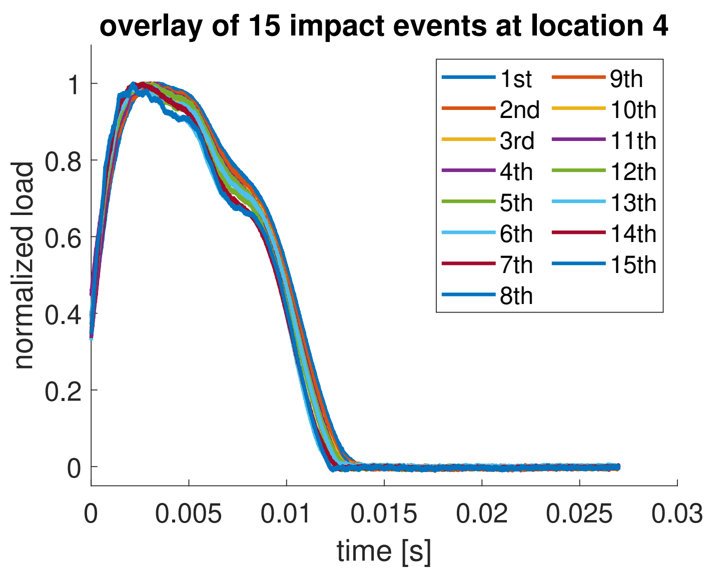

Figure 3.7: Comparison of the load signal originating from multiple impacts at a location on the SHERLOC panel. For location reference see Figure 3.9.

3.5.2 FBG passive sensing

Building upon the information gathered from the initial tests with the Modally Tuned® impact hammer, an extensive set of passive impact event sensing tests was carried out.

The FOS-FBG consisted of five FBGs per fiber with 50 mm distance between two gratings and were already bonded to the SHERLOC panel using thermoplastic adhesive earlier (Figure 3.2). There was one fiber on each stiffener foot (left and right to the bay) and the bay respectively. This sensor network ensured a good coverage of the entire section. Each grating wavelength was interrogated at a focus point [117, 120, 121](see Figure 3.8) using a 10 MS/s sampling rate. A 0.1 s long measurement sample was triggered through the hammer's load signal.

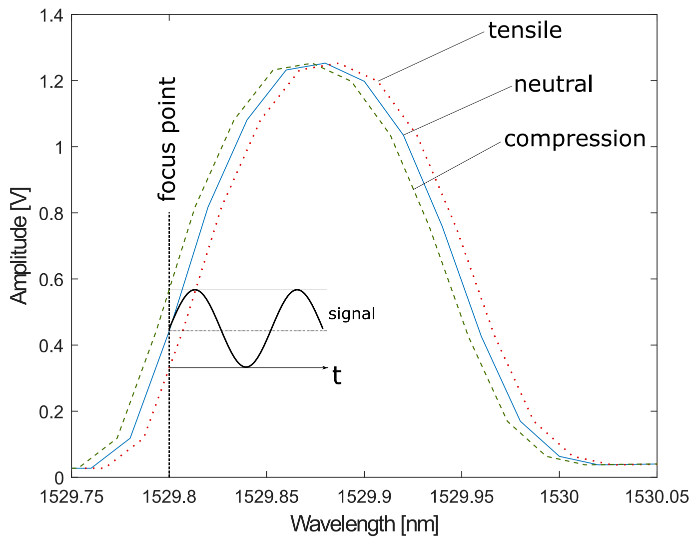

Figure 3.8: Selection of a FBG focus point and strain measurement principle

In total there were 24 predefined impact locations oriented as a grid covering the entire monitored surface area (Figure 3.9). As the tunable laser source cannot switch between individual FBG focus points (acting in a narrow band configuration) so quickly as to capture the entire impact event across all five grating locations on a fiber, the measurements had to be split. Each location was impacted 15 times and captured by a different FBG every time. In total 360 (24 locations, 15 times) measurements were taken this way and analyzed using MATLAB®.

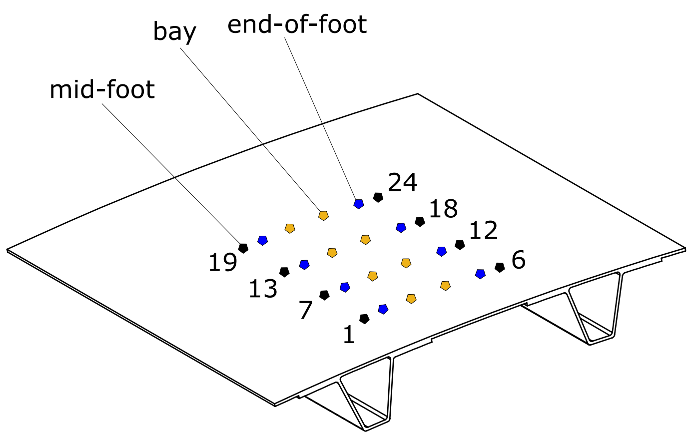

Figure 3.9: Schematic indicating the 24 impact locations completely covering the monitored area.

The results from these measurements are presented in Figure 3.10 - 3.14. Since the measurements were taken from multiple successive impacts with slightly different impact force amplitudes, the signals were normalized to maximum amplitude equals one for better comparison. A flexural wave propagating across the five FBG locations can be observed (Figure 3.10). Given the high sampling frequency, the wave pattern is reflected in great detail. It becomes evident, that several waves at different frequencies are propagating at the same time slightly obscuring the individual wave packets. Nonetheless, the information gathered provides useful information on the impact event.

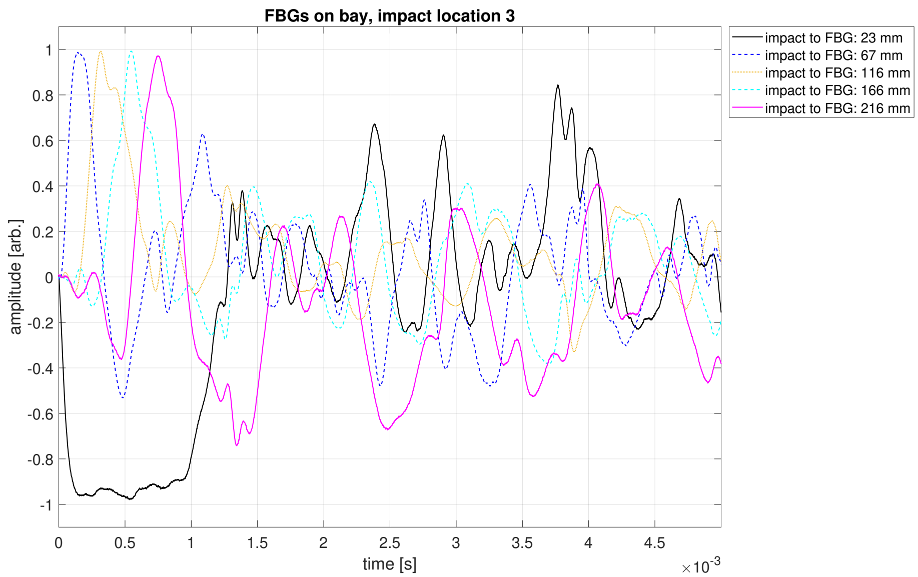

Figure 3.10: Non-damaging impact occurring at location 3 (ref. Figure 3.9) and captured by the five FBGs mounted on the bay.

Figure 3.11 shows an impact in the bay area of the panel zoomed-in on the first wave packet. The FBG closest to the impact site shows an opposite sign to the ones further away. This indicates tensile strain closer to the impact location, compared to compressive strain further away. Also, the broad relatively flat part of the signal on the closest FBG indicates saturation of the photo detector. This occurs when the power received is out of range due to a large signal amplitude.

Another observation to make is that the further the wave packet travels the more dispersion of different frequencies occurs. Such behaviour is marked by higher frequency, lower amplitude oscillations occurring at the beginning of the large first wave packet.

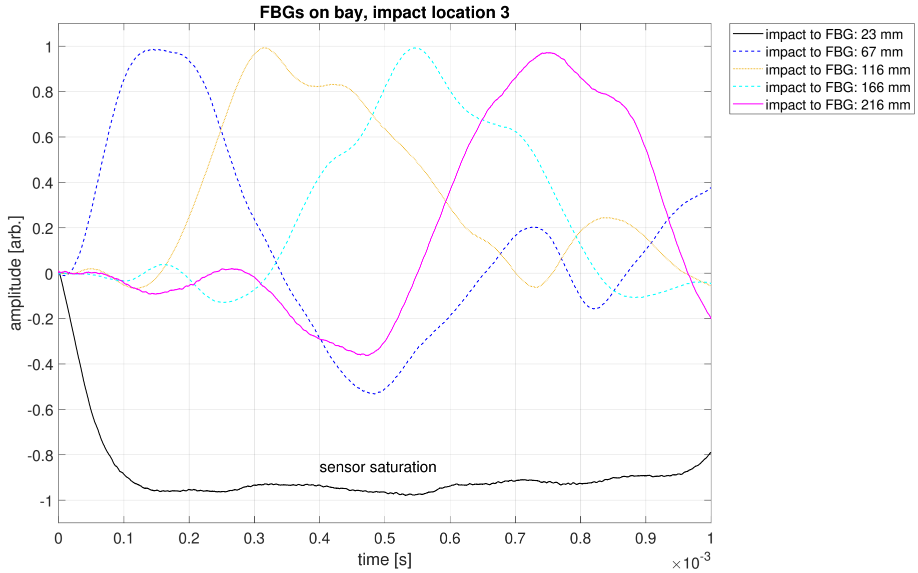

Figure 3.11: Zoomed-in view on the first wave packet of the impact event displayed in Figure 3.10.

For impacts in the foot area of the stiffened composite panel see Figure 3.12, similar conclusions can be drawn as for the bay area. This is expected since the material properties and composite ply orientations are the same. The only difference is the total thickness of the lamina in this location being two times that of the bay. Again, the individual wave packets are clearly discernible and the presence of multiple frequencies is evident.

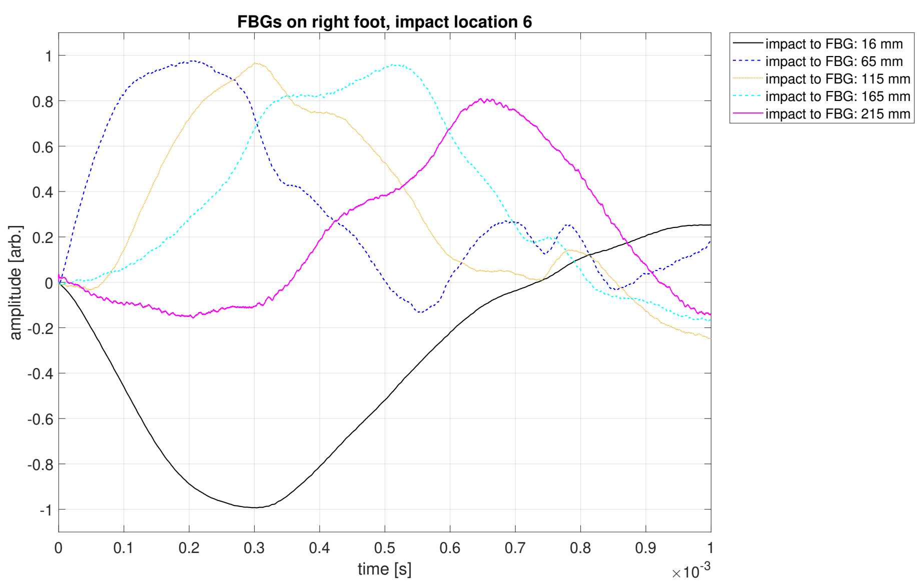

Figure 3.12: Non-damaging impact occurring at location 6 (ref. Figure 3.9) and captured by the five FBGs mounted on the right foot of the stiffener.

Building on the measurements obtained for the individual FBG and impact location combinations, a novel methodology was developed for full field strain reconstruction to show the response of the composite plate upon an impact. To be able to compute synthetic strain values at locations not monitored by an FBG a few assumptions are made:

- Material properties are considered quasi-isotropic.
- Circular wave-front propagation pattern is assumed.

Based on these assumptions, a 3$^{\text{rd}}$ degree polynomial model was created for every time stamp to compute the missing strain values. The distance between the impact location and the FBG is used as an independent variable. The model is created based on the 15 existing measurement points (Figure 3.13). The experimental data is subject to a scatter due to the superposition of different frequencies. However, the 3$^{\text{rd}}$ degree polynomial fit is able to capture the underlying major wave-motion satisfactorily.

With the model in place, strain points in locations not originally monitored can be calculated and a full-field representation of the plate's deformations is possible. Figure 3.14 presents the reconstructed plate deformation. As visible from the experimental data, a large initial wave packet travels across the plate originating from the impact location at [0 mm, 55 mm]. The panel representation itself has a length and width of 215 and 155 mm respectively. This is exactly equal to the monitored area.

Overall the excellent ability of FBGs to monitor the highly dynamic load case of an impact event is shown. The ability of MHz-range data acquisition bandwidth preserves all of the signal's information content. Several unique monitoring aspects are enabled through this data quality. Besides the tracking of individual wave packets, their propagation and morphology in a full-field strain reconstruction is enabled. These are all important factors when considering a SHM system.

Finally, whilst passive impact detection based on FOS-FBG has been published before [122–127], there are some aspects of the implementation shown herein not presented before. Novel aspects include the use of a thermoplastic adhesive and vacuum bagging method for FOS application, monitoring on a full-scale curved stiffened fuselage panel covering different laminate thicknesses and the idea of merging the data obtained from 15 FOS-FBG for the same impact location to create a full-field strain representation.

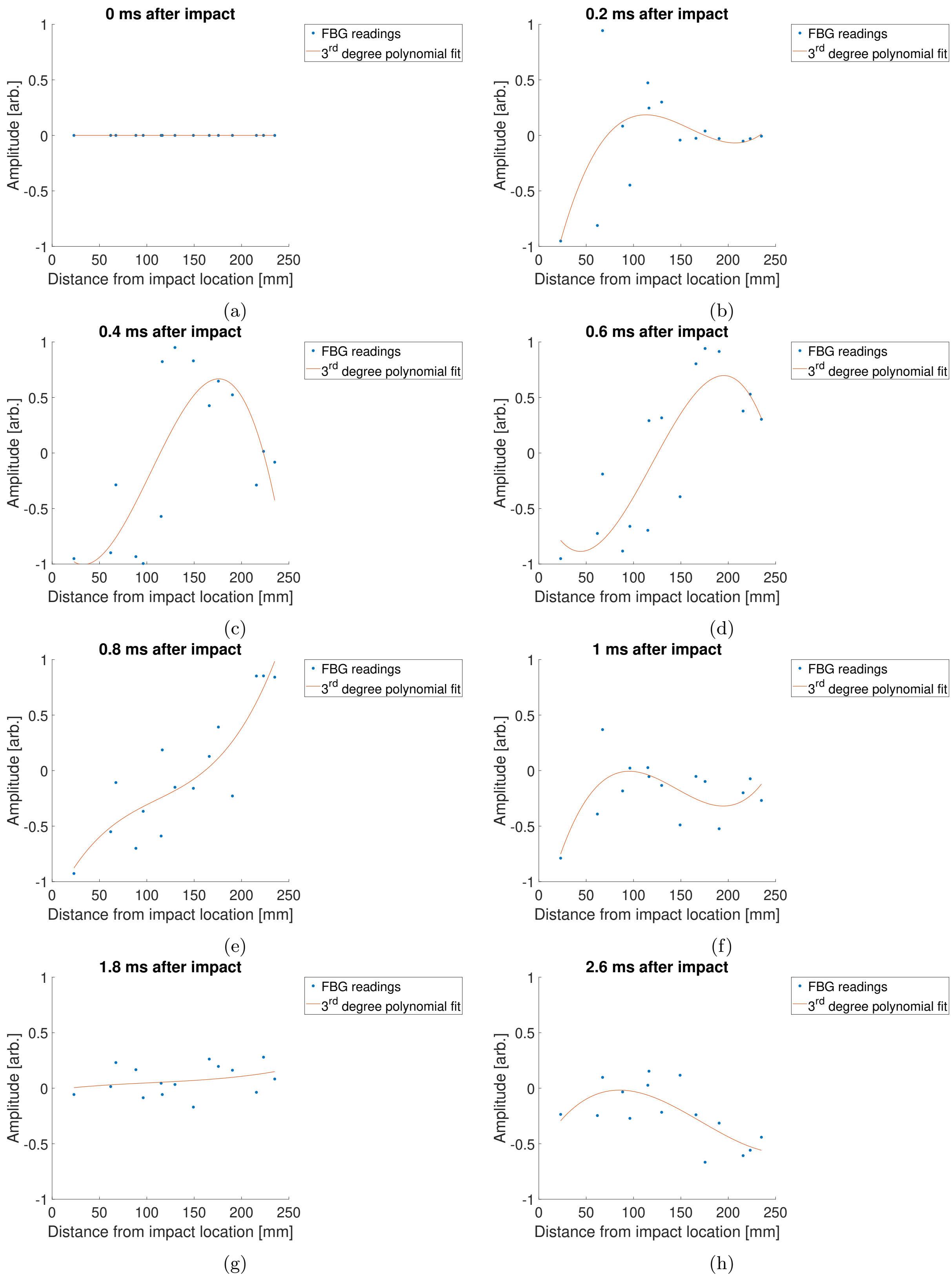

Figure 3.13: Wave propagation monitored at 15 different FBG locations across the panel viewed at increasing time intervals.

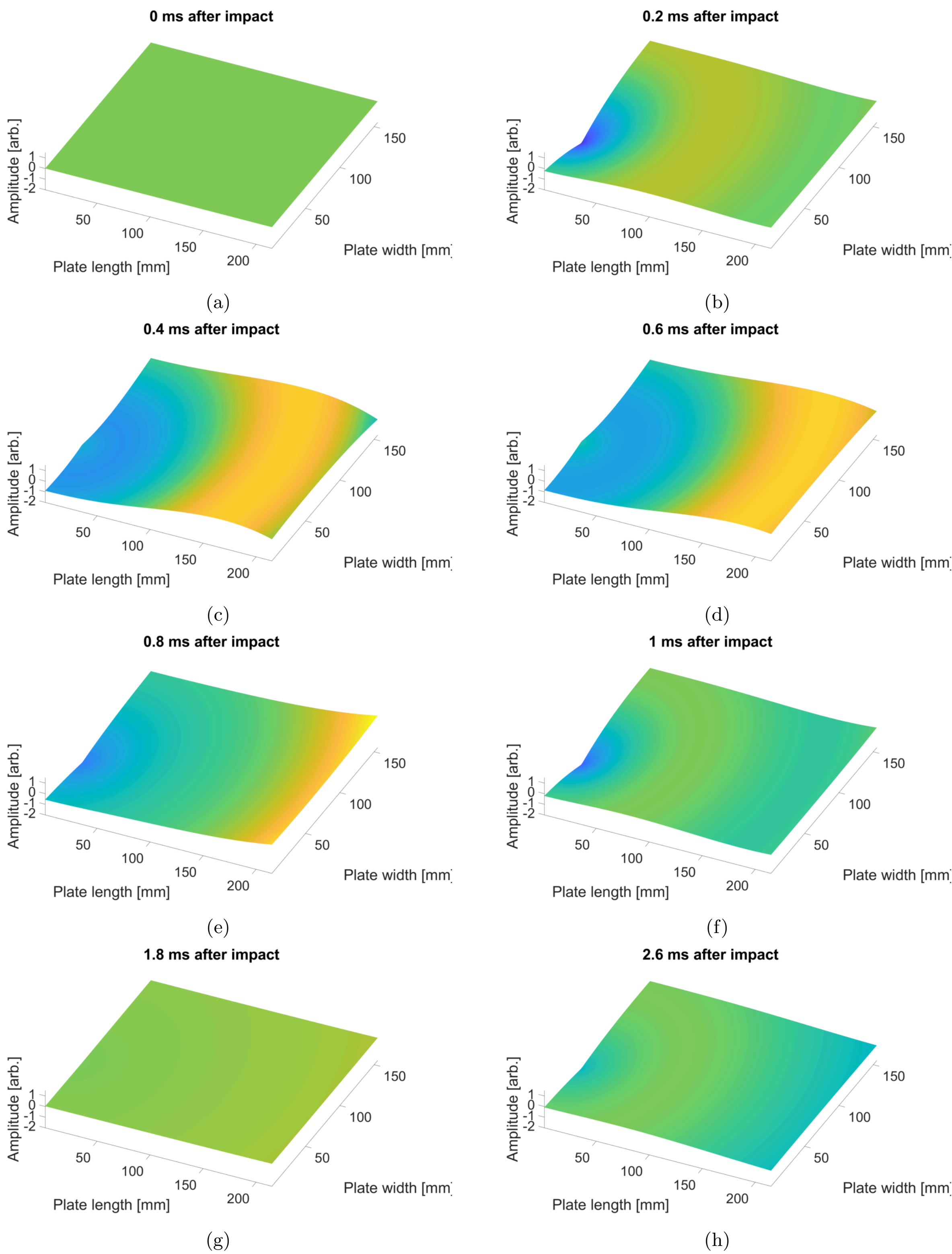

Figure 3.14: Plate deformation reconstructed from FBG readings viewed at increasing time intervals.

3.5.3 FOS-OBR passive sensing

At the same time as the experiments described above were carried out with FOS-FBG sensors, the distributed FOS-OBR system was acquiring data as well. The frequency shift measurements were acquired at 100 Hz which is 5 orders of magnitude lower than for the FBG. However, one of the benefits of OBR is that it does not require a focus point search and adaptation. Additionally, the entire section can be monitored with a single fiber. This means a single impact event at one location is enough to create a data set that spatially covers the entire monitored area.

Figures 3.15, 3.16 and 3.17 present the results obtained from a single turn covering the entire monitored area. As there were 24 impact locations on the monitored area (Figure 3.9), there are also 24 clearly visible peaks in the figures. Each figure shows a maximum and minimum envelope for a single fiber section which encompasses the data of the entire length of bonded FOS-OBR (around 450 mm for each fiber section).

These peaks, despite being monitored at the highest possible data acquisition rate of 100 Hz, hold very limited information content. Most of the times their width is only a few samples wide and their height is relatively inconsistent. Such a behaviour can be explained by considering the extremely low acquisition rate when compared to the speed at which such an impact event dies down.

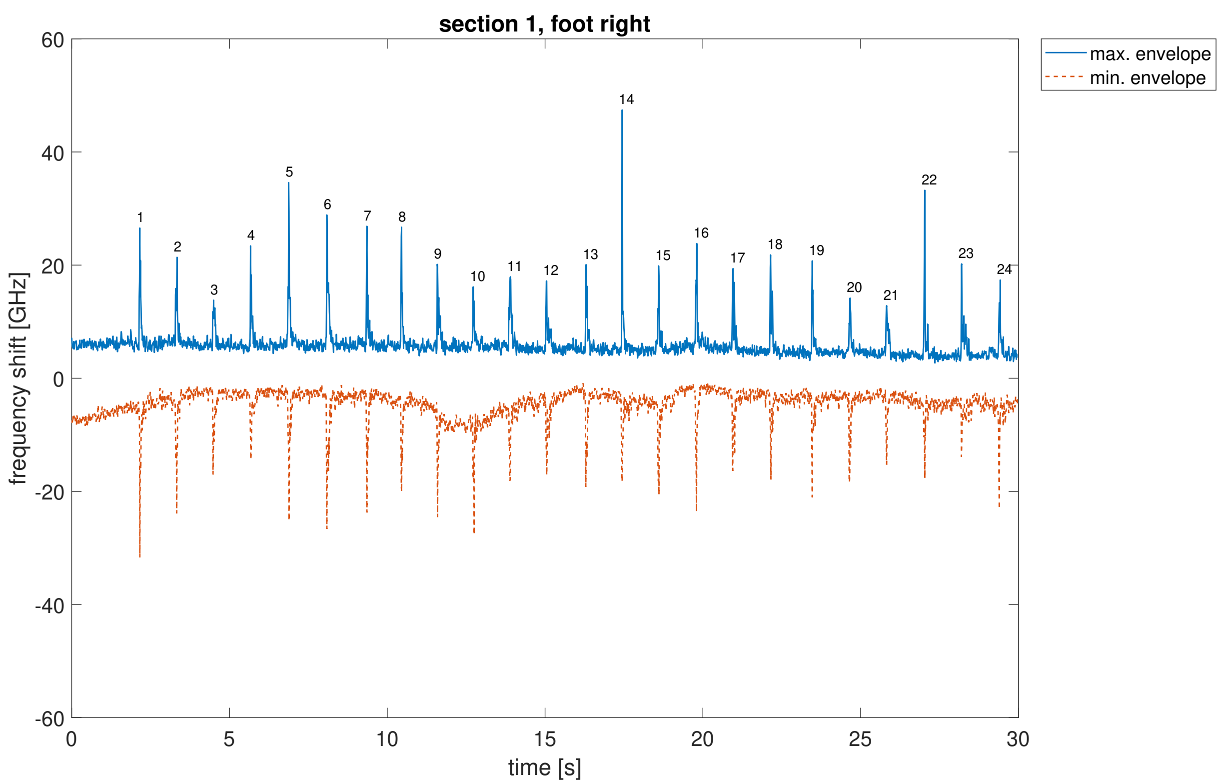

Figure 3.15: Passive impact events monitored by FOS-OBR, fiber section: foot right.

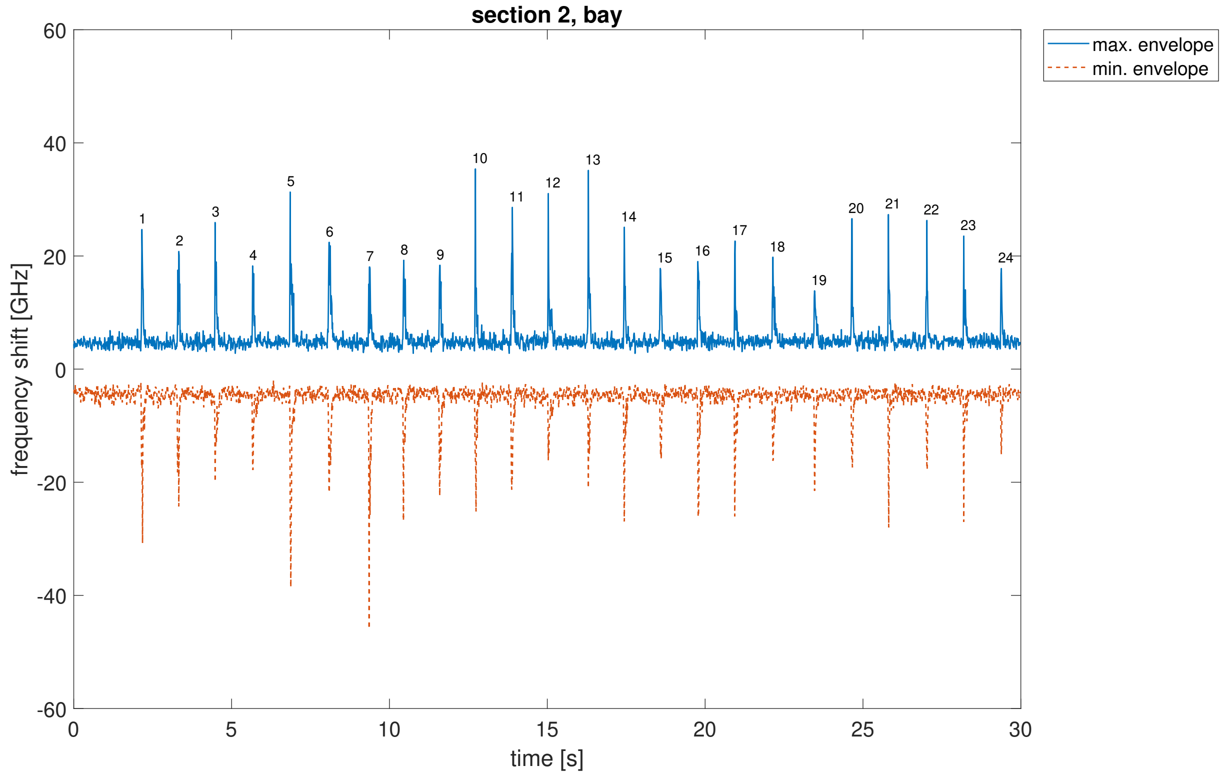

Figure 3.16: Passive impact events monitored by FOS-OBR, fiber section: bay.

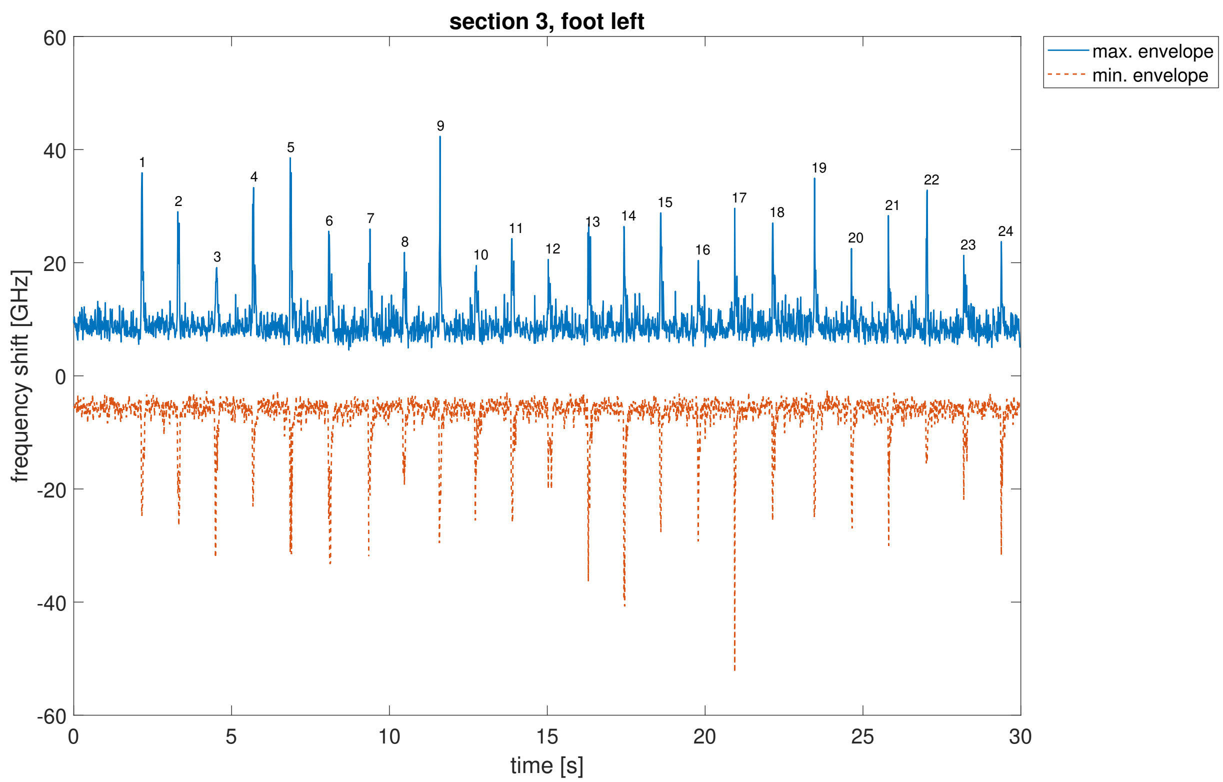

Figure 3.17: Passive impact events monitored by FOS-OBR, fiber section: foot left.

3.6 PZT-FBG active sensing

3.6.1 Introduction to hybrid measurements

Using a PZT transducer to generate waves within a structure is a commonly exploited method for SHM. Typically Lamb waves are actuated selectively for their relatively low attenuation when travelling great distances. In a conventional SHM setup, those actuated waves are being received by a PZT transducer. This can be the same transducer that created the perturbation in case of the pulse-echo method [58], or another PE element when the pitch-catch method is used [128]. The receiving transducer converts the strain into voltage (see 'inverse piezoelectric effect' in section 2.2.3), which is captured by the DAQ.

However, PZT transducers have certain advantages (light weight, low power, multi-modal excitation, used both for active and passive sensing), as well as disadvantages (extra weight from wiring, electromagnetic interference). Similarly, FO sensors have electromagnetic immunity, light weight, multiplexing and high strain sensitivity, but they are passive sensors only. There exists a technique that utilises the advantages of both PZT and FOS.The FOS-FBGs are used to measure the strains caused by the actuation (Figure 3.2), in an active sensing set-up. This is done in a similar manner as described in section 3.5.2. Again, a focus point is required in order to capture strain data at 10 MS/s. This focus point, i.e. a specific wavelength provided by the tunable laser source to the FOS-FBG, serves as a neutral baseline. Any contractions or extensions resulting from the UGW are detected as a voltage increase or decrease at the photo detector.

A more detailed description of the method used in this part of the research can be found in the works of Lambinet [117,120,121] and Xu [76,129]. They have developed and continuously improved the systems used. The combination of PEs and FOS-FBG for SHM investigations is commonly referred to as hybrid Lamb wave measurement [6, 117, 121, 130]. In this work, hybrid measurements were carried out to further investigate this method in general and better understand the other applications possible for a component that has a FOS-FBG installed already from earlier process monitoring.

In order to perform an active hybrid measurement, where a PE transducer is used to create a perturbation and a FOS-FBG receives the strains in pitch-catch mode, a measurement path needs to be defined. Such a path consists of one actuator and one sensor location. A wave or wave packet excited by the actuator travels in all directions in the plate and the sensor records these perturbations caused by the strain wave as an output signal. This signal is then evaluated for any features that could contain information about potential damage or degradation of the material on the path. This is the same method as used for UGW based damage detection.

Here the FOS-FBGs are again used for their high strain sensitivity. In addition to their high sensitivity, FOS-FBGs are not affected by electromagnetic interference. Such electromagnetic noise is an unwanted phenomenon adversely affecting signal quality. Such noise can originate from the measurement devices itself ("cross-talk" [116]) or the environment.

3.6.2 Results obtained by hybrid measurements

Using the sensor configuration depicted in Figure 3.2 a five cycle Hanning-windowed actuation signal at 50 kHz was delivered to the PZT. A sample of the input signal is shown in Figure 3.18. Three distances between the actuating PZT and the sensing FOS-FBG were chosen (see Figure 3.19) to show the effect of the distance between them on the time of arrival (TOA) and amplitude. These were 50, 100 and 150 mm along the extrusion direction of the SHERLOC panel and within the bay section.

With the wave propagating along the extrusion direction of the panel (Figure 3.19), the main UGW wave packet hits the FOS-FBG's grating parallelly, whilst reflections originating from the omega stiffener hit the FBG sideways. It is expected that the results from parallelly propagating waves will be of significantly higher signal quality than those perpendicular. This is owing to the pronounced directionality [123] of the FOS-FBG 2.2.1.1.

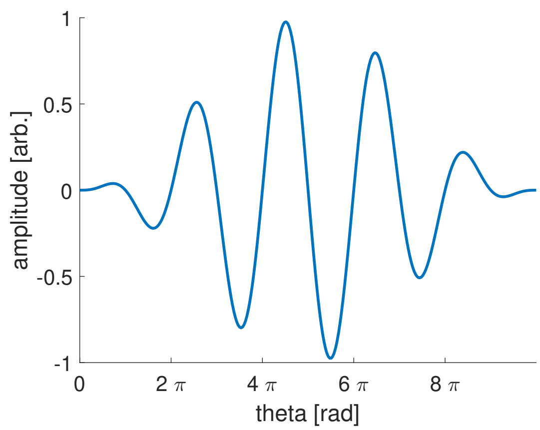

Figure 3.18: A five cycle Hanning-windowed signal.

In Figure 3.20 the obtained readings from the FOS-FBG are shown. The signals were processed in MATLAB® with a digital bandpass-filter prior to plotting. The graph contains three measurements, each of them acquired at a different FOS-FBG but actuated from the same PZT. This means each individual line represents a specifc distance between the actuator and sensor. The features of the actuation signal can be clearly identified.

Secondly, the TOA increases with increased distance whilst the amplitude decreases at the same time. This is exactly as expected. Further, the presence of a second wave packet is visible, with the second one having a much lower amplitude, just slightly above the noise floor. This is likely to be a reflection.

The noise visible in Figure 3.20 is random and limited to a relatively small bandwidth. This is likely the result of the high sensitivity of the system itself and slight variations owing to the power output of the tunable laser source. The level of noise present in a SHM system is an important factor to be aware of and needs to be actively managed. That is because only signals clearly discernable from noise can effectively be processed.

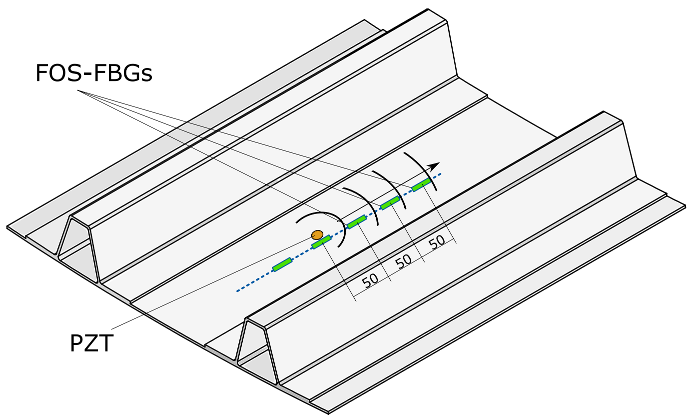

Figure 3.19: Active hybrid: PZT and FOS-FBG locations.

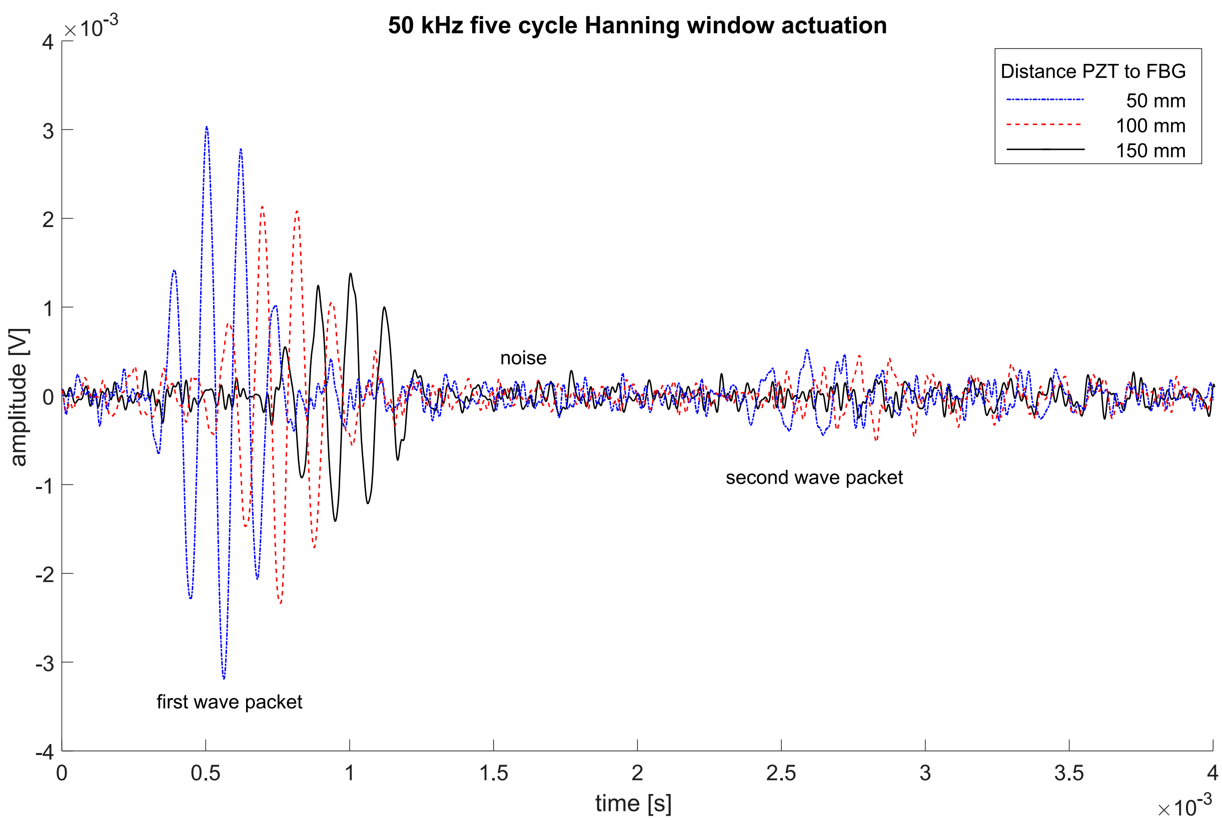

Figure 3.20: Active hybrid measurements with distances of 50, 100 and 150 mm between PZT and FOS-FBG.

Overall, the results obtained show that the hybrid sensing method is able to detect the Lamb waves present within representative composite structures. The signal quality for the first wave packet is good and offers a large enough signal-to-noise ratio to support high fidelity, data-driven damage assessments as discussed in literature [117].

The fact that FOS-FBG can be successfully combined with PEs on complex and representative structures to facilitate Lamb wave-based SHM techniques (ref. section 2.2.2) is significant. Both these sensing technologies have their unique benefits and downsides. Being able to combine them, but also use them independently opens the possibility for varied and multifunctional PM and SHM applications.

Chapter 4

Development of process monitoring techniques: technology down-selection

4.1 Technology selection process

In chapter 2 a range of possible technologies have been identified as potential candidates when it comes to integral PM and SHM. In chapter 3 PE and FOS have been extensively tested in SHM settings to better understand their working principles. Table 2.1 and Table 2.2 summarize different monitoring techniques and are evaluated for their suitability to monitor a range of parameters under processing conditions.

With most composite components, differently to metallic ones, the material is created at the same time as the part takes shape. Liquid polymeric resins are initially mixed and combined with reinforcement fibers. This sets several challenges that need to be overcome by a potential sensor: Firstly, the stiffness of a composite rises by the order of several magnitudes as the resin cures. This means that in the early curing stages the sensor cannot be affixed to a solid structure for protection from mechanical loads. Such loads could be pressure, mold closure movements, erosion or mismatched surfaces. Also, not being able to hold a sensor in the desired location means that it might get moved around by resin flow and not stay where it is needed.

Secondly, temperatures seen in manufacturing processes can reach several hundred °C. Especially when it comes to thermoplastic composites. Furthermore, the dimensions of a composite component change quite significantly throughout the manufacturing steps. During consolidation it is not uncommon to experience >10% decrease in thickness. This is the result of applying pressure (both positive and negative). A sensor and its wiring need to be able to survive the high loads and subsequent relative movement. For a component to comply to dimensional requirements, machining processes are common. These are challenging when sensors or wires are embedded and exit through the periphery of a component.

Considering all the above it is still necessary to produce valuable process information and capture parameters important for successful manufacturing. This chapter gauges technologies that were found most promising following a search in published literature.

A set of experiments was carried out by the author for the assessment of the existing technologies and to evaluate their performance in realistic environments. The results are presented to demonstrate the aptitude of specific techniques when it comes to PM and SHM and to make a down-selection of sensor technologies for further development within this PhD research. Together with a theoretical treatment of the technology in question by means of literature references, analytical and/or numerical modelling those experimental results are used to conclude the suitability of a given technology.

4.2 Introduction of pre-selected technologies

4.2.1 Principles of required sensing density (spatial and temporal)

Independent of the selected physical sensing technology, it is important to consider the required density of measurement points in a temporal and spatial sense to gain a meaningful insight into the phenomenon in question. Should the phenomenon be one that affects a large area, the number of sensors and associated density of measurement points in a spatial sense can be reduced. A potential example could be the monitoring of a component's temperature. Here a single measurement could be sufficient to estimate the condition for a large section. Whereas, if the condition only affects a very small area or changes significantly depending on the location a measurement was taken, a more dense network is required. One example for this would be measuring local pressure which is not representative of the distribution over larger areas. Arguably, required densities can sometimes be subjective and the definition of an optimal sensor placement strategy is subject to an entire research field.

In a temporal sense, the density of measurements needed to capture a specific event are more straightforward but need to be viewed in conjunction with the above. For a given event, be it an impact, vibration, load gradient etc. the speed at which said event occurs is governed by the mechanical properties of the component to be monitored and the event itself. It is usually possible to ascertain the propagation speed and duration of the signal to be captured using first principle calculations. Such calculations will give an insight into the required acquisition rates. Examples for a long and short event respectively would be the monitoring of a bridge that is subjected to transient loads due to traffic compared to a ballistic impact onto an aircraft. In the case of the bridge it is probably sufficient to capture measurements at frequencies of a few Hz or below. When considering the impact on an aircraft, several hundred kHz of acquisition rate are necessary to get a full picture.

The state of the art technology in sensor design, data acquisition and data processing technology forms a feasibility barrier and careful decisions need to be made to get the best result. In most cases (PE, FOS and certain electrical property-based technologies), the element defining the acquisition rate is an oscilloscope or a digitizer, where several hundred MHz are possible. Oscilloscopes or digitizers are used to measure voltage across a piezoelectric element or a photo-detector. The second frontier is how quickly a system can switch between channels (PE and electrical property-based technologies) or tune its wavelength (FOS and distributed FOS). This is important when distributed sensors or sensor networks are needed. When designing a monitoring regime all of these factors need to be considered and optimised (Figure 4.1).

For easy segregation, in this work the following definitions are used: 1) point sensors deliver measurements for a single location, typically at very high rates , 2) distributed sensors which cover larger areas at lower rates.

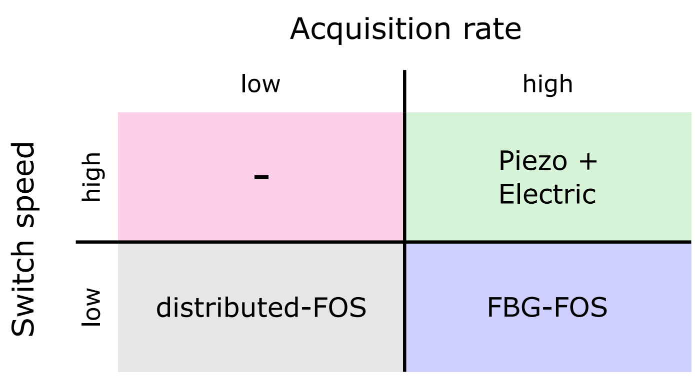

Figure 4.1: Switch-over speed vs. acquisition rate of chosen monitoring technologies.

When considering the acquisition rate for a specific physical parameter the Nyquist rate forms the lower bound, below which a signal suffers an unacceptable loss of quality and cannot be reconstructed anymore to its true information content. The Nyquist rate is $\geq$ 2x the highest frequency content that needs to be captured. Given a signal with a frequency of 250 kHz the Nyquist rate is 500 kHz which is the minimum rate a data acquisition system neeeds to be capable of delivering.

4.2.2 Piezoelectric devices

PE SHM transducers have arguably reached the highest levels of commercialization and industry acceptance. They are available in many different shapes and sizes, as well as material combinations. Figure 4.2 shows two commercially widespread and commonly used configurations. A DuraAct patch transducer is pictured next to two disk-type transducers with different electrode configurations (all by PI Ceramic GmbH, Germany). Whilst all of these transducers are based on the same PIC255 ceramic, the patch transducers offer greater protection of the brittle disk and can be viewed as more durable when it comes to handling.

To function as sensors, they need to be in physical connection with the structure and in electrical connection to the acquisition unit. They generate electrical charges corresponding to the mechanical stress they are subjected to. Such stress can originate from vibrations or mechanical waves present in the structure they are connected to.

If the application requires the PE to also work as an actuator, a suitable power source and waveform generator is required. In this case the PE generates waves within the structure through the physical connection between the PE and the structure. The tight control over the actuation wave forms and frequencies enable highly targeted monitoring of specific locations and conditions. Wave propagation properties are highly dependent on the mechanical properties of the monitored structure [53] and can therefore be used to inform about the structural health of a structure (ref. section 2.2.2).

Besides the ability to detect and/or enforce mechanical waves within a structure, PEs are also sensitive to their boundary conditions. These boundary conditions can be either: free, one-sided contact or embedded. A free PE is suspended within a fluid and its contractions and extensions are inhibited only by the force required to move the fluid [88]. In one-sided contact the element is bonded to a structure on one of its major faces. This leads to the inhibition of contractions and extensions which can be measured in terms of electromechanical impedance (EMI) [68]. The embedded condition means complete enclosure of the PE within the structure. As such the contractions and extensions are inhibited in a three-dimensional fashion. In the latter two cases discussed, the level of inhibition is dependent on the properties of the connection between the PE and the structure as well as on the mechanical properties of the structure itself.

Given the many ways in which a PE's properties are affected by the material it interacts with, the exploitation of such a dependence is sought for PM.

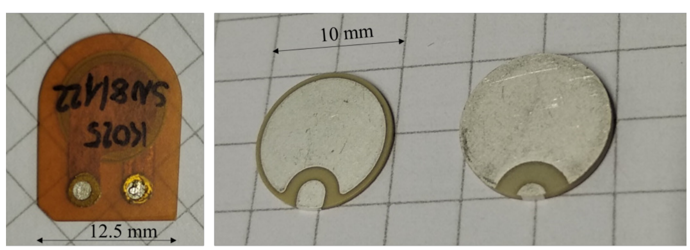

(a) (b)

Figure 4.2: Two types of PZT actuators (a) DuraAct patch transducer (used in chapter 3) and (b) circular PZT wafers (used in section 4.3.1)

4.2.3 FOS

At first glance, the capability portfolio of FOS places them ideally for PM. The high temperature sensitivity of FOS-FBG make them ideal temperature sensors, whereas their strain sensitivity can be exploited to study residual stresses [25, 99, 102, 103, 109, 110]. Exposing parts of the fiber core to surrounding media (exploiting Fresnel reflection [131]) or by applying specialised coatings has seen them being used in determining chemical compositions of different media [132–135]. However, given their fragile nature [136], they were not able to widely out-compete more traditional measurement devices like TCs and dielectric sensors yet. One noteworthy exception is the degree of cure monitoring of a CNT-reinforced composite. Since the CNTs make dielectric sensing impossible, Fresnel reflection presents itself as a viable option [98]. Limited efforts have been made, however, to expand the field of application for FOS into the sensing of other physical changes occurring in composites manufacturing processes. The author proposes in this work the use of FOS for monitoring physical quantities thus far not yet widely explored.

One main area is the sensing of in-mold pressure and compaction pressure of dry fiber reinforcements. Pressure is an important factor in many composite processing techniques and especially for those where a high degree of resin flow is required (i.e. Resin Infusion under Flexible Tooling (RIFT), Resin Transfer Molding (RTM), etc.). Since the compaction pressure varies drastically over a given area, distributed FOS has a major benefit when compared to other FOS-based techniques. It allows the user to define a custom fiber layout to capture data at a very high spatial resolution whenever required.

Figure 4.3 depicts a typical FOS-FBG as commercially available. The sensor shown here consists of a piece of optical fiber with two FBGs written into it (i.e. the sensitive areas visible through the two red color markings). The working principle and manufacturing of FOS-FBG have been discussed in section 2.2.1.1. In order to interrogate the sensor, connectors are added on either side of the FBGs with some length of fiber to allow placement of the sensor where required. Depending on whether the reflected or transmitted spectrum is analyzed, the laser source and photo detector are located on the same side or opposite side of the FBGs.

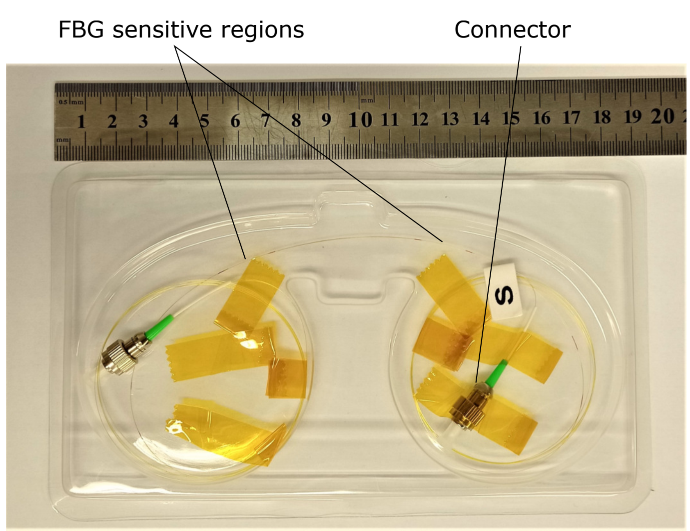

Figure 4.3: FOS-FBG sensors before installation.

4.2.4 Electrical properties-based sensors

When exploiting changes in electrical properties for the purpose of PM and SHM, one finds two main approaches: 1) at least one of the constituent materials is electrically conductive [64, 65] and directly used as electrodes, or 2) a sensing device is introduced to provide the measurement interface [63].

Since carbon fibers are generally quite good electrical conductors several solutions exist where this property is used for evaluating changes of electrical properties [64, 65]. Additionally, the polymer matrix material of a composite can be made conductive through the use of additives (e.g. Carbon Nano Tubes [78, 137]). Such methods are not within the scope of this work as the focus lies on the development of specifically designed and optimized devices.

As laid out in Chapter 2 the most important composite manufacturing process parameters are temperature, degree of cure, fabric wet-out and pressure. In order to be able to monitor these, a measurement strategy needs to be defined that suits the abilities of the materials and devices that can be manufactured. For measuring the degree of cure, the works of Bekas et al. [67] are referenced. They used printed interdigitated electrodes (IDE) in an impedance spectroscopy setup for cure monitoring. This requires direct contact of the electrodes to the resin and good conductivity. This device could also be used to detect the presence and location of the flow front as impedance values will be greatly different in the presence or absence of resin on the device's surface.

For pressure monitoring a capacitor as proposed by Valentine et al. [138] forms the basic building platform. As such, the sensing device needs to be made from two conductors, separated by a dielectric and allow for the thickness of the dielectric to vary with the pressure acting upon it. A certain level of elastic behaviour is therefore required.

Finally, the material needs to be able to inform the structural health of a monitored component. To achieve that some form of strain sensitivity is desirable 4.4 [139].

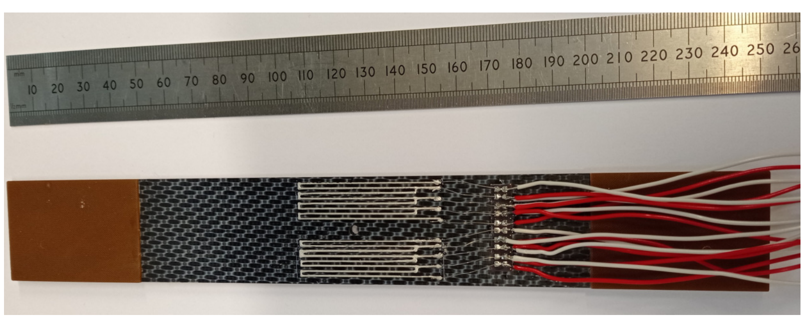

Figure 4.4: Tensile test specimen with a printed strain gauge.

Analyzing all the above, a qualitative material properties profile can be derived:

- High conductivity
- Molding, shaping or printing may be necessary to create different devices for different purposes
- Compatibility with a dielectric
- Elastic behaviour
- Temperature resistance >180 °C

Upon completion of an initial description of the sensing devices itself, the integration into structures and the connection to acquisition apparatus' needs to be considered. Typical methods in use are standard metallic wires and printed circuits that include the wiring up to a terminal [67,116,140]. Given the additional weight of external wiring and associated wire management, integrally wired sensors and wires are strongly desired. Such wires need to be as thin as possible to save weight and be deposited at predefined locations as required. Manual handling of such delicate devices would cause their deterioration. Considering this requirement, additively manufactured sensors and cables become a necessity.

4.3 Experimental demonstration

Whilst some previous works have reported on several aspects of PM either experimentally or theoretically, it was important to demonstrate the most promising technologies in a realistic composite manufacturing environment to assess the maturity and reliability of the monitoring systems. To this end, a range of experiments was conducted and conclusions were drawn from the individual results which are reported in this section.

The chapter first explores the idea of manufacturing tool-based PM. For this purpose a simple flat resin infusion mold is manufactured and instrumented using FOS-FBG and PZT sensors. Several important processing parameters are being evaluated using these technologies.

FOS' multiparameter monitoring capabilities are demonstrated next. Both FOS-FBG and FOS-OBR are used to measure: e.g. the degree of cure, temperature, strain and lateral pressure. The pressure monitoring aspect is demonstrated numerically first and verified in an experiment. Novel results have been achieved in this area of research.

Lastly, electrical sensing methods are explored and demonstrated. Limitations in their manufacturibility have lead to the development of novel 3D-printed flexible devices to which Section 7.1 is dedicated.

4.3.1 Mold-based piezoelectric monitoring

Inspired by the promising results reported by other researchers [10, 30, 87] a mold-based manufacturing monitoring solution has been devised and tested in this research for a resin infusion process. PZT transducers were used to the mold so that PM was possible. They were bonded to the mold such that they would demold along with the component to be manufactured (Figure 4.5). Following this proposed method, at the end of the process one would receive a fully instrumented structure for which a complete manufacturing monitoring dataset is available too. This approach was chosen to represent a precursor study for subsequent industrialization.

The focus on a future industrialization was an important guiding principle for selecting an appropriate sensorization process. PZTs are inherently fragile and present significant challenges around sensor placement and embedding into uncured composites. To protect the transducers, the rigidity and the control of the mold provided was exploited.

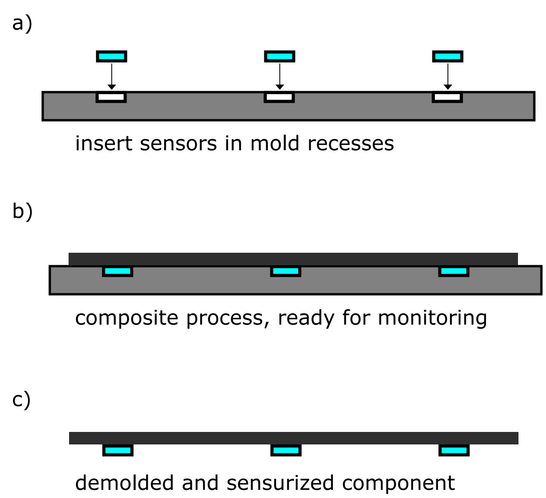

Figure 4.5: "Smart" mold sensorization concept

4.3.1.1 "Smart" mold design

Whenever a mold is designed, several aspects need to be considered. Among others the most important are:

- Complexity of the component to define mold making process
- Molding process (process definition includes materials, temperatures, pressures, etc.)
- Definition of molded faces (which face needs to have good quality finish)
- Component release (how will the component be retrieved from the mold)

These factors drive the decision making process and have a major influence on the component that is going to be made. For the "smart" mold a simple 2D plate was initially aimed at, reducing the complexity and allowing the use of stock materials. As the entire research project evolved around next-generation composite manufacturing processes, a RIFT mold was designed. This decision also means, that only one face can have molded finish as the other was going to be determined by the vacuum bag. At this point, the decision was made to go with a GFRP mold, which is a standard mold-making material in industrial applications given the close resemblance of mechanical and CTE properties to the produced component. This decision also meant easier machining of recesses for the sensors. Finally, the release of the manufactured component was to be accomplished using a non-porous Teflon® film that is bonded to the mold. Again, this is industry best-practise.

4.3.1.2 Manufacturing of the ”smart” mould

A 3 mm thick GFRP plate was cut to size and prepared for the mold making. In a first step, the recesses for the monitoring sensors had to be machined. This was done on a three-axis CNC machine using an end mill. The recesses had to be precise in diameter and depth as the composite component's surface quality depended on the flushness of the sensors to not induce waviness. The sensors were then inserted into the mold and covered with an inkjet printed Kapton (Lohmann Technologies (UK) Ltd, Milton Keynes) film. This film had a printed silver ink circuit on it to allow connection to the sensors. The sensors were connected to the film using silver filled epoxy adhesive (Figure 4.6).

With the mold now completed, several aspects needed to be validated. These results are presented below.

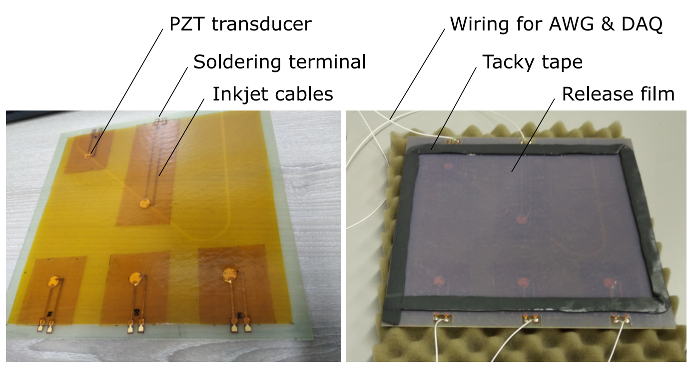

Figure 4.6: ”Smart” mold as built with and without the release film attached to the surface

4.3.1.3 Wave propagation study

The smart mold with installed sensors was first characterised on its own to understand whether all sensors were in good working order and that the wave propagation properties were as expected. A typical feature to assess is to study the time of arrival (ToA) of wave packages in a pitch-catch configuration. For this purpose, a five cycle Hanning-windowed signal at 200 kHz was used (see Figure 3.18). The input signal is created by an arbitrary waveform generator (AWG) and directly supplied to the transducers. The entire actuation and measurement execution was handled by an in-house developed measurement platform, named LASAR [141]. The ToA in pitch-catch is defined as the time a signal travels from the actuated transducer to the sensing transducer. The time is dependent on the material properties of the propagation media and the distance the signal needs to travel [53]. In Figure 4.7 the relationship between ToA and distance travelled is presented. Each data point represents a measurement performed on a sensor pair. In total 10 pairs were evaluated, covering many different directions and distances ranging from 70 mm to 200 mm. The fit-line was forced through the origin. The high degree of linearity is expected and indicates that the material properties are similar in all directions. The results also suggest that signals are able to travel in a radius of 200 mm.

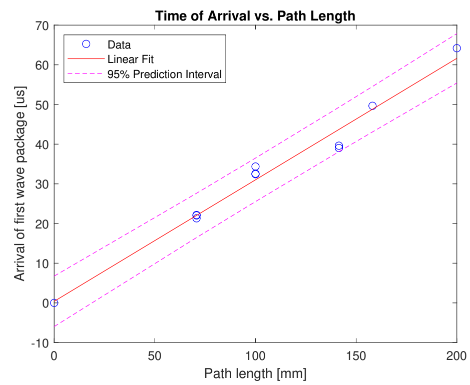

Figure 4.7: "Smart" mold ToA for different transducer pairs confirming linearity

To evaluate the ability of the mold to carry signals over great lengths without a loss of information, a large amplitude is required. A signal's amplitude is measured in volts directly at the receiving transducer. It is expected that the release film dampens the travelling signal and leads to a reduction in amplitude. However, a severe dampening could negatively affect the sensing capabilities of the smart mold. To evaluate this, a five cycle Hanning-windowed signal at 200 kHz was again used in a pitch-catch configuration. Two representative sensor pairs were chosen for a sensitivity analysis to study the impact the non-porous release film has on signal quality.

The two sensor pairs chosen are transducer 1-2 and 1-5 (refer Figure 4.8 (a)) since they are equidistant and any differences can be attributed to the addition of the release film. First a reference state is recorded with only the tacky tape, but no release film. After that, three strips of release film have been added to the mold with increasing length (Figure 4.8 (b)-(d)).

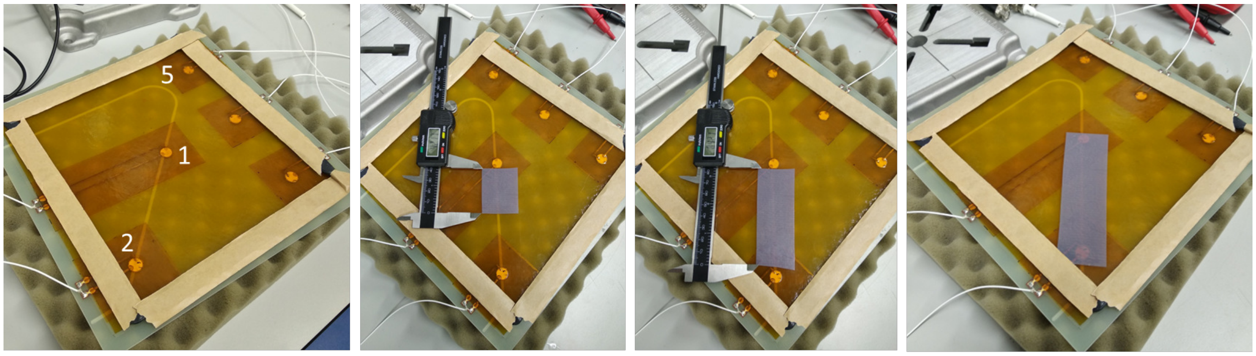

(a) (b) (c) (d)

Figure 4.8: "Smart" mold release film induced dampening study. a) bare mold without any film, b) half of the path is covered c) the entire path length is covered but the transducers ares not d) the entire path including the transducers are covered with release film.

As expected, the waveform on the path 1-2 and 1-5 are relatively similar in amplitude and general appearance (Figure 4.9 (a)). This confirms the suitability of the chosen sensor pair for further investigations. After confirming that, a roughly 40 mm long strip of release film is placed directly on the propagation path between transducer 1 and 2 (see Figure 4.8 (b)). The film caused the signal to be dampened significantly with an amplitude drop of more than 70% (Figure 4.9 (b)). Upon adding even longer strips of release film (Figure 4.8 (c)-(d)) and thereby covering more and more of the direct path between the transducers 1 and 2, the amplitude dropped even further (Figure 4.9 (c)-(d)).

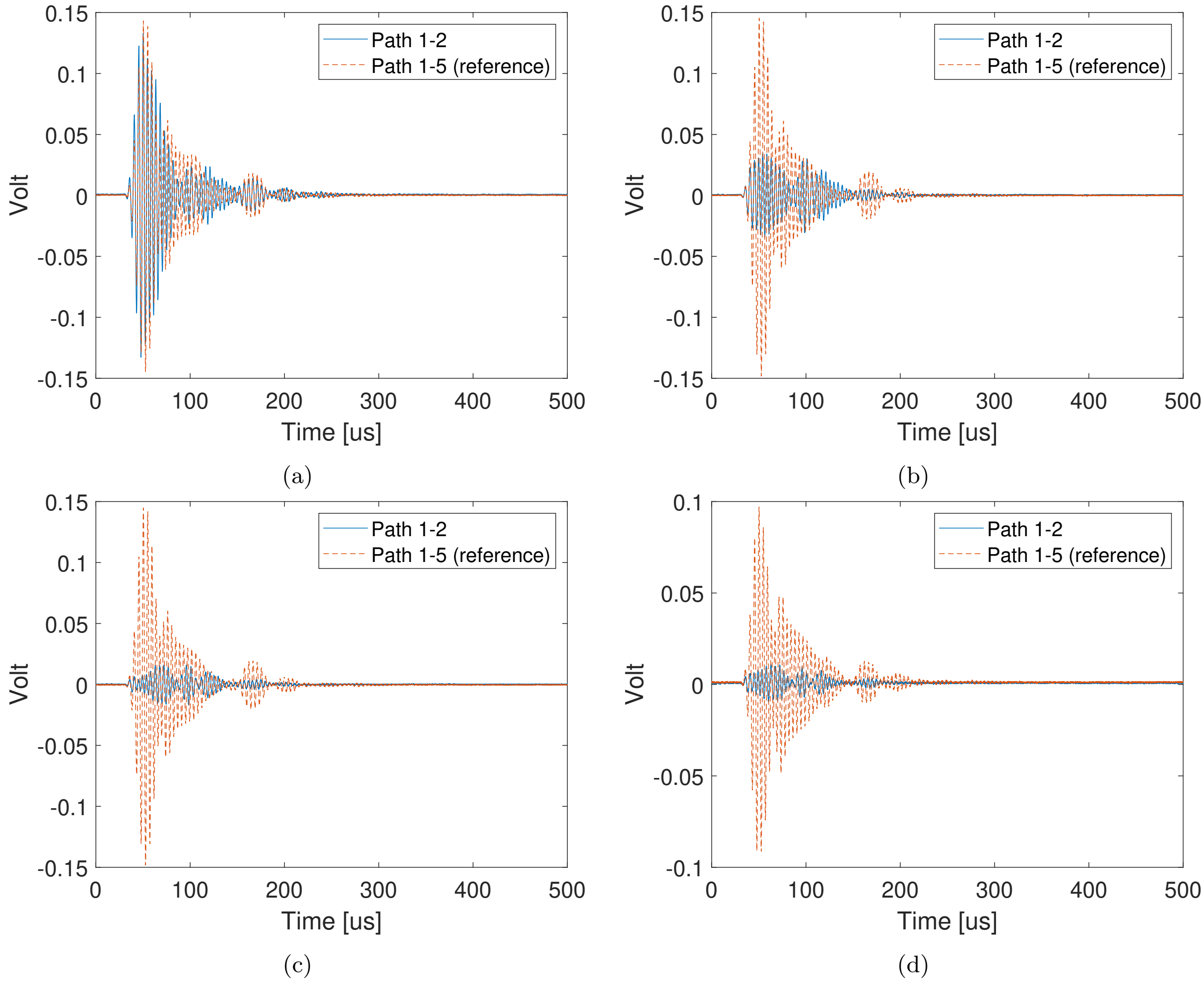

Figure 4.9: Wave propagation study with different levels of release film cover. Ref. Figure 4.8 for the corresponding pictures showing the release film cover. a) bare mold without any film, b) half of the path is covered c) the entire path length is covered but the transducers ares not d) the entire path including the transducers are covered with release film.

When plotting the maximum amplitude against the length of the release film strip, the impact becomes evident. The maximum amplitude drops from just under 0.14 V on the bare mold down to just over 0.01 V (Figure 4.10). This is problematic, as it severely limits the range signals can travel with high enough amplitudes to carry information about the process.

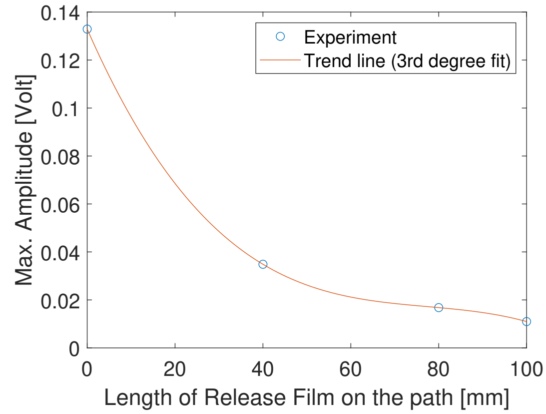

Figure 4.10: "Smart" mold dampening caused by the release film

4.3.1.4 Secondary poling of PZTs

Given the high temperatures that are needed for certain composite manufacturing processes (exceeding 300 °C) the Curie temperature of many piezoelectric materials is reached leading to depoling and finally the loss of its piezoelectric properties. When proposing a holistic entire-life cycle monitoring technique it was necessary to ensure PEs could be poled during or after the process [96] to retain their unique properties (ref. also Figure 2.17). To do this, high electric fields are required and a test apparatus was designed using spring-loaded electrodes in a 3D-printed poling fixture (Figure 4.11).

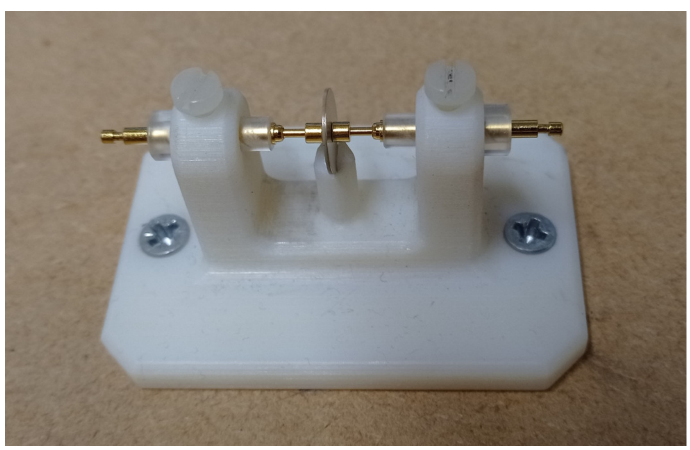

Figure 4.11: Poling fixture

To test the apparatus, a set of PIC255 PZT elements was subjected to 350 °C for extended periods. To test the response to that heat-treatment and to have a comparable metric, EMI measurements were taken before heat-treatment and after. In Figure 4.12 a significant decline in impedance signifies the partial loss of piezoelectric properties after the Curie temperature was surpassed and depoling occurred. In a second step the depoled elements were taken and placed inside the poling fixture ready for the application of an electric field. A high voltage power source (LT series, Glassman High Voltage Inc.) was used for the poling process. A field of 1.5 to 2 MV/m was applied to the electrodes, ensuring to stay below the breakdown strength of air which is around 3 MV/m. This is important as otherwise the two electrodes would create a spark due to the break down of the surrounding air. The voltage to apply can easily be calculated by multiplying the field strength by the distance between the two electrodes. For a 0.5 mm thick wafer, at a field strength of 2 MV/m requires 1 kV. Figure 4.12 shows that the poling was successful since the EMI response (measured on an Impedance Analyzer E4990A, Keysight) after poling is producing similar or higher impedance response than before depoling.

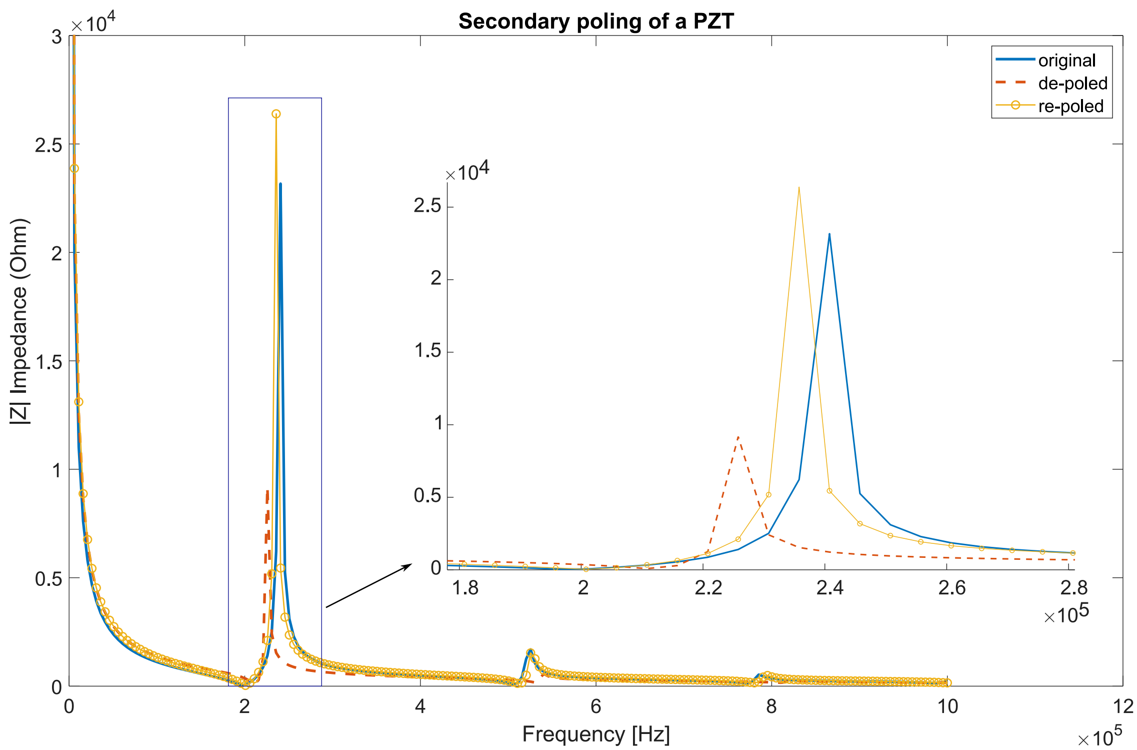

Figure 4.12: Electromechanical impedance measurement confirming successful secondary poling

4.3.1.5 Liquid detection with PZTs

Another important aspect that could be proven to work well when it comes to PM using PZTs was their sensitivity to being covered by a liquid. This leads to a decrease in impedance during EMI measurements. Figure 4.13 shows the response of a PZT element in air and then immersed in water. The impedance at the first resonance frequency is lowered by one order of magnitude and can therefore be taken as a reliable indicator for the presence of liquid. This is useful when considering liquid resin infusion processes during which the void space between individual fibers is replaced by the resin. A sensing element able to differentiate those two states thereby is able to inform the flow front position as it passes the element.

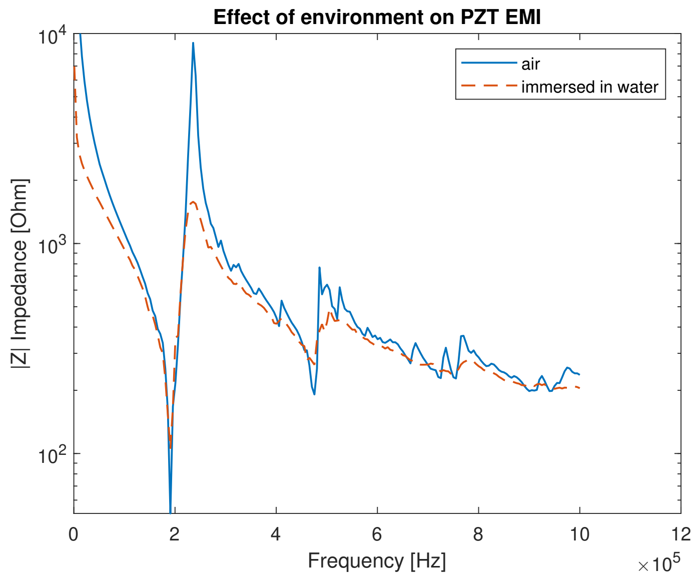

Figure 4.13: Effect of different media on EMI measured by a PZT

4.3.1.6 "Smart" mold conclusion

Despite encouraging initial results, the "smart" mold concept was scrapped due to significant limitations in wave propagation. This was mainly caused by the non-porous release film used to cover the mold. Secondly, the difficult installation procedure of PZTs along with their brittleness rendered them not suitable for such an application. Finally, the surface quality that can be expected from such a solution was likely to be not satisfactory for manufacturers. Therefore, the concept of a "smart" mold was abandoned at this stage of the project. However, the deeper understanding for individual components of the setup aided in the technology down-selection process.

4.3.2 Novel piezoelectric sensor architectures

Since one of the major limitations with ceramic PEs is their extreme brittleness, the search for alternative materials lead to polymeric PEs. This section reports on experiments carried out manufacturing such polymeric PE transducers.

4.3.2.1 Printed piezoelectric-polymer sensors

Polyvinylidene fluoride (PVDF) is a polymer with piezoelectric properties. Its mechanical properties are much more favourable when it comes to brittleness and conformability, however, the piezoelectric field strength is significantly lower than that of ceramic piezoelectric material. In this work, it was tried to utilize printing techniques to create customized piezoelectric sensing devices (ref. section 2.2.3).

Printing of P(VDF-TrFE) short for poly(vinylidene fluoride-co-trifluoroethylene) requires the polymer to be dissolved in a solvent. The solvent used was cyclopentanone (Sigma-Aldrich) and the polymer powder was a P(VDF-TrFE) with a 25% TrFE content by Piezotech®. Dissolution of 25w% polymer powder in the solvent was achieved by suspending an airtight container filled with solvent and the powder in a water bath. The water temperature was controlled at 65 °C by a thermostat connected to the hot plate and a magnetic stirrer bar ensured the water mixes well and has a constant temperature throughout. Another magnetic stirrer bar was put inside the container with the solvent and powder to ensure efficient mixing and a quick dissolution (Figure 4.14).

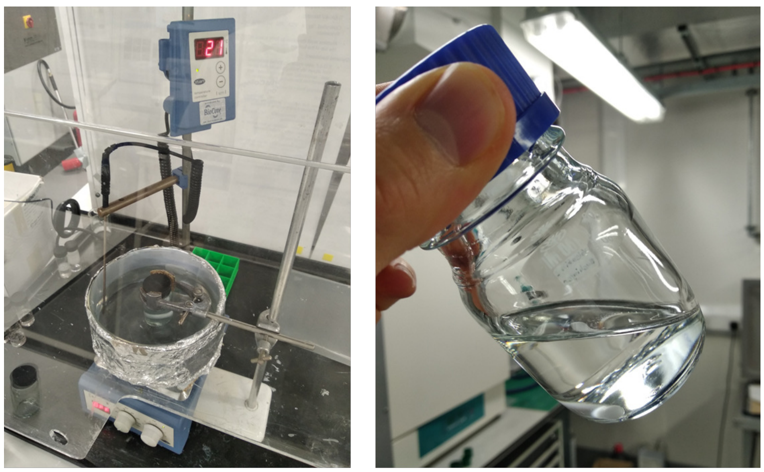

(a) (b)

Figure 4.14: Making of a printable P(VDF-TrFE) ink (a) dissolution setup with hot-plate and water bath , (b) the completed ink with the magnetic stirrer bar visible inside the bottle.

When planning for the printing, two methods were considered: 1) Inkjet printing on a FUJIFILM Dimatix Materials Printer and 2) screen printing using custom made screens.

Given the tight viscosity requirements of the FUJIFILM Dimatix Materials Printer of 10-12 mPas [142] and the lack of control on that parameter during the chosen ink-making process, the inkjet printing was not explored further at this stage. However, an improved process with tighter control on the viscosity could open a new route for manufacturing specialized piezoelectric devices.

Realizing the limitation posed by available ink-making equipment and the target application, a low-tech approach to screen printing was demonstrated on an IDE. For that, a set of IDEs was cut from copper tape and placed onto a glass plate for better handling and insulation. Using adhesive tape a screen was created around the IDEs to enable the use of a knife edge for spreading the ink equally across the surface of the IDE (Figure 4.15).

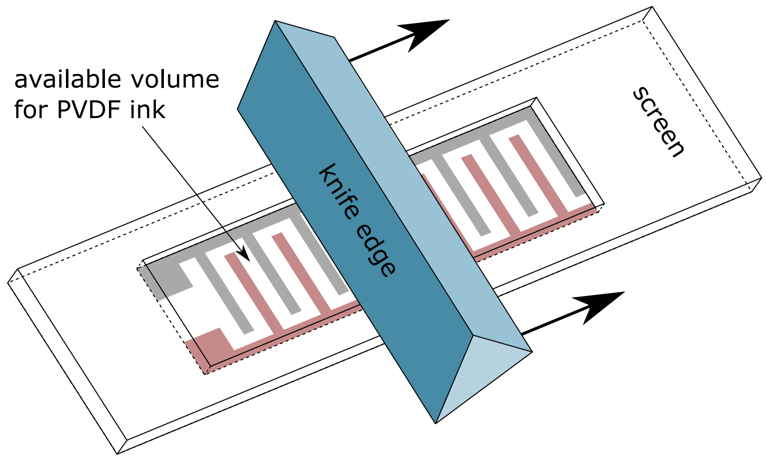

Figure 4.15: Screenprinting of P(VDF-TrFE) onto an IDE.

Once the cyclopentanone in the ink had evaporated, the device was annealed at 140 °C for 60 minutes. The annealed polymer does not yet possess piezoelectric properties. In order to obtain them, the material needs to be poled by applying a strong electrical field. Here the unique benefit of the IDE design becomes evident. As discussed earlier, the piezoelectric field strength is significantly lower than that of piezoceramics. In most cases piezoelectric devices are poled through thickness (direction 3, see Section 4.3.1.4). To utilize them as transducers, however, they are usually bonded to a host structure such that in-plane perturbations are exploited (direction 1 and 2). Most piezos exhibit a lower coupling in this configuration (coupling parameters , d_{13} and d_{23} are lower than d_{33}, see section 2.2.3.2). It would therefore be beneficial to have a poling technique that yields in-plane poling. An IDE can deliver such capability since its IDEs enforce an in-plane electrical field (Figure 4.16).

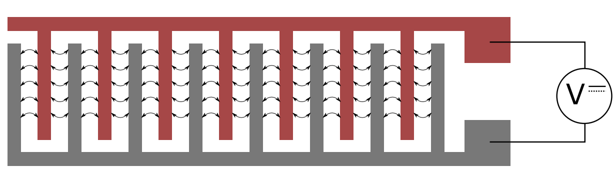

Figure 4.16: Poling of PVDF through an IDE.

For successful poling an electric field of more than 50 MV/m is required [59]. This is significantly above the break-down strength of air, which is around 3 MV/m [143]. This means that in order not to cause such a break-down, the opposing electrodes cannot be exposed to air and need to be covered completely by the P(VDF-TrFE)-ink. This proved to be difficult using this simplistic screen printing method. During poling trials, repeatedly sparks were observed near the break-down strength of air originating from the edges of IDE-fingers (Figure 4.17) indicating incomplete coverage. Upon closer inspection of the IDE's coating, it became evident that the ink forms a convex drop adhering to the electrode and having sufficient thickness but fading out towards the edges. It is at those edges where the sparks form and then lead to the breakdown of the surrounding air (Figure 4.17). The author would like to draw the reader's attention to a similar work [144] where IDEs made from PVDF have been successfully demonstrated concurrently to the author's work. This research direction was abandoned at this stage.

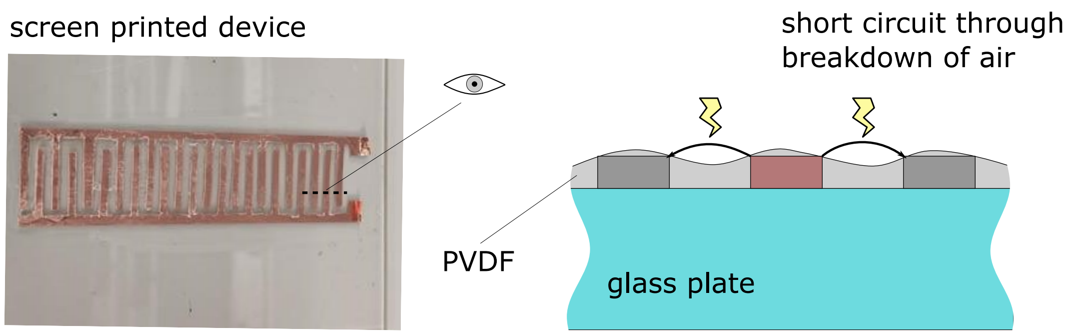

Figure 4.17: Short circuit occurring during poling of P(VDF-TrFE) due to breakdown of air.

4.3.2.2 Etched metallized PVDF sensors

Laser micromachining (etching) of metallized PVDF was also considered as a potentially viable manufacturing route for flexible piezoelectric sensing devices (Figure 4.18). This machining technology offers a high degree of precision and highly customized devices are possible. Metallized PVDF on the other hand, can be purchased off the shelf and is produced in relatively large quantities. For this purpose, screen-printed PVDF sheets (PolyK Technologies LLC, PA USA) with a sintered silver-electrode thickness of 12 µm were etched using an Oxford Lasers Micromachining equipment.

First, a simple IDE pattern was designed using a CAD software and a machining program created using the AlphaCAM software package. A test-run using regular printing paper was performed to confirm the setup. A slighly hihger degree of burn in areas where individual machining paths started or ended was noticed. The default program, without a lead-in was expected to cause more burn as the energy input at the starts and ends of a path was higher than during normal feed. To counteract this, a different machining strategy with arc lead-in was prototyped on paper (Figure 4.18 (b)). This ensured that the laser beam would already be moving when entering the IDE. When creating the prototype shown in Figure 4.18 (b) the laser power was set to full power also when performing the lead-in in order to make it visible. This would not be the case when actually machining the IDE. During lead-in only 10% of peak power was be applied.

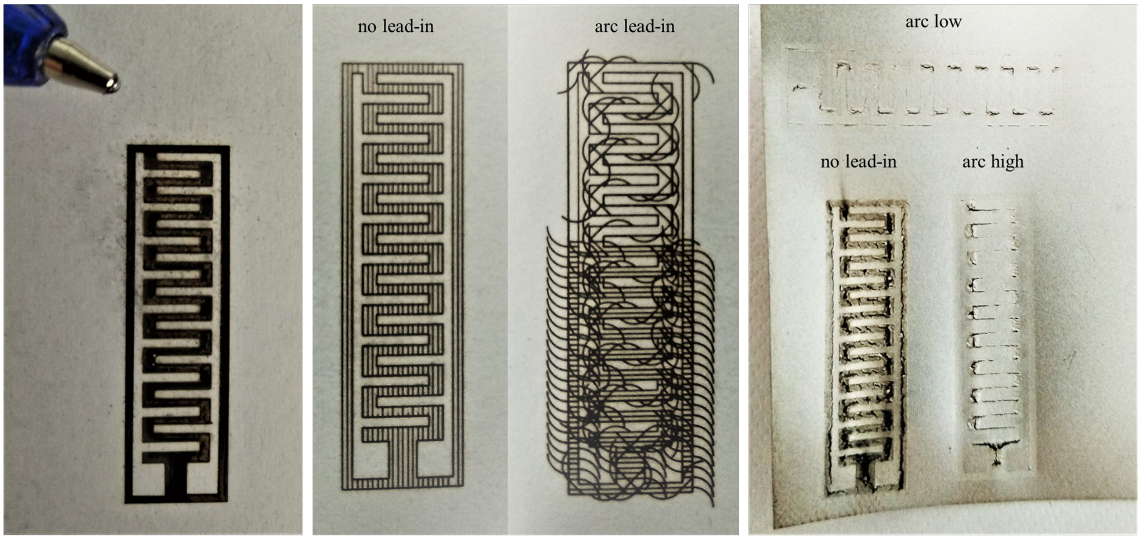

(a) (b) (c)

Figure 4.18: Laser micromachining results (a) desired outcome - machining of paper, (b) comparison of two machining strategies, (c) machining outcomes of the two strategies on silverized PVDF sheet.

After prototyping the machining strategies on paper, the two concepts were tested on the metallized PVDF sheet. A first observation was that the energy levels used on paper did not work on the silver. After increasing the energy levels a degree of coloring was observed and this setting was used to actually machine the IDEs.

Figure 4.18 (c) shows the outcomes of machining. Several observations can be made. Firstly, the sheet bends excessively due to a large temperature difference between the top and the bottom electrode. Secondly, not using a lead-in causes major burns on the starts and stops of the laser. However, even when using the arc lead-in the power distribution over the surface of the IDE still appears inconsistent. Finally, a reduced power setting was used. Whilst the level of burn is lower, the distribution around laser starts and stops is still prevalent.

In private discussions with Dr Shihai Zhang at PolyK, it was confirmed that PVDF with an electrode thickness in excess of a few ten nanometers cannot be reliably etched using lasers and this direction was abandoned.

4.3.3 FOS based monitoring

In literature (see chapter 2) FOS have been used to monitor a multitude of crucial composite processing parameters. This section reports on the experiments carried out as part of this PhD research with the mission to identify a suitable method for industrialized application.

4.3.3.1 Fresnel cure monitoring

Any polymeric resin undergoes significant changes throughout a composite manufacturing process. Thermoplastic resins typically pass their Tg (unless glass transition occurs below room temperature), melt, crystallize (if semi-crystalline) and freeze again (Figure 4.19) upon completion of the molding process. Thermosets, in uncured condition, typically drop in viscosity upon mixing. They then gel, vitrify, fully cure and finally pass below their Tg before cooling down to room temperature [145]. With these different morphologies come changes in the mechanical and optical properties of the polymeric material [16, 98, 100–102].

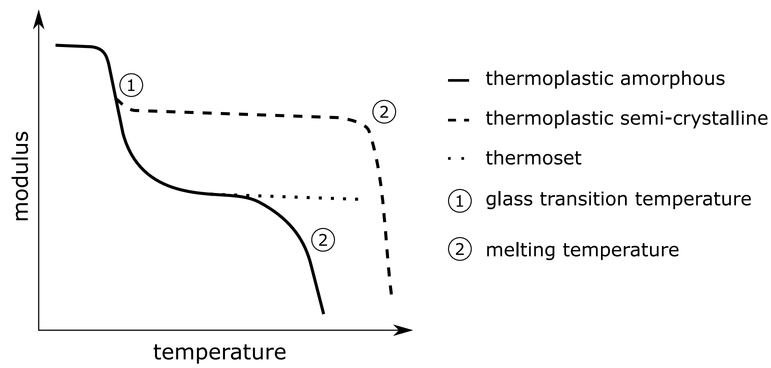

Figure 4.19: Schematic representation of modulus changes experienced by polymers upon heating

When exposing a non-terminated end of an optical fiber cable (the fiber has only been cleaved, without splicing-on a termination fiber or a connector) to a polymer, the light experiences Fresnel-reflection at the interface between the fiber's glass core and polymer. The level of reflection is dependent on the refractive index difference between the fiber core and the polymer. This refractive index changes as the polymer undergoes morphology changes whereas the one of the glass remains unchanged [131]. Therefore, any change in the reflective response of the fiber end comes from the polymer and a sensing element is formed. Fresnel measurements were performed using a setup consisting of a tunable laser source (TSL-710, SANTEC CORPORATION), circulator (6015-3-APC, Thorlabs) and photodetector (APD130C/M, Thorlabs) controlled by a custom National Instruments™ LabView program.

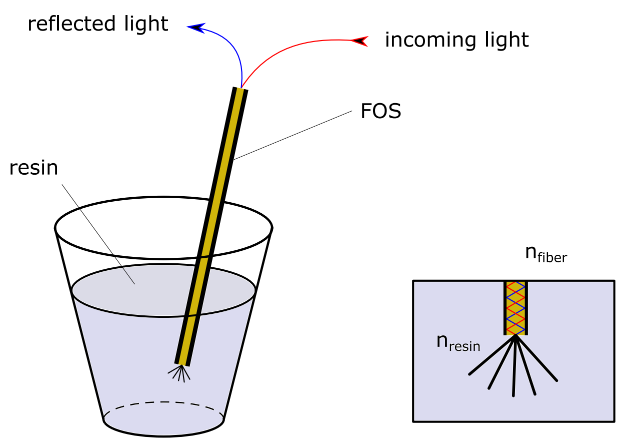

Figure 4.20: Experimental setup for cure monitoring by evaluating the changes in Fresnel reflections occurring at the fiber/resin interface

In Figure 4.21 the response over time at the non-terminated optical fiber cable is plotted. After mixing of a small batch of PRIME® 20LV infusion epoxy resin by Gurit and commence of curing a significant drop in the reflected power is observed. This drop corresponds to the state of low viscosity discussed earlier. After the curing reaction continues a sharp rise in reflective power is observed followed by a plateau. The plateau indicates the completion of the curing reaction. The obtained results agree very well with previously published data [16].

In order to implement such a system successfully, it is important to ensure that any changes picked up originate from the curing reaction only. This can be achieved by using a reference measurement arm as described by Dell'Anno et al. [16]. They report that having an unterminated fiber end, exposed only to air allows to correct for changes in the light intensity at the laser source and for losses.

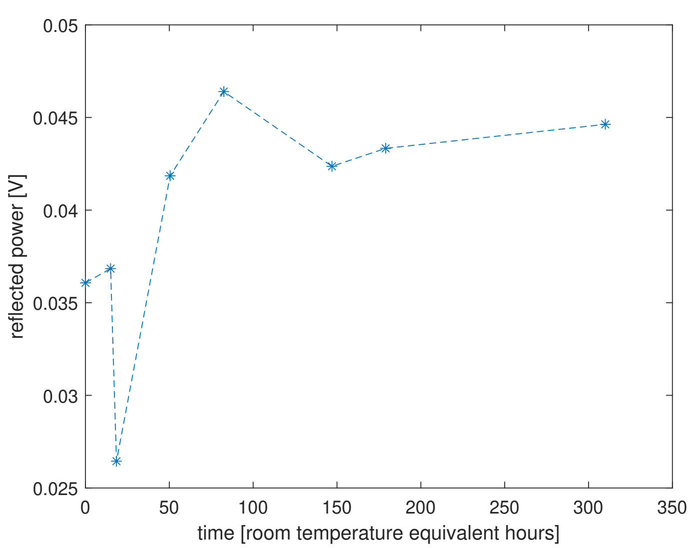

Figure 4.21: Cure monitoring using Fresnel reflections at the embedded fiber end

4.3.3.2 Temperature measurement with FBGs

FBGs are highly sensitive to changes in the physical distance of the Bragg gratings within the fiber [44, 146–148]. As such, they are ideally suited as strain sensors. Another use case is measuring temperatures by computing thermal strains. There are two ways a FBG can be used to measure temperature, either free or bonded. In the free condition the fiber is immersed in the environment that it monitors and no other strains act onto the fiber. Whereas in the bonded condition, the fiber is fixed to or embedded into a component. The main strain components originate from the surrounding material as it restricts or enforces strains onto the fiber.

To calculate a temperature from strain the relevant CTE of the fiber or the material that the fiber is bonded to needs to be known or established [109, 147]. When fibers are firmly connected to a host structure for temperature monitoring, it is important to consider that the fiber's grating is affected both by thermal as well as mechanical factors. Being able to differentiate these sources of wavelength shift is an active research field with several solutions offered: 1) isolating the FBG from mechanical strains by encapsulating it [149], 2) clever exploitation of unique properties of FBGs (spectral hole shift or peak reflectivity) [107] and 3) methods of source separation [150–152].

To demonstrate the temperature monitoring capability of FBGs in a realistic use case, a set of experiments was carried out using FBGs in both free and bonded condition which were then exposed to elevated temperatures. Figure 4.22 shows a spectrum of a typical FOS with three FBGs written onto it. They are at 1530, 1540 and 1550 nm respectively and characterised by a distinct and large peak which makes identification easy. All FBG measurements were performed using a setup consisting of a tunable laser source (TSL-710, SANTEC CORPORATION), circulator (6015-3-APC, Thorlabs) and photodetector (APD130C/M, Thorlabs) controlled by a custom National Instruments™ LabView program.

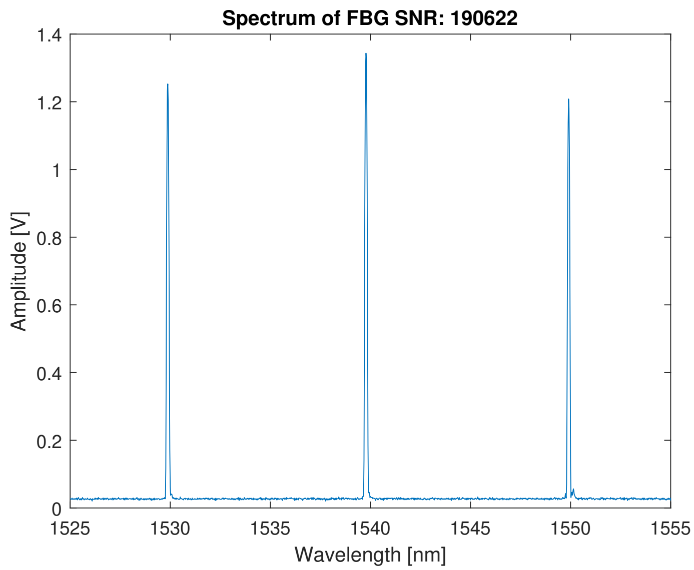

Figure 4.22: A spectrum of a typical FBG sensor with Bragg gratings at 1530, 1540 and 1550 nm respectively

A temperature measurement is enabled by tracking the position of the peak over time. Since the CTE for the material was not known at this point, a separate independent temperature measurement was required for calibration. A K-type TC placed right next to the FBG was used for this purpose (Figure 4.23). The temperature gradient necessary to perform the measurements was created by a hot air gun (Bosch GHG 660 LCD). Overlaying the TC and FBG measurements for both the free condition (Figure 4.24) and bonded condition (Figure 4.25) reveals the close agreement between measurements obtained by the TC and the FBG.

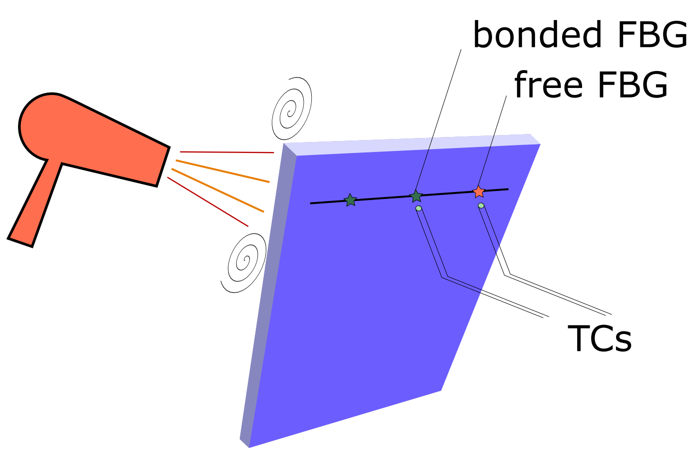

Figure 4.23: Experimental setup used to monitor the temperature of a plate using FBGs

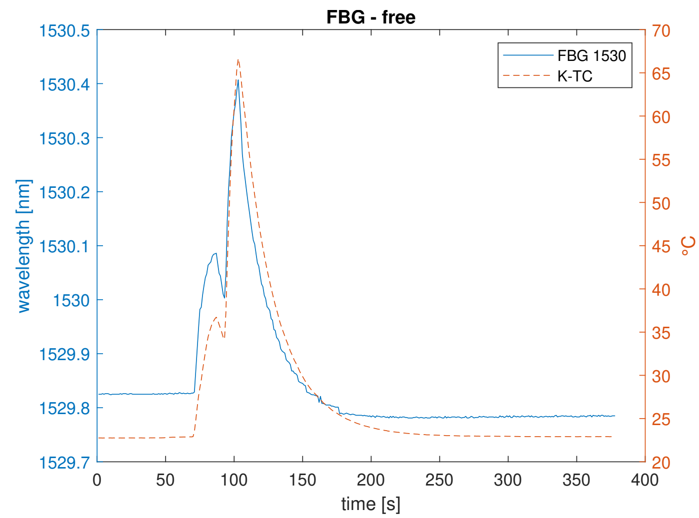

Figure 4.24: Free FBG sensor with Bragg gratings at 1530 nm being exposed to a transient temperature

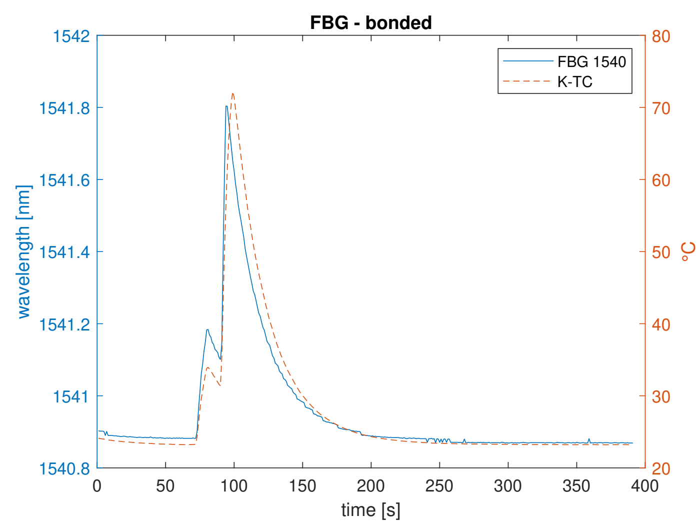

Figure 4.25: Bonded FBG sensor with Bragg gratings at 1540 nm being exposed to a transient temperature

Having both the actual temperature at the monitoring location as well as the wavelength shift now allows the plotting of calibration curves (Figure 4.26 and Figure 4.27). Two facts are noteworthy: 1) there is a distinct difference in slope between heating and cooling for both configurations tested and 2) the slopes differ between the free condition and the bonded condition as expected.

Predicting temperature sensitivities derived from Equation 2.3 and Equation 2.4 for a central wavelength of 1530 nm, yields:

- For the free condition: $1.02 \times 10^{-2}\ \frac{nm}{^{\circ}C}$.
- For the bonded condition: $2.91 \times 10^{-2}\ \frac{nm}{^{\circ}C}$, whereas for the GFRP the following is considered: CTE for E-Glass fiber: $5.25\ \frac{ppm}{^{\circ}C}$, CTE for Epoxy: $40\ \frac{ppm}{^{\circ}C}$, a fiber volume fraction of 0.45 and simple rule of

mixtures is used to calculate the composite CTE.

When comparing the empirically obtained temperature sensitivities (Figure 4.26 and Figure 4.27) with the predicted ones, good overall agreement can be noted with uncertainties related to unknown material properties and necessary simplifications.

The difference in slope for heating and cooling can be explained by considering the forced heating and natural cooling caused by the hot air gun. This leads to a temperature gradient within the panel (see Figure 4.28) where the face with direct air flow is hotter than the opposing side where the measurement was taken (ref. Figure 4.23). Upon stopping the forced heating, the panel's temperature stabilizes and begins to drop naturally and equally from both exposed sides by dissipation leading to a much more linear temperature versus wavelength shift relationship. This is also similar to the trends observed in section 3.4 and reported in previous works [147,148], albeit it is more pronounced in the current work. Such limitation could potentially be overcome in future work by changing the experimental design. Using a more reproducible heat source is recommended (e.g. an oven rather than a heat gun) along with allowing the panel to soak at the temperature of interest for a defined time before a measurement is performed as compared to taking transient measurements.

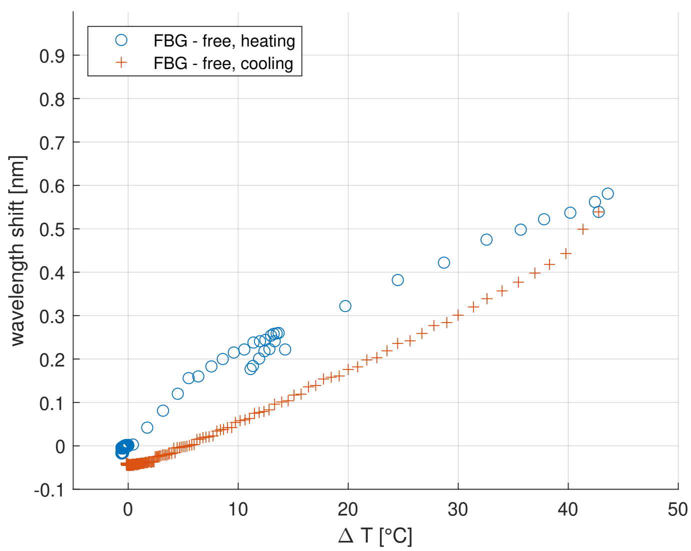

Figure 4.26: Free FBG sensor with Bragg gratings at 1530 nm being exposed to a transient temperature

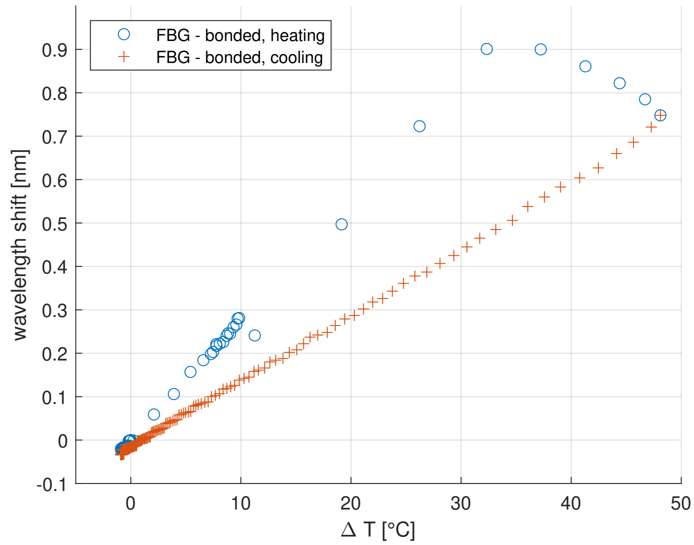

Figure 4.27: Bonded FBG sensor with Bragg gratings at 1540 nm being exposed to a transient temperature

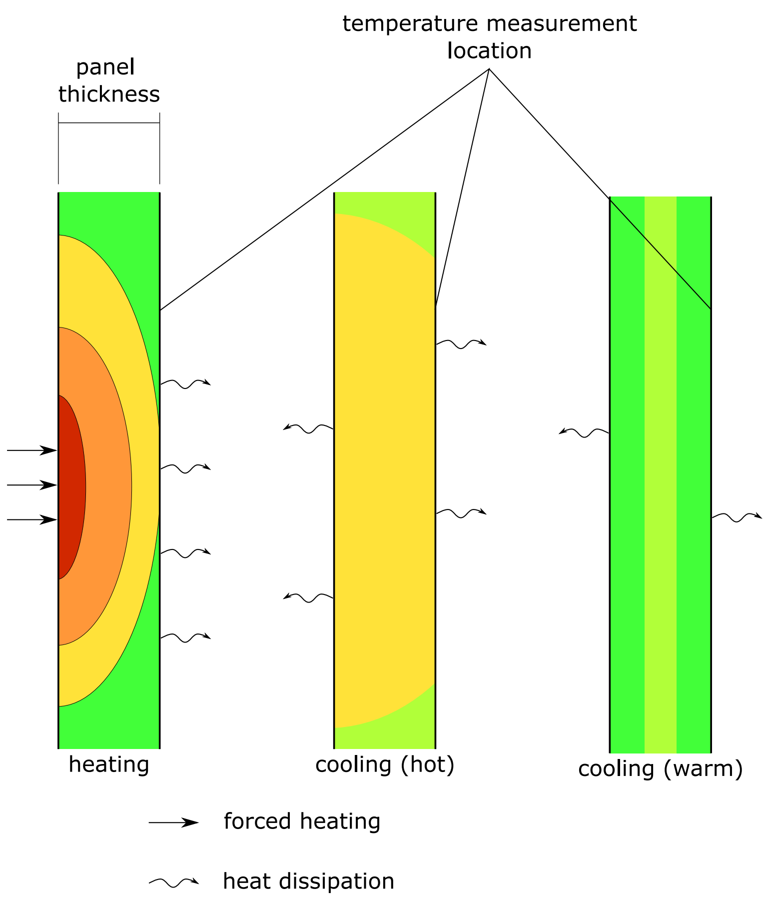

Figure 4.28: Schematic temperature gradient within a panel subjected to forced heating followed by natural cooling.

4.3.3.3 Distributed FOS temperature measurement

Similar to FBGs (ref. section 4.3.3.2) distributed FOS are highly sensitive to physical changes to the fiber in the form of mechanical strain and/or temperature. To demonstrate the temperature monitoring capability of a structure instrumented with a distributed FOS an experimental setup was created using a thermal camera (Teledyne FLIR, USA) and a programmable flash light (C-CheckIr, IrNDT USA) heat source (Figure 4.29). The heat source is used to create a transient temperature field on the structure. This field is evaluated using the thermal camera whilst also capturing measurement data from the embedded distributed FOS (performed with ODiSI B by Luna Inc., Blacksburg, VA, United States). All data processing is performed in MATLAB®.

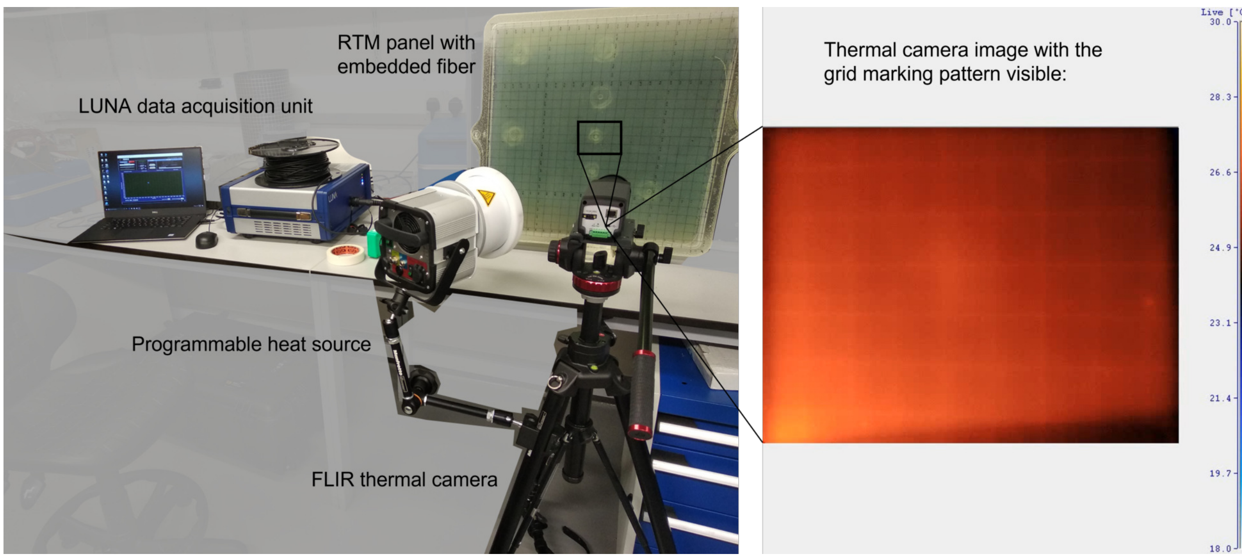

Figure 4.29: Temperature monitoring of a plate-like structure using distributed FOS and verified with a thermography excitation and evaluation method.

Plotting the obtained frequency shift from the distributed FOS data against the temperature measured by the thermal camera, reveals a linear relationship (Figure 4.30). The plotted experimental data is a local average over the measurement window of the thermal camera. This window is roughly 160x140 mm. Such a linear correlation is expected and can be quantified at 1.9781 GHz/°C. This correlation highlights the ability of the distributed FOS to monitor the temperature of structures during manufacturing or in-service.

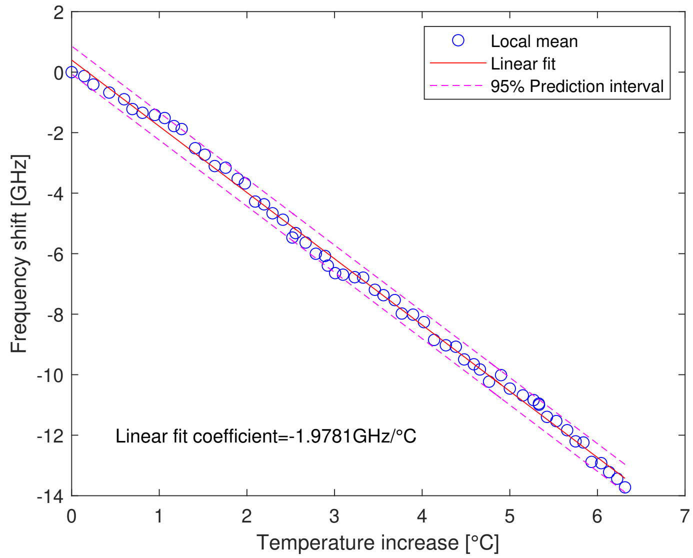

Figure 4.30: Temperature measurements by embedded distributed FOS (OBR)

4.3.3.4 Distributed FOS vacuum pressure measurement

This section is widely based on the publication by Buchinger and Sharif-Khodaei [153].

With pressure, or the lack of, being responsible for many of the typical composite manufacturing flaws mentioned in section 2.1.3 a successful manufacturing monitoring system needs to also be able to deliver reliable pressure measurements. The current state of the art is to capture this parameter at a system level (centralized vacuum line/pump) and within a vacuum bag. Such a monitoring approach delivers measurements only at those discrete locations with no information for the actual component being manufactured. However, when setting up a new process or when troubleshooting rejects, it is highly desirable to have such information available at a high spatial resolution. Using a distributed measurement device such as a FOS-OBR, paired with a sensor layout to suit the component in question, allows one to capture readings across the entire surface.

The chosen setup focuses specifically on the aspect of vacuum pressure monitoring. An ODiSI B Interrogator (by Luna Inc., Blacksburg, VA, United States) is employed to obtain the Rayleigh backscattering signature of a High Definition Sensor with a length of two meters (by Luna Inc., Blacksburg, VA, United States, model type: HDS02LC220P) for this study. The sensor was embedded beneath four layers of four-harness satin woven glass fiber onto an aluminum plate. A vacuum pump was connected to a resin catch pot with a vacuum gauge, which in turn was fed through the vacuum bag and thus applying vacuum to the panel (Figure 4.31). A resin inlet was included for completeness (lower left corner) but was sealed off during the experiment to retain the system vacuum.

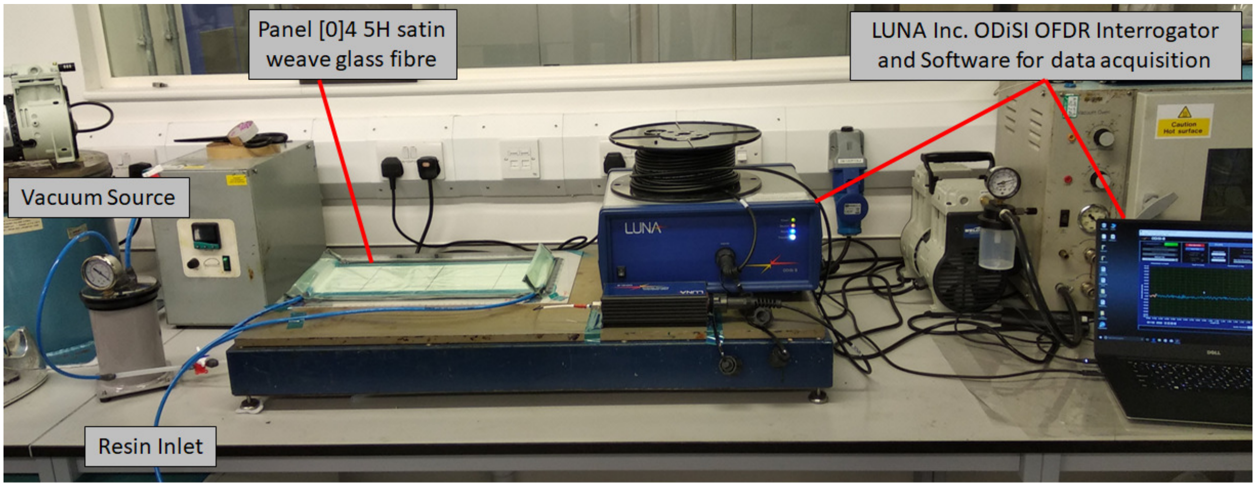

Figure 4.31: Vacuum pressure monitoring setup simulated for the RIFT process.
Reprinted by permission from Springer Nature: Springer Nature, European Workshop on Structural Health Monitoring. EWSHM 2022. Lecture Notes in Civil Engineering, vol 253. Springer by Rizzo, P., Milazzo, A. (eds) ©2023

The sensor was taped onto the mold in a serpentine shape leading to five distinct segments oriented along the length of the panel (Figure 4.32). It shall be noted that the fiber was only taped down in the bend regions but was free and only slightly pre-strained in the straight sensing portion. The sensor was configured in the LUNA software package to a gauge length of 2.6 mm yielding 600 discrete gauges distributed on the panel. Sensor mapping was performed to remove the curved segments from the logging file as the readings in those segments would skew the results. Such mapping is achieved by touching the fiber at the locations between which the segment of interest lies. Touching the fiber leads to clearly identifiable peak which is detected and stored in the interrogation software.

A vacuum bag was constructed around the panel which was ensured to be leak-proof before running the experiment. The processed data logging function provided by the LUNA ODiSI B software package was used to record a frequency shift reading every 0.1 seconds over the entire time of the experiment. All data post-processing was performed in MATLAB®.

To demonstrate the ability of the chosen monitoring system to inform the vacuum level and to detect possible detrimental conditions, the routine defined in Table 4.1 has been designed. It contains typical vacuum application and venting ramps as well as a pump failure and a bag leak.

Table 4.1: Representative vacuum application cycle with detrimental conditions simulated.

Activity	**Section ID**
Initiate full vacuum application	(I) to (II)
Pump failure/interruption (vacuum retained in bag)	(II)
Commence full vacuum application	(III) to (IV)
Bag leakage (vacuum level in the bag dropping)	(V) to (VI)
Recovery to full vacuum	(VII) to (VIII)
Venting of bag (vacuum drops to ambient pressure)	(IX)

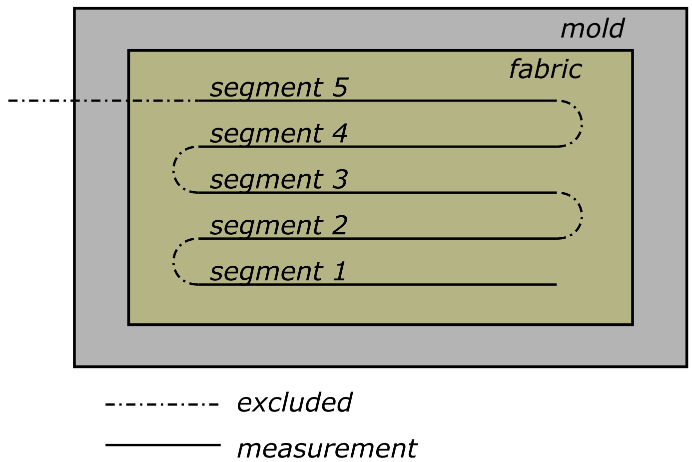

Figure 4.32: FOS-OBR layout on the rectangular RIFT plate.

Overlaying the frequency shift readings obtained by the FOS-OBR system with the vacuum pressure in the bag on a time-series plot (Figure 4.33), it can be seen that they follow very similar trajectories. Both the overall shape and relative magnitudes agree well. The raw data was denoised for plotting by averaging over ten consecutive samples. Also the data presented is only of the centermost individual gauge (fiber section 3, at half length).

Initially, even though the pressure linearly rises, the frequency shift remains relatively unchanged until at (I) a sudden rise occurs, incidentally coinciding with the simulated pump failure. As the pressure remains constant during the 25 s (Section (II) through (III)) of pump outage, so does the frequency shift measurement. After commencing vacuum application, the frequency shift rises along with the pressure until both reach a plateau at around (IV). The simulated bag leak, occurring at (V), is marked by a stark drop in pressure and frequency shift before reaching another brief plateau as the leak is closed (Section (VI) through (VII)). After that, it can again be observed that a subsequent rise (VIII), holding phase and drop (IX) are clearly indicated by corresponding frequency shift readings.

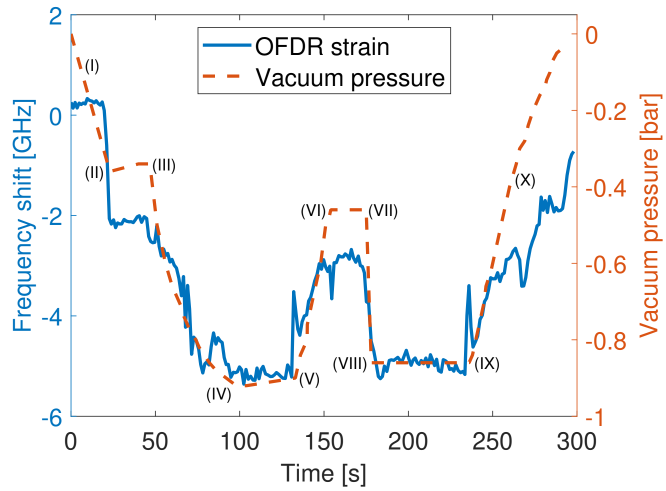

Figure 4.33: FOS-OBR readings of the centermost individual gauge overlaid with the pressure readings from a vacuum gauge [153].

Upon further inspection, there appears to be a tendency that at the onset of changes in vacuum levels, short periods of erratic readings with both positive peaks (leak stabilization at (VI), reaching full pressurization at (VIII) and towards the end of bag venting at (X)) and negative peaks (reaching full pressurization at (III), leak initiation at (V) and ventilation at (IX)) can be observed. The cause for these peaks lies in the large dynamic excursions, leading to uncertainties within the ODiSI-B's peak-matching algorithm. However, they do not affect the excellent event detection capability that was observed during the entire experiment as they were of short duration and the readings returned to the baseline immediately after.

Given the success in tracking different vacuum levels based on operation modes, a directly attributable relationship between pressure and frequency shift was hypothesized. To test such a relationship the frequency shift and pressure data were resampled. In addition, the plateau regions were removed as they would have added weight in those regions and affected the fit. Plotting pressure as a dependent variable over the frequency shift measured (Figure 4.34) confirmed that indeed there is a linear relationship.

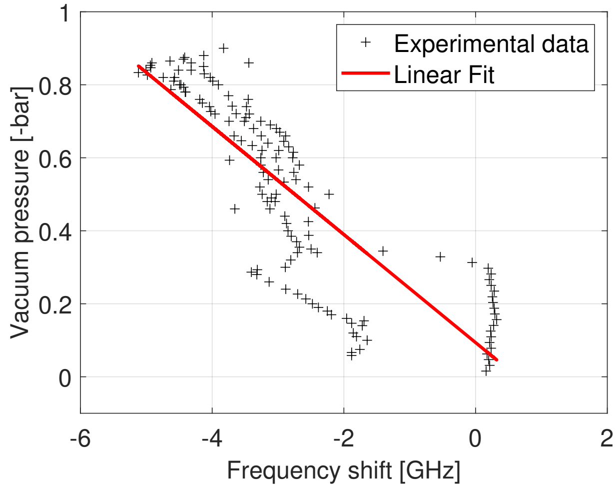

Figure 4.34: FOS-OBR readings vs. pressure linear model. The linear model applies for vacuum pressures below -0.3 bar.

Reprinted by permission from Springer Nature: Springer Nature, European Workshop on Structural Health Monitoring. EWSHM 2022. Lecture Notes in Civil Engineering, vol 253. Springer by Rizzo, P., Milazzo, A. (eds) ©2023

As noted earlier, there is a region below -0.3 bar where the experimental values diverge from the linear fit to both sides. In this region, depending on whether there is a positive or negative pressure gradient, readings seem to lag for some time, until a sudden change occurs. This behavior is more prominent for the loading than it is for the unloading phase and hence is responsible for a slight origin-offset towards a negative intercept on the frequency shift axis.

Overall, the results obtained by this method are encouraging. Beyond the capability to relate observed frequency shift to bag vacuum levels, both a pump failure and a ruptured vacuum bag were successfully detected by the system.This observation leads to the general description of the working principle of vacuum pressure measurements using a FOS-OBR under a reinforcement stack as pictured in Figure 4.35 which will be explore further in chapter 5.

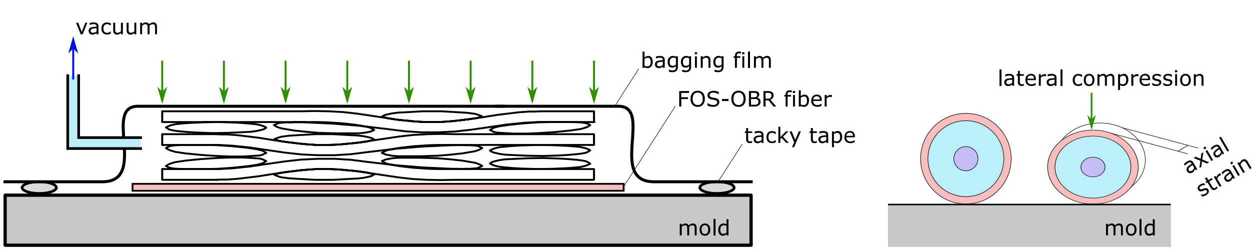

Figure 4.35: Hypothesized physical principle for pressure sensitivity of a FOS-OBR.

4.3.3.5 Distributed FOS sensor manufacturing

For the purpose of manufacturing monitoring, the FOS needs to fit the component and manufacturing process to be monitored. The OEM's FOS only come in specific lengths and with connectors already installed. When integrating fibers into composite components and in order to ensure they are able to survive the manufacturing conditions, it may be necessary to use the FOS without connectors or with speciality connectors. This meant that a manufacturing method for custom sensors to the specific requirements needed to be developed. This preliminary task started by selecting a suitable fiber. FOS-OBR sensors for embedding need to fulfill a certain set of characteristics in order to be used for composite monitoring. All parts of the fiber need to be selected such that they match the use case. In order to sustain elevated temperatures, the coating needs to be polyimide.

The fiber itself needs to be relatively insensitive to microbending. This is because the pressure acting on the sensor during manufacture can be significant and in addition, the weave structure of the reinforcement adds waviness (Figure 4.36). These factors should not lead to a loss of signal. Losses are incurred due to light leaking from the core through the cladding due to localised microbending. Specialist optical fibers are commercially available which have reduced microbending losses and are therefore ideal candidates.

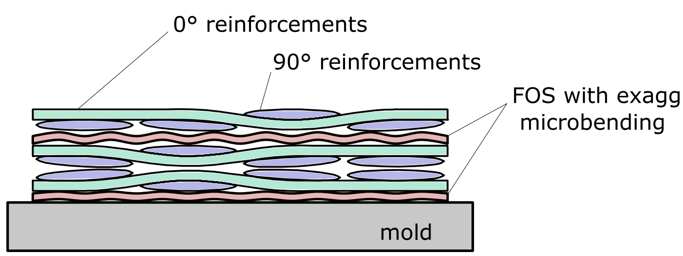

Figure 4.36: Microbending in FOS caused by embedding into composites.

Additionally, the fiber end needs to be treated such that there is minimal reflection from the end face. This can be achieved by splicing in a coreless termination fiber. For splicing the fiber needs to be stripped of its polyimide coating and cleaved. polyimide adheres very well to the optical fiber and can only be stripped using non-mechanical methods. In a preliminary step therefore, a stripping method needed to be derived. Based on the input received from the supplier of the FOS, one suitable method includes the use of a flame to char the polyimide. Doing so, leads to exposure of the bare fiber but it also affects the fiber in unwanted ways. It was found that extensive heat application leads to bending and increased brittleness.

The best results were obtained when using the flame of a regular lighter for only a fraction of a second. This will very briefly lead to a flare up and charring at only a small area. The fiber at this stage is still covered with the charred polyimide. This can then be removed using isopropyl alcohol solvent and lint free wipes. This allows for a maximum of control as it is important to only remove as much of the coating as is absolutely necessary. For the cleaving, it is important to align the now stripped fiber with the cutting blade and ensure that the parts of the fiber where it will be held in the cleaver is still coated with polyimide as the fiber will break in an uncontrolled manner when that is not the case.

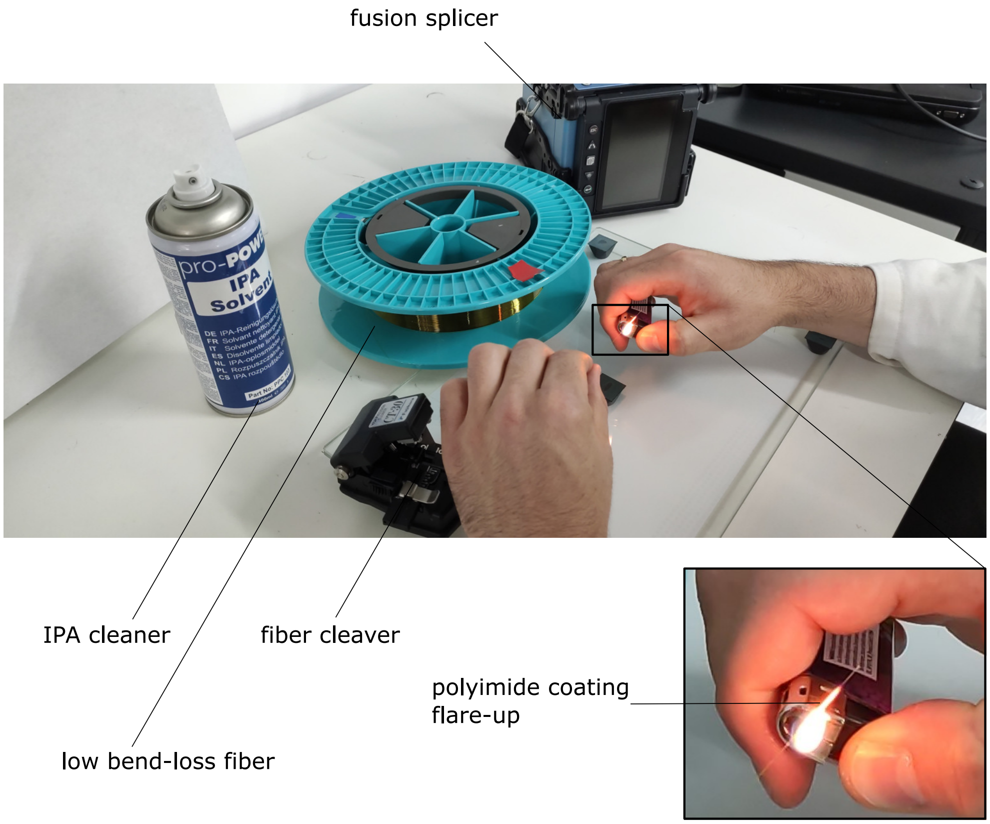

Figure 4.37: Preparation of a polyimide coated low bend-loss fiber for splicing.

At this stage, the fiber is ready to be spliced. For this a Fujikura 70 fusion splicer is used. The splicer is equipped with several splicing modes, where the AUTO mode worked well for both pig-tail splices as well as termination splices. In Figure 4.38 a successful termination splice is depicted. The distributed FOS is on the left side, whereas the coreless termination fiber is on the right. The core is clearly visible in the image. The splice location is a weak spot as the protective coating is missing and needs to be replaced.

Two options exist 1) restoration of the coating using a fiber recoater (FSR-05, Fujikura) or 2) a splice protector consisting of a metallic wire with a thermoplastic sleeve is used. Once all these variables were defined and the sensor was manufactured the obtained signals were compared to an off-the-shelf sensor from the OEM.

It can be seen that the outcome both in terms of signal stability (Figure 4.39) as well as overall characteristic (Figure 4.40) are well behaved and equal to the OEM sensor. This confirmed the ability of the developed manufacturing method to deliver high quality sensors.

Figure 4.38: Image of a successful termination splice.

Figure 4.39: Comparison of OEM sensor with manufactured sensor - scanning along its length

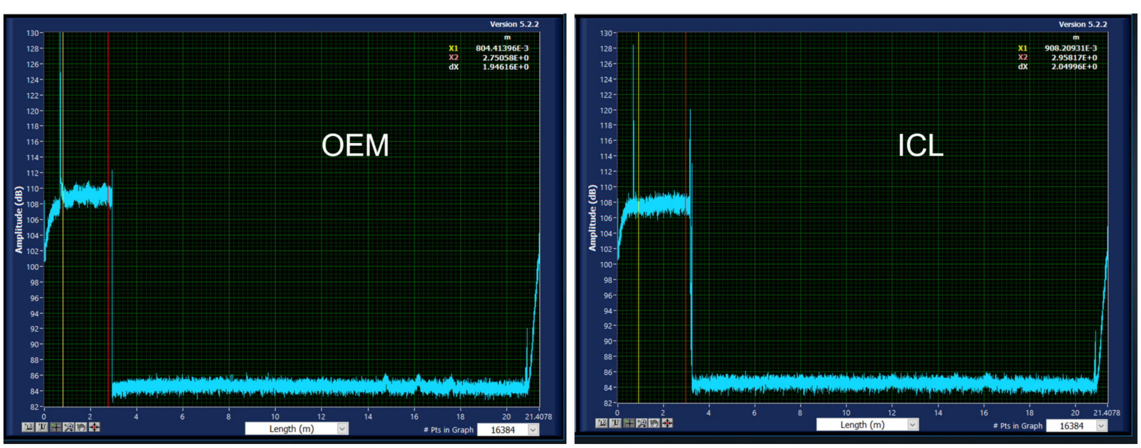

Figure 4.40: Comparison of OEM sensor with manufactured sensor - full spectrum

4.4 Summary

This chapter presented a large array of experiments carried out by the author in order to answer the question which of the sensing techniques identified by the literature search (section 2) is the most suitable. Three main technological directions have been explored: PE, FOS and electrical sensing.

PEs are arguably the most widely used SHM sensors and exist in many different shapes, sizes and material combinations. Their ability to both sense and actuate place them ideally for SHM purposes. However, severe limitations to do with their fragility and susceptibility to high temperature depolarization places significant restrictions on their usability for composite PM.

Three main types of FOS have been studied in this chapter. Both FOS-FBG and FOS-OBR have been successfully used for temperature monitoring and FOS-OBR also for pressure sensing applications. Fresnel reflection based devices have been shown to work well when it comes to quantifying changes occurring within the polymeric matrix materials. After considering the pros and cons of each sensor technology, FOS-OBR have shown to posses the most suitable capability profile when it comes to PM. Their ability to cover large areas far outweighs the drawback of low acquisition rates. Most composite manufacturing processes do not require data at shorter intervals than 0.1 s. Whilst the low acquisition rate might compromise their ability to perform certain SHM tasks, the FOS-OBR technology has been chosen for further investigations during which their SHM capability will receive heightened attention.

With the experience gathered from the experiments carried out for PEs and FOS, a fairly accurate profile of desired quality parameters had been compiled. Efforts trying to manufacture and put to use **electrical sensors** that fit that profile have proven unsuccessful. However, in chapter 7 this technique has been referred to when creating a novel sensing material and manufacturing platform with promising initial results and great potential for future work.

Chapter 5

Deployment of an integrated PM and SHM system for a GFRP plate

This chapter is widely based on a publication by Buchinger and Sharif-Khodaei [49].

Significant research efforts have in recent years derived composite manufacturing processes that deliver faster, cheaper and more repeatable products whilst still maintaining outstanding mechanical properties, typical for composites. One such process family utilises liquid polymeric resins to impregnate dry fiber reinforcement stacks and thereby enables the use of cheaper raw materials, higher degrees of automation and design freedom. VaRTM is a representative example from this process family.

In parallel to that development, sensor-based SHM technologies promise to provide an insight into the structural integrity of a specific component at any given point in time. Whilst traditional SHM applications require the sensors be fitted to the structure after it has been manufactured, this work presents ways the sensors can be integrated during manufacturing and used for PM.

Standalone PM methods for RTM manufacturing process have an important role to play in modern manufacturing setups. Torres [154] reviewed commonly used manufacturing monitoring techniques and besides the widely established methods based on TCs, pressure transducers and dielectric sensors, microwires [155] and time domain reflectometry [37,39] have also produced promising results. The only passive method allowing a flexible and distributed monitoring, however, remain optical fibers [112,114,149,154,156–160].

The developed manufacturing monitoring strategy builds upon the findings from section 4.3.3, utilizing FOS to evaluate and detect potentially harmful processing conditions early in the manufacture. Having such capabilities could mitigate the risk of failure and also allow for process improvements. Whilst FOS have been shown to be useful for manufacturing monitoring applications previously, significant limitations remain.

Those are either owed to the choice of sensor configuration like FOS-FBG [161,162], LPG [163,164] or Fresnel reflection [165] which all are point-sensors, delivering a value for only very few locations on the component or the process/material - sensor interaction exploited for monitoring. These typically are based on direct resin - fiber interaction [162,165] or bending-induced losses within the optical fiber [161,163,164]. The latter typically only offers an on/off type response and renders the sensor non-usable after the process is complete. Such a response does not allow a quantified measure for in-mold pressure, fabric compaction or fiber-volume fraction.

FOS-OBR offer a clear advantage when it comes to surface coverage and they have been applied to liquid resin manufacturing processes before [153, 156, 166, 167]. They also have successfully monitored the subsequent life of a component [168–173].

The emphasis in this research lies on retrieving performance characteristics that inform about the quality of the employed process in a quantified manner. Thereby giving the manufacturer the ability to change the process trajectory for the better. This is achieved through a low bend-loss single mode (SM) optical fiber and exploiting its opto-mechanical properties.

FBG-based FOS have been successfully used to determine transverse loads or pressure more general in literature [99, 100, 104, 107, 108, 174, 175]. A laterally loaded FOS-FBG tends to develop a second reflectivity peak with a spectral hole between those peaks [107, 108, 174], see Figure 2.23. Tracking the peaks and spectral hole allows the derivation of pressure as a function of their shift. The appearance of the second peak is a result of birefringence [99, 174] in the fiber. This means that the acting lateral load leads to the two orthogonal polarization modes being affected differently for birefringent fibers (ref. Figure 2.23) and a specific interrogator, able to capture those modes independently, is required [104, 176]. This is a limitation given the need for additional hardware (polarization splitter and a second photo detector [176]).

This technique has another major downside when considering industrial application. It requires an extremely high degree of control on fiber placement and orientation. As the technique exploits the affect pressure has on the polarization axis, those axis need to be aligned with the loading directions [72,100,103,107,108,174]. Such a level of control will be very difficult to obtain during industrial composite manufacturing and is therefore not considered further.

Another method proposed by Correia et al. [175] is to coat part of the FOS-FBG's sensitive region with pliable material and exploit the axial stretch caused by lateral compression to infer the transverse loading. This technique does not cause birefringence within the fiber.

FOS-OBR are herein applied to the lateral compaction monitoring of a dry fiber stack. The information gained from this technique sheds light on the level of compaction, panel thickness, fiber volume fraction and permeability in a distributed manner. Such parameters could previously not be captured live over a large area and process quality decisions are now possible online. The compaction process is modelled in Abaqus to establish the relationship between fiber-optical measurements and the state of compression within the fabric. Subsequently, an FOS-OBR sensor is integrated within the mold of a VaRTM manufacturing setup to quantify the quality of the process.

5.1 Problem definition

5.1.1 Manufacturing

In the most abstract form, a resin infusion process's constituents are the fibrous reinforcement, the polymeric resin and a way of pressure application (vacuum and/or positive pressure) and retention to aid infusion and reduce gaseous entrapments. From a manufacturer's viewpoint, it is desirable to achieve minimal time and maximum laminate quality employing the most simple set up. Mathematical treatment of the problem has lead to involved models [177], however, they still are based around Darcy's law of flow through a porous media as in Equation (5.1)

$$q = \frac{-k}{\mu} \nabla p \tag{5.1}$$

where q is the instantaneous flow rate (process output), k the permeability (property of the reinforcement), μ the dynamic viscosity (property of the resin) and ∇p pressure drop (process input).

It can be concluded that for a given fiber reinforcement (this definition includes the weave pattern and ply orientation as permeability is strongly influenced by that) and resin, the flow is proportional to the pressure differential between the injection pressure acting on the resin pot and the vent pressure (typically atmospheric pressure or vacuum).

Having established that ∇p is the process variable of most importance for the infusion process itself, it is evident that any integrated manufacturing and health monitoring system has to be able to provide information on the pressure levels with sufficient spatial resolution.

The state of the art is to monitor pressurisation at a system level (press, resin pot, resin feed-lines) or at discrete locations (in-mold pressure sensors). Such an approach is at best an indicator and requires the decision on sensor placement to be made at a very early stage in the manufacturing process design. Using an FOS-OBR type sensing solution allows one to capture readings across the entire surface of a component and gives the ability to react to problems occurring late in development or even in an existing production environment.

5.1.2 Pressure as a main process characteristic

In addition to being the driving force during fiber bed wet out, pressure plays a major role during the entire manufacturing process. It impacts all major quality characteristics of a composite, like: the laminate thickness, fiber volume fraction, void content and yarn and fiber alignment [2, 178–182].

The components of pressure within a section of composite during manufacture include: the externally applied pressure (imparted through the mold or a vacuum bag), which is counteracted by the fabric, injection pressure at the port and an optional application of vacuum at the vent (Figure 5.1) and their respective counterforces (omitted in the figure).

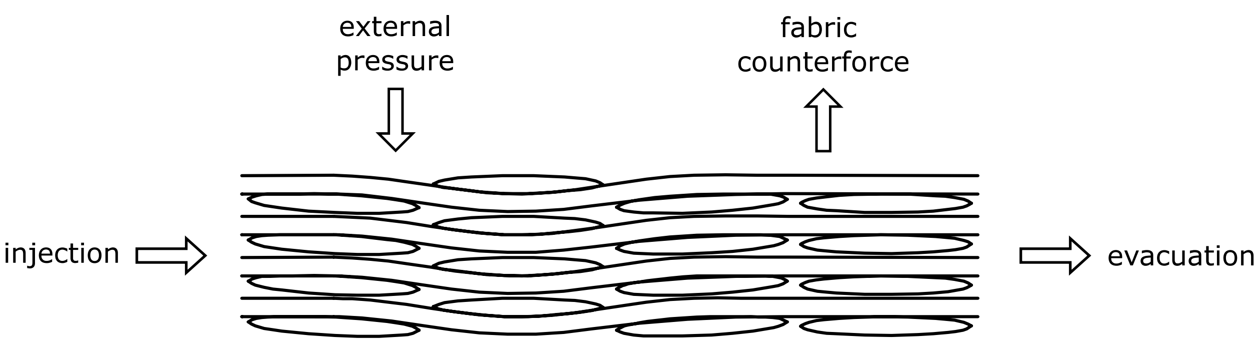

Figure 5.1: Loads acting on fabric during manufacture [49].
This is an 'Accepted/Original Manuscript' of an article published by Taylor & Francis Group in Advanced Composite Materials on 30 Nov 2021, available online: https://wwww.tandfonline.com/10.1080/09243046.2021.2001910.

Considering all those factors, it becomes evident that the true state within the material is complex and cannot be reasonably inferred from measurements at a system level or discrete locations. Additionally, the fabric's lateral loading is an aspect of composite manufacture which is difficult to measure directly using conventional pressure transducers.

5.1.3 FOS-OBR based pressure sensing

Rayleigh backscattering based OBR is described in detail in section 2.2.1.2. Equation 2.5 introduced earlier can be linearly approximated by Equation 5.2, given strains and wavelength shifts are small. This relationship is exploited further throughout this chapter in order to relate back and forth between physical strains within the optical fiber and how they impact optical measurements.

$$\frac{\Delta\lambda}{\lambda} = \Delta\varepsilon_{11} - \frac{1}{2}n^2\left[p_{11}\Delta\varepsilon_{22} + p_{12}(\Delta\varepsilon_{11} + \Delta\varepsilon_{33})\right] \tag{5.2}$$

where $\Delta\varepsilon_n$ are the 3D-strain components, $p11 = 0.113$, $p12 = 0.252$ are the strain-optic coefficients following

[51] and $n = 1.4459$ is the Refractive Index [52].

5.2 Compaction model

The ability to predict the FOS output is vital for the implementation and testing of the proposed monitoring system. Building upon Equation 5.2 the requirement for a 3D strain field within the fiber arises. To obtain this, a numerical model was set up.

Microsections were used to establish the input parameters for the compaction model. An approximately 25 mm x 25 mm large piece of fabric was embedded in polyester mounting resin (KLEER-SET, Metprep Ltd., GB) and analysed using a Zeiss Axio Imager.M2m optical microscope. The yarn and fiber dimensions (Table 5.1) were used to create a corresponding 3D-model of the fabric using TexGen v3.12.0 Fabric Modeller ([183]). An Abaqus dry fiber file was exported and used for further numerical treatment of the problem.

Table 5.1: Fabric properties

Weave style	**Fiber Diameter** (μm)	**Fibers per yarn** (count)	**Yarn width** (mm)	**Yarn height** (mm)
4HS satin	9	1300	1.3	0.15

A full characterisation of the compaction behaviour as described by Valkova et al. [184] was performed. The sample made up of four fabric layers was placed between two self-aligning plates with a diameter of 50 mm. The load exerted on the sample was recorded by a 50 kN load cell fitted to the upper cross-head of an Instron®5960 universal testing machine and displacements via a Imetrum Video Gauge™. The fitting parameters a, b, c and d describe the lateral compression behaviour (Equation 5.3) and were obtained using a problem based nonlinear least-squares optimisation scheme in MATLAB®. The optimisation scheme was repeated several times starting from predefined parameters and halted upon observing convergence of parameters. The fit to the experimental data can be observed in Figure 5.2.

$$E_{22_{yarn}} = ae^{bV_{f_{yarn}}} + ce^{dV_{f_{yarn}}} \tag{5.3}$$

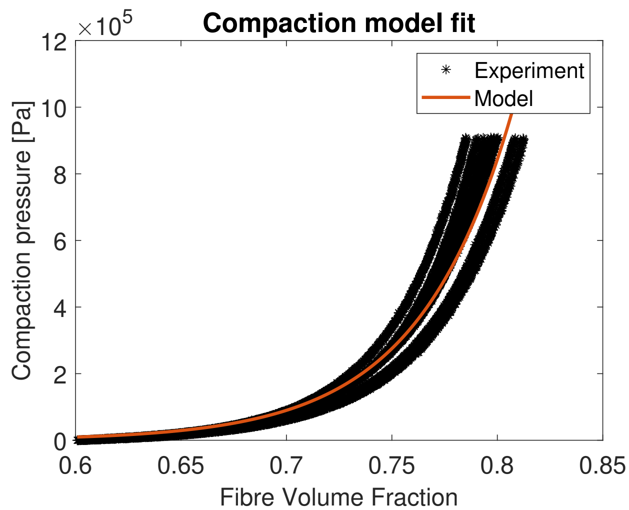

Figure 5.2: Response to compaction pressure: $E22_{yarn}$ model compared to experimental data.
This is an 'Accepted/Original Manuscript' of an article published by Taylor & Francis Group in Advanced Composite Materials on 30 Nov 2021, available online: https://wwww.tandfonline.com/10.1080/09243046.2021.2001910. [49]

This material model was implemented as a user subroutine (based on the work by Valkova et al. [184]) in Abaqus Explicit (VUMAT) along with a friction coefficient of 0.2 for glass fiber yarns sliding along each-other, as well as between a yarn and metallic surfaces ([185, 186]). This value was implemented in Abaqus' contact formulation for tangential behavior.

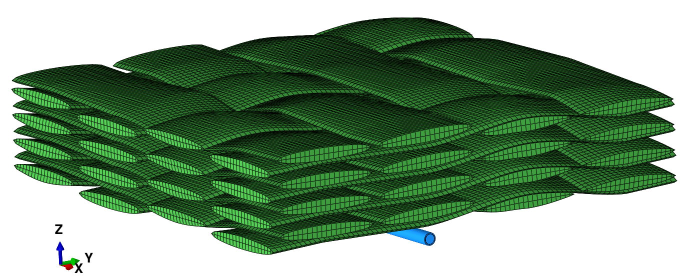

Figure 5.3: Representative volume element of the fabric stack and the optical fiber.
This is an 'Accepted/Original Manuscript' of an article published by Taylor & Francis Group in Advanced Composite Materials on 30 Nov 2021, available online: https://wwww.tandfonline.com/10.1080/09243046.2021.2001910. [49]

The fabric model (Figure 5.3) consists of rigid top and bottom plates (not shown in the figure), 32 yarns (3,400 elements each, type C3D8R) and the optical fiber which is modelled as a glass main fiber (125 µm diameter consisting of 12,320 elements, type C3D8R, with an assumed Young's Modulus of 70 GPa and a

Poisson's ratio of 0.25) coated with polyimide to a total diameter of 150 µm (6,720 elements, type C3D8R, with an assumed Young's Modulus of 2.5 GPa and a Poisson's ratio of 0.34).

The load is applied through displacement control of the upper rigid plate. The multi axial strain response within the optical fiber is captured and used as input for the calculations of the predicted wavelength shift (Equation 5.2). The plotted data (Figure 5.8) represents the envelope for the entire fiber segment modelled. At small levels of top-platen downward displacement, the expected shift is minimal but it increases once surpassing 0.3 mm. Overall the trend observed suggests a divergent power-law relationship between the platen stroke (i.e. level of compaction) and optical frequency shift. The evolution of the compaction process and associated fabric morphology changes are shown in Figure 5.4. Strain build-up inside the optical fiber is illustrated in Figure 5.5.

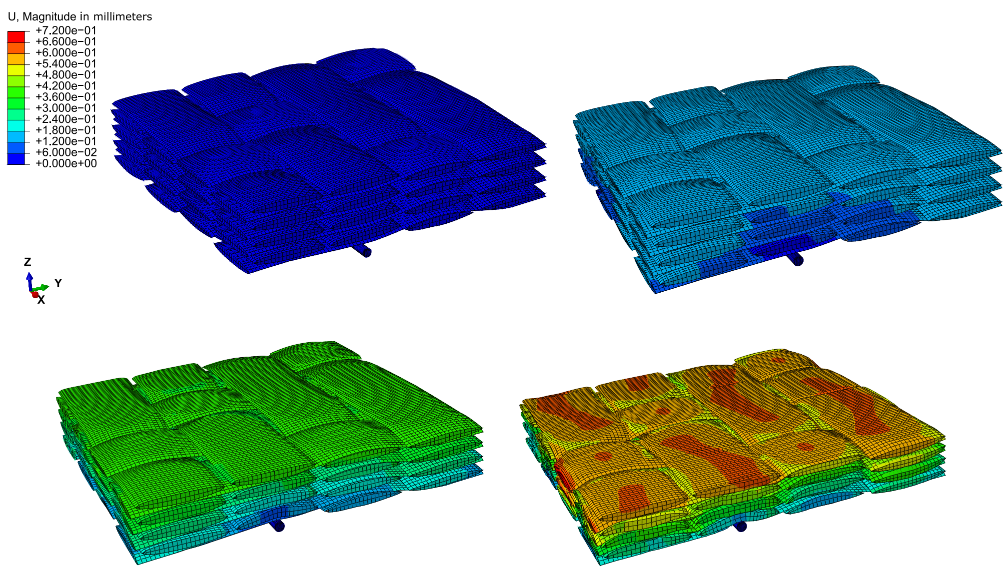

Figure 5.4: Compaction model output showing the displacement of the fiber tows relative to each-other and the general fabric morphology.
This is an 'Accepted/Original Manuscript' of an article published by Taylor & Francis Group in Advanced Composite Materials on 30 Nov 2021, available online: https://wwww.tandfonline.com/10.1080/09243046.2021.2001910. [49]

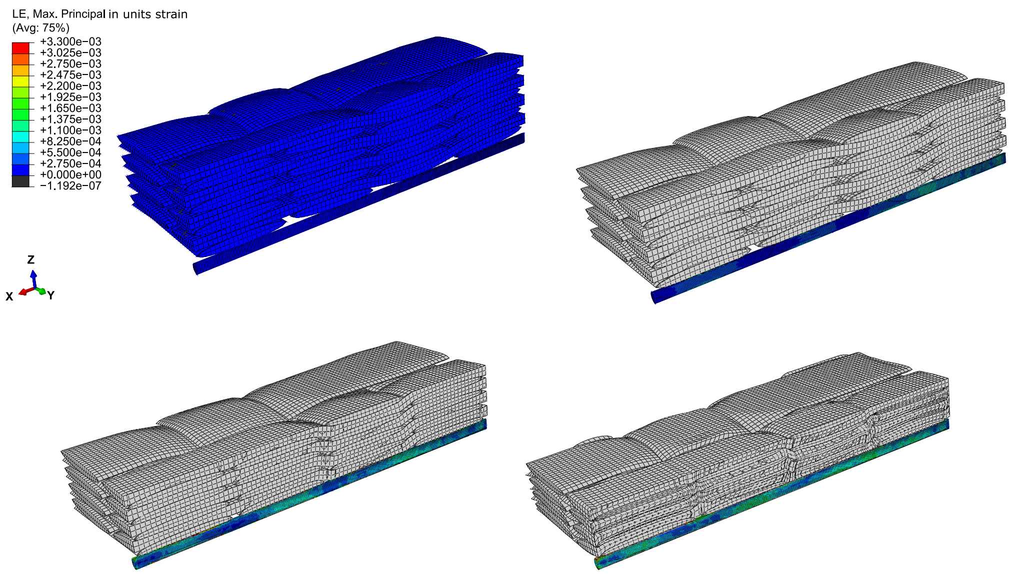

Figure 5.5: Compaction model output showing the evolution of optical fiber strain.
This is an 'Accepted/Original Manuscript' of an article published by Taylor & Francis Group in Advanced Composite Materials on 30 Nov 2021, available online: https://wwww.tandfonline.com/10.1080/09243046.2021.2001910. [49]

To confirm assumptions made about the FOS actually being transversely loaded microsections were made (Figure 5.6). These microsections were focused on the FOS and show clearly how the fiber is held in place and firmly packed between the reinforcement fibers. This confirms the assumption that the FOS will actually be compressed laterally only and that all load is locally concentrated directly at the fiber.

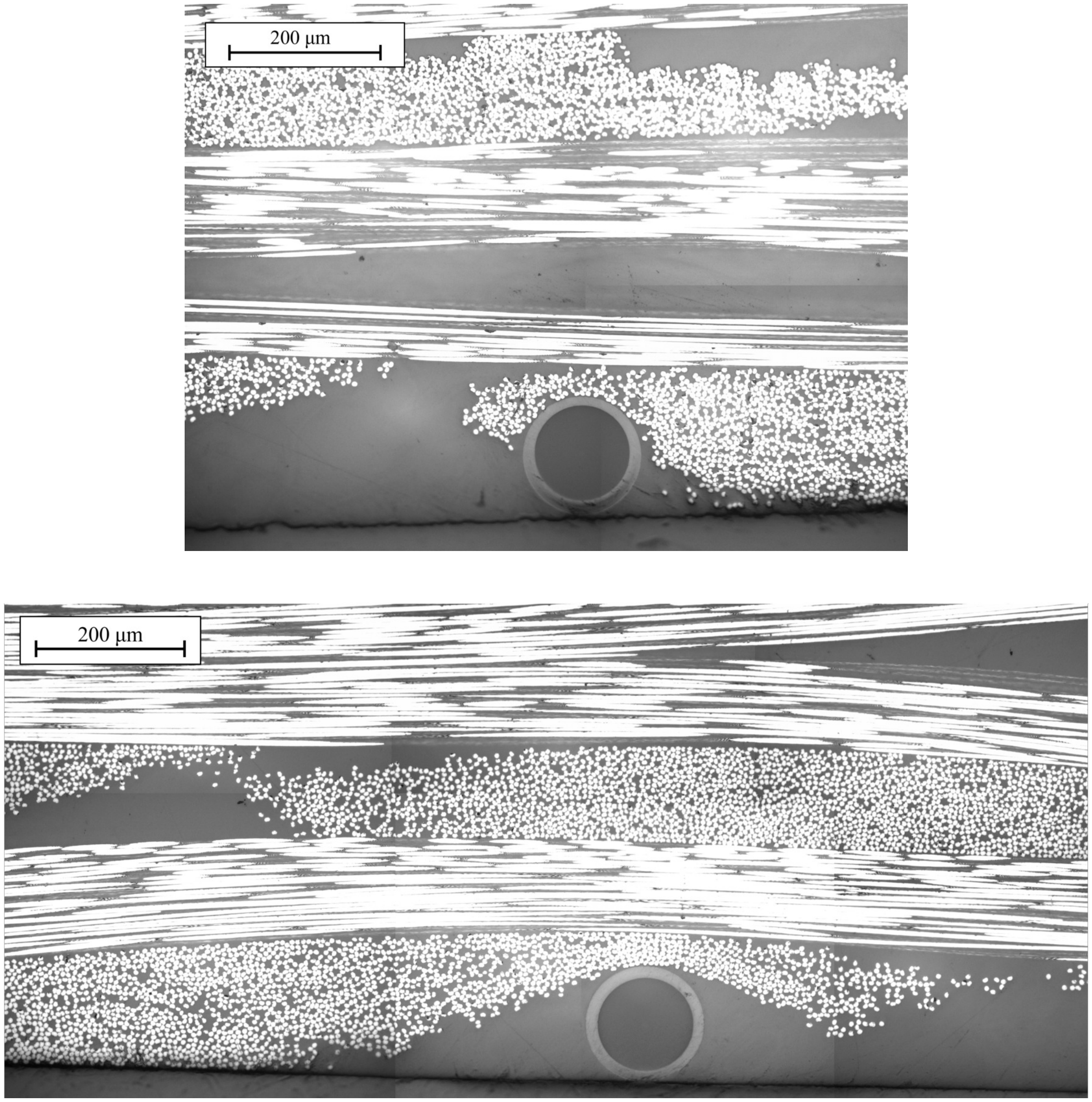

Figure 5.6: FOS embedded in a composite laminate beneath the bottom-most layer confirming assumptions about lateral compression.

5.2.1 Model validation

To verify the applicability of the developed model, a separate experiment was set up. The FOS was laid into a serpentine shape, placed underneath four layers of glass fiber fabric (square pieces of 155 mm side length) and compressed between two stainless steel platen. The top-platen was mounted to a self-aligning fixture ensuring an even pressure application at a motion-controlled rate of 0.1 mm/min. To ensure proper contact between the platen and the fabric a threshold counterforce of 10 N was chosen (equals a 1.4e-4 MPa compressive pre-load). Upon reaching this value, force and displacement readings were set to zero and the test commenced.

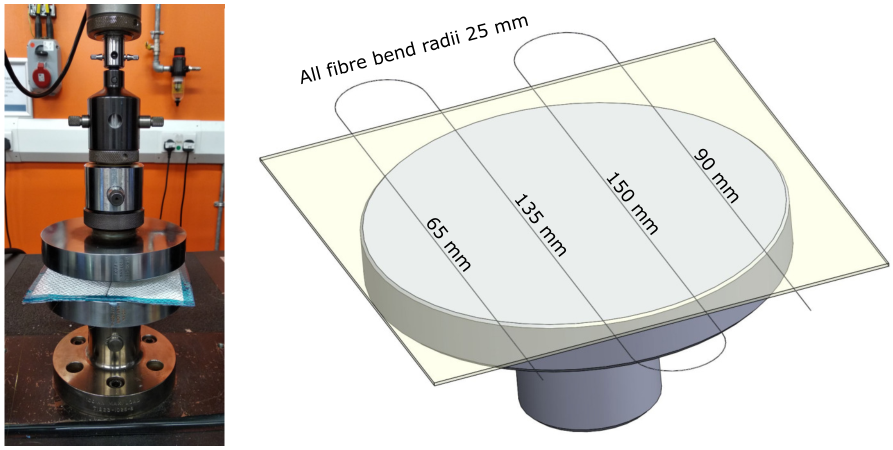

Figure 5.7: Compaction of a four-layer fiber bed in-between two rigid platen (150 mm diameter) with the sensor laid out in serpentine.
This is an 'Accepted/Original Manuscript' of an article published by Taylor & Francis Group in Advanced Composite Materials on 30 Nov 2021, available online: https://wwww.tandfonline.com/10.1080/09243046.2021.2001910. [49]

Experimental verification of the proposed modelling scheme in Figure 5.8 reveals an offset of about 0.1 mm towards a greater platen stroke. This can be explained by the small force acting at low levels of compaction and the resulting uncertainties around the starting point. In the model, contact between the plate and the fabric occurs by default from the onset. Such contact cannot be guaranteed during experimental testing as the initial distance between the platen was taken when a threshold force was surpassed. This introduces a mismatch between the boundary conditions present in reality versus what has been assumed for the model which is difficult to quantify. In the figure the experimental data has been shifted 0.1 mm towards the left to accommodate for this circumstance. Additionally, the model generally overestimates the expected frequency shift. This can be attributed to uncertainties around the true material properties of the optical fiber.

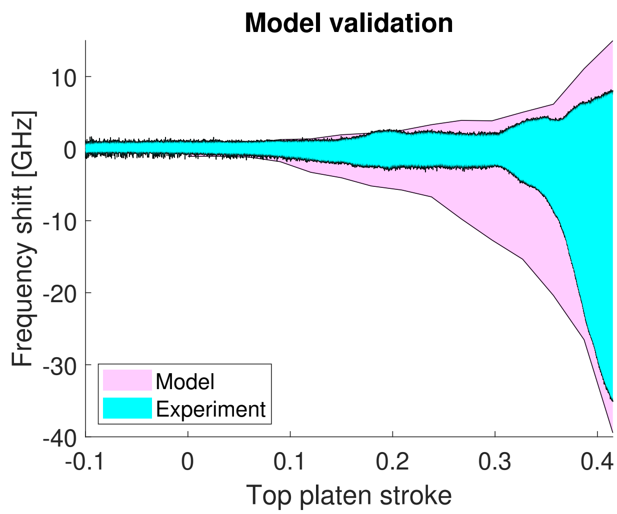

Figure 5.8: Optical frequency shift derived from the strains derived from the Abaqus model (entire modelled unit cell) and translated into shift through opto-mechanical equations in comparison to experimental values measured and averaged across the entire platen area (ref. Figure 5.7).
This is an 'Accepted/Original Manuscript' of an article published by Taylor & Francis Group in Advanced Composite Materials on 30 Nov 2021, available online: https://wwww.tandfonline.com/10.1080/09243046.2021.2001910. [49]

5.3 VaRTM manufacturing monitoring study

To demonstrate the suitability of the presented monitoring technique an actual part manufacturing trial was performed using VaRTM.

5.3.1 Set up

Building upon the encouraging results obtained by Sanchez et al. [166] and Chandarana et al. [171] using FOS-OBR systems as a proof of concept, an ODiSI B Interrogator (by Luna Inc., Blacksburg, VA, United States) is employed to obtain the Rayleigh backscattering signature of a fiber sensor.

Ten layers of the four-harness woven glass fiber fabric were cut to shape and laid into a test panel tooling (Figure 5.9) by Composite Integration Ltd (Saltash, UK). The mold fills from the resin inlet port at the left side of the mold inwards. The blue arrow indicates the vacuum outlet with the general resin flow paths indicated (orange). Once the fabric is laid into the mold it is closed using bolts along the circumference and ready for resin injection.

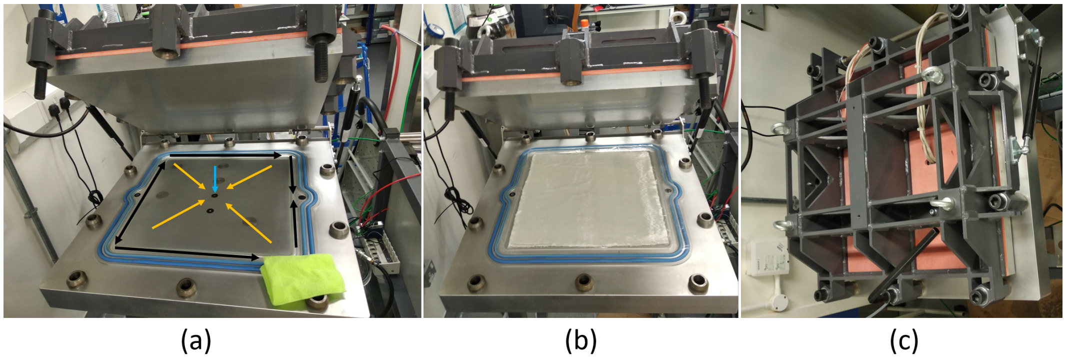

Figure 5.9: Depiction of the RTM mold used for the experiment. (a) the empty mold with the resin distribution channels at the circumference (black arrows) are highlighted; (b) the fabric laid into the mold; (c) closed tooling ready for resin injection.
This is an 'Accepted/Original Manuscript' of an article published by Taylor & Francis Group in Advanced Composite Materials on 30 Nov 2021, available online: https://wwww.tandfonline.com/10.1080/09243046.2021.2001910. [49]

5.3.2 RTM plate manufacture

A 5 m long section of Fibercore Ltd SM1500(9/125)P was used as FOS. This fiber has a diameter of 125 µm, polyimide coating, a mode field diameter of 9 µm and a numerical aperture 0.15. Previous experiments showed that this fiber provides consistent results and due to its bend insensitive nature is well suited for embedding into composites. The fiber was placed on top of the glass fiber stack in a serpentine shape and held in place by local stitching (Figure 5.10). The sensor was configured to a gauge length of 2.6 mm yielding 962 discrete gauges distributed on the panel. The processed data logging function provided by the LUNA ODiSI B software package was used to record a strain reading every 0.1 seconds over the entire time of the experiment. During data processing, the fiber was split into five sections to utilise the information around local and spatial differences in the measurements. All data post-processing was performed in MATLAB®.

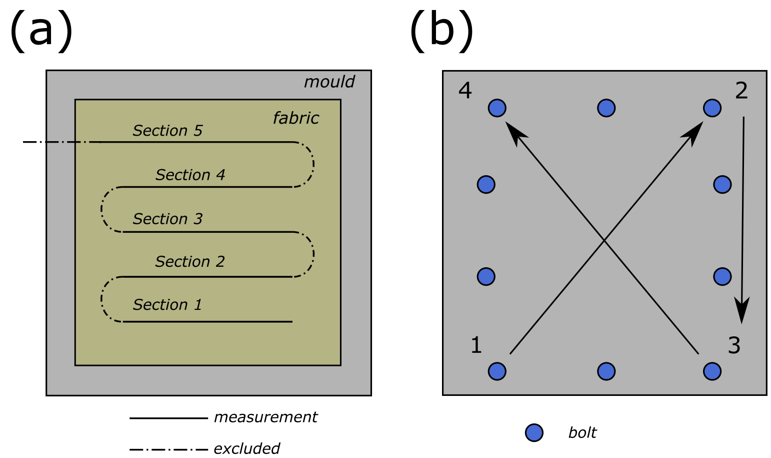

Figure 5.10: Panel layout (a) indicating the fiber bed (yellow, 500 mm × 500 mm) and the sensor position (serpentine). (b) The bolts were tightened in a diagonal sequence as indicated for the first 4 bolts.
This is an 'Accepted/Original Manuscript' of an article published by Taylor & Francis Group in Advanced Composite Materials on 30 Nov 2021, available online: https://wwww.tandfonline.com/10.1080/09243046.2021.2001910. [49]

The FOS-monitoring was initiated during mold closure to monitor the compaction of the fabric stack. Since the mold is closed and held closed by manually tightened bolts, slight differences in applied torque lead to minor differences in the laminate thickness. In order to demonstrate the capability to detect such differences in compaction levels, the experiment was carried out with deliberate differences in final torque. The bolts along Section 1 of the fiber have seen the highest torque whereas the bolts situated along Section 5 the lowest.

A Sicomin SR 8100/SD 8824 Epoxy system was mixed at a 100:22 ratio by weight. It was loaded into a Hypaject MK III – 6 Litre injection unit by Magnum®Venus Products and heated up to a temperature of 30°C for injection. The vacuum port on the tooling was connected to a resin catch pot and vacuum pump. The vacuum was maintained below -0.9 bar throughout the injection process. Upon the resin reaching its final temperature, it was injected into the mold with a positive pressure of 2.5 bar. As the advancing resin front reached the vacuum line and got sucked into the vacuum hose the connecting hose was pinched using a hemostat when no more air bubbles were observed in the resin. The injection pressure was held constant for a further five minutes to ensure complete wet out before being clamped as well and shut off. Heating the upper and lower plates of the mold to 40 °C commenced the resin cure.

5.4 Experimental results and discussion

In Figure 5.11 the readings of the entire VaRTM process are shown. The data presented is averaged over ten time samples to remove noise and per fiber section for clarity. As expected the readings start at 0 as this was the last Tare applied to the acquisition system. A slight drift can be observed at first which can be attributed to the mold being physically closed and the stack being brought in contact with the upper mold half for the first time. Following complete closure, torque is applied to the locking bolts and the fabric stack is compacted. The fully tightened mold is ready for resin injection. This occurs at around 2000 s and is marked by a massive jump in amplitude. This large spike can be explained by the sudden change in pressure conditions within the tool as it changes from being at negative pressure to changing to positive due to trapped air within the injection unit's connection hose. This can be pictured as a sudden inflating of an enclosed, airtight volume.

Upon completion of the infusion process and upright pressurisation without resin flow to allow an even distribution, the injection unit is shut-off and another baseline shift occurs. From there on the filling process is complete until the curing step commences at around 5000 s. This is marked by a smooth almost linear decrease in the optical frequency shift. At this point another tare is recommended in order to monitor the cure with a common origin. When presented with the view of the entire process in terms of optical frequency shift the individual process steps stand out owing to their unique characteristics. This in itself renders the system a great tool for overall process state monitoring.

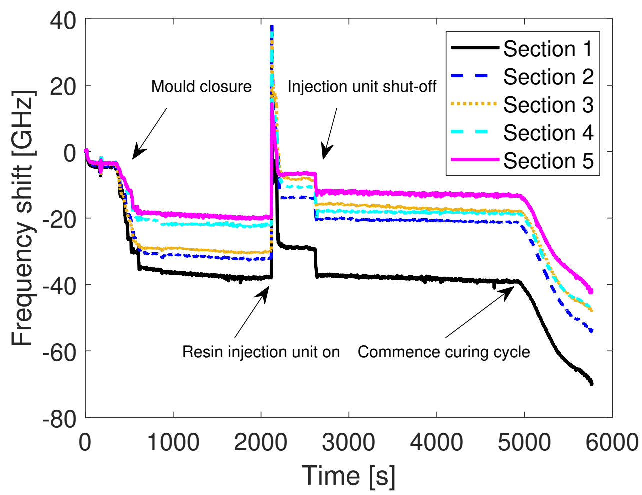

Figure 5.11: FOS-OBR frequency shift obtained during the entire RTM process.

Zooming into more of the details and evaluating the readings obtained during the first phases of VaRTM, additionally illustrates the process quality monitoring aspect of the presented system. Over the course of mold closure and bolt tightening (Figure 5.12) a linear decrease in frequency shift is observed as predicted by the Compaction model. The step wise appearance is explained by the fact, that the mold is closed bolt by bolt leading to plateaus when changing over the allen key.

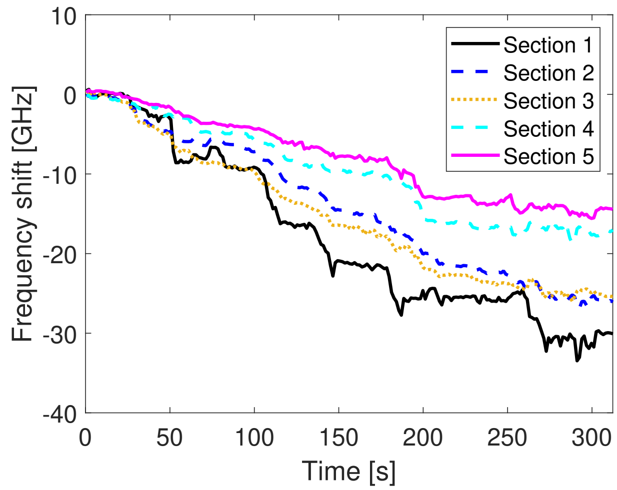

Figure 5.12: Measured optical frequency shift observed during the compaction phase. *This is an 'Accepted/Original Manuscript' of an article published by Taylor & Francis Group in Advanced Composite Materials on 30 Nov 2021, available online: https://wwww.tandfonline.com/10.1080/09243046.2021.2001910.* [49]

Comparing the five different sections with each-other a roughly 20 GHz gap is present between the final readings of Section 1 and Section 5, suggesting a different level of fabric compression. The relationship between stack compression and optical frequency shift is given through the lateral load that is transferred through the fabric and finally acts on the optical fiber. As such it is corresponding to the tightening torque. The resulting closing force pushes the upper plate down on the fabric and as a result it is compressed. The observed differences clearly suggest non-uniform mold closure as a result of inconsistent bolt torque leading to non-uniform compaction across the panel surface and in consequence to thickness and fiber volume fraction differences.

Post curing the manufactured panel was inspected and its thickness was recorded on multiple locations using a Deep Throat Micrometer (RS PRO, Range 0 mm to 25 mm). As expected, the thickness varies greatly across the surface and the distribution correlates well with the obtained FOS-OBR results (Figure 5.13). Both for the frequency shift and the thickness a mean value was used for correlation.

Whilst it is understood that bolt clamped VaRTM molds are typically only used for small components, these findings can easily be applied to any given shape and closing mechanisms. This is done by exploiting the fact that panel thickness is indirectly proportional to the fiber volume fraction of the composite (Equation 5.4 and 5.5). Once a fiber volume fraction distribution is known, employing Kozeny-Carman's equation provides the relationship between permeability and fiber volume fraction [187].

$$V_{total} = V_{mold} = V_{fiber} + V_{resin} \tag{5.4}$$

$$v_{fiber} = \frac{V_{fiber}}{V_{mold}} \tag{5.5}$$

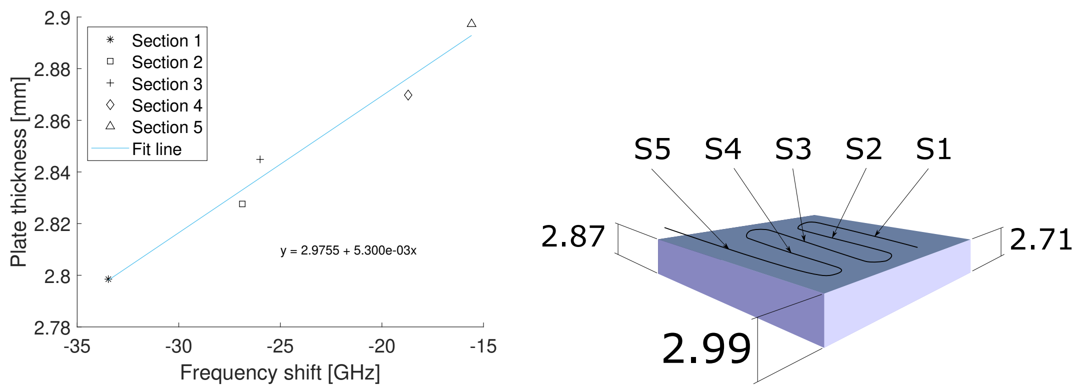

Figure 5.13: Measured plate thickness plotted against frequency shift and panel representation indicating fiber layout with selected thickness measurements.
This is an 'Accepted/Original Manuscript' of an article published by Taylor & Francis Group in Advanced Composite Materials on 30 Nov 2021, available online: https://wwww.tandfonline.com/10.1080/09243046.2021.2001910. [49]

5.5 Conclusions

The merit of FOS-OBR sensors as process monitoring devices was demonstrated through rigorous FEM modelling and experimental testing. First an existing model for fabric compaction was adapted for the studied GFRP and the FOS was added to the composite stack. In a second step the 3D-strain field resulting from compaction was used to calculate the effect on the optical properties of a fiber. The obtained results were experimentally validated and a good agreement was observed.

Extending the initial theoretical study of the problem, a manufacturing trial was performed to evidence the suitability of the proposed technique in an industrial environment. During VaRTM panel manufacture a fiber sensor was integrated at the mold closure stage and through deliberate variation in applied torque at certain locations, a non-uniform fabric compression level and part thickness was simulated. It could be shown that both the entire VaRTM process can be monitored as well as errors can be clearly detected with the proposed FOS-OBR based manufacturing monitoring technique. Additionally, it was possible to deduce a linear relationship between panel thickness (or fiber volume fraction) and measured frequency shift. Such capability can offer deep insights into the quality of the final component at the onset of manufacture with the ability to react or adjust. The choice of a distributed sensing method allows the determination of the location and extent of any deviation. Manufacturers then have the ability to take directed action immediately and avoid defective products.

Chapter 6

Integrated PM and SHM applied to representative aerospace components

FOS-OBR has previously been proven to produce high fidelity PM information both numerically and experimentally (see chapter 5). Building upon the results obtained from a two-dimensional component, an extension towards more complex structures is presented in this chapter.

6.1 Selection of demonstrators

Modern aircraft are comprised of a myriad of individual parts, with different levels of complexity. Therefore, to demonstrate the capabilities of the developed PM/SHM solutions on realistic parts, two demonstrators with different complexities and challenges have been selected in this research. After considering composite structures that have found widespread use and also are feasible to be manufactured and tested within our facilities, two elements have been chosen: 1) a tapered flat panel and 2) a C/U-section stiffener.

The tapered panel combines several unique benefits and challenges of composites within a relatively simple geometry. The fact that a taper resulting from an internal ply-drop off allows the thickness of a structural element to vary without having to perform any machining is an important one. Inside the composite panel, the individual plies are still continuous, leading to good integrity. However, when considering manufacturing processes with enclosed molds the taper can be challenging to manage. This becomes evident when looking at the cross-section of a typical ply drop-off (Figure 6.1). As the position of the drop-offs is usually depending on manual positioning tolerances, fraying of the dry fabric, distortion or general misalignment, such areas are prone to experience lower or higher consolidation pressures, leading to problems during manufacturing. These include low fiber volume fractions due to lack of consolidation, porosity due to low pressure or dry spots due to high pressure. Such local problem areas are ideally suited for localised PM technologies like FOS. They have large impact on product quality but are spatially rather small and known beforehand. As such they offer high returns for minimal effort for manufacturers and were chosen for this work.

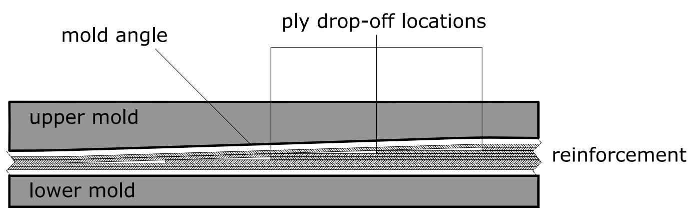

Figure 6.1: Cross section of a ply drop-off during molding

In addition to the issues around getting such tapers molded correctly and to a high quality, they also are subject to different loading compared to their surroundings. When considering a simple tensile loading case, an out-of plane opening load is formed to compensate for the misalignment of acting forces. Such behaviour is amplified by bending where a force/stress gradient is present in the structure already.
To illustrate the above Abaqus simulations of the tapered panel were performed. The model consists of 3D elements making up the individual plies and cohesive elements representing the resin layer between plies. This approach was chosen to show the tendency for delaminations in the taper regions. Figure 6.2 and 6.3 show the opening loads and shear loads acting on the cohesive elements respectively. Note that certain plies have been removed from the images to reveal high load concentration areas. The panel was subjected to a central bending load and it was constrained on all four edges to represent a differential pressure load acting on a typical skin panel in an aircraft fuselage configuration.

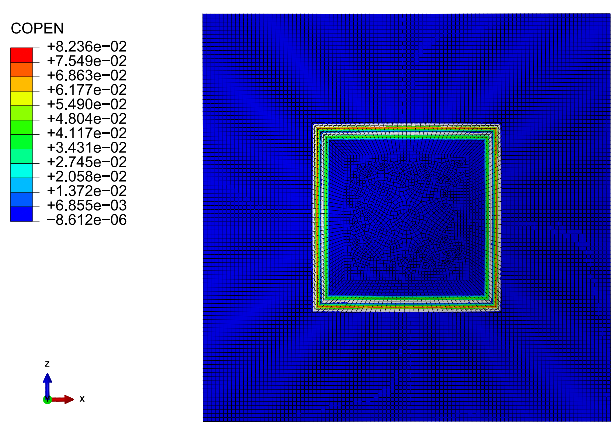

Figure 6.2: Abaqus model to show the opening loads on the taper (bottom view, only last ply showing

As can be expected, a crack opening load is present at the taper. Such an out-of-plane load case is not ideal for composite structures as it directly subjects the resin holding together the individual plies to high loads. In itself, this is a manageable scenario as expected by simple analytical calculations. However, considering that these loads are present in an area of concern from a manufacturing point of view, the superposition of both warrants additional measures.

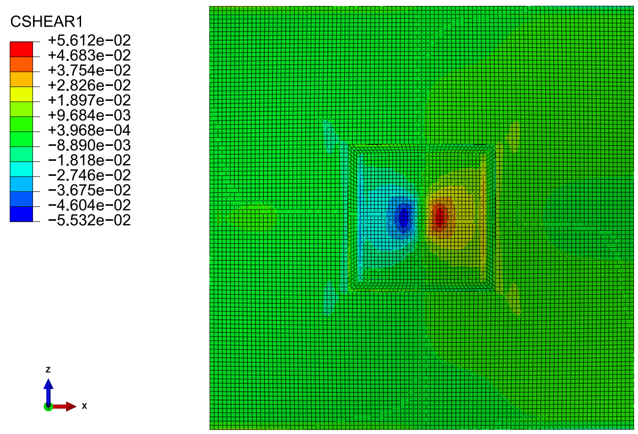

Figure 6.3: Abaqus model to show the shear loads on the taper (bottom view, first two plies removed)

The C/U-section stiffener was chosen as the second demonstrator since it represents the geometry widely used for aircraft frames or ribs. Those are essential structural elements in modern and legacy aircraft alike. They consist of two flanges separated by a web, joined together by two radius sections (ref. Figure 6.31). From a manufacturing point of view these simple structures are oftentimes produced using high-throughput processes like infusion, RTM or press molding. Using a press with die-matched tooling for consolidation and molding, typically brings up the challenge of selecting a suitable mold opening plane to foster proper consolidation (Figure 6.4a). This is owing to the fact that the flanges and the web are typically at normal angles to each-other which makes it hard to enforce consolidation pressure on the vertical faces. When using vacuum bagging based methods the consolidation of flat sections is less of an issue but the radius section can become tricky in both male and female tooled configurations (Figure 6.4b). A high fidelity PM tool would be beneficial for both of these configurations. Due to limitations around the available machinery the researcher had access to, the RIFT method using a vacuum bagging for resin infusion is used.

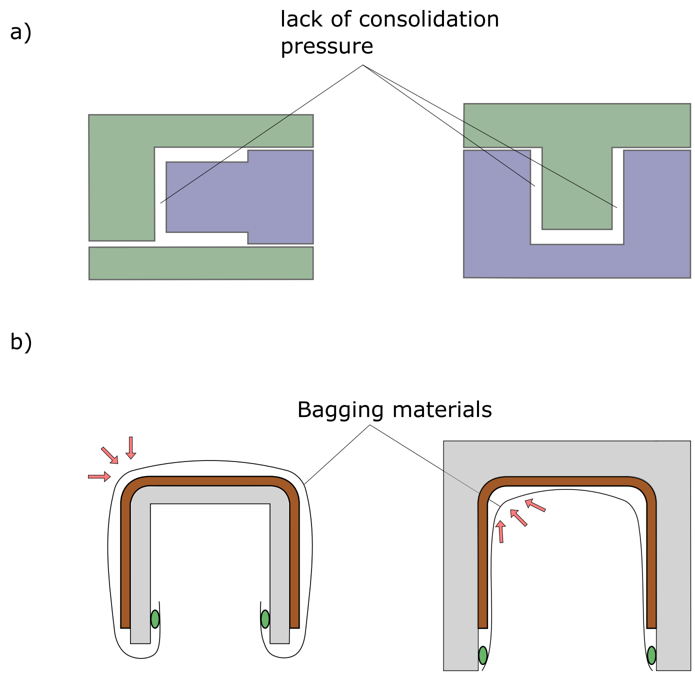

Figure 6.4: Geometrical challenges with stiffener consolidation. a) press molding b) vacuum bag consolidation.

With two representative demonstrators chosen: 1) the flat tapered panel manufactured by a closed mold process and 2) the C/U-profile manufactured by RIFT, the following sections will introduce the studies carried out in more detail. First, the manufacturing processes used will be described and the chosen monitoring methodology introduced. After discussing the manufacturing monitoring results, the planned SHM experiments are put forward. Together, the obtained PM and SHM datasets help in gauging the fidelity of the FOS-OBR technique for reasonably complex demonstrators.

6.2 Tapered panel (manufactured by VaRTM)

6.2.1 Process monitoring

6.2.1.1 Method

The taper was achieved through a combination of ply drops in the woven fabric and a 3D-printed die that fits the resulting recess and physically molds the depression. The taper with a 1:30 ratio (1 ply-drop over a length of 30 times the ply thickness) leaves a central square section of 150x150 mm with a thickness of 1 mm made up of 4 plies and a surrounding section with a thickness of 2 mm and made up of 8 plies. The 3D printed die was covered with non-porous Teflon® film to ensure easy demolding and secured in place onto the upper mold using polyimide tape.

6.2.1.2 Materials

The reinforcement fabric was a 2x2 Twill weave with 210g areal weight made up from 3k 'ProFinish' carbon fiber by Easy Composites Ltd (Stoke-on-Trent, UK). The ProFinish relates to a process of stabilization using an epoxy compatible binder. Binders are commonly used in industrial applications to ease manufacturing and was therefore included in this study as well. All plies were cut to shape using an automatic ply cutter and assembled in dry condition under clean room conditions. After stackup, the fabric was ready for the RTM process for which a Sicomin SR 8100:SD 8824 Epoxy system was mixed. It was prepared at a 100:22 ratio by weight and a Hypaject MK III – 6 liter injection unit by Magnum®Venus Products was used for injection. To ease resin flow the unit was preheated to 30°C.

6.2.1.3 Setup

As indicated in section 6.1 the taper with associated ply drops requires monitoring throughout the entire process (ODiSI B by Luna Inc., Blacksburg, VA, United States) to ensure good quality. In order to be able to compare the taper section with solid parallel sections the fiber needs to be routed such that a large area of both the 1 mm and 2 mm sections are covered sufficiently. Finally, when considering the future use as a SHM sensor, the fiber should capture as many different angles as possible to ensure a whole strain field can be computed. In Figure 6.5 the final layout is presented fulfilling all the above requirements.

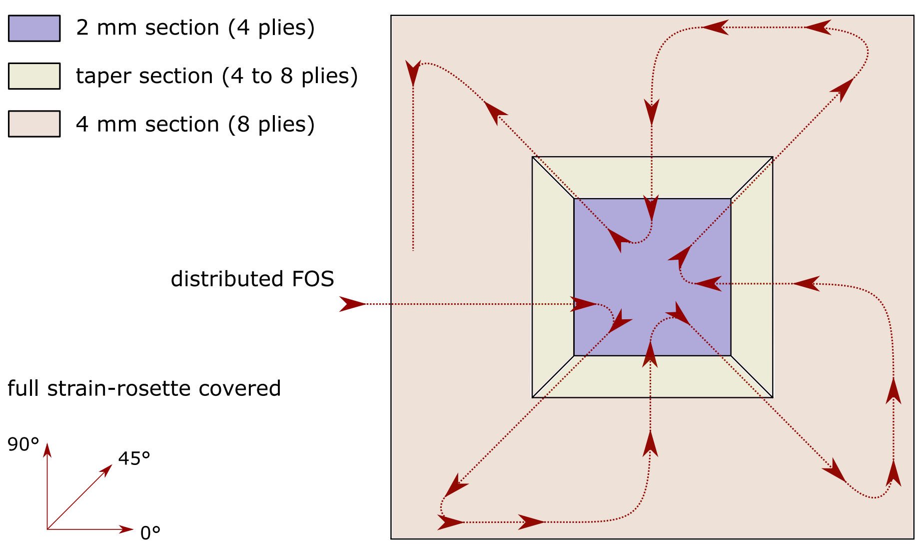

Figure 6.5: Layout of the FOS integrated on the top layer of the tapered RTM panel

The flat panel mold and overall setup as described in section 5.3.1 was used for the manufacture of the tapered panel. In addition, an in-mold pressure sensor (IMPS) with a range of 0 to 10 bar was fitted to the mold. The sensor is a ceramic ECT type and provides 0 to 10V output (EL-35-0029 by Composite Integration, Saltash UK). This allows the tracking of in mold vacuum and pressure at a specific location (see Figure 6.6a) and will serve as a reference for the FOS-OBR readings.

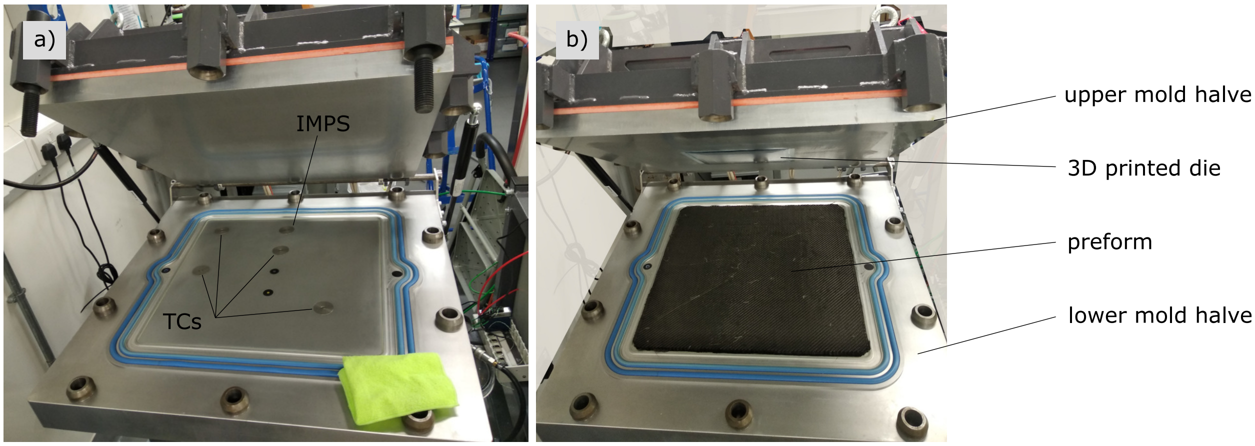

Figure 6.6: a) RTM mold with the TC and IMPS locations. b) Carbon fiber preform placed inside the RTM mold with the 3D printed die installed on the top mold halve.

To ensure that the FOS-OBR remains at it's intended location (ref. Figure 6.5), the fiber was stitched in place using a circular carpet needle and a Nylon thread (Figure 6.7). As the fiber was superficially placed on the preform it would be in contact with the upper mold halve once closed. This greatly helps with protecting the fiber during mold closure and throughout the manufacturing process as the solid and straight surface of the mold could act as a guide for the fiber and protect it from damage. Since the fiber diameter is small the two circular mold seals were able to form an air-tight mold closure without the loss of vacuum.

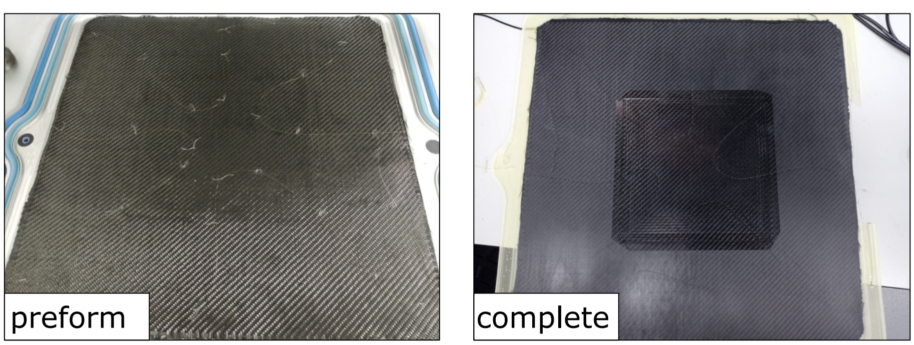

Figure 6.7: The preform with FOS-OBR stitched in place before and after the RTM process.

Figure 6.8 shows the true position of the FOS-OBR after manufacturing. The image was obtained through tracking of the visual fiber path on the SOLIDWORKS CAD package. It can be confirmed that the stitching indeed was able to hold the fiber in place throughout the process and knowledge about the actual poosition is useful for subsequent SHM usage of the FOS-OBR.

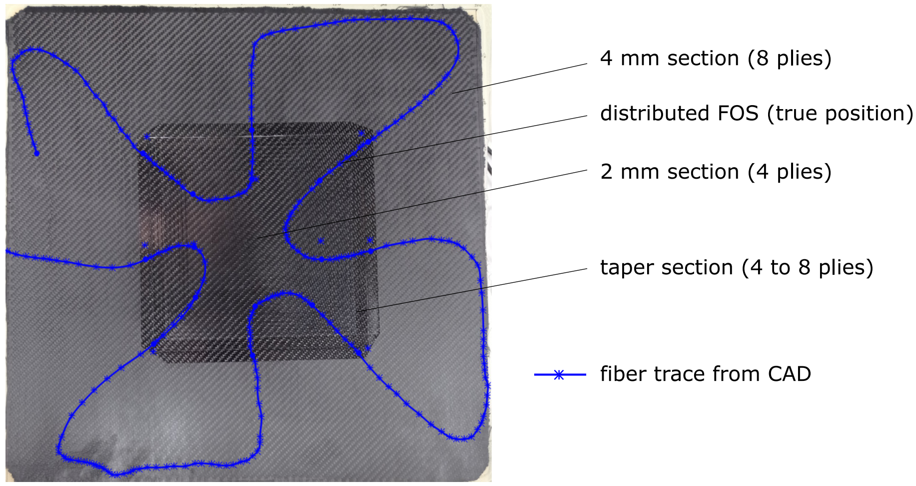

Figure 6.8: True fiber trace of the FOS-OBR after the RTM process used for sensor mapping for SHM.

6.2.1.4 Results

The entire VaRTM process was monitored for the whole time using three different sensors: 1) FOS-OBR, 2) the in-mold pressure sensor and 3) TCs. Figure 6.9 shows the measurements obtained using all three methods.

Overall the process steps are clearly identifiable from the readings of the different sensors. The first step is the manual closure of the mold and tightening of the bolts (Figure 5.9). This first step of the process is only visible in the FOS-OBR data and as discussed in chapter 5 is important for the quality of the manufactured panel.

Upon complete closure, the vacuum supply is switched on. This is clearly visible from the in-mold pressure readings. The pressure drops very sharply from atmospheric conditions down to a high quality vacuum. Again, the FOS-OBR sensor is able to pick up this change in the loading conditions within the preform and the drop in pressure is marked by a further decrease in the frequency shift.

After the full application of the vacuum the supply is switched off to test for the tightness of the setup. During that time, the injection resin was mixed. Over the course of 40 minutes the vacuum slowly dropped to 0.6 bar relative pressure. During this phase there is a intermittent gap in the FOS-OBR dataset. This was due to the fact that data-acquisition was stopped for around 20 minutes whilst preparing the resin for injection. However, the drop in pressure is clearly visible in the overall trend for that phase.

As the mold was considered sufficiently air tight, the vacuum supply was switched on again which can be seen from both in the in-mold pressure readings and the FOS-OBR. With a high quality vacuum present within the mold the setup was ready for resin injection.

The onset of the resin injection is marked by a steep increase of the in-mold pressure up to 3.5 bar, which corresponds to the target pressure set on the injection unit. The injection is also visible on the FOS-OBR, whilst the temperature remained relatively unchanged. This is important as it indicates that the temperature of the resin was similar to the one of the mold and any changes in the FOS-OBR were purely due to the resin injection commencing.

Once the mold was completely filled and the resin front reached the vacuum port in the mold, the injection unit was disconnected and the pressure began dropping again back to atmospheric pressure where it remained. Again, this process step is also clearly visible in the FOS-OBR data and the in-mold pressure sensor.

After waiting for just over an hour for the curing reaction to start naturally, the temperature of the mold was increased to above 35°C to accelerate the curing reaction and to understand the effect of raised temperature on the sensor's readings. As expected, the TCs and FOS-OBR show the increase in temperature clearly whilst the in-mold pressure sensor registers an intermittent peak. The cause for this peak could not be ascertained.

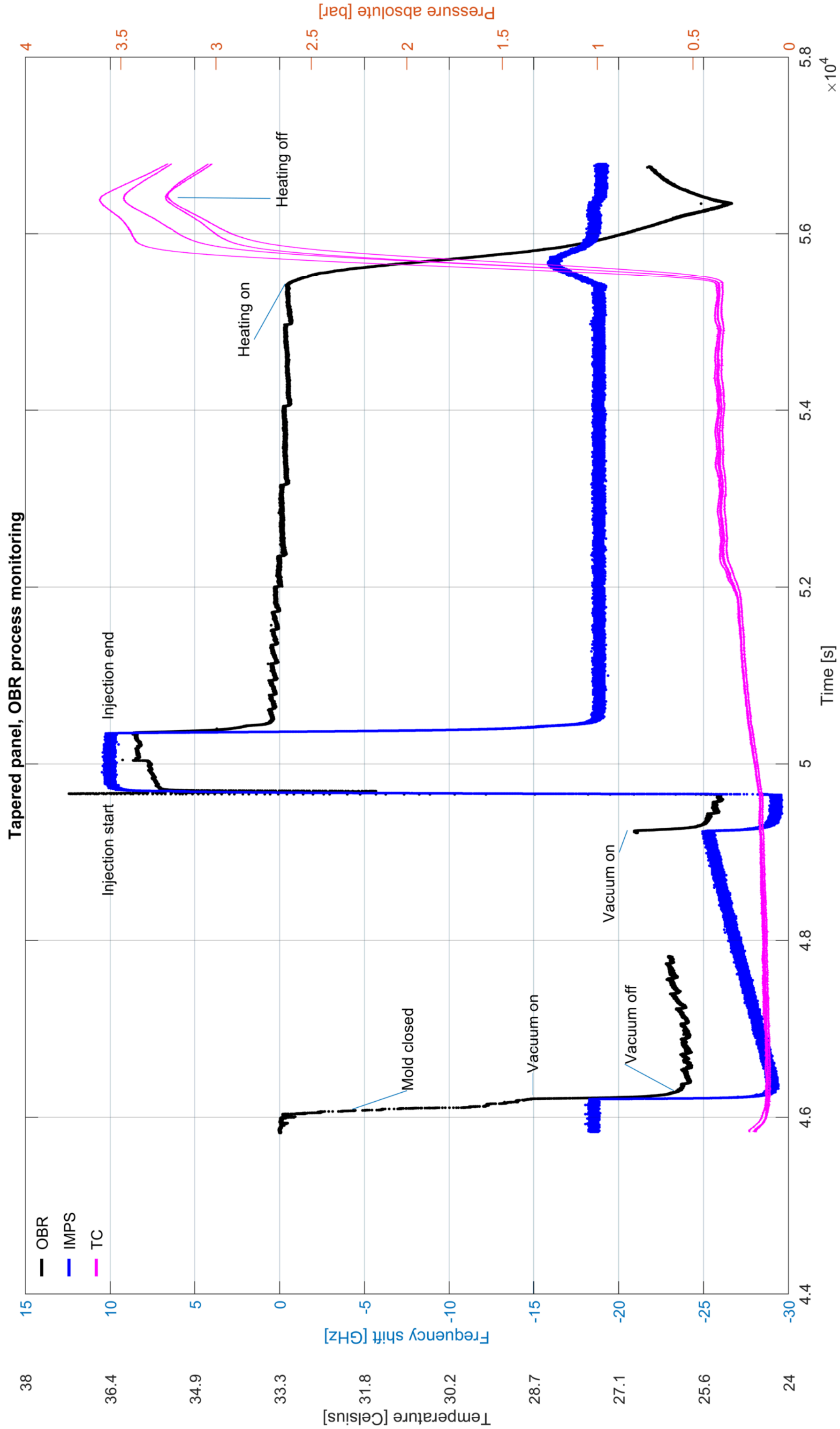

Figure 6.9: Entire PM measurement of the tapered RTM panel

Microsections were used to establish the intertow fiber volume fractions for the individual taper sections. Approximately 25 mm long pieces were cut from the panel at the desired locations (ref. Figure 6.12) and embedded in polyester mounting resin (KLEER-SET, Metprep Ltd., GB). The microscope pictures (Figure 6.10) were made using a Zeiss Axio Imager.M2m optical microscope.

To determine the area between individual fiber tows the image processing tool ImageJ [188] was used to analyse the microsections. First, a rectangular section of the image is selected and cropped. By choosing appropriate threshold values, the areas representing the tows can be split from the rest of the image (Figure 6.11 and the pixels counted that make up the tows. Subtracting the area of the tows from the total area gives the area taken up by the intertow resin. Finally dividing the intertow area by the total image area gives the fraction. This method admittedly is subjected to uncertainty. This uncertainty stems from the fact that a single cut surface is analyzed and used as a representative value for a larger area. Also the choice of threshold values is somewhat subjective. However, the method was deemed as appropriate for the given purpose.

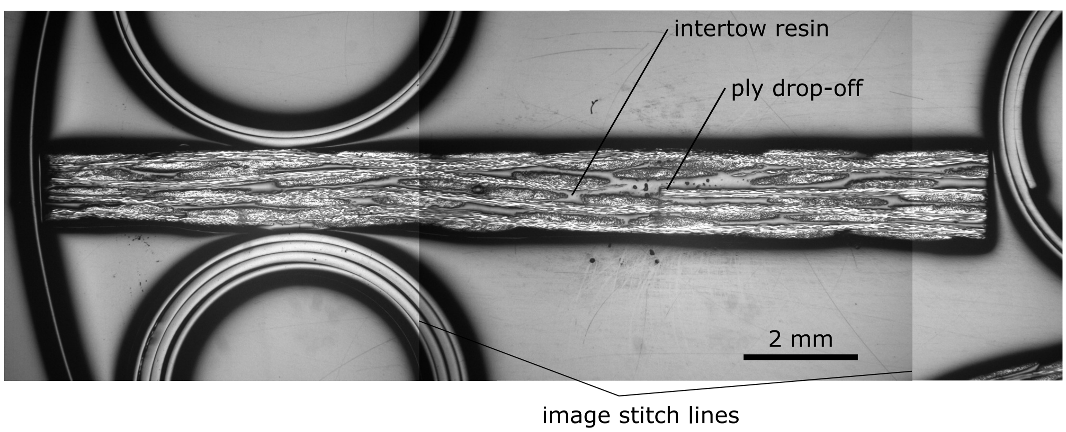

Figure 6.10: Microsection showing a taper section with the intertow resin and a ply drop-off marked.

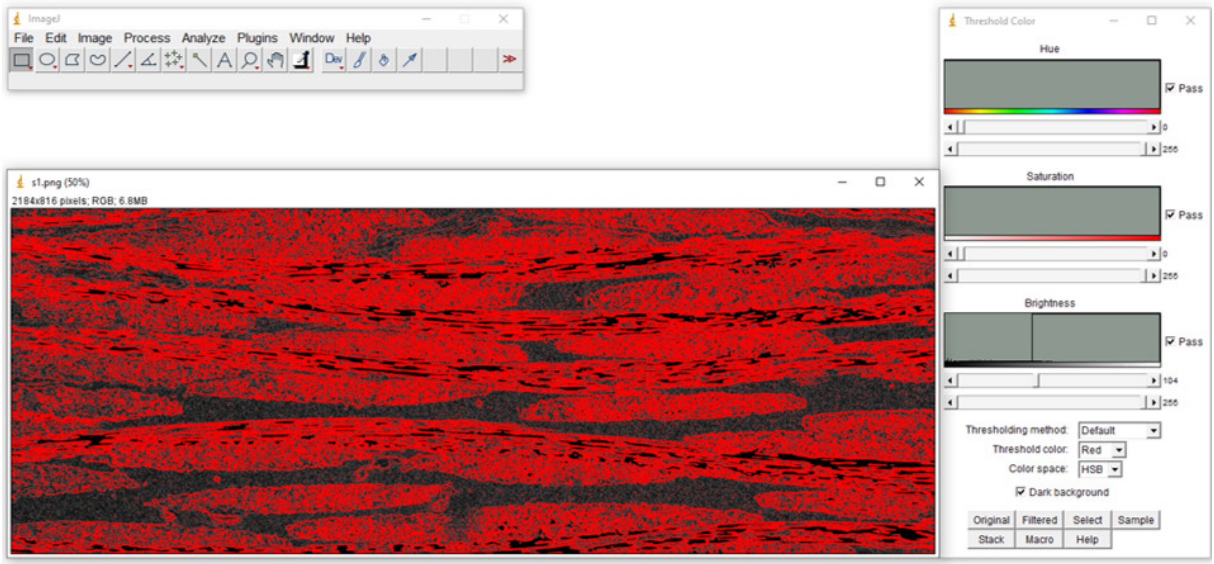

Figure 6.11: Determination of the intertow volume fraction using the ImageJ software [188].

In Figure 6.12 the individual sections are shown with the reported intertow resin fraction value. In total there are eight individual values, one for each taper section. The values range from 0.11 up to 0.19 indicating that between 11 and 19% of the image area was resin between the tows. Whilst a definitive explanation for these differences cannot be given with absolute certainty, it is likely that the die on the top mold-halve (ref. Figure 6.6) was not perfectly aligned with the corresponding ply drop-offs in the preform. Such an instance is very common in manual layup processes where slight angle deviations occur and are considered already at the component design stage.

With the die not perfectly aligned with the recess on the preform resulting from the internal ply drop-off, different levels of compaction can be expected. The higher the level of compaction, the less space is available between tows for resin to occupy and vice-versa. Having established this relationship previously in chapter 5, it is expected that the FOS-OBR integrated on the top layer would be able to give insights into the actual pressure conditions within the tapered sections.

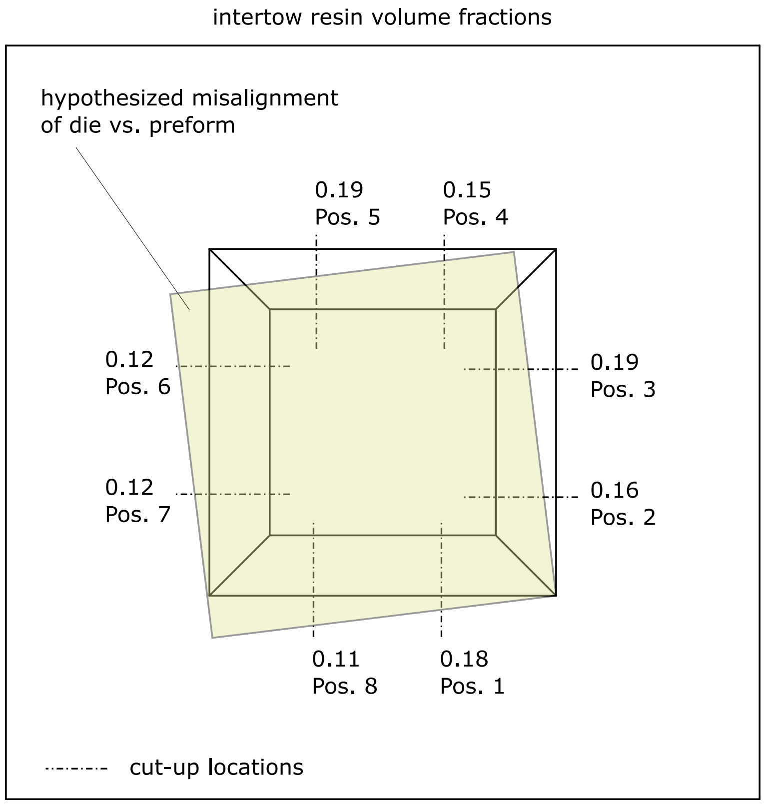

Figure 6.12: Location of microsections performed with corresponding intertow volume fractions. One possible root cause for differences observed is the misalignment of the die with the preform (shown exaggerated in above figure).

The relationship between frequency shift and intertow volume fraction is shown in Figure 6.13. Here the measured frequency shift is averaged for the length of FOS-OBR that covers the width of the taper and plotted against the nearest available volume fraction value. A general tendency for a linear relationship can be seen. This is as expected considering the results obtained in chapter 5.

However, the level of error is higher for the tapered area than it is for the flat panel. An increased level of error is somewhat conceivable and expected considering the general higher level of complexity and localized effects on pressure distribution. Further studies will be required to better understand the root cause for the higher levels of error. Nonetheless, the ability to predict the amount of resin in a taper section is a very useful tool.

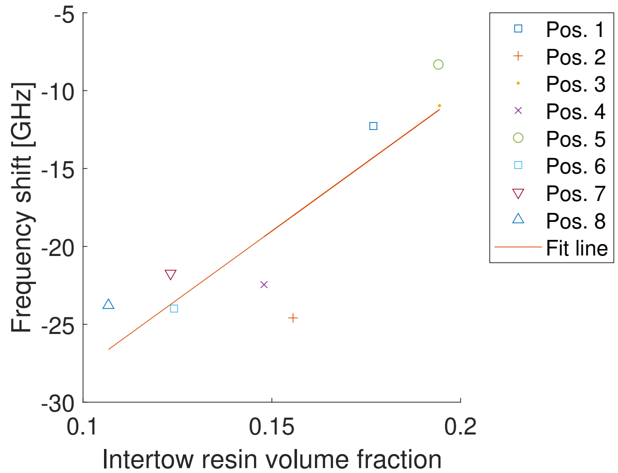

Figure 6.13: Frequency shift vs. intertow fiber volume fraction for the taper sections.

6.2.2 Structural health monitoring

To demonstrate the ability of the FOS-OBR to monitor the structural health of the manufactured tapered panel a set of experiments was carried out. They were aimed at simulating load conditions an aircraft component would be subjected to throughout its life. This includes static loads and impact loads. For both types of load scenarios a wooden frame was constructed to support the panel at its edge. The overall dimensions of the panel were 500x500 mm and the panel was supported over a 50 mm wide section all around leaving a 400x400 mm section unsupported at the centre. The static loads were simulated by adding masses at the centre of the panel leading it to bend.

The impacts were focused on the tapered section since this was an area of particular interest. In Figure 6.14 the panel is shown supported on the wooden frame with the tapered section pointing downwards. The circular artefacts visible on the panel surface are caused by imprint from TCs and the in-mold pressure sensor.

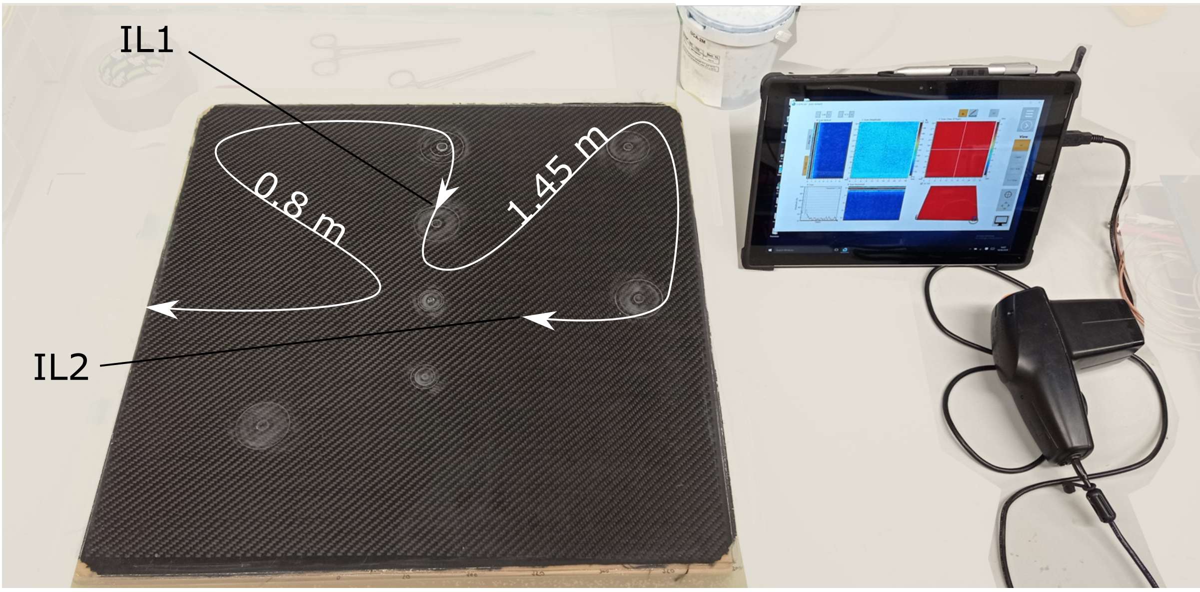

Figure 6.14: Tapered panel ready for testing, supported on a wooden frame. The white line indicates the pathlength of the integrated FOS-OBR. IL1 and IL2 indicate the impact locations.

6.2.2.1 Experimental setup

The supported panel with its integrated FOS-OBR was monitored throughout the experiments. For the static tests, the fiber was connected to the ODiSI B interrogator and data acquisition system (by Luna Inc., Blacksburg, VA, United States) and interrogated at 10 Hz.

For dynamic impact monitoring the interrogation frequency was set to 100 Hz.

To establish whether any damage was caused to the panel and for reference purposes, a DOLPHICAM (dolphitech UK, Cambridge, UK) ultrasonic scanning device was used. The DOLPHICAM offers A, B and C-scan capability and in Figure 6.15 a stitched scan image of the entire tapered panel can be seen before impact. The tapers are clearly visible, manifested through their difference in panel thickness. Since the scanning is a manual process the stitched images are at times slightly angular which does not affect the overall NDI capability.

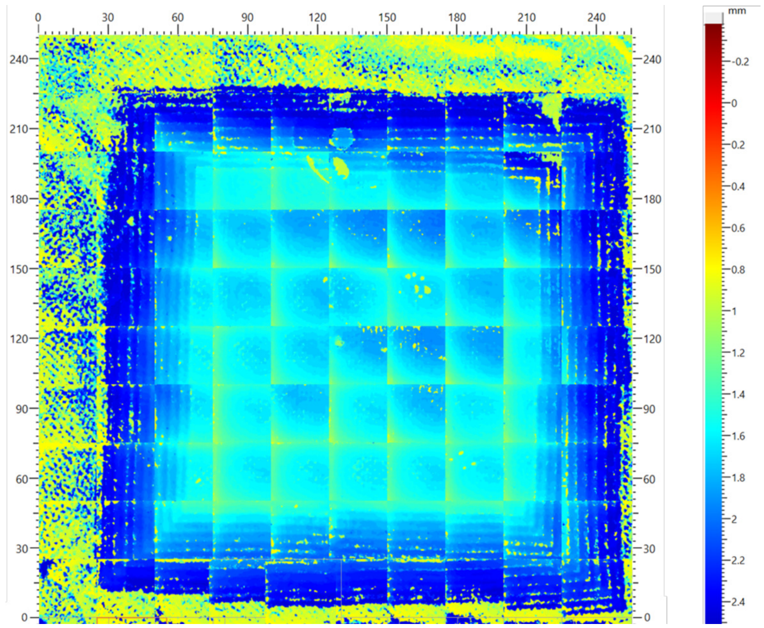

Figure 6.15: C-Scan (amplitude) of the tapered panel in pristine condition.

Similar to the integrity check performed with the DOLPHICAM, a pristine measurement of the FOS-OBR spectrum was carried out. Whilst this does not provide a live and continuous insight, the spectrum holds information about the integrity of the sensor and its reflectivity. In Figure 6.16 the entire spectrum is shown with the integrated section characterised through a wave-pattern. Figure 6.17 is a zoomed-in view of the same spectrum.

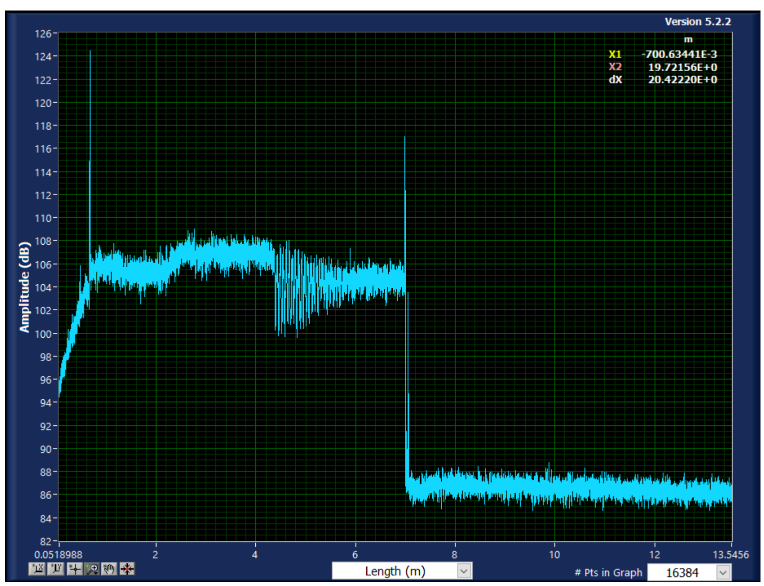

Figure 6.16: FOS-OBR spectrum of tapered RTM panel

The pronounced wave-like pattern (Figure 6.17) is an artefact of waviness of the integrated fiber. Such waviness may originate from the ply drop-off sections as well as from the weave pattern of the fabric. They lead to reflections within the distributed-FOS and where light bounces back and forth. Such artefacts negatively impact the measurement capability of the OBR system. Possible implications of this condition are: in-stable baselines, fluctuations and loss of signal over large parts of the sensor. As far as could be ascertained within this work, the major cause for the difficulties during measurement arise from the peak-matching algorithm within the OBR software. As signals are still received for sections on either side of the missing part (see Figure 6.18), this suggests the wave guide is still intact. A cause not related to the physical measurements itself is suspected for the low measurement fidelity. However, despite the difficulties during measurements, the dataset obtained still was able to reveal useful SHM data when passed through a five-sample moving average smoothing operation (Figure 6.18).

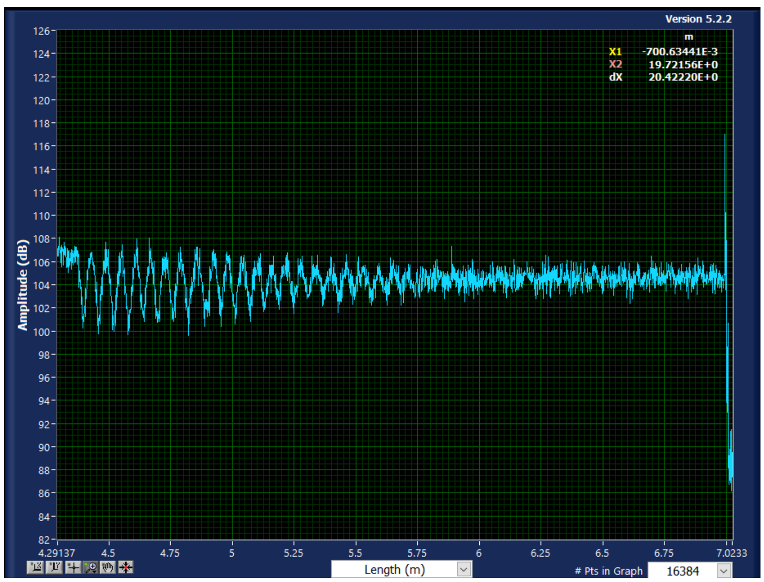

Figure 6.17: FOS-OBR spectrum of tapered RTM panel zoomed-in on the integrated section.

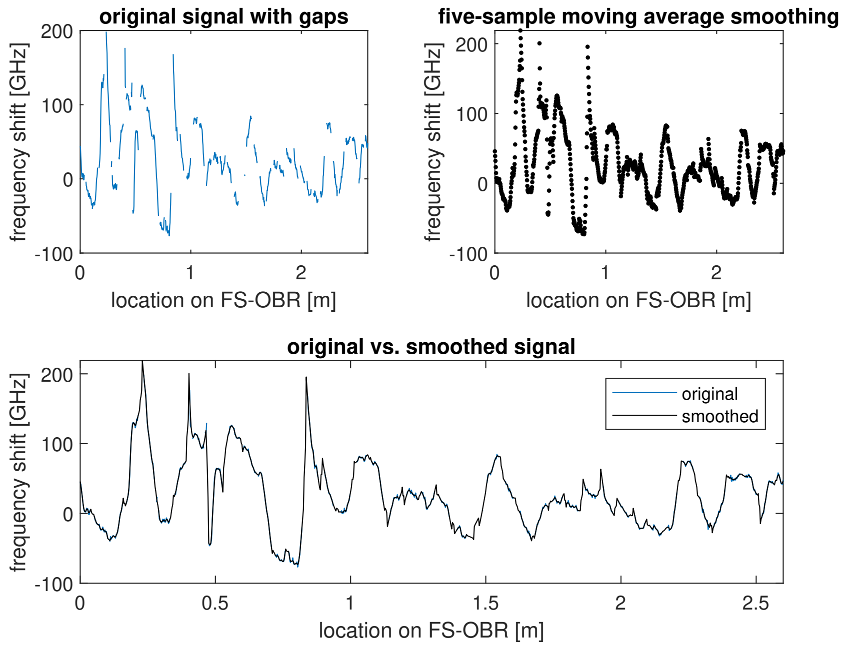

Figure 6.18: A sample FOS-OBR measurement obtained during an impact at IL1 showing the original signal with gaps, the smoothed signal using a five-sample moving average and both of them overlaid.

6.2.2.2 Static load monitoring

Static, or quasi-static loads occur in structures during their regular and intended use. For an aircraft those are e.g. pressurization of the cabin, cruise flight loads, on-ground loads due to the lack of lift on the wing, etc. To show what insights an integrated FOS-OBR can provide, a set of five non-damaging loading and unloading cycles are carried out.

The tapered panel was resting on the wooden frame (see Figure 6.14) and weights were added to the central part of the panel, where its thickness is lowest (comparable to the simulated load case in section 6.1). Three different weights (0.9 N, 2.7 N and 25 N) were applied in ascending order (0.9 N to 25 N) and then again in descending order (25 N down to 0.9 N) yielding five measurements.

Figure 6.19 shows the obtained average frequency shift (averaged over the entire panel surface). The five distinct regions away from the baseline correspond to the loading cycles. Besides a linear increase in average frequency shift with increasing load (see also Figure 6.20) a slight long term baseline shift can be observed. The LUNA ODiSI B's handbook mentions a temperature gradient as a possible root cause for this slight, highly linear shift. As established earlier (see section 4.3.3.3) embedded FOS-OBR are sensitive to changes in panel temperature. This can be compensated for by establishing a temperature compensation method (ref. section 2.4.3.3).

Overall, static loads are clearly and reliably captured qualitatively and quantitatively by the integrated

FOS-OBR. This feature could be used for strain-based damage detection methods (section 2.2.1).

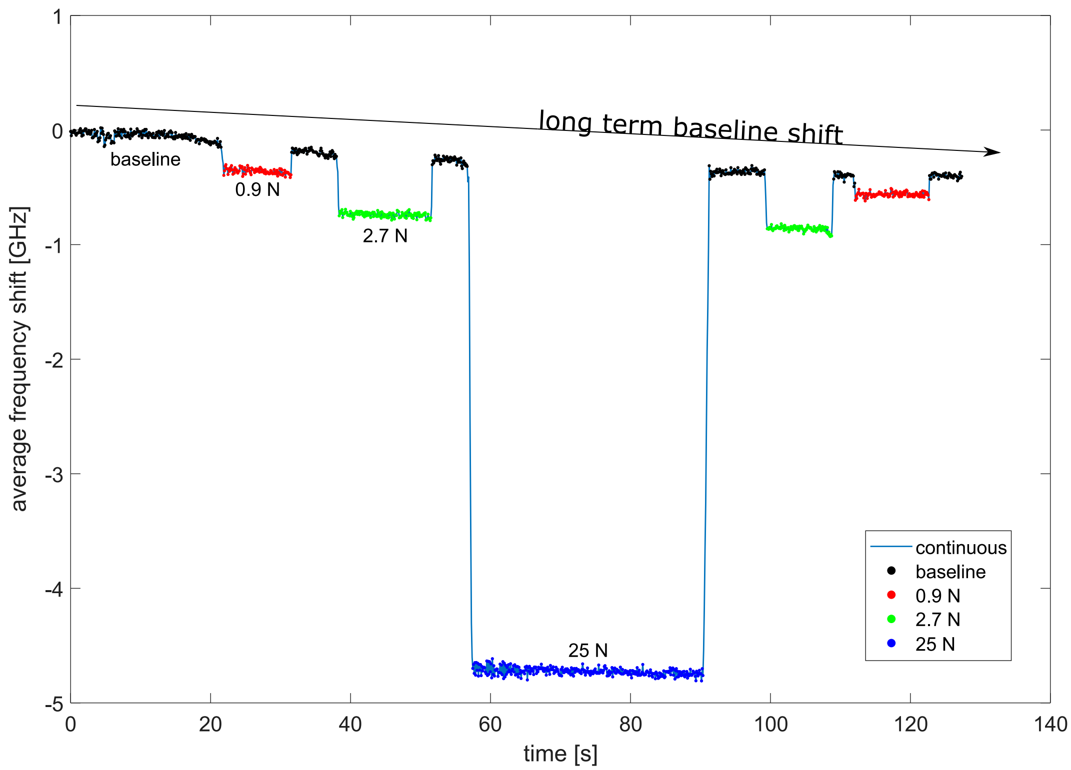

Figure 6.19: FOS-OBR static load monitoring.

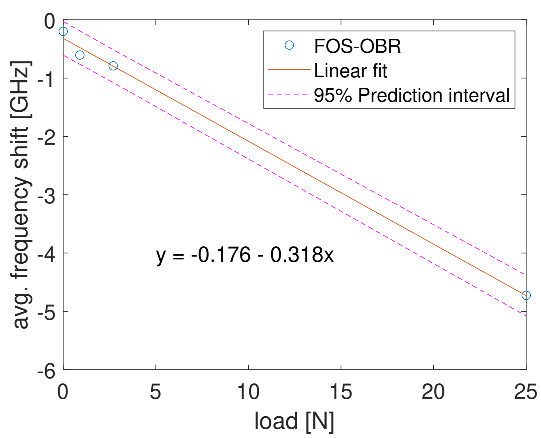

Figure 6.20: FOS-OBR static load monitoring - linear fit.

When considering a reading taken whilst the panel was loaded with 25N (see Figure 6.21) one can identify repeatable features within the data. These can be directly linked to the local FOS routing. The large positive peaks are related to the relatively sharp bends occurring at the centre of the tapered panel, whilst the wider peak sections are the peripheral bend areas. Besides the spatial information from the FOS-OBR system itself, these data features can be used to locate and contextualize any measurement obtained.

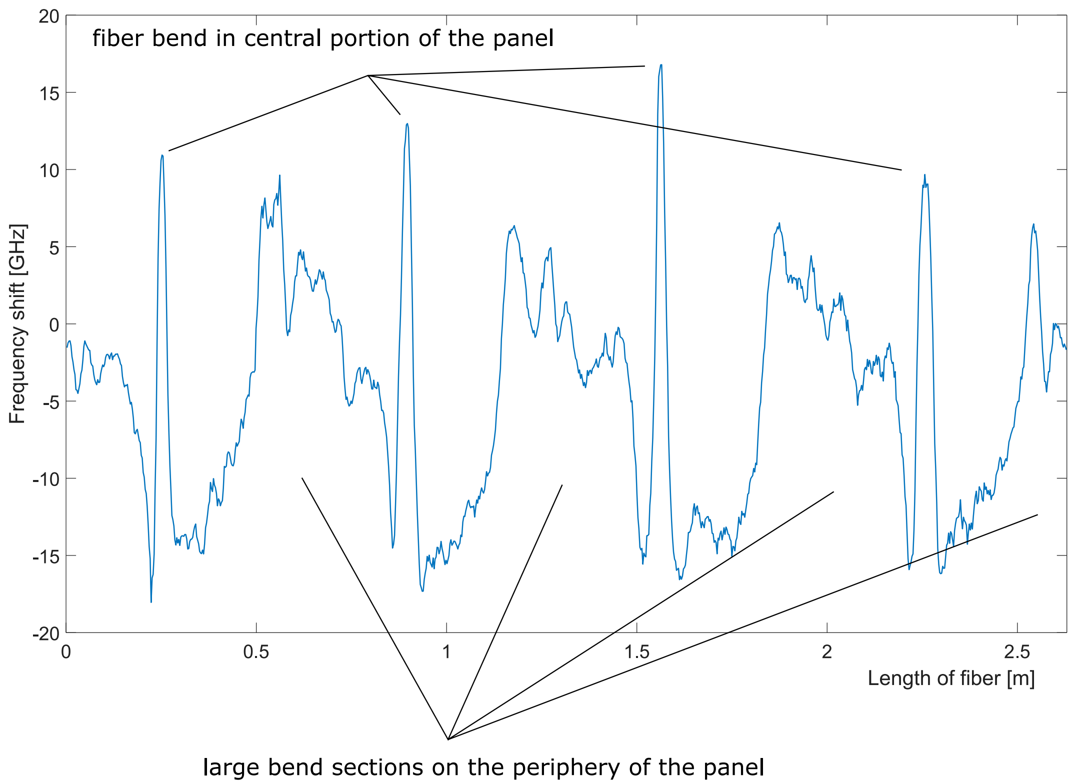

Figure 6.21: Frequency shift plotted along the length of the embedded fiber whilst loaded with 25N. Refer Figure 6.8 for orientation.

6.2.2.3 Impact damage creation

Despite their detrimental effects on structures, impact events occur relatively frequently in the life of aircraft and a good understanding about the effect they have is crucial. Lab testing methods make use of an impactor that hits the structure with a defined weight and velocity. In this case, a mass of 2.6 kg was dropped from a height of 815 mm and guided by a pipe to ensure control over the impact location. The part of the impactor that hit the panel had a pointy tip with a radius of 10 mm.

In total two impacts were performed at the locations shown in Figure 6.14. After every impact, C-Scans were performed to evidence any damage that occurred on the panel. In both cases the impact location was visually detectable (Figure 6.22) indicating the energy level was above the level one would expect to see for BVID events. However, the goal for this study was to understand whether impact events can be successfully detected with the integrated fiber.

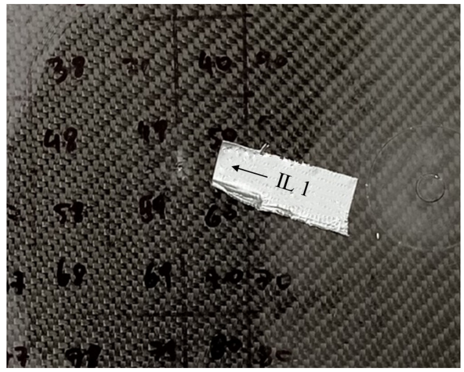

Figure 6.22: Visible impact damage at the first impact location.

6.2.2.4 DOLPHICAM damage assessment

Figure 6.23 and 6.24 show the amplitude and Time of flight (ToF) results obtained by the DOLPHICAM for the first impact. A cross-shaped damage pattern is visible following the 0/90° fiber angle of the woven carbon-fiber fabric used to manufacture the panel. What is important to note is that the damage is much larger on the DOLPHICAM images than it is visually. This is a major issue and typical for composites as it means even if damages appear small, they could be much larger within the laminate.

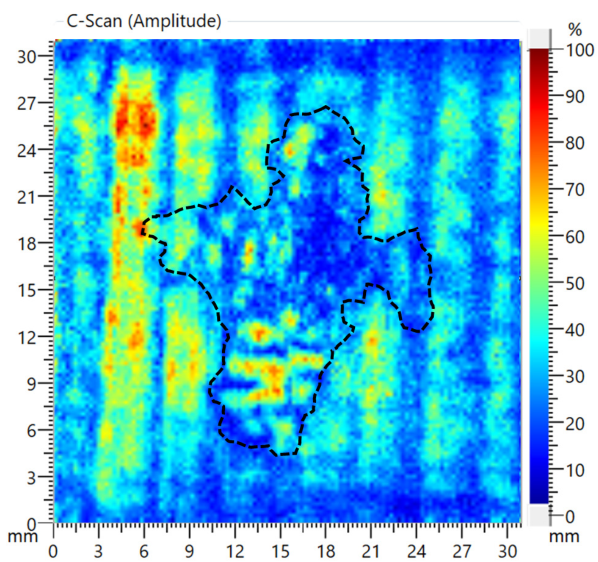

Figure 6.23: DOLPHICAM amplitude C-Scan image of the first impact location.

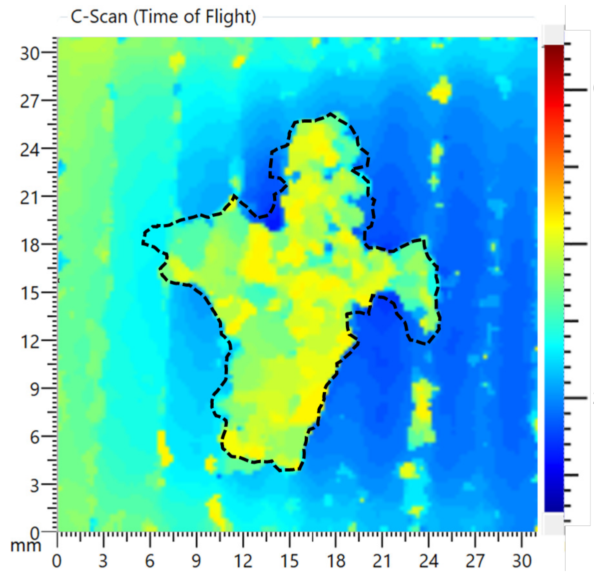

Figure 6.24: DOLPHICAM ToF C-Scan image of the first impact location.

Figure 6.25 and 6.26 show the damage resulting from the second impact. Whilst the impactor had the same mass and was dropped from the same height as the first impact, the resulting damage is much larger. In this instance the panel was physically damaged such that the laminate completely broke and one could see light passing through the crack from one side of the panel to the other.

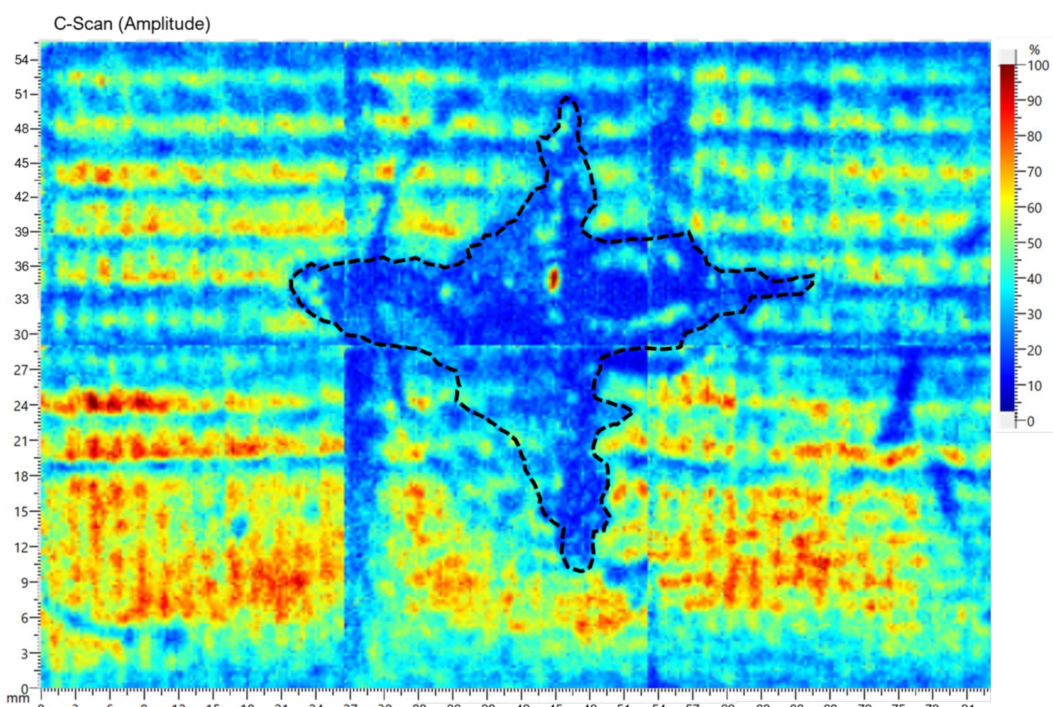

Figure 6.25: DOLPHICAM amplitude C-Scan image of the second impact location.

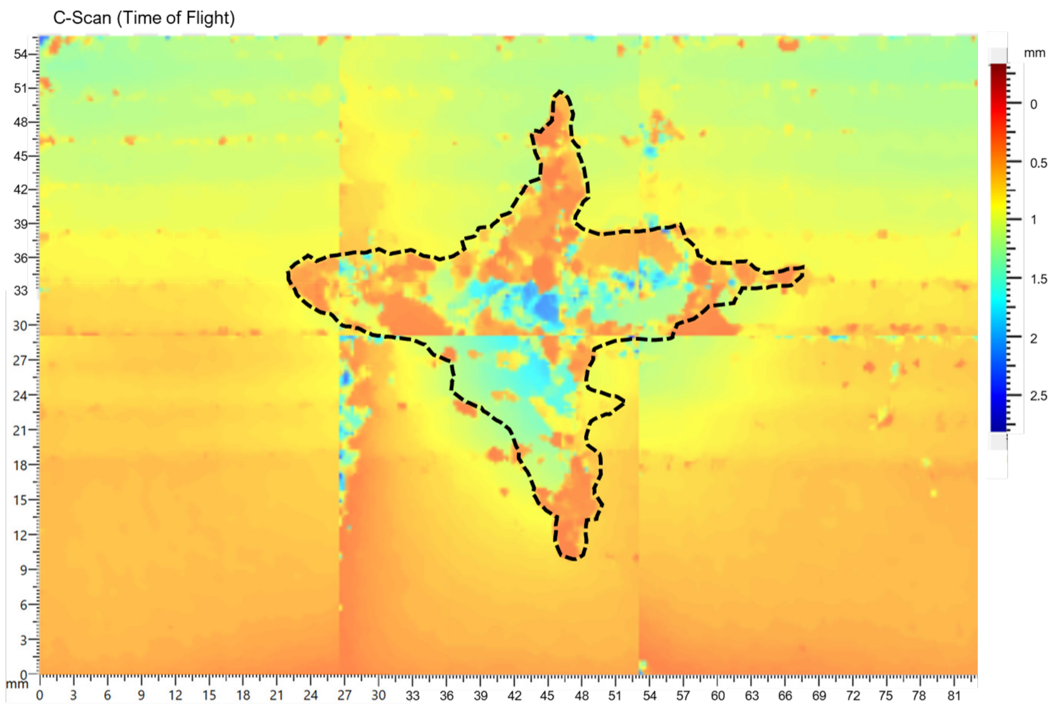

Figure 6.26: DOLPHICAM ToF C-Scan image of the second impact location.

6.2.2.5 FOS-OBR strain-based impact detection method

Strain-based SHM methods have been described in section 2.2.1. In the current setup it is expected that the presence of damage will locally affect the strain field that is measured on the FOS-OBR [77].

The LUNA ODiSI-B interrogator was connected to the integrated FOS-OBR and used to monitor the impact events at a maximum acquisition rate of 100 Hz. In Figure 6.27 the frequency shift is plotted for the entire length of the integrated FOS-OBR. The data included reflects three timestamps: 0.4 s and 0.2 s prior to the impact and one selected exactly in the instance the impact event occurred. The data at timestamps before the impact serves as a reference state to compare against. It can be seen that there is not any discernable difference between them, confirming their usefulness as reference data.

Considering the readings obtained at the time of the impact, a large negative peak can be observed just before 1.5 m of FOS-OBR. This point coincides perfectly with the impact location (Figure 6.14) and clearly indicates that an impact had occurred.

Whilst it is useful to detect an impact event as it happened, it may sometimes be the case that this moment is not directly captured. This may be due to a lower acquisition rate being used or the inspection of certain areas is performed only periodically and not concurrently. In such a case, the presence of a significant damage should be found as well. For this purpose the measurements presented in Figure 6.28 are included. As before, the graph shows the frequency shift plotted against the integrated length of the FOS-OBR. Again, two timestamps are shown: 1) several minutes before the impact and 2) several minutes after the impact event had occurred.

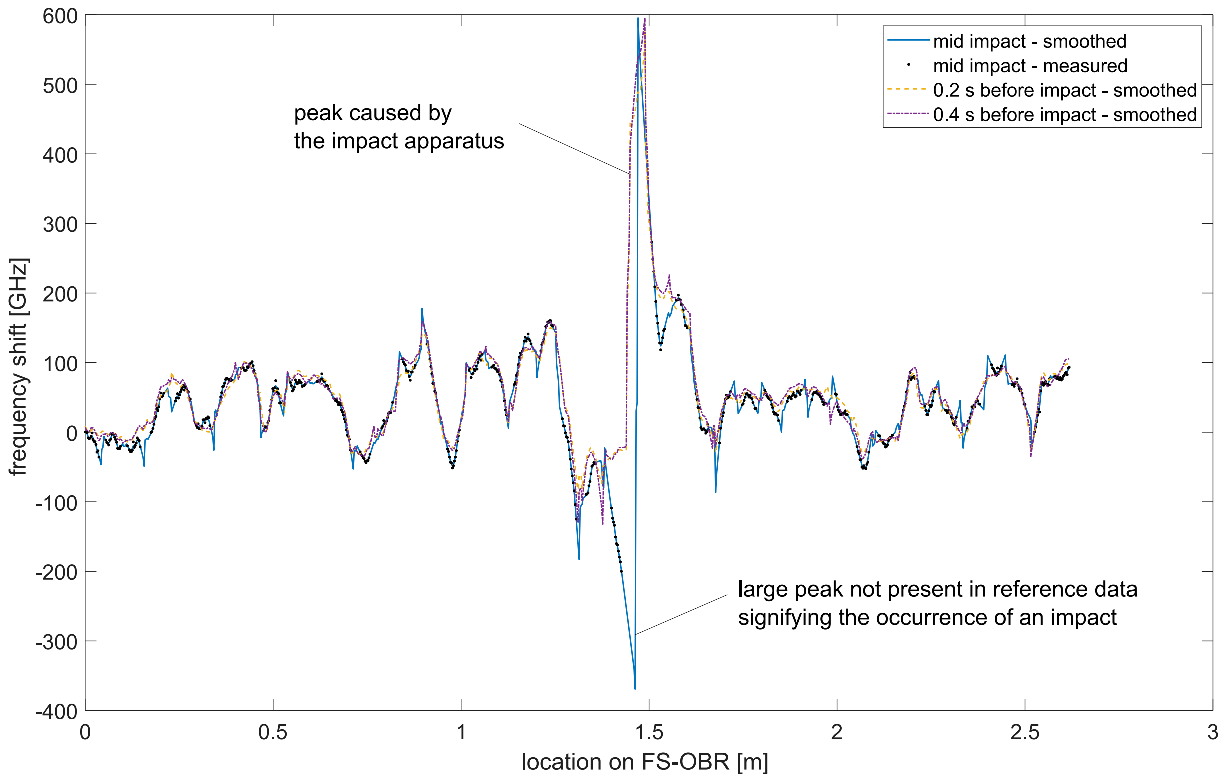

Figure 6.27: Frequency shift response obtained at IL1 during the impact event and immediately prior to it.

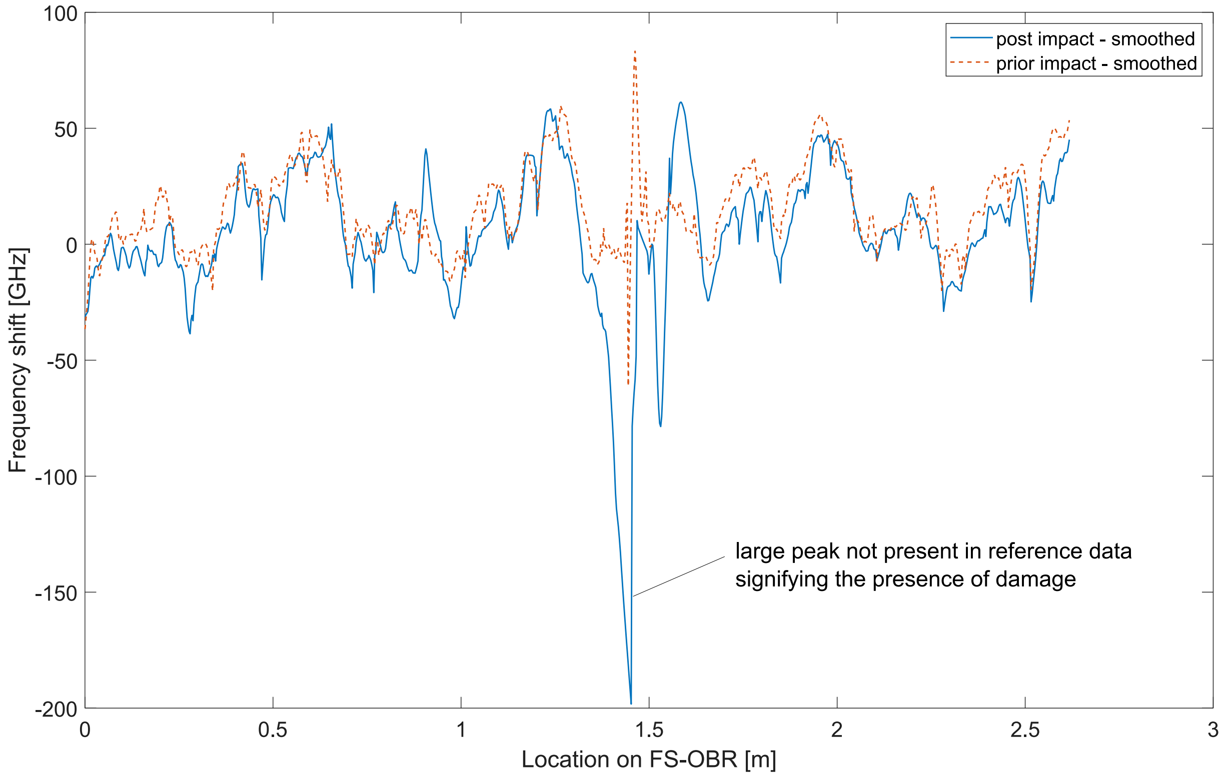

Figure 6.28: Post-impact permanent strain profile change as a result of the impact damage at IL1.

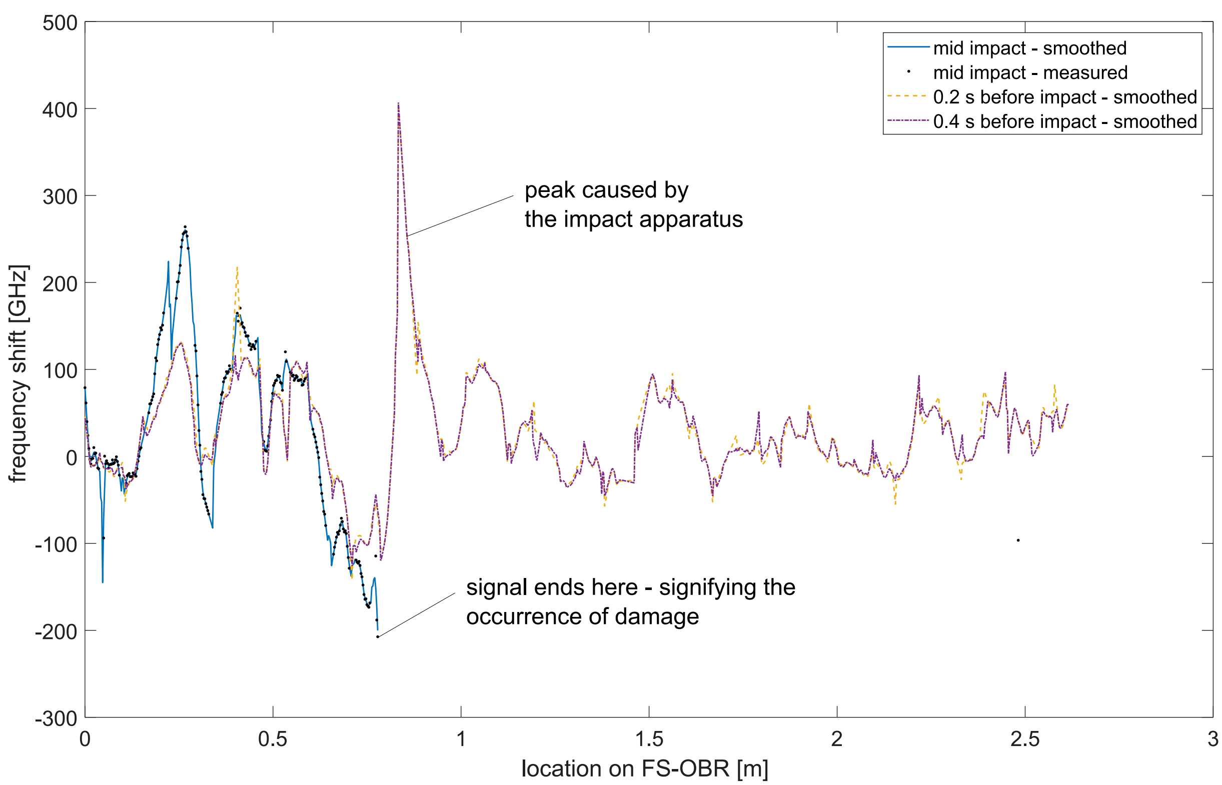

Figure 6.29: Frequency shift response obtained at IL2 during the impact event and immediately prior to it.

At a length of roughly 1.45 m a large negative peak accompanied by a smaller, second negative peak at 1.55 m mark the location of the impact clearly. When comparing the data to the pristine state before the impact, a clear distinction is possible and the presence of damage can be confirmed. Again, when comparing the position with the FOS-OBR layout in Figure 6.14 a very precise defect localization is enabled.
Analyzing the data collected at IL2, a rather similar result was obtained. Figure 6.29 shows the dynamic response with measurements taken 0.4 s and 0.2 s before the impact and one set whilst the impact occurred. As discussed earlier (Section 6.2.2.6) the second impact lead to fiber breakage and therefore the dataset obtained during the impact, has no more data after roughly 0.8 m of integrated path length.
The fact that no more data can be collected beyond a certain point is a clear indication of a major damage event. When considering the FOS-OBR layout in Figure 6.14 the predicted damage location again perfectly coincides with IL2's actual location. This once more confirms the excellent damage detection and localization ability of this monitoring system.
A suggestion to make for a future implementation would be to route the fiber in and out of the component to be monitored. This is in opposition to terminating the fiber inside the component as done here. With a free fiber end at the fiber ingress and egress gives access to the embedded part of the fiber from two sides. Having two fiber ends would then allow the interrogation of both parts individually should a fiber break occur within the panel as a result of damage. Referring to the method described above (see Figure 6.28), where the permanent post impact strains are used to confirm damage, that method could aid in distinguishing between actual structural damage and damage only to the FOS-OBR.

Important remarks: The data in Figures 6.27, 6.28 and 6.29 has been smoothed with a five sample window moving average wherever indicated. This was necessary to calculate missing values caused by fluctuations (Figure 6.17). Both in Figures 6.27 and 6.29 a large positive peak is visible near the impact location. This is due to the impact apparatus resting on the panel and causing it to bend slightly.

6.2.2.6 FOS-OBR spectrum-based impact detection method

Besides establishing a damaging impact based on the FOS-OBR strain profile, the integrated fiber can also be used to analyse the spectrum. Figure 6.30 shows the spectrum of the same integrated distributed-FOS as in Figure 6.16 after the tapered panel had sustained an impact causing catastrophic damage (Impact 2). During that damage event the fiber was broken with parts of the fiber no longer connected to the OBR system. What is remarkable, however, is the ability of the intact piece of fiber to still produce useful information. Firstly, as can be seen from the difference in overall length of the fiber, the location of fiber breakage can be clearly established. As the path of the fiber is known and mapped the location of the newly "terminated" fiber gives a precise damage location (see Figure 6.14).

Secondly, the intact fiber can still be used as a monitoring device and therefore provide useful insights into the progression of the now present damage to the panel. To the knowledge of the author, such a capability has not yet been reported for OBR-based SHM systems. This is significant as most other monitoring systems would immediately fail in the case of a broken link to the sensor. However, given the distributed nature of OBR strain monitoring, the entire fiber acts as a sensor and thereby enables the above mentioned capability.

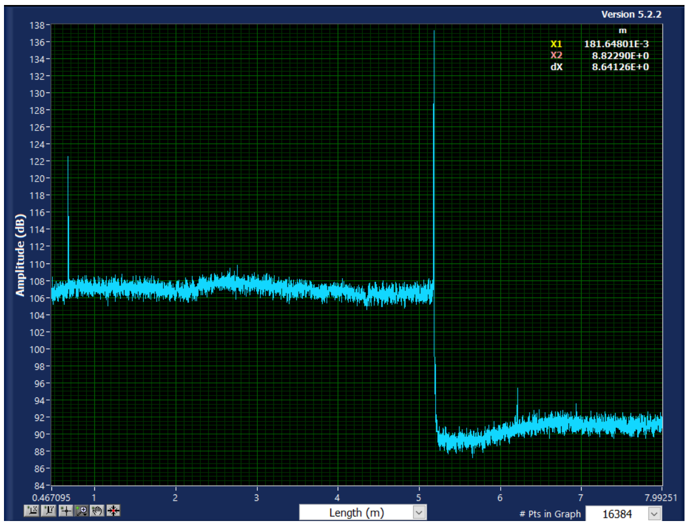

Figure 6.30: FOS-OBR spectrum of tapered RTM panel after the large mass impact.

6.3 U-beam resin infusion

One major benefit of composites is the ability to directly mold complex three-dimensional structures without the need for secondary forming. This allows for integral components, i.e. reduced part count. Additionally, plate-like components are frequently reinforced using stiffeners. Such stiffeners come in different shapes with the most frequently used being C/U-,Z- and Omega-profiles. The stiffeners and reinforced plates are typically produced separately and later on bonded or riveted together. Given the importance of such structural elements in aircraft construction and challenges of their manufacturing (e.g. porosity, resin dry areas in particular in curved corners), the second demonstrator considered in this research is a C/U-section profile which is manufactured and monitored with the proposed PM-SHM system.

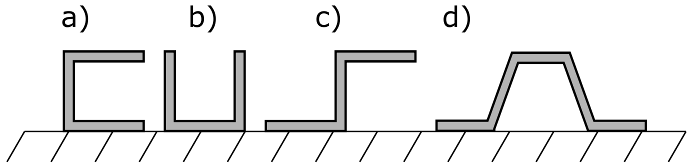

Figure 6.31: Comparison of typical stiffener shapes: a) C-profile, b) U-profile, c) Z-profile, d) Omega-profile

To manufacture such a stiffener it is required to choose a molding process that is capable of delivering the chosen shape and allow for vacuum application and resin wet-out. Both RTM and resin infusion processes are able to deliver those prerequisites. However, given the complexity of an RTM mold and associated costs and lead-times, the classical RIFT was chosen. The next sections provide more detail on the setup and work undertaken.

6.3.1 Method

An aluminium mold was first manufactured using an off-the-shelf U-profile. This was machined using a radial end-mill to shape two 6 mm radius fillets. These are required to allow the material to drape around the corners and avoid fiber damage. The entire mold is 1.4 m in length out of which 1.2 m are usable for manufacturing. Before every molding cycle a coat of mold release (227CEE, Marbocote Ltd.) is applied to the aluminium surface to allow easy demolding after the resin has cured and the stiffener is completed. The FOS-OBR sensor is applied directly to the mold using small drops of UV curing adhesive (UV683, Permabond). This secures the fiber and ensures a small pre-tension. Four layers of four-harness satin woven glass fiber fabric are laid up on the mold and FOS in a 0/90 sequence is applied. The entire stack is covered with one layer of peel-ply and flow medium each. In the final step before infusion a vacuum bag is constructed around all the above.

The vacuum bagging for resin infusion in general and when PM in particular requires specific attention. As indicated in Section 5.1.2 the pressure acting on the fabric stack has a significant impact on the quality and mechanical properties of the final composite. Additionally, it plays a major role in driving the resin through the porous fiber bed to wet out the fabric and form the matrix holding the reinforcement in place. It is therefore important to achieve a properly sealed vacuum bag before commencing with infusion. The FOS sensor, however, requires connection to the LUNA data acquisition system and therefore needs to lead through the vacuum bag in a way that neither affects the vacuum levels inside the bag, nor causes damage to the FOS. This was solved by applying a strip of polyimide tape on the FOS. The tape holds the fiber in place, guides it along the mold and by firmly pressing it down onto the fiber sideways ensures that there is no air-way. The tape also fulfills a fourth goal, namely protecting the fiber from getting stuck on the tacky tape and risking damage to the FOS during removal of the vacuum bag and sensor cable retrieval.

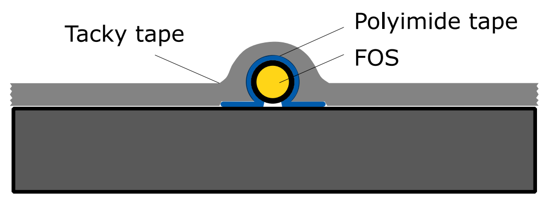

Figure 6.32: FOS vacuum bagging egress

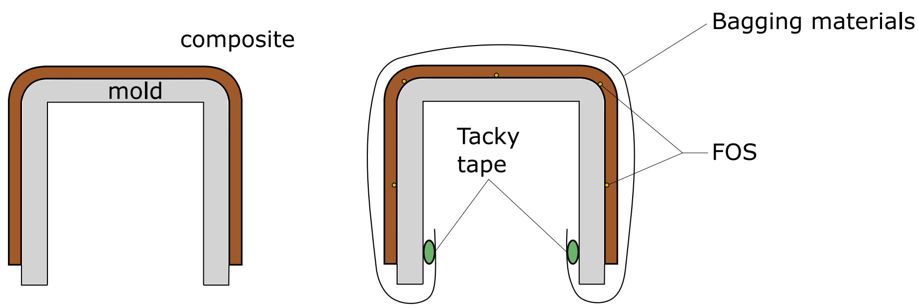

Figure 6.33: Cross section of the stiffener mold showing FOS location and vacuum bagging strategy

6.3.2 Process monitoring

In an initial production run, weaknesses of the manufacturing technique and geometry are revealed and a suitable monitoring technique is chosen. Figure 6.34 highlights the main problems occurring in the radius. Two main types of errors are observed: porosity and dry spots due to lack of resin. This means that any monitoring technology used needs to allow for presence in the radius section (Figure 6.35). Due to its flexibility and small footprint FOS-OBR are chosen for this study.

Figure 6.34: Manufacturing defects found in an initial production run

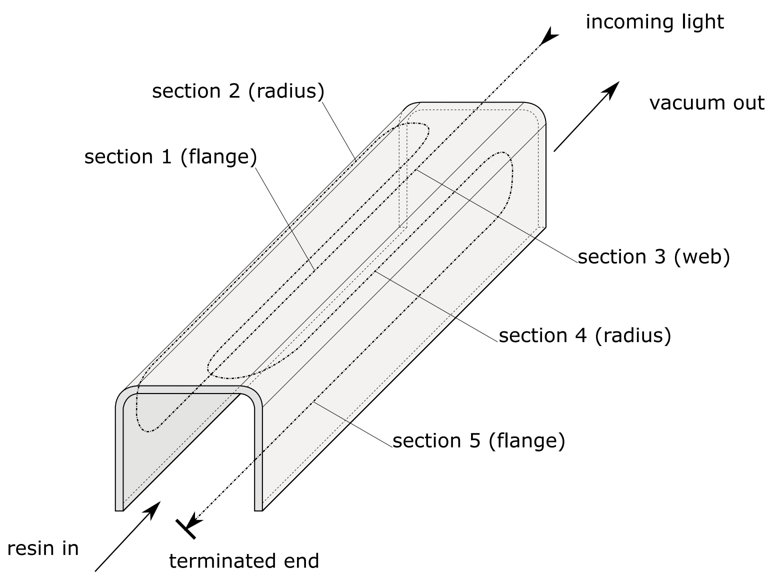

Figure 6.35: Location of the FOS-OBR in the U-beam.

6.3.2.1 Materials

The beam section was made up of four layers of four-harness woven glass fiber fabric. The fabric was cut into individual plies with 500 mm length and 145 mm width. The beam was laid up with butt-splices between the individual layers which were ensured to be no closer than 25 mm of each other. This ensures a uniform thickness and good mechanical properties.

A Sicomin SR 8100/SD 8824 Epoxy system was prepared at a 100:22 ratio by weight and put in a large paint mixing bucket ready for infusion. The infusion setup comprised of a 6mm polyvinyl chloride vacuum hose that connects the resin reservoir to the vacuum bag's inlet. From there the resin enters a resin distribution spiral which delivers resin across the entire cross section of the beam. The fabric is covered with PP180 polyester peel ply and FM100 infusion mesh to facilitate a quick infusion process. Vacuum is drawn from the other side of the beam through a microporous vacuum line (MTI hose) which ensures a complete infusion by not blocking the vacuum line with resin prematurely. All of the mentioned materials were purchased from Easy Composites (Stoke-on-Trent, UK).

6.3.2.2 Setup

To capture the progression of the resin flow along the beam's extrusion direction (1.2 m) two cameras were used. They were set up on either side of the mold at an elevated downward facing position such that all surfaces could be captured. The peel ply was equipped with tracer lines which were oriented perpendicular to the extrusion direction of the beam and used as a reference for flow front propagation.

The LUNA OBR system was setup with a gauge length of 2.6 mm and the previously mounted FOS-OBR had a total length of 8 m out of which 5.5 m are integrated within the beam. It was interrogated at 10 Hz continuously throughout the entire process with a tare performed just before vacuum application.

Throughout the infusion the vacuum pressure was measured using a dial vacuum gauge attached to the resin catch pot at the vacuum side of the setup.

Figure 6.36 and 6.37 show the flow front progression at equally spaced timestamps as captured by the camera. Initially the flow front progresses very fast until its speed stabilizes at around 3 minutes into the process. When observing the saturation of color in the infused areas, a section at the flow front with brighter color becomes evident. This represents the flow front position within the infusion mesh which is dissimilar to the position within the glass fiber fabric. Upon comparing the videos obtained from the left and right side a uniform flow progression is observed, indicating a good and uniform resin feed rate and permeability within the fabric, peel ply and flow media setup.

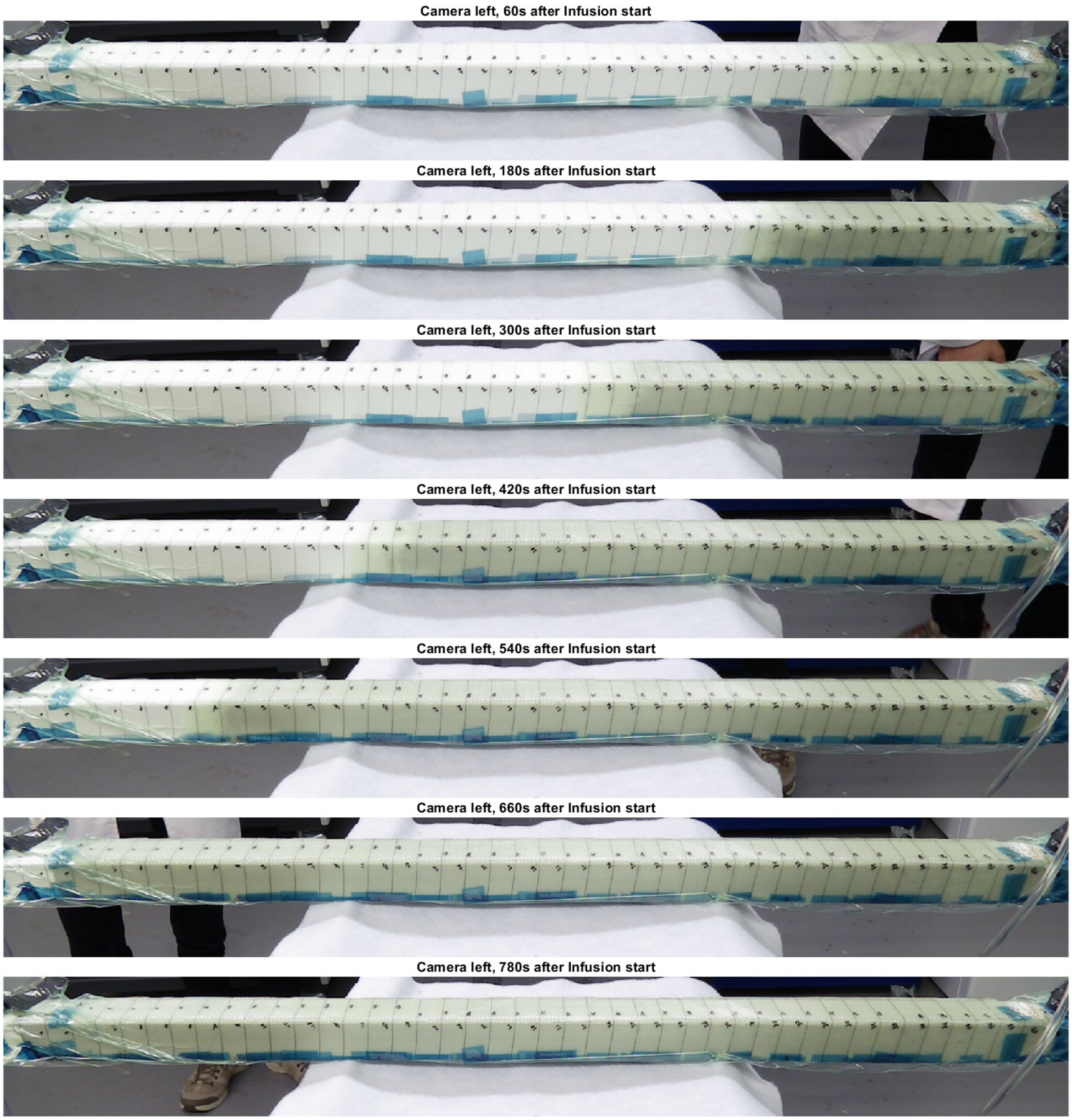

Figure 6.36: Infusion filmed from camera left at selected timestamps

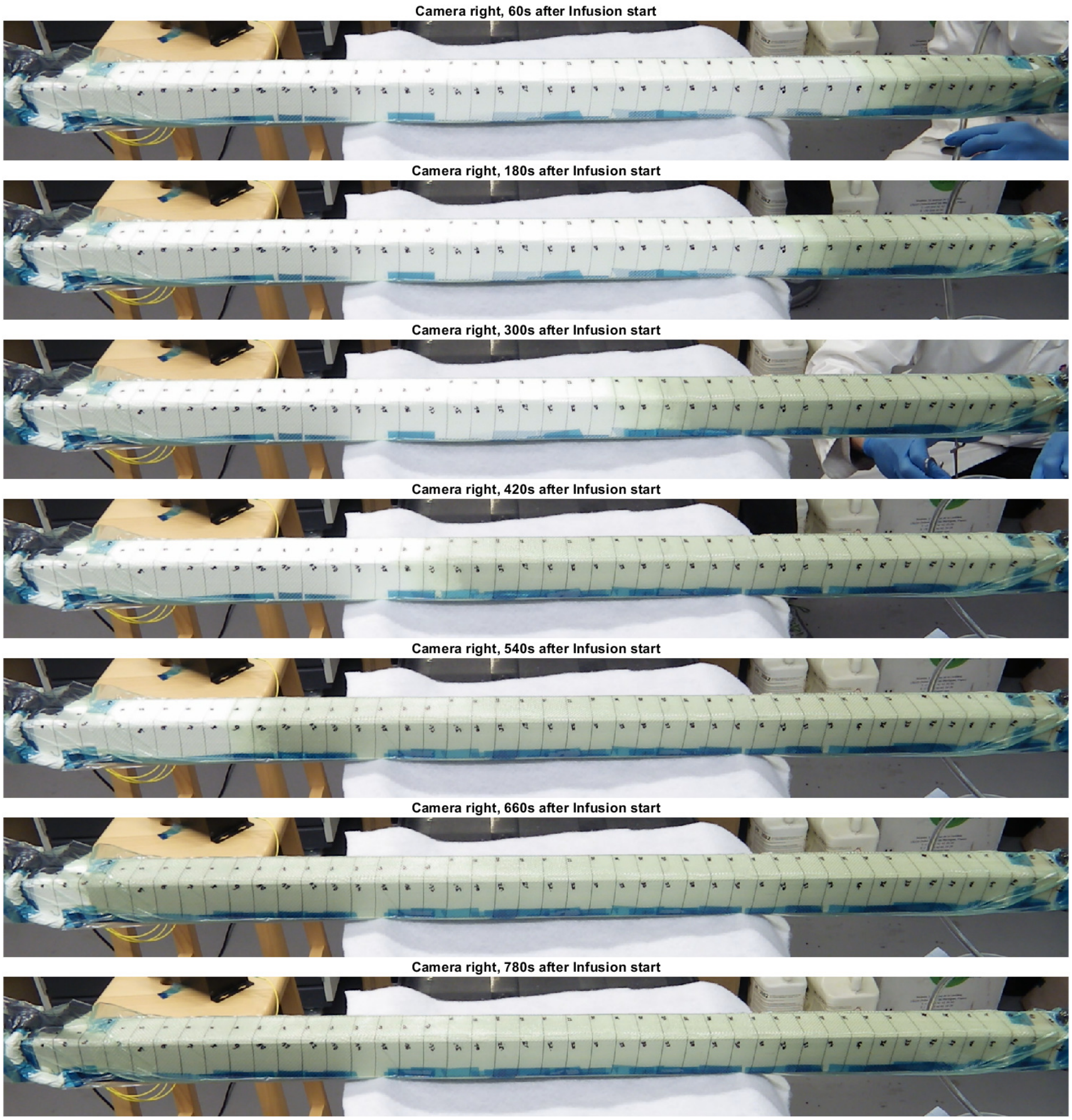

Figure 6.37: Infusion filmed from camera right at selected timestamps

After completing all the preparatory steps and setting up the cameras for flow front monitoring, the infusion process was initiated by applying vacuum to the bag. The FOS-OBR measurement results are presented below in chronological order as the infusion process progressed. The data plotted in Figure 6.38, 6.40, 6.41 and 6.43 is averaged along the entire length of the relevant section. This has been validated by comparing readings across several spanwise sub-sections where no notable difference in relative amplitude, gradient or presence of individual features has been observed.

As observed in previous experiments and modelling, upon vacuum application a lateral force acts onto the fiber leading to diverging amplitudes of frequency shift (Figure 6.38). The frequency shift reaches a plateau at roughly 22s indicating the bag's vacuum levels have reached a stable value. Sections 1 and 2 (ref. Figure 6.35 to locate the individual sections) show normal behaviour, whereas Sections 3 through 5 show a sinusoidal wave-like pattern with increasing amplitude which begins at around 10s in the process and only stabilizes after 35s. The readings obtained from Section 4 and Section 5 are in phase with different amplitudes, however, the measurements on Section 3 are shifted by half a period. The cause for this unusual artefact could not be established at this point. One possible explanation could be that a small leak within the tacky tape had formed, which under specific vacuum conditions would have closed and reopened until it finally closed. A second possibility was the formation of a pocket within the vacuum bag that was disconnected to the main bag (e.g. a crease in the bag due to tension whilst the bag settles, see Figure 6.39) and had a different level of vacuum. Once a certain level difference was surpassed that pocket would connect and disconnect again from the main bag to equalize the pressure. Regardless of what was the cause, a stable and high quality of vacuum is important for a quick and high quality infusion process. Having confirmed that, the infusion could be kicked-off.

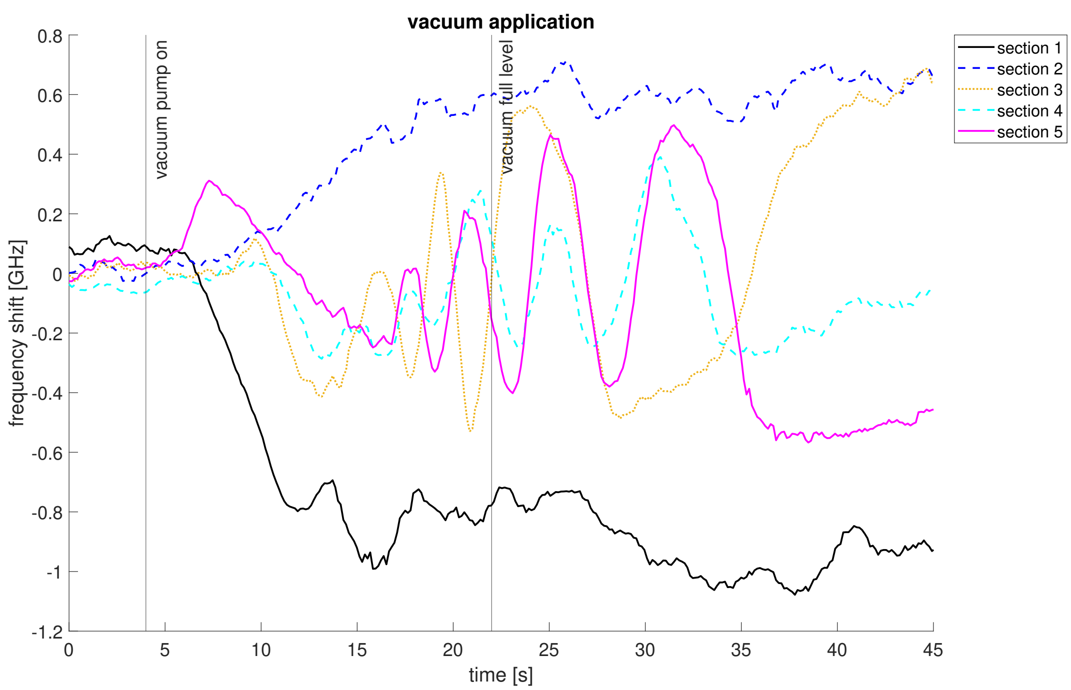

Figure 6.38: OBR readings obtained during vacuum application to the U-beam (each section averaged over entire length).

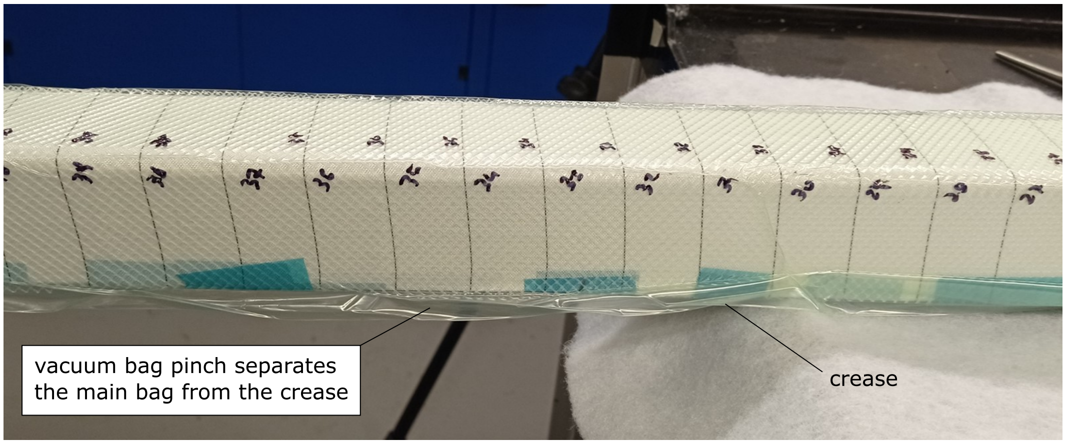

Figure 6.39: Picture of a crease in the U-beam's vacuum bag which may be the cause for fluctuations picked up by the FOS-OBR.

Once the desired vacuum level was reached the epoxy infusion resin which was previously weighed and set aside was mixed thoroughly using wooden spatulas ensuring no visually detectable air bubbles were formed or entrapped in the resin. This made a degassing step after mixing obsolete and saved time. In order for infusion to start the hose on the resin side had to be opened. This lead to an intermittent loss of vacuum which can be clearly identified in the corresponding OBR readings (Figure 6.40). Upon dipping the open end of the hose into the resin, vacuum levels quickly rise and reaching peak levels again, repeating the sinusoidal pattern in the same manner as it did previously. From that onward the infusion progressed normally for 200 s.

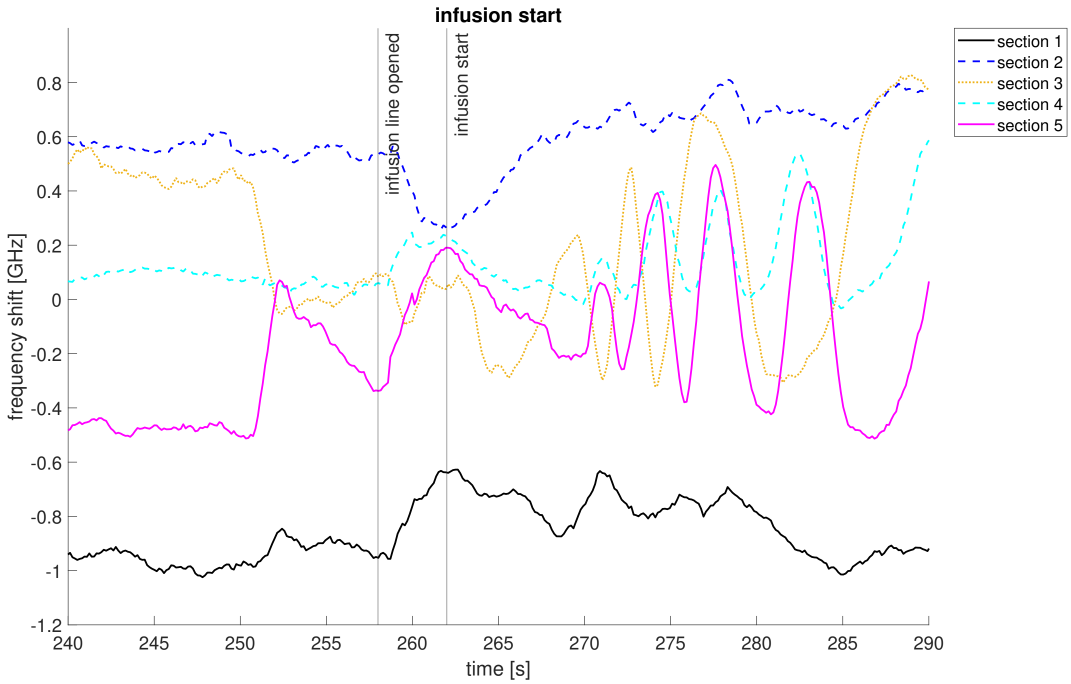

Figure 6.40: OBR readings obtained during the early stages of infusion (each section averaged over entire length).

After approximately 500s a kink that formed in the resin supply hose (Figure 6.42) was noticed. An attempt was made at correcting it using a set of tweezers to restore the original diameter and straight routing. Such a kink could limit the resin flow and lead to different pressure conditions within the bag. This condition is potentially harmful to the process as it slows it down and when using fast reacting resins, this could lead to unsatisfactory mold filling and premature onset of the curing reaction.

The kink and the rectification attempts are clearly visible in the corresponding OBR measurements (see Figure 6.41) rendering the system as an excellent capability to detect such conditions at the instance they occur. Such a phenomenon would be impossible to capture using a vacuum monitoring only. The impact the kink had on the OBR readings is most prominently visible for Sections 3 through 5 (ref. Figure 6.35 to locate the individual sections). It manifests itself in a large shift of the baseline indicating a change in the lateral compression conditions. This can be expected given the fact that the kink serves as a seal on the resin side, leading to the vacuum levels in the already infused section approaching that of the resin catch pot as opposed to the levels at the resin port, i.e. atmospheric pressure. As can be seen in the OBR readings the kink was fixed for a short while until it appears to have formed again to a lesser extent at around 780s in the process.

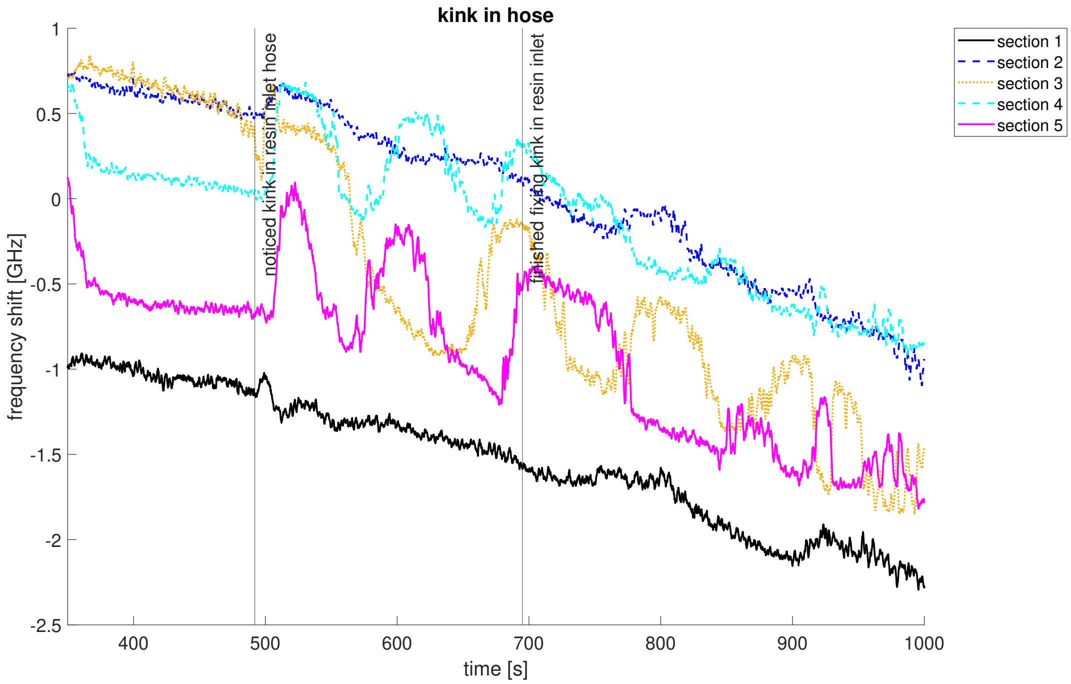

Figure 6.41: OBR readings obtained during noticing and correcting a kink in the infusion hose (each section averaged over entire length).

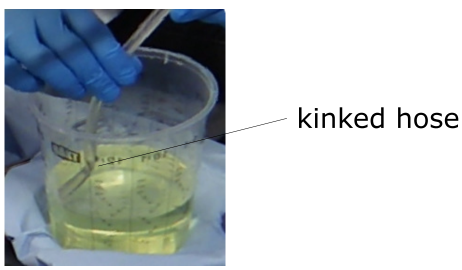

Figure 6.42: Kink in infusion hose

Towards the final stages of the infusion process the readings stabilize (Figure 6.43). This is due to the advanced flow front reaching the vacuum line and therefore leading to almost atmospheric pressure conditions inside the bag. Nonetheless, minor handling operations are visible in the OBR data through baseline shifts and changes in fluctuation amplitude. Such minor processing artefacts are impossible to monitor using vacuum gauges or pressure transducers.

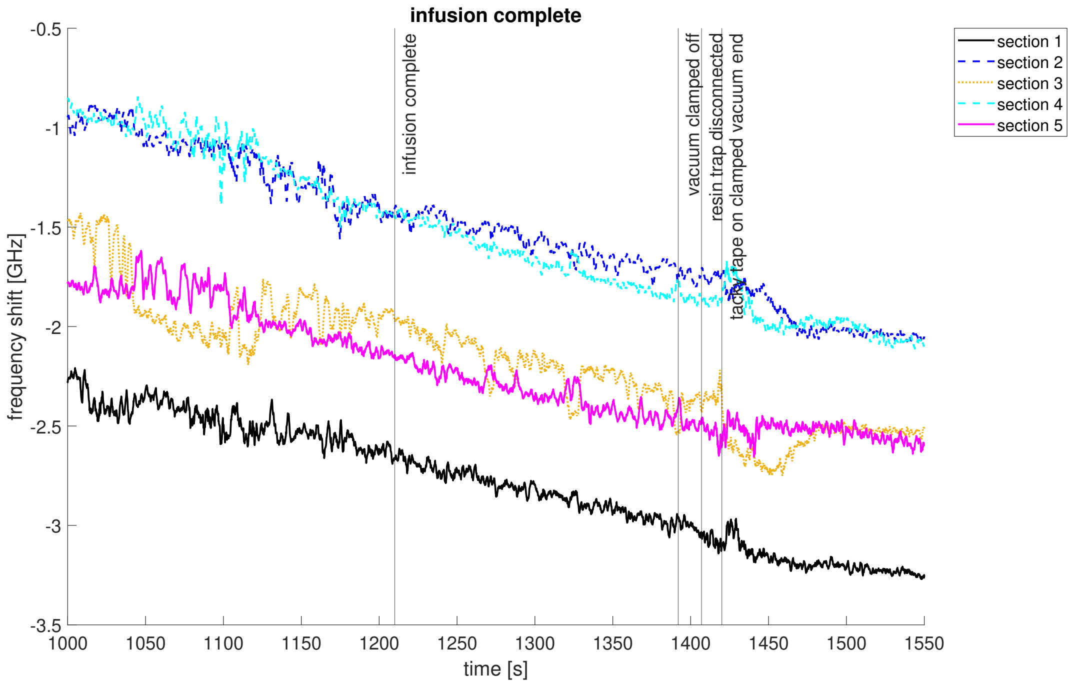

Figure 6.43: OBR readings obtained during the final stages of the infusion process (each section averaged over entire length).

6.3.3 SHM study on U-beam

6.3.3.1 Setup

To evidence the benefit of having the FOS-OBR integrated into the component for SHM, a three-point bending experimental setup was devised. Since the U-beam was too large for a standard Universal Testing Machine, a hydraulic press equipped with a FUTEK LLB400 button load cell was used for load introduction (Figure 6.44). The beam was supported using 200 mm long machined wooden blocks on both span-wise ends.

To avoid excessive localized bending of the web caused by the relatively small diameter (8 mm, see insert on Figure 6.44) of the button of the load cell, a 50x50 mm aluminium plate with a thickness of 1.5 mm was bonded to the U-beam.

During initial trial runs it was also noticed that the U-beam bent excessively which lead to the beam lifting away from the wooden support blocks at the edges (a gap of up to 10 mm was observed). This changed the boundary condition to a pin at the wooden block's edge closest to the center of the beam. A C-clamp was used to clamp the beam vertically with a 75 mm wide wooden plate to protect the beam. This intervention ensured that a longer section of the beam was in vertical contact with the wooden blocks and more closely resembled a clamped condition.

The load cell data was acquired at 100 Hz with a FUTEK IHH500 Digital Display connected to a laptop running the SENSIT Test and Measurement Software. The FOS-OBR was interrogated using the LUNA ODiSI-B at a rate of 10 Hz.

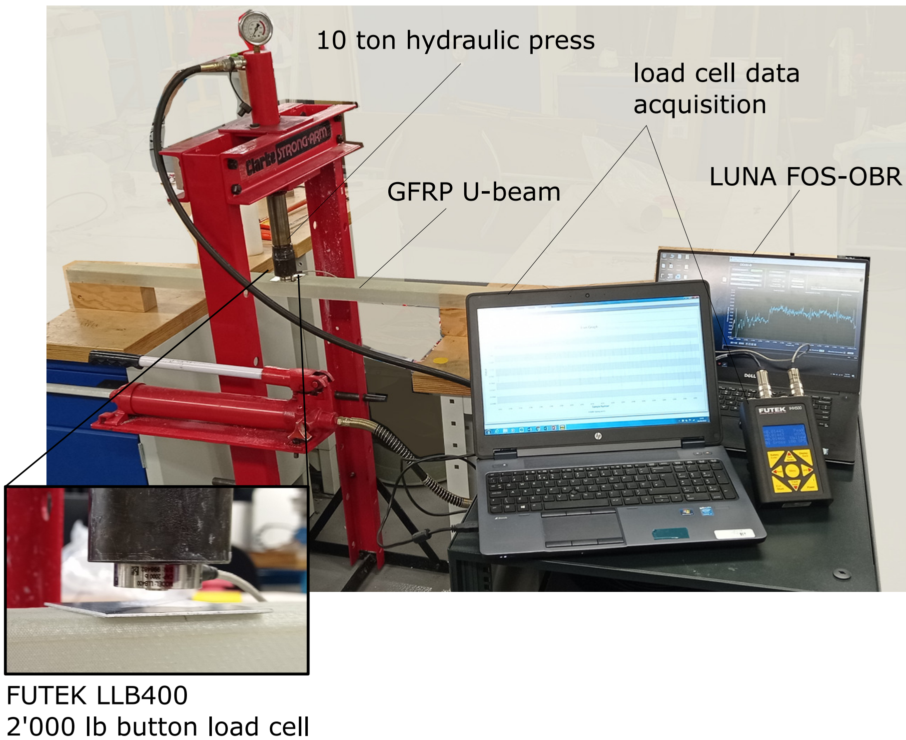

Figure 6.44: Three-point bending experimental setup for U-beam.

6.3.3.2 Load monitoring and damage detection

With an overall length of 1.2 m and two 200 mm wide wooden blocks acting as supports, the span-width of the beam was 800 mm. Any loads were applied along the medial z-axis of the beam (Figure 6.45).

Loads of up to 100 N were introduced by increasing the pressure on the hydraulic press with the handle. This meant that after every pump-action the load remained unchanged for a few seconds until the next pump stroke was performed. A step-wise load increase is the result of this circumstance.

Decreasing load gradients could be achieved by opening a valve on the press. The gradient could be somewhat controlled by how far the valve was opened. Despite the high level of required manual control, the maximum load could be repeatably reached with less than 1 N of accuracy.

In Figure 6.45 the artificially created damages can be seen. Two types of damages were introduced: cut slots and drilled holes. They were created successively as the ballooned number indicates. At first a 20 mm long and 2 mm wide slot was cut on the right flange, 120 mm away from the centre in the positive y-direction and 16 mm below the web. Secondly, a 25 mm long and 2 mm wide slot was cut on the web, 150 mm away from the center in the negative y-direction and 10 mm away from the center in the positive x-direction. Lastly, a 3 mm hole which was then opened up to 8 mm diameter was drilled into the web, 80 mm away from the center in the positive y-direction and 10 mm away from the center in the negative x-direction.

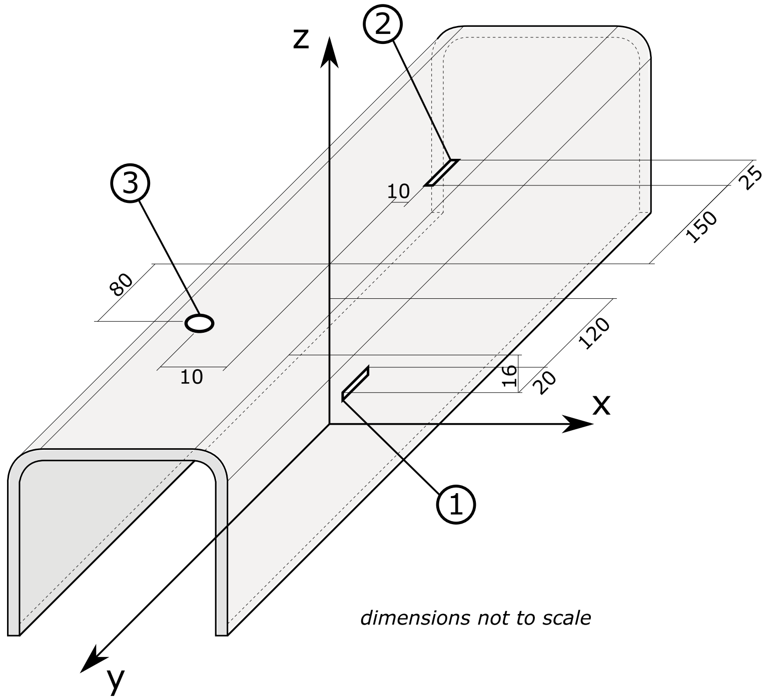

Figure 6.45: Damage location and sizes in the order of damage creation (1 thru 3).

At first, three pristine loading and unloading cycles were performed. The data collected during these cycles is used as an undamaged reference state. Additionally, in this experiment the overall load monitoring capability of the integrated fiber became evident. In Figure 6.46 the frequency shift observed in the web and one of the flanges is plotted. For reference, a simple representation of the beam's setup is shown as well. This representation is to scale and three distinct sections are clearly marked. Going from left to right, they are: left support (200 mm width), the load introduction point with its 50x50 mm Aluminium plate and the right support (200 mm width).

Analyzing the corresponding frequency shift data plotted above and below the beam representation, these three distinct sections (2x support and load introduction) are clearly identifiable as they empose a unique strain profile. Another observation to make is the magnitude of the frequency shift. The black solid line is the data captured at 10 N external load whereas the blue dashed line is captured at 20 N. In both the web and flange areas this doubling in load resulted in a doubling of the magnitude of frequency shift.

Finally, the opposing sign of the frequency shift highlights the obvious fact that whilst the flanges experience tensile strain, the web is in compression.

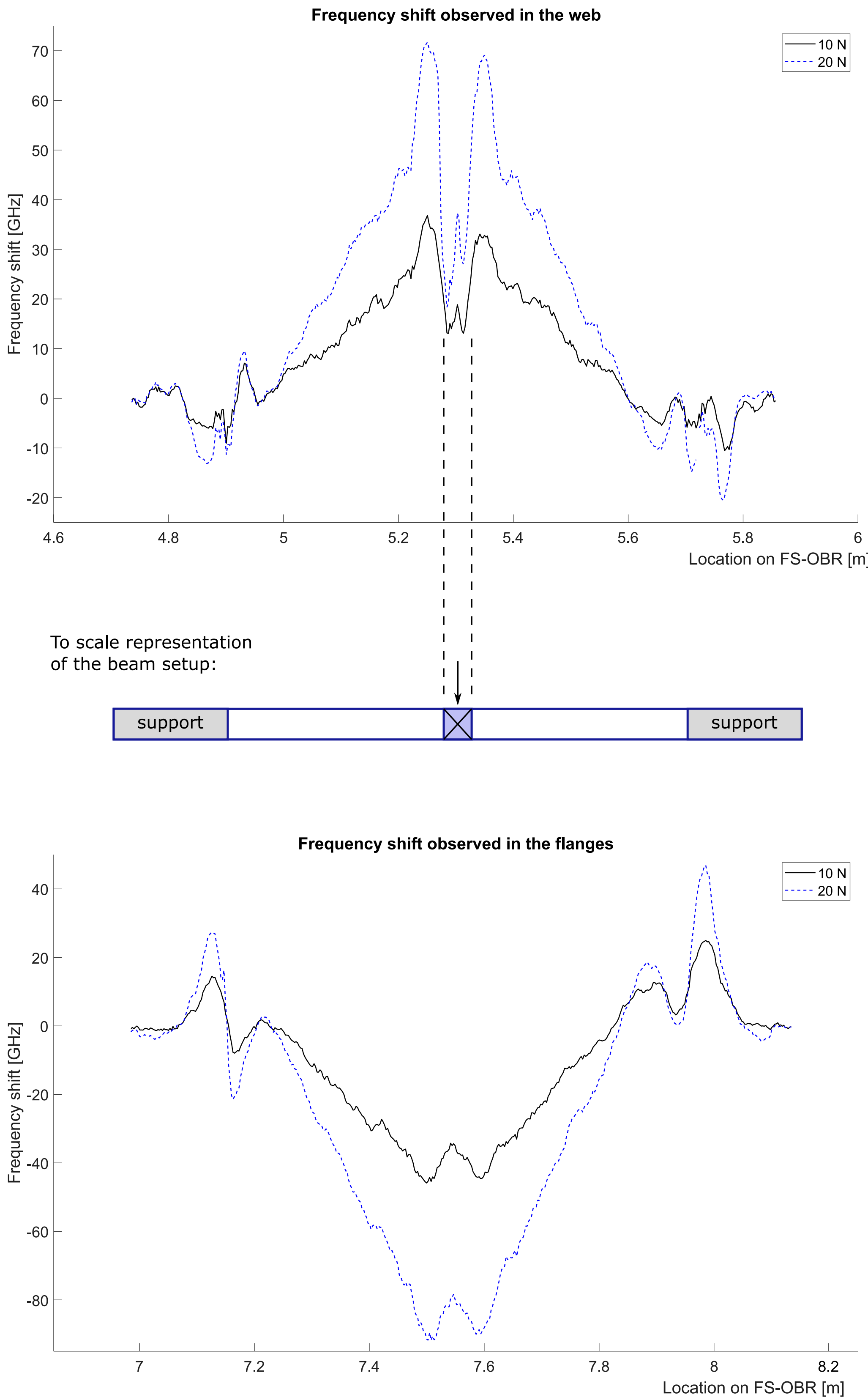

Figure 6.46: Load monitoring with integrated FOS-OBR. The load introduction and support geometries are clearly recognizable from the data.

With the reference data collected, the experiment continued with the introduction of the artificial damage. After such a damage was introduced another loading and unloading cycle was performed and the data collected is compared to the pristine state.

The first slot, located in the flange was not discernible from the strain data. Since the flanges are under tensile loading (ref. Figure 6.46), the longitudinal slot's presence does not impact tensile mechanical properties in a significant manner. Unfortunately, since the fiber could not be compromised by performing perpendicular cuts, the longitudinal slots were the only artificial damages possible.

The second slot was cut into the web of the U-beam. In Figure 6.47 the in-plane buckling that occurred during the three-point bending can be seen. Several local valleys and peaks are visible with a half-length of roughly 85 mm. This buckling is responsible for the relatively good damage detection capability on the web. Since the cut in this configuration does affect the local shear-modulus of the U-beam, the presence of the damage can be detected (see Figure 6.48 and 6.49).

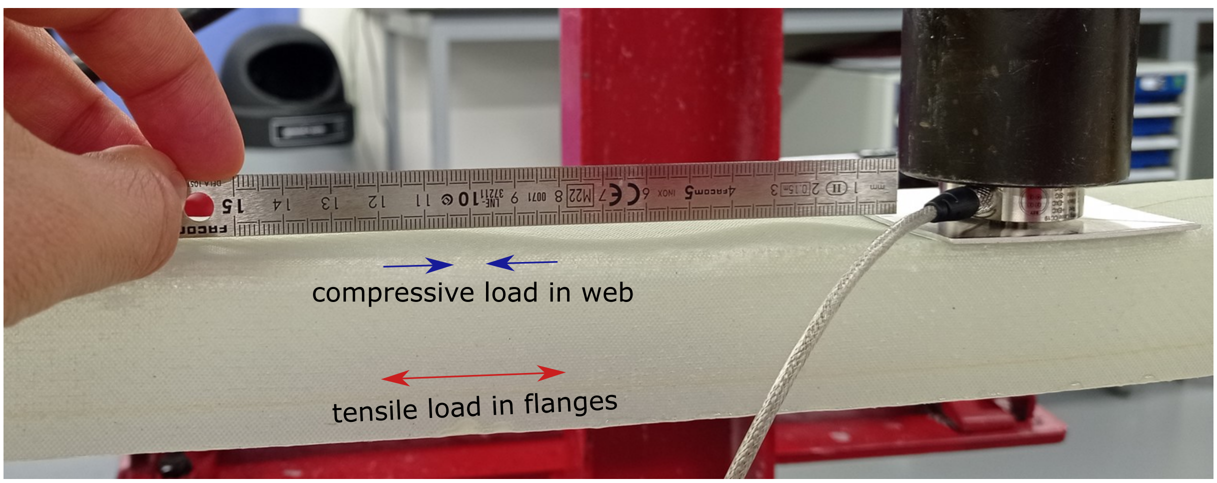

Figure 6.47: In-plane buckling observed on the web of the U-beam during three point bending.

Figure 6.48 shows a zoomed-in view on the section surrounding the cut on the web. The three black solid lines represent the pristine data, whereas the red dashed line is data collected with the slot present. A local increase in frequency shift of 20% is noted. When considering the length of the slot shown to scale in Figure 6.48 it is obvious that not only is the presence of the damage clearly highlighted, but also its size. When mapping the fiber's length on the structure it is also possible to determine exactly the position of the slot. Having such detailed information about a damage is crucial for a high-fidelity SHM-system.

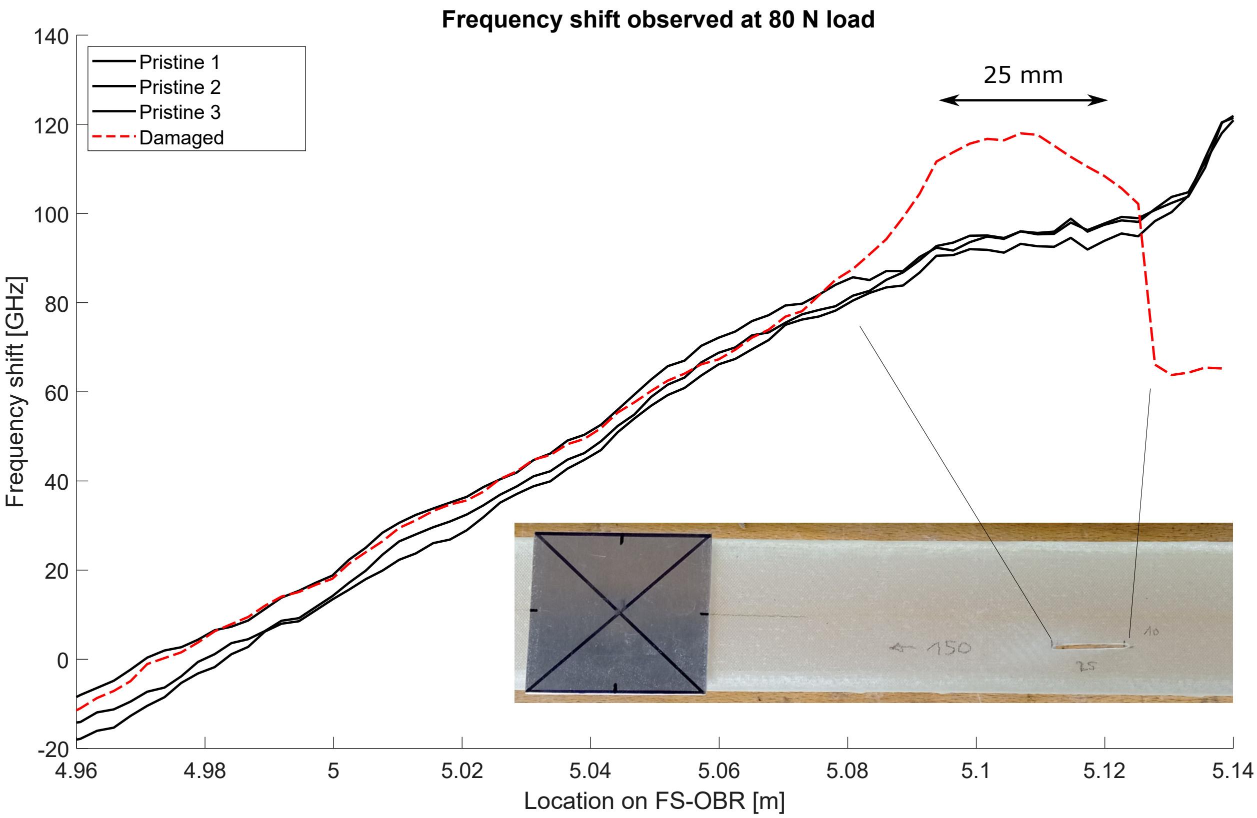

Figure 6.48: Location of the 2nd cut clearly visible on the frequency shift versus length graph (the three pristine lines are repetitive experiments to show repeatability).

The current frontier of SHM is the determination of remaining useful life of a component. This requires knowledge about the impact a damage has on the load-bearing capability of a structure under investigation. Figure 6.49 reveals, that FOS-OBR can deliver useful information about the load-bearing capability as well. The data plotted in Figure 6.49 is the mean frequency shift over the affected area, identified in Figure 6.48 against the applied load. The black crosses (+) represent the pristine data, whereas the red circles is the dataset with the damage present.

In both cases, the load increases linearly initially up until 80 N for the pristine case and 60 N for the damaged case. After the linear increase, the frequency shift's gradient changes signs, indicating the local strain switches from compressive to tensile due to the onset of buckling (Figure 6.50).

Since buckling conditions typically are not desired in engineering structures the reduction in the onset load can be interpreted as a reduction in the structure's load-bearing capability. This is a unique and highly valuable insight into the structural health of a component.

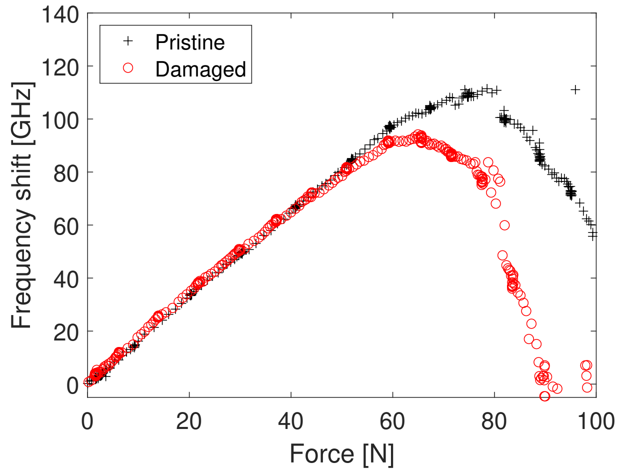

Figure 6.49: Frequency shift versus load in the region of the 2nd cut.

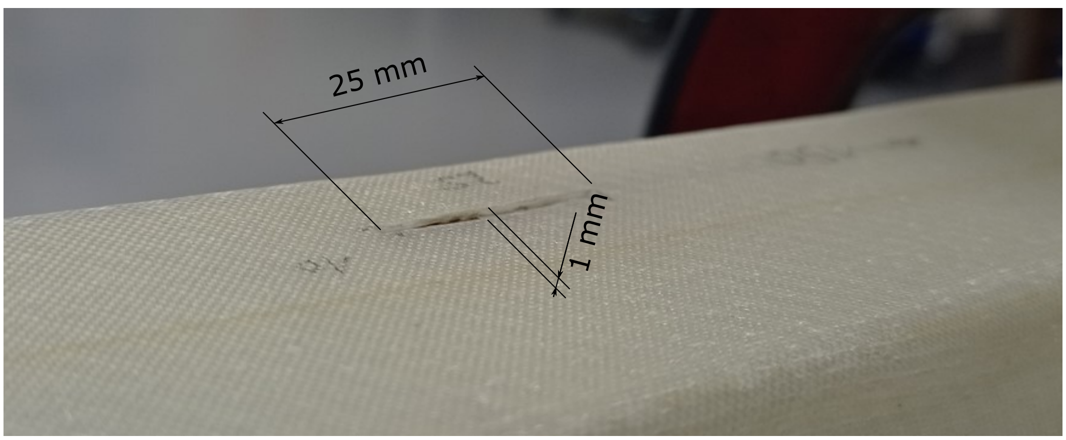

Figure 6.50: Effect of 2nd cut on the buckling behaviour of the U-beam.

Despite the success in detecting the slot in the web it is important to also highlight limitations owing to this SHM method. It was noted earlier that the first slot could not be detected. Similarly, the presence of the hole could not be identified from the FOS-OBR data. This is again due to the fact that the hole does not affect the local strain field. Figure 6.51 shows the web still buckles as previously noted (ref. Figure 6.47). The area around the hole can be seen unaffected and conforming entirely to the local strain field.

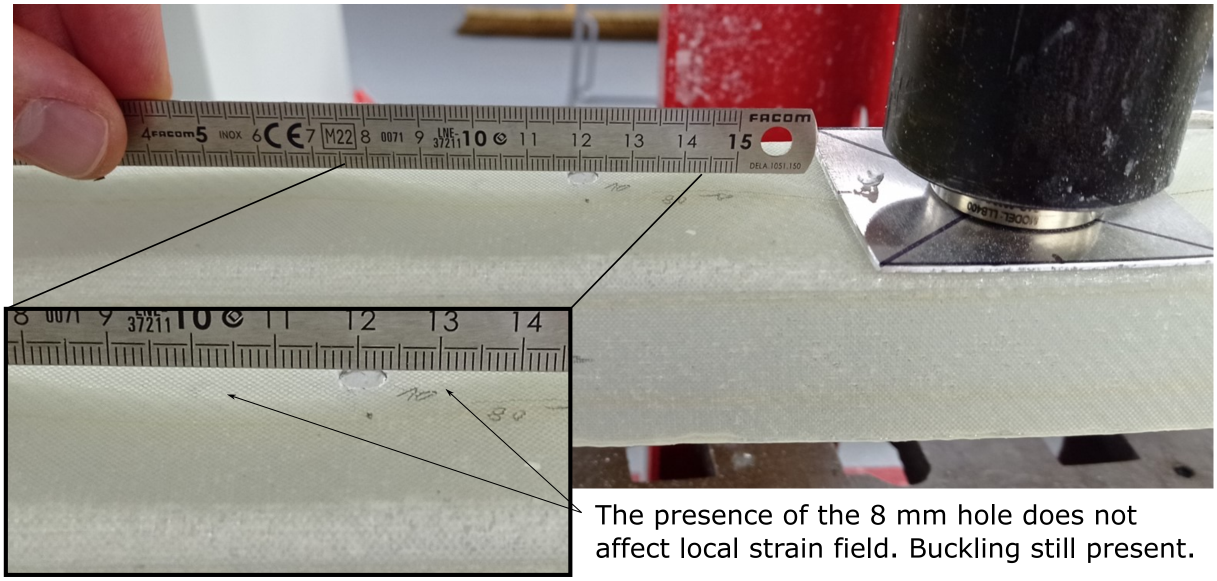

Figure 6.51: Effect of drilled hole on the buckling behaviour of the U-beam.

6.4 Conclusions

So far, the FOS-OBR PM technology has been applied only to 2D structures. In this section, the application on a fairly complex and representative structure has been shown. The monitored U-beam had a length of 1.2 m, relatively tight corner radii (6 mm) and both the web and flanges measured 50 mm in length.

The manufacturing was monitored with an FOS-OBR from the earliest process stages onwards. During the RIFT infusion process, the sensor provided insights into the vacuum conditions within the bag. Besides other artefacts, the most notable discovery was the ability to detect a kink that formed within the resin feed-line. Such a kink restricts the flow of resin and affected the fabric compaction. After manually intervening, the kink was rectified and the success of this action could be verified from the FOS-OBR readings. This is a significant improvement over legacy technology as it would be impossible to detect such a condition otherwise and the component would display inferior quality.

After the resin cure was complete the fully sensurized beam was immediately ready for its use without the need to install further sensing hardware. To simulate in-service loading conditions a three-point bending set up was used. Bending loads of 100 N were applied to the centre of the beam causing it to bend and buckle. The FOS-OBR allowed the monitoring of all of these phenomena with a dense spatial resolution.

In a final step, artificial damages in the form of slots and holes were introduced. The goal was to understand whether the presence of such damages could be detected with the FOS-OBR. Only one of the slots could successfully detected whereas the other slot and the holes remained undetected. This highlighted the fact that for reliable degradation monitoring, the effect a potential damage has on the structure needs to be known before implementing SHM solutions. In the shown case, only the slot on the web affecting the local buckling response was detected. Remarkably, however, once the defect was identified, both the exact location and length of the slot were visible in the strain response with high precision.

Considering all the above in conjunction, two main conclusions can be drawn: 1) the FOS-OBR can successfully be integrated into complex structures and deliver useful information and 2) the system needs to be selected with great care to ensure it is sensitive enough for the conditions of interest.

Chapter 7

Development of novel sensing elements for integrated PM and SHM

7.1 Flexible printed strain gauges and crack detectors

This section is based on the publication by Buchinger, Sharif-Khodaei and Aliabadi [139].

Advances in wearable electronics and soft electronics have lead to the development of novel manufacturing techniques for electronic circuitry. The work presented in this section is inspired by a publication from Valentine et al. [138] and an attempt is made to utilize the unique properties of the flexible printed devices for PM and SHM.

At first multifunctional inks are developed that can be successfully printed using an available 3D-printer. The ink has to fulfill several unique requirements: 1) bond well to the substrate to be printed on, 2) have good electrical conductivity to ensure high measurement fidelity and 3) must not short-circuit when printed onto electrically conductive substrates, like CFRP.

After testing the ink on several substrates (including thermoplastic composites, which are particularly challenging to bond to) and printing increasingly complex sensing devices, limitations with the existing printing equipment became evident. A novel sensor application workflow and process is developed based on a robotic arm.

The complete system (ink and robot-based 3D-printing) is finally demonstrated by directly printing sensing devices onto a tensile test specimen. Strain sensing and damage detection capabilities are shown in a mechanical test.

7.2 Development of multifunctional inks

In order to print any matrix material, its viscosity needs to be reduced to low enough levels to allow dispensing. Viscosity can either be reduced by melting or by dissolution in a solvent. In this work the main matrix material is BASF Elastollan BCF 35 A12 P TSG which is a thermoplastic polyester-polyurethane (TPPU). This material comes in roughly 2 mm diameter granules, has excellent mechanical properties (refer Table 7.1) and exhibits a high degree of elastic stretch. In order to create devices from this material two different types of ink are required. One that is loaded with silver flakes to make it conductive and one that is neat TPPU. The silver flakes had a purity of 99.95% with an average particle size of 2-5 microns and were produced by Inframat Advanced Materials (Manchester, CT 06042 USA). To derive a printable ink the TPPU was mixed with the solvents dimethylformamide and tetrahydrofuran. Mixing was enforced by using a magnetic stirrer inside an airtight container placed on a stirrer plate. The silver particles for the conductive ink were added in a later stage at which all the TPPU granules were fully dissolved. Again, a magnetic stirrer was used to disperse the silver particles. A proper dispersion is hard to quantify and therefore a relatively long stirring time of roughly 18 hours overnight was chosen. Both the initial dissolution of the TPPU as well as the dispersion of silver particles was done at room temperature.

Table 7.1: Material properties of BASF Elastollan BCF 35 A12 P TSG [189]

Property	**Value**	**Unit**	**Test method according to**
Hardness	37	Shore A	DIN ISO 7619-1 (3s)
Density	1.18	g/cm^3	DIN EN ISO 1183-1-A
Tensile strength	20	MPa	DIN 53504-S2
Elongation at break	1050	%	DIN 53504-S2
Tear strength	36	kN/m	DIN ISO 34-1Bb
Abrasion loss	135	mm^3	DIN ISO 4649-A

7.3 Sensor design process

In order to quantify the ability of such a sensing device to reliably function in PM and SHM scenarios two types of sensing devices were derived: 1) strain gauges for standard strain measurements and 2) crack detectors to identify damage and track its progression (see concept in Figure 7.1). An important design feature for those sensors is the smallest reliably printable width of a conductive wire. This dimension is dependent upon the final viscosity of the ink, the nozzle diameter and printing speed. These three parameters need to be optimised.

For resistance based applications where strains or cracks are detected based on strain readings, an extra step is required when used in conjunction with carbon fibers. Since CFRP are highly conductive, the silver ink cannot come in direct contact with it. Therefore a layer of insulating neat TPPU ink is needed to form the interface to the CFRP.

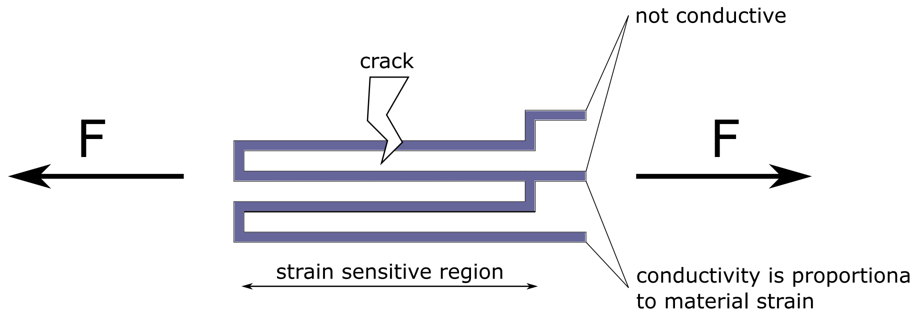

Figure 7.1: Illustration of the basic concept of a flexible strain sensor and crack detector.

7.4 Sensor manufacturing

A major limitation with prefabricated sensors is their inflexibility when it comes to adjusting to complex part geometries which are typical for aircraft composites. This inflexiblity stems from two facts: the sensing elements are brittle (PZT see Figure 7.2 and many FOS) and the wiring needs to cover great lengths requiring extensive wire management, or worse, drives up weight. In order to solve this problem, 3D printing of both the sensor and wiring directly onto components is selected. To achieve this, the dispensing nozzle needs to be mounted to a system that is capable of moving in at least three dimensions. In this work experiments were carried out on two different systems. One being a custom made high precision 3D printer, the other being an off the shelf robotic arm. They are presented in more detail below.

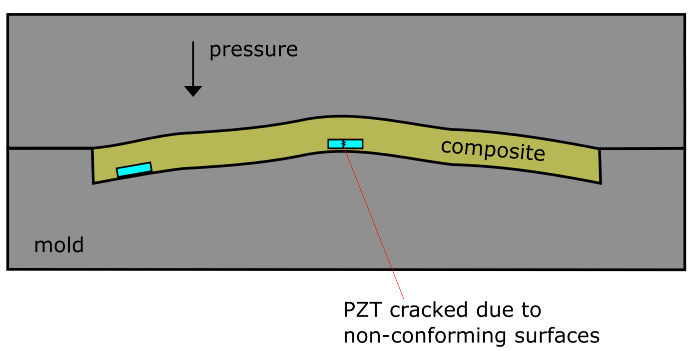

Figure 7.2: Illustration of PZTs cracking due to brittleness

7.4.1 High precision 3D printer

The printer (Figure 7.3) was designed and built by Raza et al. [190]. For the purpose of the presented work only the continuous direct write nozzle was used. It is connected to a Nordson EFD Ultimus™ V dispensing unit and controlled by a National Instruments™ LabView program. A textfile containing the subsequent coordinates of points to cover is provided to the software which then issues move instructions to the x,y,z-stages.

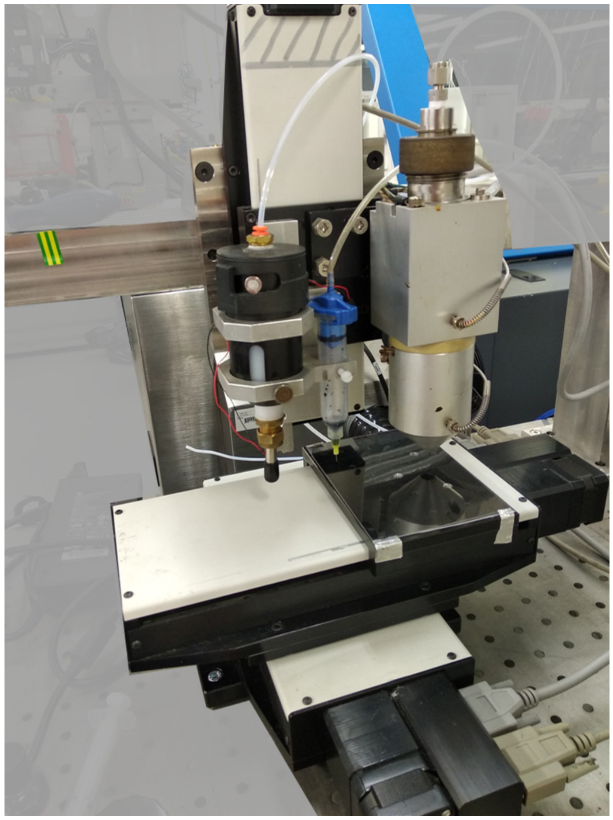

Figure 7.3: Custom made high precision 3D printer

Figure 7.4: Nordson EFD Ultimus™V dispensing unit

Whilst in theory this printer is capable of moving in all three axis at the same time, the relatively small printing area (a single 'move' command could not be longer than 20 mm) meant that the prints executed were 2D and relatively simplistic (see Figure 7.5). Nonetheless, it was possible to test the concept and characterize the printed devices.

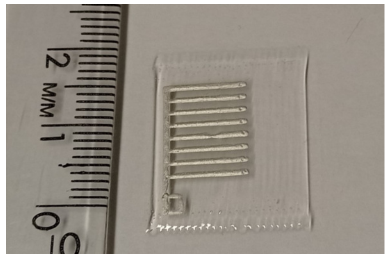

Figure 7.5: One half of an IDE printed with the High precision 3D printer.

7.4.2 DoBot MG400 - robotic arm

Automation efforts across most industries have lead to a steady decline in costs for industrial robots. In composites known applications include: automated layup and inspection processes, surface preparation, assembly and machining. This trend is likely to continue and robots will become common place in many manufacturing shop floors. The level of precision and degrees of freedom make them ideal candidates for the printing of sensors and associated wiring. In this work a DoBot MG400 robotic arm with four degrees of freedom and a precision of ± 0.05 mm was equipped with a Nordson EFD Ultimus™V dispensing unit.

The benefit of using an off the shelf hardware package is revealed when it comes to the realisation of unique sensor designs. In Figure 7.6 the workflow chosen for this work is shown. First the device with its desired configuration is drawn in a CAD package. This offers the ability to consider the structure to be printed on during the design phase.

When the sensor design is complete, it is exported in standard triangle language (*.stl*) which is common place in 3D-printing operations. Such a file can then be imported into a slicer of choice. A slicer is a piece of software used to dissect the three-dimensional body to be printed into slices that together make up the body. Each slice is a single layer that gets printed. Here the Ultimaker Cura software package is used (Figure 7.7). Important settings like the material and processing parameters can be set to suit the application. In the end a *.gcode* file can be exported which has all the movement- and printing commands. In order to make it compatible with the DoBot MG400 a custom MATLAB® routine was developed to turn the *.gcode* commands into a language that can be interpreted by the robot. This step is straightforward as the *.gcode* file already contains all the necessary information and acts merely as a translator.

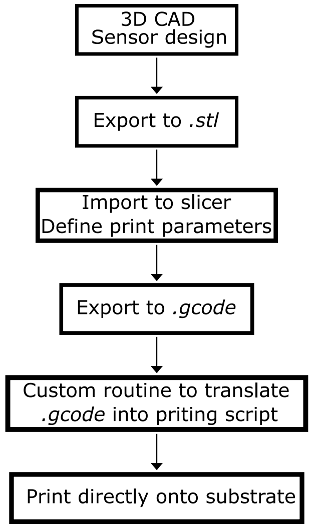

Figure 7.6: Flowchart illustrating the process of generating print files for the robotic arm

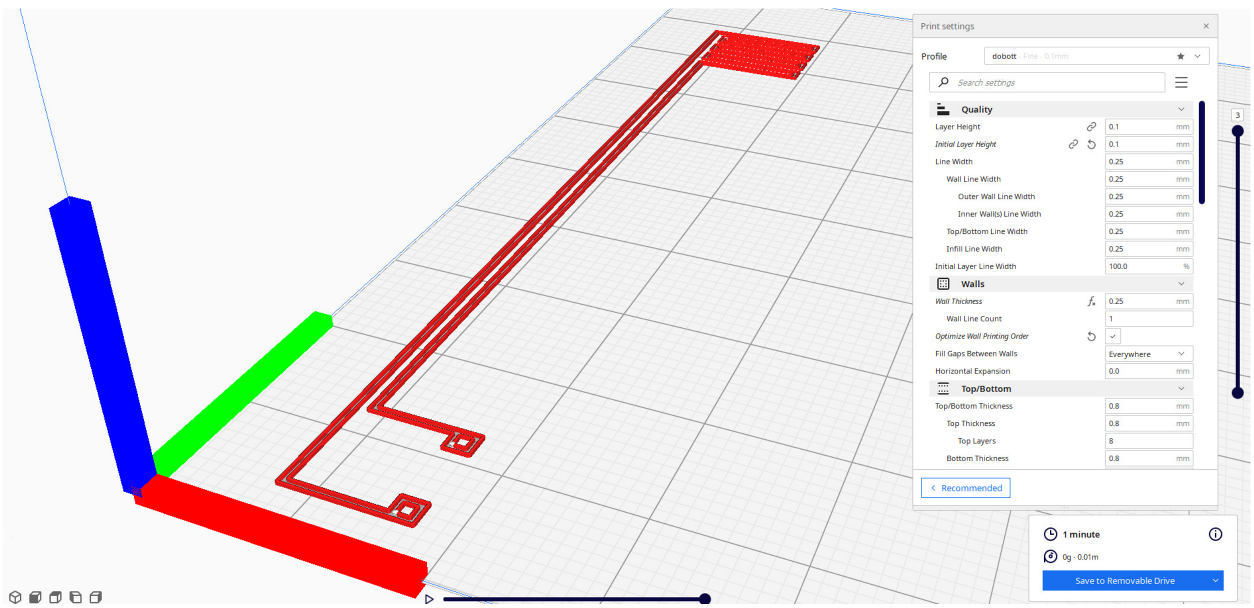

Figure 7.7: Slicing operation in Ultimaker Cura

7.5 Experimental demonstration

As highlighted by Valentine et al. [138] the devices produced from the above mentioned materials are suitable for two physical parameters. Strain leads to material stretching and therefore separation of silver flakes. During the separation of silver flakes the resistance increases and this increase can be used as an indicator for strain levels. A second application is for pressure sensing. For this application a multilayered sensor design is required. Two conductive layers are separated by a layer of insulating ink. By doing so, a capacitor is formed whose capacitance is proportional to the physical lateral distance between the two layers. Given the softness of the TPPU a pressure sensor is formed. In the present work, this material- and process combination is used to derive devices for strain monitoring and crack detection. The crack detection ability is hypothesized to be an extension of the material's resistance proportionality to strain. Should a crack occur in the monitored structure the material faces very high degrees of strain, up to a point of separation. Upon reaching a threshold, the network of silver flakes breaks up and the material no longer is conductive. This indicates damage and can be used to monitor critical locations or track the progression of damage.

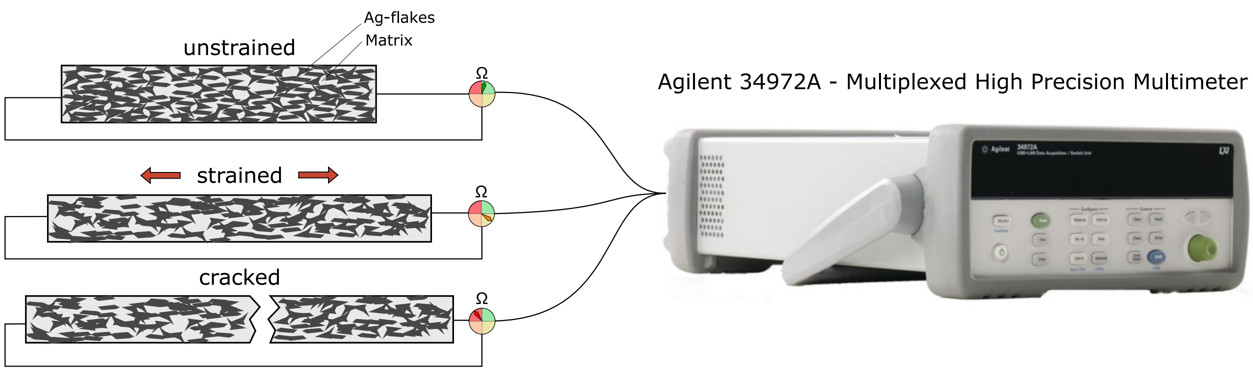

Figure 7.8: Strain measurements using flexible ink

7.6 Mechanical testing

To establish strain sensitivity of the developed device, two samples were tested on an Instron 5985 universal testing machine fitted with a 250 kN load cell and wedge action tensile grips. The first sample was not monitored as it was only used to establish an approximate failure load and to ascertain the failure mode. This was important to ensure the printed sensor was at the right location to experience damage. As expected, the failure originated from the hole and extended along the 90° direction of the specimen (refer Figure 7.9). A jagged vertical separation line is visible, corresponding to FM3. Figure 7.9 also highlights the extremely high degree of stretch the printed TPPU can endure whilst remaining fully bonded in the areas which are still in contact with the sample.

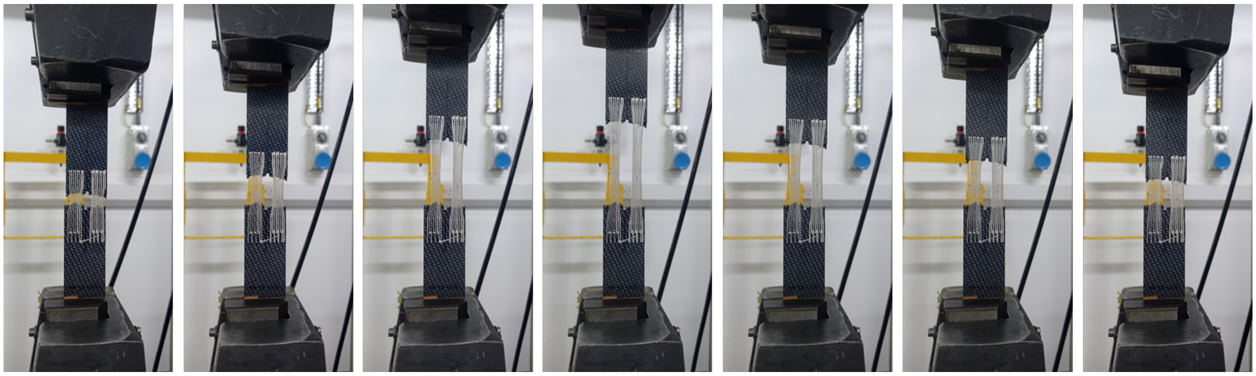

Figure 7.9: Extreme stretchability of the printed strain sensor

The second sample was also tested using the configuration as described above. However, to capture the change in resistance as the sample is stretched and experiences damage, it's printed gauges were connected to an Agilent 34972A multiplexed multimeter. This device directly measures the resistance of the individual regions at 0.7 s intervals.

The first specimen failed abruptly and violently at around 45 kN without any prior indication or damage forming. This condition is unfavourable when establishing the reliability of the measurements as it allows for only single use. To maximise the number of measurements on a single specimen, several loading cycles at sub-critical load levels were performed (0 to 20 kN at a rate of 0.5 mm/min). After four repetitions (identified in the plots as Pristine # 1 thru 4), a small damage is introduced using a diamond file to create a 1.5 mm deep and 2 mm wide V-shaped notch on the right laminate edge in the same horizontal plane as the hole is located. Again, several load cycles are performed (small notch # 1-3) before increasing the size of the notch (large notch 1 and 2) and finally bringing the sample to failure. This was done to demonstrate the post-failure crack-opening monitoring using the flexible sensor.

7.7 Results

The resistance measurements are presented in several graphs below (Figure 7.10 to 7.13). Overall, a clear and highly linear relationship between acting force and obtained change in resistance is observed. It shall be noted that the amplitude of change between individual regions (Pristine # 1 thru 4) are inconsistent, however, they are very consistent across repeating cycles at the same region. This suggests variations during the sensor manufacturing (line width, local variations in silver content, etc.). Given the high repeatability of subsequent tests (Pristine 1 thru Pristine 4) such variations can easily be accounted for using linear correction coefficients. The authors do not suggest such coefficients at this stage as the phenomena is still subject to ongoing investigations.

Further, it was noticed that when removing the load at the end of the experiment, the resistance only reaches its initial value after a long asymptotic phase (see Figure 7.11). It was therefore decided to plot resistance change and not absolute values.

Upon detailed inspection of the individual plots one can further note a distinctly higher level of non-linearity for laminate edge regions (Figure 7.10 a) and Figure 7.12 d)). Since the sensitive regions are very close to the laminate edge (< 2 mm) it is expected that such variations are the result of edge effects, including the formation of minor, non-critical matrix cracks. When considering the measurements of the regions away from the edge (Figure 7.10 b-d)) the merit of the developed devices becomes evident. The elastic region is marked by a highly linear resistance-change/load relationship as expected.

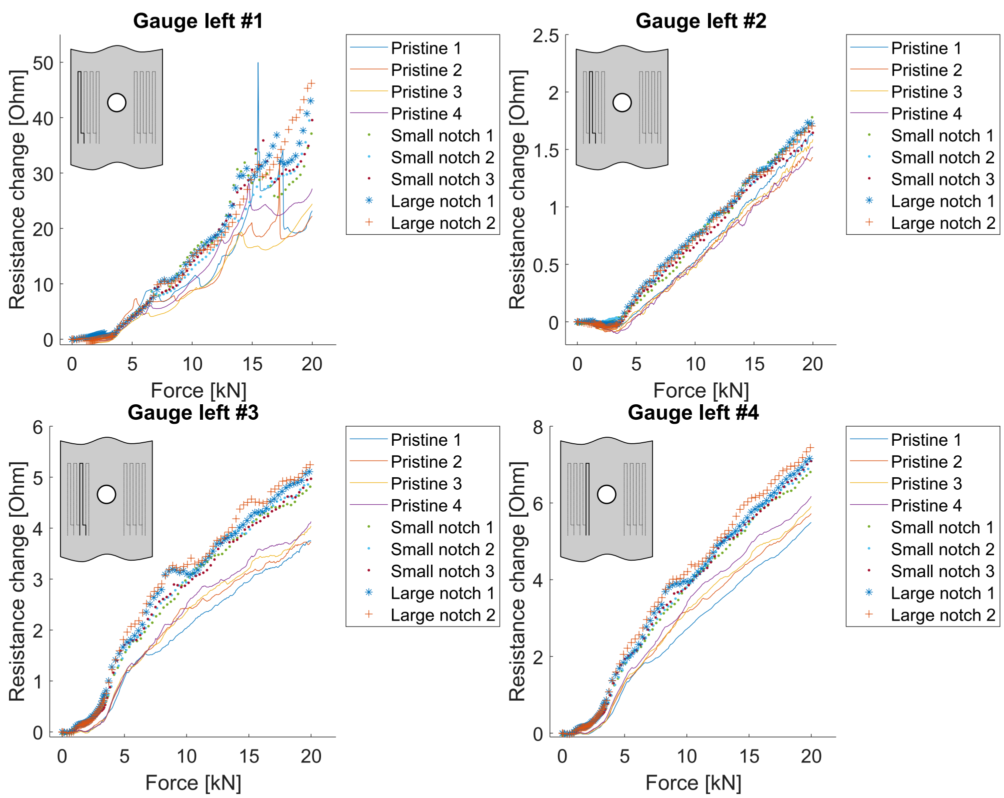

Figure 7.10: Resistance measurements obtained from the gauge located on the left side of the sample.

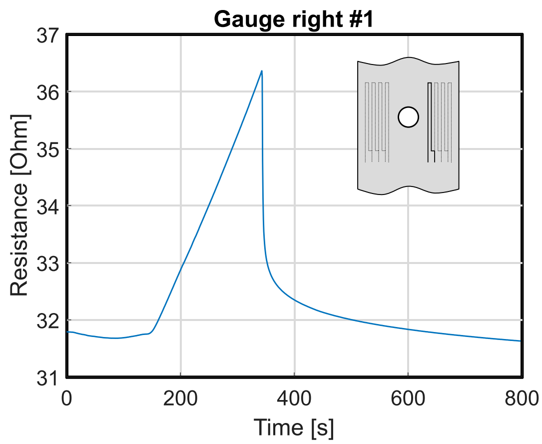

Figure 7.11: Resistance plotted versus time illustrating asymptotic resistance decay upon unloading.

Additionally, the presence of a damage in the form of an artificially created notch is clearly indicated through an increase in resistance by up to 50%. The notch leads to an increase in compliance of the sample, i.e. the notched sample stretches more than the pristine one at the same load. The higher level of stretch leads to greater resistance. A damage can be detected by comparing the current resistance levels with the pristine state. If there is a significant increase, the mechanical properties of the material have reduced, indicating the presence of damage. The readings also are sensitive to the size of the notch as resistance values for the enlarged notch are again higher than those for the small notch.

Further, a comparison of the readings obtained on the left gauges, i.e. the notched side (Figure 7.10), with those on the opposite side with no notch present (Figure 7.12) is performed. In Figure 7.12 a-c) again the elastic region presents a high degree of linearity for the regions away from the edge. However, the impact the notch has on the resistance measurements and therefore on the strains experienced by the material are less obvious. When zooming-in on these graphs (Figure 7.13) the difference between the two conditions does become visible. Again, a clear separation can be made between pristine and damaged states of the sample. It is evident that the strain sensitivity of the individual devices is qualitatively very similar, however, quantitatively they are different. This highlights the need to further the understanding of what causes these differences in strain sensitivity.

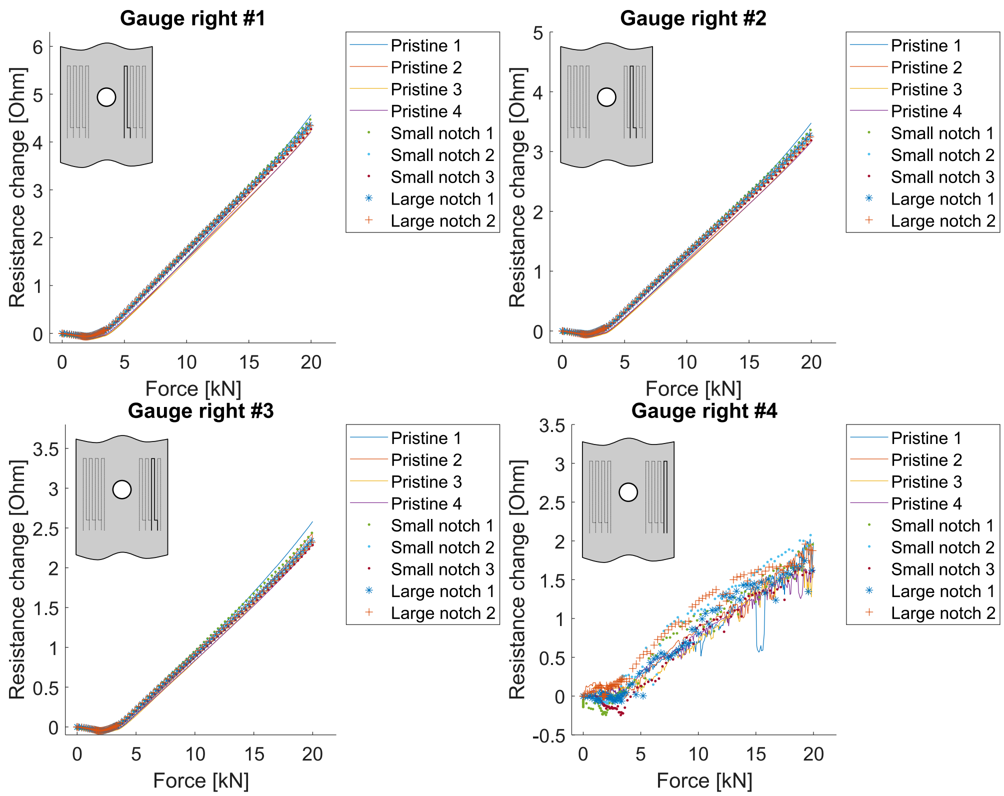

Figure 7.12: Resistance measurements obtained from the gauge located on the right side of the sample.

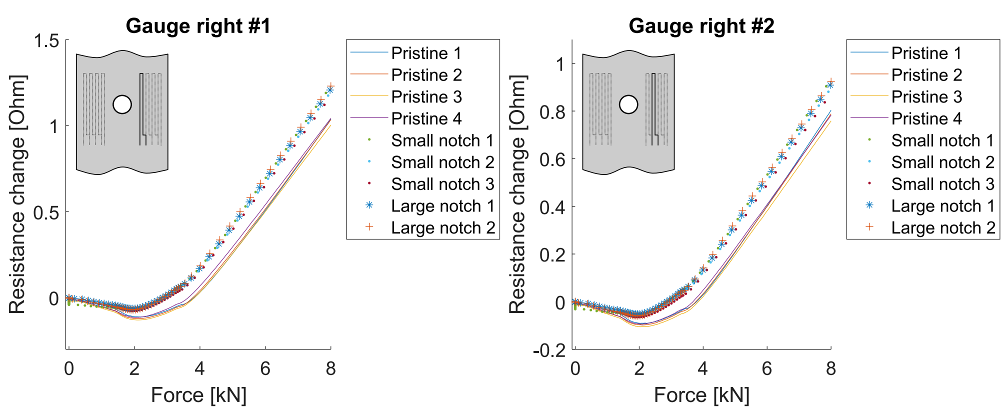

Figure 7.13: Detailed view on the resistance measurements obtained from selected individual sensitive regions located on the right side of the sample.

Finally, after the sample ultimately failed and the two halves separated, the devices were able to still capture resistance data. This demonstrates that the devices can survive ultimate failure of the sample. Figure 7.14 shows that five out of the eight sensing regions survived the breakage of the sample which resulted in an initial gap between the sample halves of 4.2 mm (inset in Figure 7.14). The universal testing machine is used to separate the halves in a controlled way even further at a constant rate of 0.5 mm/min. Upon further separation, the devices showed an immediate increase in resistance because of increased stretching experienced by the sensor. Such post-failure capability could aid in tracking the growth of existing damage.

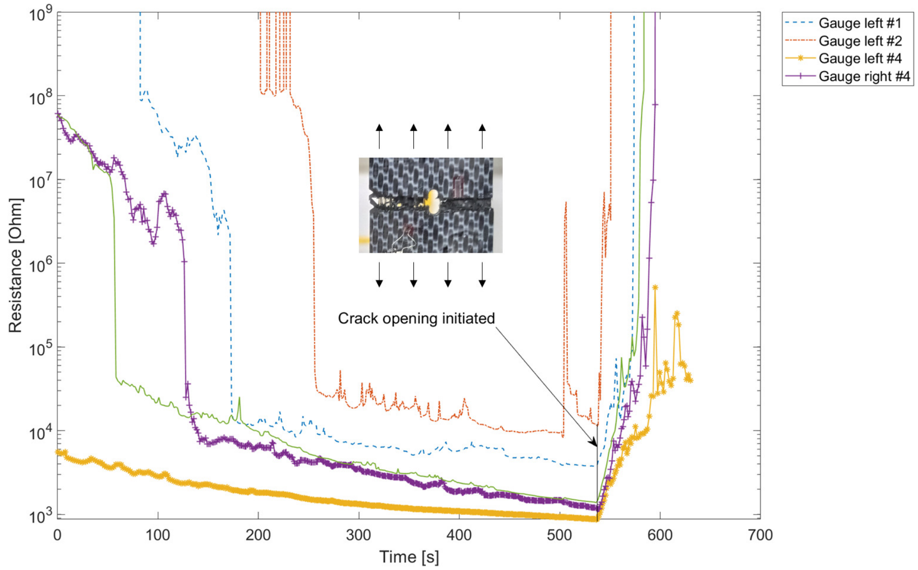

Figure 7.14: Post break capabilities of a printed strain sensor.

7.8 Conclusions

In this section a novel strain sensing and damage detection device is presented. It uses highly flexible TPU inks and a robotic arm to deposit the inks on an OHT composite sample. The device has shown excellent strain sensitivity and was able to detect the presence of damage. The sensor was directly printed on a thermoplastic composite coupon, where it showed excellent bonding capability. In addition, the device is shown to survive the ultimate failure of the OHT specimen and continue to function as a displacement sensor. Such a device could enable highly automated sensorisation and presents itself as an ideal candidate for future SHM applications. The advantages of the developed sensor is its flexibility, capability to be printed directly on composite part, conformity to curved and complex geometries, and its stretchability.

Further work is required to understand and manage the strain sensitivity of the devices. Figure 7.15 highlights some of the causes for inconsistent resistance results. They all occur during ink deposition, but are related to problems during ink making (presence of gelled particles, differences in viscosity, etc.). In order to resolve these issues, a tighter process control is required when manufacturing the ink. Once a sufficiently high repeatability and predictability of resistance values has been achieved these printed devices should be applied to different structures and loading conditions.

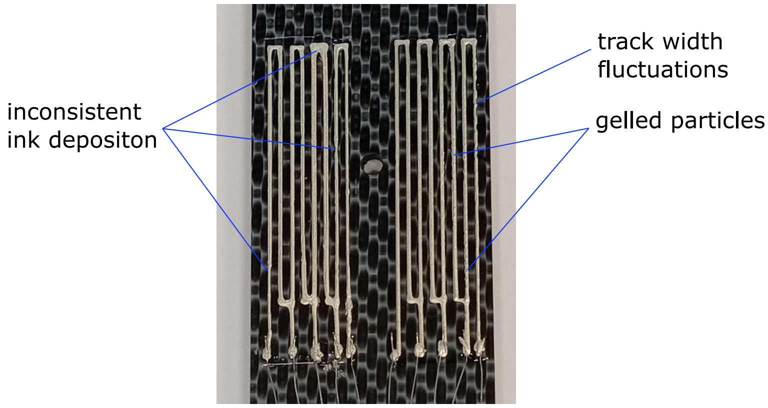

Figure 7.15: Inconsistent printing quality observed which affect the strain sensitivity of devices.

Chapter 8

Conclusion and future research

In this section the main findings of the thesis are reviewed. A recap on the set goals and objectives in section 1.2 will provide a structured summary and give an overview of the research reported on.

8.1 Conclusions

The prospect of an integrated PM and SHM solution for polymer matrix composites is investigated in great detail within this thesis. The ability to monitor such diverse aspects of a component's life cycle as manufacturing parameters and in-service damages could open the door for much wider use of composites, but also offer significant efficiency improvements.

However, given the diverse sensing environments and conditions, any proposed system needs to be able to perform tasks that sometimes are diametrically opposite to each other. One such example is a high degree of flexibility to reach points of interest versus survivability in high pressure and temperature settings. This thesis reports on the efforts undertaken by the author in order to identify a suitable solution for this integrated monitoring task.

The thesis is split into six main chapters which are briefly introduced in the following paragraphs.

In chapter 2 the necessary background information is provided and relevant literature is reviewed. At first, the current state-of-the-art in composite manufacturing processes is presented. Both thermoset and thermoplastic matrix processes are considered and the most common flaws stated. These flaws informed the choice of parameters which a suggested integrated PM and SHM platform needs to be capable of monitoring. A basic introduction into the very active research field of SHM provides the reader with an overview of the working principles of strain based and ultrasonic guided wave based monitoring approaches. The technologies employed to deliver such solutions are presented in detail in order to support a down-selection for further experimental testing. Finally, two successful case studies are introduced. One deals with the implementation of piezoelectric elements for RTM and the other showcases a fully automated PM and SHM solution.

A thorough technology demonstration and selection can be found in chapter 4. All work presented has been carried out by the author to support decision making on what technology shows the most promising characteristics for integrated PM and SHM. Piezoelectric elements, fiber optical and electrical sensing devices are all employed in realistic composite manufacturing environments. It is found that piezoelectric elements are usually too inflexible and brittle to survive the significant pressures and deformations typical for a composite manufacturing process. Distributed fiber optic sensing technology based on optical backscattering reflectometry technology showed the most promising results of all the existing technologies reviewed.

Chapter 5 is mainly based on a journal publication achieved by the author of this thesis. It deals with the demonstration of the FOS-OBR technique for vacuum assisted resin transfer molding PM. A 500x500 mm GFRP plate is manufactured. The results obtained both numerically as well as experimentally prove the aptitude of FOS-OBR to produce valuable insights into the reinforcement compaction and fiber volume fraction.

With the successful identification of a suitable technology completed, Chapter 6 reports on efforts to expand the usage of FOS-OBR on more complex structures and different manufacturing processes. In a first step, a tapered CFRP panel is manufactured using VaRTM and monitored with the optical sensing fiber completely embedded in the structure. The same fiber has then been used to extract SHM data and in both cases detailed findings were enabled by the chosen technique. Secondly, a GFRP U-beam stiffening element with a length of 1.2 m is manufactured using the resin infusion under flexible tooling process. Again both PM and SHM data is collected using FOS-OBR and the results are presented.

The final chapter 7 deals with the creation of novel sensing devices based on the findings made so far. It is found that above all, mechanical flexibility is the main hurdle when it comes to integrating sensors into composite manufacturing processes. This has to do with the need to reach the point of interest and the large pressure and temperature gradients that are present. The latter two lead to large deformations within a component as it takes shape. To accommodate such limitations a novel sensing platform is proposed based on highly flexible, 3D-printed devices. This chapter covers the development of the material as well as the manufacturing workflow and application to a tensile test specimen. It is shown that the developed device was capable of measuring strain with high enough sensitivity to detect the presence of artificial damage.

The research findings and conclusions of the work presented in this thesis can be summarised against the set aims and objectives:

- **Aim 1:** Identify what SHM technologies have potential for PM
  - *Objective 1:* Identify important processing parameters for composite manufacturing that need to

be monitored.

Despite the development of new composite manufacturing processes which allow for more automation, the underpinning parameters for a high quality product have stayed the same. A list of the mostly reported manufacturing flaws is presented in section 2.1.3. From this list and the associated literature, it was noted that temperature, pressure and the determination of chemical changes occurring in the matrix are most important.

- *Objective 2:* Perform an extensive literature search for established SHM techniques being used in a PM setting.

  SHM is a very active research field with a plethora of available techniques and specialised sensing technologies being proposed. However, only a fraction of those are useful in a PM setting. It was important, therefore, to dedicate section 2.4 specifically to reported attempts at closing the gap between PM and SHM. It was found that PEs, FOS and electrical sensors posses the most promising characteristics. These sensing technologies are hence selected for further demonstration in Chapter 4.

- *Objective 3:* Present case studies of successful, integral PM and SHM implementations.

  Successful previous attempts by researchers to fully integrate SHM technology during the composite manufacturing process are presented in section 2.4.5. These studies include the use of PE sensors for RTM PM [10,30]. They also highlight strategies for packaging sensors and overcoming limitations. One of them being that high processing temperatures could render PEs unusable. Hufenbach [96] et al. found a clever way to perform the poling of active PE elements whilst the manufacturing is still ongoing. Such previous successes motivated the author to further pursue this direction as it was clear that there is a real benefit for operators and manufacturers.

- **Aim 2:** Demonstrate PM capabilities of pre-selected technologies numerically and in a realistic manufacturing environment.

  - *Objective 1:* Experimentally verify pre-selected technologies in a realistic manufacturing environment.

    Chapter 4 is dedicated to the development of a PM technique based on previously reported technologies in realistic composite manufacturing settings. The chapter contains the description of experimental setups and the corresponding results for technologies ranging from FOS-FBG, FOS-OBR, PE ceramic, polymeric PEs and electrical sensing. The results obtained are used to draw conclusions on their usability (see Objective 3 below).

- *Objective 2:* Consider sensor integration and protection strategies.

  Besides the fact that a specific sensor needs to be able to produce useful measurement data, it is important to also consider their implementation and protection. Since significant loads act on them during composite manufacturing, a mold based approach was put forward for PEs (section 4.3.1.1). However, this approach had its own limitations which are reported. Fiber optic sensors have shown to be able to deal with those limitations better, but require protection nonetheless. Section 4.3.3.5 is concerned with the selection of suitable optical fibers, coatings and the placement within components. Following these procedures allows for the successful integration and gathering of in-process data as well as for SHM.

- *Objective 3:* Perform a down-selection to a single technology.

  Experimental evidence suggested with increasing certainty, that FOS-OBR possessed the most suitable sensing capabilities and was able to survive the harsh processing conditions the best. Section 4.4 summarises the findings of the technology selection process that led to this decision.

- **Aim 3:** Develop an appropriate PM-SHM technique for a novel use case.

  - *Objective 1:* Show numerically the sensor's working principle.

    With FOS-OBR selected as the most suitable technology, the underpinning sensing working principle was shown by means of finite element analysis. Section 5.2 provides the details. It was shown how the FOS-OBR readings could be predicted when subjected to lateral reinforcement compaction. A four layered woven dry fiber stack was modelled using an Abaqus Explicit formulation. The strains seen by the optical fiber were then translated into optical frequency shift, the native unit of measure for FOS-OBR. A validation experiment showed good agreement between the numerical model and the measurements obtained directly from the fiber.

  - *Objective 2:* Develop in-house sensor manufacturing route for chosen technology.

    One major limitation of FOS-OBR initially was that the sensors needed to be bought from the OBR equipment OEM, with limited ability to customize them. Customization was required to accommodate different physical dimensions of the components to be monitored or in order to protect the sensor better from adverse handling. In section 4.3.3.5, the manufacturing steps involved in making a high quality FOS-OBR sensor in-house are described.

- *Objective 3:* Develop a PM-SHM solution for two prototypes, representative of complex aeronautical structures.

  With a successfully proven sensing technology at hand and a process of customizing the sensors, the technique was used on more complex geometries and with different manufacturing processes to further establish its usefulness. Chapter 6 describes the build, PM and SHM of a 500x500 mm tapered CFRP panel and a 50x50x1200 mm GFRP U-beam stiffener. Both components were fitted with a FOS-OBR during the manufacturing process and later subjected to damaging load scenarios. Useful information on the processing conditions as well as the damage mechanisms and their severity could be obtained. The increased complexity, however, also highlighted shortcomings and areas in which further work is required.

- **Aim 4:** Proposal of a novel monitoring technique that considers the learnings made and extends PM capabilities.

  - *Objective 1:* Develop a sensor profile with desired mechanical and monitoring properties.

    Taking into consideration that mechanical flexibility of the sensor itself is of high importance when it comes to actually implementing an integrated PM and SHM system, the search for a highly flexible carrier material lead to 3D-printable thermoplastic polyurethane. In section 7.2 the making of a printable ink for both insulation as well as electrical conduction is described in detail. This material and the process of how to make an ink is based on a paper by Valentine et al. [138] and it has been for the first time extended to SHM purposes.

  - *Objective 2:* Develop in-house sensor manufacturing route for the chosen technology.

    Another limitation faced by PM as well as SHM is the ability to actually place the sensing elements in the location of need. Current SHM technologies still require a high degree of manual labour when placing and installing sensors. In section 7.4.2 the author proposes a highly automated, robot-based 3D-printing process and workflow for fully automated sensor creation and installation directly onto substrates, including 3D geometries. The process was demonstrated to work with the above described ink.

  - *Objective 3:* Demonstrate the novel technology in PM and SHM settings.

    In the final stage, the above developed sensor printing process and ink was used to print strain sensing and crack detection devices directly onto CFRP tensile specimen. Section 7.5 describes the mechanical tests performed and also presents the results obtained. Overall a high level of linearity is observed with sufficient sensitivity in order to detect the presence of an artificial damage.

8.2 Relevance

Composite manufacturing is inherently expensive. This is due to high raw material cost, expensive cold storage facilities and a high degree of manual labour. It is desirable for **composite manufacturers** to drive down component rejection rates caused by quality concerns. The FOS-OBR technique has been shown to be able to measure local pressure distribution and predict fiber volume fractions. These are important process and component quality parameters. The FOS-OBR has the potential to inform the manufacturer in real time of any detrimental conditions to mend or stop the process and save costs. In addition, the reduced rejection rate means a more sustainable product as recycling of composite materials still is a difficult challenge today.
To **SHM engineers** the presented work is relevant in several ways. The work carried out to improve early integration of sensors into structures opens pathways for more efficient sensor placement and time savings in manual installation. Secondly, this thesis adds to the understanding around what phenomena FOS-OBR can in fact monitor and what not. It was shown that it is critically important to keep in mind what impact a certain defect will have on the structure and place sensors accordingly. One such example is given in section 6.3.3 where in a U-beam in three-point-bending condition, out of two slits made, only one of them was detected. However, the great flexibility of optical fibers and the ability to monitor large areas with FOS-OBR has shown remarkable damage detection and localization on the tapered CFRP panel in section 6.2.2.5. Lastly, the newly developed sensor manufacturing workflow based on robtic 3D-printing allows for a step-change in efficiency when it comes to the placement and wiring of sensors.
The author also expects that **composite part operators** responsible for the maintenance of their infrastructure will find this work particularly pertinent to their operations. They will receive the combined benefit of a more efficiently produced component with improved SHM capability.

8.3 Future work

To ensure the techniques proposed in this thesis can be progressed further to higher technology readiness levels which can be applied in industry and on-board of aircraft, several challenges remain to be explored further. It is also appreciated that certain aspects of the developed solution are somewhat immature at this moment. To overcome these remaining challenges it may even require the application of knowledge across different disciplines. In order to provide a structure to the proposed future work streams the following segmentation seems suitable:

- Proposed improvements to the FOS-OBR PM-SHM system:
  - Increase the amount of manufacturing processes in scope: As discussed in section 2.1, composites manufacturing processes are constantly being improved and increasingly automated. It would therefore be pertinent to expand the list of manufacturing processes that the proposed solution has been successfully demonstrated for. Whilst liquid resin techniques have been covered in detail in this thesis, the author suggests to expand towards automated prepreg processes like ATL and AFP as they are likely to be utilized more and more for the manufacture of near-future aircraft programs. The use of prepreg may also require autoclave curing which presents its own challenges when considering the routing of FOS. Figure 8.1 shows a prepreg autoclave mold designed by the author. The mold offers ingress and egress points for the FOS. The position of the ingress and egress points is such that the fiber is directly guided towards the lateral embedding position. This reduces the risk of localized bending and potential breakage. All areas in contact with the FOS are polished and any edges have been rounded to 1 mm radius in order to prevent sharp edges which could damage the fiber. This mold will be used in the near future to demonstrate the FOS-OBR for autoclave PM.
  - Couple the OBR with other measurement technologies: The FOS-OBR technique has been shown to work well whenever the fiber is subjected to mechanical loads or temperature gradients. An interesting prospect of FOS, however, is their ability to be spliced together with other functionalized fibers or by exploiting the interaction of the fiber itself with its environment. As such it would be beneficial to experiment with novel fiber coatings and fresnel refractometry in an OBR context.
  - Increase the acquisition frequency of FOS-OBR: Whilst for PM the low acquisition rates of OBR are not a serious problem, SHM settings usually require a system capable of performing measurements at several hundred kHz. It is acknowledged that the number of sensitive regions and maximum acquisition rates are somewhat of a trade-off to make. However, with ever increasing computational processing power it is expected that the processing of measurement data inside an OBR system can be sped up as well. Further development of the OBR technology will be needed in order to increase its measurement fidelity when used for SHM.
  - Develop novel FOS connectors: Stable FOS ingress and egress is of significant importance and at the same time a great challenge. This becomes particularly evident when considering sensor integration at early manufacturing stages. It is common practice for structural composite components to be manufactured with excess material all around. This excess needs to be machined off

to meet installation requirements and geometrical tolerances. This, however, poses a real problem for embedded sensors and networks as it could render them unusable when cut through. It is therefore important to focus on solutions for secondary means of connection or wireless systems. One potential idea to address this problem would be free space coupling of the laser light into the FOS.

- Proposed improvements to the flexible printed devices:
  - Improve the printability of inks: The TPPU inks developed herein require further improvements in terms of their printability. This includes a thorough study of their rheological properties and how they can be controlled. Common issues encountered include: clogging of the nozzle, changes in viscosity between different batches and aging. All of those issues need to be addressed in order to achieve consistently high printing quality.
  - Predict electrical properties: By solving the above it is expected that it will become possible to produce predictive models for the electrical properties of the printed devices. Such capability would allow for highly specialized sensors to be manufactured. To achieve this, the orientation and alignment of silver flakes during printing needs to be understood and the governing factors be controlled tightly.
  - Demonstrate other sensing devices: Besides the strain sensors demonstrated herein, the capacitive pressure sensor shown by Valentine et. al [138] further devices can be developed using the proposed method. One potential field of application are IDEs which can be used for cure monitoring.
  - Print on 3D-surfaces: The author sees the greatest potential for early and widespread industrial application by fully exploiting the fact that the proposed method is capable of directly printing onto 3D shapes. This opens the door for automated sensor application and wiring over large areas. To achieve that, the printing behaviour of inks needs to be well understood in order to prevent them from flowing during printing on angular sections. Also, the use of standard 3D-printing slicers will not be possible for such applications as the generated print paths are restricted to a single z-plane. What is needed here is the implementation of a software tool that is capable of efficiently producing 3D tool paths. One possible route may be the use of computer numerical control (commonly known as CNC) solutions.
- Measures to increase maturity of the proposed methods:
  - Demonstrate realistic in-service environmental conditions: So far, all SHM experiments were carried out in laboratory conditions only. This is known not to be representative given the large temperature, pressure and humidity gradients experienced by an aircraft within a single flight.

When proposing a new technique it is imperative to identify how well it performs under these realistic conditions. The author therefore proposes to initially perform extensive testing within a climatic chamber before exposing the system to in-flight testing. These tests should also include sensitivity analyses of the capability to detect damage under these realistic conditions.

– Show fatigue and long-term behaviour: Somewhat connected to the point made above is the need to show how well the system performs on the long-run and how well it deals with fatigue. This is both true for the sensing hardware as well as the signal quality. Aircraft are known to be in use for decades and any SHM system applied to a component should be able to match the life of the said component or exceed it. A thorough fatigue testing campaign is suggested here with continuous monitoring throughout.

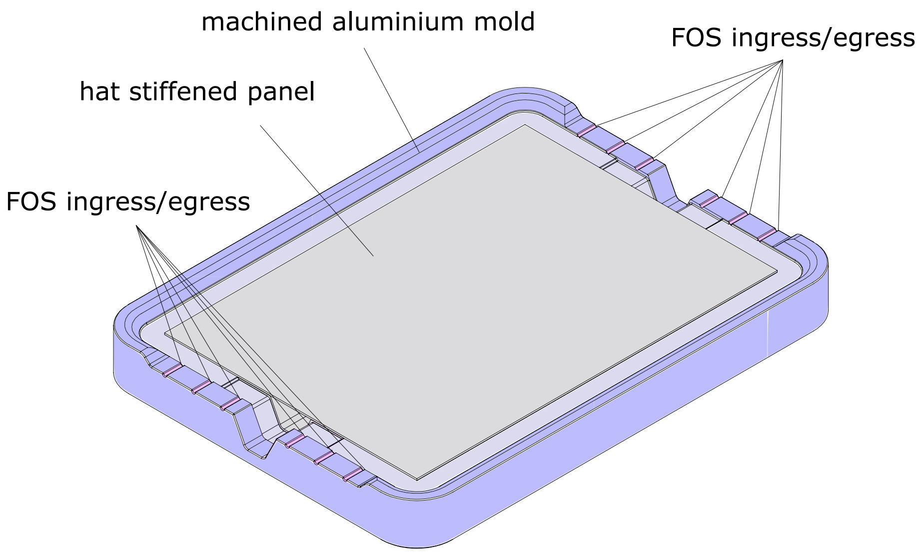

Figure 8.1: Hat stiffened mold designed and manufactured equipped and ready for FOS PM.

Bibliography

[1] Guy Norris and Mark Wagner. *Boeing 787 Dreamliner.* Zenith Press, 2009.

[2] R. A. Smith. Composite Defects and Their Detection. *Materials Science and Engineering*, III:103–143, 2009.

[3] U.S. Department of Transportation. Federal Aviation Administration and Federal Aviation Administration. Composite Aircraft Structure. Technical Report AC 20-107B, Federal Aviation Administration, 2010.

[4] Carl S. Byington, Michael J. Roemer, Gregory J. Kacprzymki, and Thomas Galie. Prognostic enhancements to diagnostic systems for improved condition-based maintenance. *IEEE Aerospace Conference Proceedings*, 6:2815–2824, 2002.

[5] Nan Yue, Zahra Sharif Khodaei, and Ferri M.H. Aliabadi. An Innovative Secondary Bonding of Sensors to Composite Structures for SHM Application. *Key Engineering Materials*, 774(August):516–522, 2018.

[6] Florian Lambinet and Zahra Sharif Khodaei. Damage detection & localization on composite patch repair under different environmental effects. *Engineering Research Express*, 2(4):1–21, 2020.

[7] Ting Dong and Nam H. Kim. Cost-Effectiveness of Structural Health Monitoring in Fuselage Maintenance of the Civil Aviation Industry. *Aerospace*, 5(87):1–24, 2018.

[8] Martin Meindlhumer, Konstantin Horejsi, and Martin Schagerl. Manufacturing and Costs of Current Sandwich and Future Monolithic Designs of Spoilers. *Journal of Aircraft*, 56(1):85–93, 2019.

[9] Alfred C. Loos. Low-cost fabrication of advanced polymeric composites by resin infusion processes. *Advanced Composite Materials: The Official Journal of the Japan Society of Composite Materials*, 10(2-3):99–106, 2001.

[10] Michael Scheerer, Zoltan Simon, Michael Marischler, and Bernhard Rittenschober. Validation of a multifunctional hybrid piezo / temperature sensor for process and structural health monitoring of

CFRP structures. In *9th European Workshop on Structural Health Monitoring July 10-13, 2018, Manchester, United Kingdom*, pages 1–12, 2018.

[11] Gardner Business Media Inc. The markets: Pressure vessels (2019), 2018.

[12] H. Hernández-Moreno, F. Collombet, B. Douchin, D. Choqueuse, P. Davies, and J. L. González Velázquez. Entire life time monitoring of filament wound composite cylinders using bragg grating sensors: Ii. process monitoring. *Applied Composite Materials*, 16(4):197–209, 2009.

[13] Amrita Kumar, Xinlin Qing, Thomas K. Delay, Shawn J. Beard, James L. Walker, Samuel S. Russell, and Mark Lin. Monitoring the integrity of filament-wound structures using built-in sensor networks. *Smart Structures and Materials 2003: Industrial and Commercial Applications of Smart Structures Technologies*, 5054(August 2003):222, 2003.

[14] Nicholas E. Ortyl. Damage evaluation and analysis of composite pressure vessels using fiber Bragg gratings to determine structural health. *Fiber Optic Sensor Technology and Applications IV*, 6004(November 2005):60040D, 2005.

[15] B. Vieille, W. Albouy, and L. Taleb. Investigations on stamping of C/PEEK laminates: Influence on meso-structure and macroscopic mechanical properties under severe environmental conditions. *Composites Part B: Engineering*, 63:101–110, 2014.

[16] Giuseppe Dell'Anno, Ivana Partridge, Denis Cartié, Alexandre Hamlyn, Edmon Chehura, Stephen James, and Ralph Tatam. Automated manufacture of 3D reinforced aerospace composite structures. *International Journal of Structural Integrity*, 3(1):22–40, 2012.

[17] Berend Denkena, Carsten Schmidt, and Patricc Weber. Automated Fiber Placement Head for Manufacturing of Innovative Aerospace Stiffening Structures. In *Procedia Manufacturing*, volume 6, pages 96–104. Elsevier B.V., 2016.

[18] M. N. Grimshaw, C. G. Grant, and J. M.L. Diaz. Advanced technology tape laying for affordable manufacturing of large composite structures. *International SAMPE Symposium and Exhibition (Proceedings)*, 46 II(4):2484–2494, 2001.

[19] Amanda Jacob. Thermoplastic composites fly on G650 tail, 2010.

[20] Richard Stewart. Thermoplastic composites — recyclable and fast to process. *Reinforced Plastics*, 55(3):22–28, 2011.

[21] S. Boria, A. Scattina, and G. Belingardi. Experimental evaluation of a fully recyclable thermoplastic composite. *Composite Structures*, 140:21–35, 2016.

[22] B. Zheng, M. Li, T. Deng, H. Zhou, Z. Huang, H. Zhou, and D. Li. Process–structure–property relationships of thermoformed woven carbon-fiber-reinforced polyether-ether-ketone composites. *Polymer Composites*, 10:3823–3834, 2019.

[23] Daichi Tatsuno, Takeshi Yoneyama, Kiichirou Kawamoto, and Masayuki Okamoto. Hot press forming of thermoplastic CFRP sheets. *Procedia Manufacturing*, 15:1730–1737, 2018.

[24] Casey Keulen, Bruno Rocha, Afzal Suleman, and Mehmet Yildiz. Design of an Embedded Sensor Network for Manufacturing Process Monitoring, Quality Control Management and Structural Health Assessment of Advanced Composite Structures. In *Proceedings of the ASME 2010 International Mechanical Engineering Congress & Exposition*, pages 197–206, 2010.

[25] Alexandros A. Skordos, Ivana K. Partridge, Athanasios Dimopoulos, Stephen W. James, Edmond Chehura, Ralph P. Tatam, and Stephen J. Buggy. Fibre grating refractometer sensors for composite process monitoring. *Optical Measurement Systems for Industrial Inspection V*, 6616(June 2007):661635, 2007.

[26] C. M. Stokes-Griffin and P. Compston. The effect of processing temperature and placement rate on the short beam strength of carbon fibre-PEEK manufactured using a laser tape placement process. *Composites Part A: Applied Science and Manufacturing*, 78:274–283, 2015.

[27] T. K. Slange, L. Warnet, W. J.B. Grouve, and R. Akkerman. Influence of preconsolidation on consolidation quality after stamp forming of C/PEEK composites. *AIP Conference Proceedings*, 1769(October 2016):1–6, 2016.

[28] N Liebers, M Buggisch, M Kleineberg, and M Wiedemann. Autoclave infusion of aerospace ribs based on process monitoring and control by ultrasound sensors. In *The 20th International Conference on Composite Materials, Copenhagen, 19-24th July 2015*, pages 1–10, 2015.

[29] D. G. Aggelis and A. S. Paipetis. Monitoring of resin curing and hardening by ultrasound. *Construction and Building Materials*, 26(1):755–760, 2012.

[30] Michael Scheerer, Zoltan Simon, Michael Marischler, and Bernhard Rittenschober. A Multifunctional Piezo and Temperature Sensor for Process and Structural Health Monitoring of CFRP Strucutres Made by Resin Transfer Molding. In *Structural Health Monitoring 2017: Real-Time State Awareness and Data-Driven Safety Assurance: Proceedings of the 11th International Workshop on Structural Health Monitoring*, pages 2555–2562, 2017.

[31] T B Hudson. *Real-time Cure Monitoring of Composites Using a Guided wave-based System with High Temperature Piezoelectric Transducers, Fiber Bragg Gratings, and Phase-shifted Fiber Bragg Gratings.* Thesis doctor of philosophy, North Carolina State University, 2017.

[32] In-Kyung Park, Doo-Sung Lee, and Jae-Do Nam. Equivalent processing time analysis of glass transition development in epoxy/carbon fiber composite systems. *Journal of Applied Polymer Science*, 84(1):144–154, 2002.

[33] S. M.R. Kazmi, Q. Govignon, and S. Bickerton. Control of laminate quality for parts manufactured using the resin infusion process. *Journal of Composite Materials*, 53(3):327–343, 2018.

[34] Boming Zhang, Zhanjun Wu, and Danfu Wang. Composite cure process optimization with the aid of fiber optic sensors. *Industrial Sensing Systems*, 4202(December 2000):15–20, 2000.

[35] Sébastien Gueroult, Aurélie Lebel-Lavacry, Chung Hae Park, Laurent Bizet, Abdelghani Saouab, and Joël Bréard. Analytical modeling and in situ measurement of void formation in liquid composite molding processes. *Advanced Composite Materials*, 23(1):31–42, 2014.

[36] Nacef Ghodhbani, Pierre Maréchal, and Hugues Duflo. Ultrasound monitoring of the cure kinetics of an epoxy resin: Identification, frequency and temperature dependence. *Polymer Testing*, 56:156–166, 2016.

[37] Christopher Buchmann, Jürgen Filsinger, and Elisabeth Ladstätter. Investigation of Electrical Time Domain Reflectometry for infusion and cure monitoring in combination with electrically conductive fibers and tooling materials. *Composites Part B: Engineering*, 94:389–398, 2016.

[38] Mehmet Yildiz, Talha Boz, Ege F. Sengun, Gokhan Bektas, Casey J. Keulen, Yusuf Z. Menceloglu, Cem Ozturk, Nazli G. Ozdemir, and Afzal Suleman. An Experimental Study on the Process Monitoring of Resin Transfer Molded Composite Structures Using Fiber Optic Sensors. *Journal of Manufacturing Science and Engineering*, 134(4):044502, 2012.

[39] Gaurav Pandey, Hope Deffor, Erik T. Thostenson, and Dirk Heider. Smart tooling with integrated time domain reflectometry sensing line for non-invasive flow and cure monitoring during composites manufacturing. *Composites Part A: Applied Science and Manufacturing*, 47(1):102–108, 2013.

[40] Muhammad A. Ali, Rehan Umer, Kamran A. Khan, Yarjan A. Samad, Kin Liao, and Wesley Cantwell. Graphene coated piezo-resistive fabrics for liquid composite molding process monitoring. *Composites Science and Technology*, 148:106–114, 2017.

[41] Rebecca Y.N. Wong, Edmon Chehura, Stephen W. James, and Ralph P. Tatam. Resin Directional Flow and Degree of Cure Sensing Using Chirped Optical Fiber Long Period Gratings. *IEEE Sensors Journal*, 17(20):6605–6614, 2017.

[42] K. O. Hill, Y. Fujii, D. C. Johnson, and B. S. Kawasaki. Photosensitivity in optical fiber waveguides: Application to reflection filter fabrication. *Applied Physics Letters*, 32(10):647–649, 1978.

[43] Mark Froggatt and Jason Moore. High-spatial-resolution distributed strain measurement in optical fiber with Rayleigh scatter. *Applied Optics*, 37(10):1735–1740, 1998.

[44] Alan D. Kersey, Michael A. Davis, Heather J. Patrick, Michel LeBlanc, K. P. Koo, C. G. Askins, M. A. Putnam, and E. Joseph Friebele. Fiber grating sensors. *Journal of Lightwave Technology*, 15(8):1442–1462, 1997.

[45] Xiaolei Li, Qizhen Sun, Duan Liu, Ruibing Liang, Jiejun Zhang, Jianghai Wo, Perry Ping Shum, and Deming Liu. Simultaneous wavelength and frequency encoded microstructure based quasi-distributed temperature sensor. *Optics Express*, 20(11):12076, 2012.

[46] Gui Xin, Li Zhengying, Wang Fan, Wang Yiming, Wang Changjia, Zeng Siyue, and Yu Haihu. Distributed sensing technology of high-spatial resolution based on dense ultra-short FBG array with large multiplexing capacity. *Optics Express*, 25(23):28112, 2017.

[47] Xin Gui, Zhengying Li, Xuelei Fu, Changjia Wang, Yiming Wang, Hongli Li, and Honghai Wang. High-density distributed crack tip sensing system using dense ultra-short FBG sensors. *Sensors (Switzerland)*, 19(7), 2019.

[48] Luna Innovations. Luna Innovations Webpage, 2021.

[49] Valentin Buchinger and Zahra Sharif Khodaei. Vacuum assisted resin transfer moulding process monitoring by means of distributed fibre-optic sensors: a numerical and experimental study. *Advanced Composite Materials*, 31(5):467–484, sep 2022.

[50] S. Miclos, D. Savastru, R. Savastru, and I. I. Lancranjan. Transverse mechanical stress and optical birefringence induced into single-mode optical fibre embedded in a smart polymer composite material. *Composite Structures*, 218(July 2018):15–26, 2019.

[51] Axel Bertholds and Réne Dändliker. Determination of the Individual Strain-Optic Coefficients in Single-mode Optical Fibers. *Journal of Lightwave Technology*, 6(1):17–20, 1988.

[52] Eli Voet. *In-situ Deformation Monitoring of Aerospace Qualified Composites with Embedded Improved Draw Tower Fibre Bragg Gratings*. PhD thesis, Ghent University, 2011.

[53] M H Ferri Aliabadi and Zahra Sharif Khodaei. *Structural Health Monitoring for Advanced Composite Structures*, volume 08 of *Computational and Experimental Methods in Structures.* WORLD SCIENTIFIC (EUROPE), feb 2018.

[54] Horace Lamb. On waves in an elastic plate. *Proceedings of the Royal Society of London. Series A, Containing Papers of a Mathematical and Physical Character*, 93(648):114–128, 1917.

[55] Yanfeng Shen and Carlos E. S. Cesnik. Modeling Guided Wave Propagation in Composite Structures Using Local Interaction Simulation Approach. In M. H. Ferri Aliabadi and Zahra Sharif Khodaei, editors, *Structural Health Monitoring for Advanced Composite Structures*, chapter 2, pages 47–92. World Scientific Publishing Europe Ltd., 2018.

[56] Ifan Dafydd and Zahra Sharif Khodaei. Analysis of barely visible impact damage severity with ultrasonic guided Lamb waves. *Structural Health Monitoring*, 19(4):1104–1122, 2020.

[57] Victor Giurgiutiu. Electroactive and Magnetoactive Materials. In *Structural Health Monitoring with Piezoelectric Wafer Active Sensors*, pages 21–49. Elsevier, 2014.

[58] The Institute of Electrical and Electronics Engineers Inc. IEEE Standard on Piezoelectricity. Technical Report 2, The Institute of Electrical and Electronics Engineers Inc., New York, 1984.

[59] Piezotech by Arkema. TDS Piezotech ® FC, 2018.

[60] Ting Dong and Nam Ho Kim. Reviews of Structural Health Monitoring Technologies in Airplane Fuselage Maintenance Perspective. In *AIAA/AHS Adaptive Structures Conference*, number AIAA SciTech Forum, pages 1–16, 2018.

[61] Iddo Kressel and Osher Shapira. Airworthiness Monitoring of the Wings of a UAV Fleet Using Fiber Optic Distributed Sensing. In *29th ICAF Symposium – Nagoya, 7–9 June 2017*, number ICAF Symposium, pages 1–5, 2017.

[62] Sung Jun Joo, Myeong Hyeon Yu, Eun Beom Jeon, and Hak Sung Kim. In situ fabrication of copper electrodes on carbon-fiber-reinforced polymer (CFRP) for damage monitoring by printing and flash light sintering. *Composites Science and Technology*, 142:189–197, 2017.

[63] Huasheng Zheng, Sirong Zhu, and Zhuoqiu Li. Continuous deformation monitoring by polymer-matrix carbon fiber sensitive layer. *Journal Wuhan University of Technology, Materials Science Edition*, 31(3):705–712, 2016.

[64] Jan Cagáň, Jaroslav Pelant, Martin Kyncl, Martin Kadlec, and Lenka Michalcová. Damage detection in carbon fiber–reinforced polymer composite via electrical resistance tomography with Gaussian anisotropic regularization. *Structural Health Monitoring*, 18(5-6):1698–1710, nov 2019.

[65] Khaled Almuhammadi, Arief Yudhanto, and Gilles Lubineau. Real-time electrical impedance monitoring of carbon fiber-reinforced polymer laminates undergoing quasi-static indentation. *Composite Structures*, 207(July 2018):255–263, 2019.

[66] Khaled Almuhammadi, Tushar Kanti Bera, and Gilles Lubineau. Electrical impedance spectroscopy for measuring the impedance response of carbon-fiber-reinforced polymer composite laminates. *Composite Structures*, 168:510–521, 2017.

[67] Dimitrios G. Bekas, Zahra Sharif-Khodaei, Dimitrios Baltzis, M. H.Ferri Aliabadi, and Alkiviadis S. Paipetis. Quality assessment and damage detection in nanomodified adhesively-bonded composite joints using inkjet-printed interdigital sensors. *Composite Structures*, 211(November 2018):557–563, 2019.

[68] Z. Sharif-Khodaei, M. Ghajari, and M. H. Aliabadi. Impact Damage Detection in Composite Plates using a Self-diagnostic Electro-Mechanical Impedance-based Structural Health Monitoring System. *Journal of Multiscale Modelling*, 06(04):1550013, 2016.

[69] Zahra Sharif-Khodaei and M. H. Ferri Aliabadi. Impact Detection and Identification with Piezoceramic Sensors: Passive Sensing. In M. H. Ferri Aliabadi and Zahra Sharif Khodaei, editors, *Structural Health Monitoring for Advanced Composite Structures*, chapter 7, pages 215–266. World Scientific Publishing Europe Ltd., 2018.

[70] R. Brett Williams, Gyuhae Park, Daniel J. Inman, and W. Keats Wilkie. An Overview of Composite Actuators with Piezoceramic Fibers. In *Proceedings of SPIE - The International Society for Optical Engineering*, pages 421–427, 2002.

[71] Xin Lu, Hang Qu, and Maksim Skorobogatiy. Piezoelectric microstructured fibers via drawing of multimaterial preforms. *Scientific Reports*, 7(1):1–12, 2017.

[72] Roger M. Groves, Edmon Chehura, Weilai Li, Stephen E. Staines, Stephen W. James, and Ralph P. Tatam. Surface strain measurement: A comparison of speckle shearing interferometry and optical fibre Bragg gratings with resistance foil strain gauges. *Measurement Science and Technology*, 18(5):1175–1184, 2007.

[73] Simone Weber, Thomas Kissinger, Edmond Chehura, Stephen Staines, James Barrington, Kevin Mullaney, Luca Zanotti Fragonara, Ivan Petrunin, Stephen James, Mudassir Lone, and Ralph Tatam.

Application of fibre optic sensing systems to measure rotor blade structural dynamics. *Mechanical Systems and Signal Processing*, 158:107758, 2021.

[74] Thomas Kissinger, Simone Weber, Edmond Chehura, James H. Barrington, Stephen Staines, Stephen W. James, Mudassir Lone, and Ralph P. Tatam. Ground vibration testing of a helicopter rotor blade using optical fibre sensors. In *Seventh European Workshop on Optical Fibre Sensors*, volume 1119902, page 5, 2019.

[75] Yunshil Choi, Syed Haider Abbas, and Jung Ryul Lee. Aircraft integrated structural health monitoring using lasers, piezoelectricity, and fiber optics. *Measurement: Journal of the International Measurement Confederation*, 125(April):294–302, 2018.

[76] Cheng Xu and Zahra Sharif Khodaei. A Novel Fabry-Pérot Optical Sensor for Guided Wave Signal Acquisition. *Sensors*, 20(6):1728, mar 2020.

[77] Alfredo Guemes. SHM of Composite Structures by Fiber Optic Sensors. In M. H.Ferri Aliabadi and Zahra Sharif-Khodaei, editors, *Structural Health Monitoring for Advanced Composite Structures*, chapter 6, pages 191–214. World Scientific Publishing Europe Ltd., 2018.

[78] D. G. Bekas and A. S. Paipetis. Damage monitoring in nanoenhanced composites using impedance spectroscopy. *Composites Science and Technology*, 134:96–105, 2016.

[79] Casey J. Keulen, Mehmet Yildiz, and Afzal Suleman. Multiplexed FBG and etched fiber sensors for process and health monitoring of 2-&3-D RTM components. *Journal of Reinforced Plastics and Composites*, 30(12):1055–1064, 2011.

[80] Xiaoming Wang, Claus Ehlers, Christian Kissinger, Manfred Neitzel, Lin Ye, and Yiu-Wing Mai. Potential of Piezoelectric Elements in the Monitoring of Composite Manufacturing Process. *Journal of Intelligent Material Systems and Structures*, 8(12):1073–1078, 1997.

[81] J. Z. Hao, C. M. Tay, C. Y. Liaw, C. Lu, and S.C. Tjin. A novel FBG pressure sensor with low temperature sensitivity. In *2003 IEEE LEOS Annual Meeting Conference Proceedings (IEEE Cat. No.03CH37460)*, pages 21–22, 2003.

[82] Ji-Ying Huang, Christophe Caucheteur, Antonio Bueno Martinez, Thomas Geernaert, Eric Lindner, Johan Vlekken, Bram Van Hoe, Jan Van Roosbroeck, and Francis Berghmans. FBGs written in specialty fiber for high pressure/high temperature measurement. *Optics Express*, 25(15):17936, 2017.

[83] Thomas Geernaert, Eric Daerden, Jan Van Roosbroeck, Ji-Ying Huang, Christophe Caucheteur, Eric Lindner, Johan Vlekken, Bram Van Hoe, Antonio Bueno Martinez, and Francis Berghmans. Packaged

FBG based optical fiber sensor for simultaneous pressure and temperature monitoring. In *SPIE Commercial + Scientific Sensing and Imaging, 2018, Orlando, Florida, United States*, volume 1065409, page 8, 2018.

[84] P. Roriz, M. S. Ferreira, K. Schuster, J. Kobelke, and O. Frazão. A Fabry-Perot sensor prototype for low-pressure measurements. *Microwave and Optical Technology Letters*, 56(12):2981–2986, dec 2014.

[85] Qingchao Zhao, Xiaohui Liu, Long Ma, Wenan Zhao, and Hongzhong Wang. Optical fiber pressure sensor based on F-P cavity in the oil and gas well. *IOP Conference Series: Earth and Environmental Science*, 64(1):1–8, may 2017.

[86] M. Cassiède, J.-L. Daridon, J. H. Paillol, and J. Pauly. Impedance analysis for characterizing the influence of hydrostatic pressure on piezoelectric quartz crystal sensors. *Journal of Applied Physics*, 108(3):034505, aug 2010.

[87] Nico Liebers, Florian Raddatz, and Florian Schadow. Effective and flexible ultrasound sensors for cure monitoring for industrial composite production. In *Deutscher Luft- und Raumfahrtkongress 2012*, pages 1–6, 2012.

[88] Keiji K. Kanazawa and Joseph G. II Gordon. The Oscillation Frequency of a Quartz Resonator in Contact with a Liquid. *Analytica Chimica Acta*, 175:99–105, 1985.

[89] Xiaoming Wang, Claus Ehlers, Christian Kissinger, Manfred Neitzel, Lin Ye, and Yiu-Wing Mai. Sensitivity of piezoelectric wafers to the curing of thermoset resins and thermoset composites. *Smart Materials and Structures*, 7(1):113–120, 1998.

[90] Francesca Lionetto and Alfonso Maffezzoli. Monitoring the Cure State of Thermosetting Resins by Ultrasound. *Materials*, 6:3783–3804, 2013.

[91] Tyler B. Hudson, Nicolas Auwaijan, and Fuh Gwo Yuan. Guided wave-based system for real-time cure monitoring of composites using piezoelectric discs and phase-shifted fiber Bragg gratings. *Journal of Composite Materials*, 53(7):969–979, 2019.

[92] PI Ceramic GmbH. Piezoelectric Materials, 2019.

[93] Xiaoning Jiang, Kyungrim Kim, Shujun Zhang, Joseph Johnson, and Giovanni Salazar. High-temperature piezoelectric sensing. *Sensors (Switzerland)*, 14(1):144–169, 2014.

[94] Shujun Zhang, Edward Alberta, Richard E. Eitel, Paul W. Rehrig, Wesley Hackenberger, Clive A. Randall, and Thomas R. Shrout. High temperature piezoelectric materials for actuators and sensors.

Smart Structures and Materials 2005: Active Materials: Behavior and Mechanics, 5761(May 2005):279, 2005.

[95] Poh-Sang Lam, Christopher Verst, Hanfei Mei, Mohammad Faisal Haider, Victor Giurgiutiu, Bin Lin, and Lingyu Yu. Piezoelectric wafer active sensors under gamma radiation exposure toward applications for structural health monitoring of nuclear dry cask storage systems. In Peter J. Shull, editor, *Nondestructive Characterization and Monitoring of Advanced Materials, Aerospace, Civil Infrastructure, and Transportation XII*, number Nondestructive Characterization and Monitoring of Advanced Materials, Aerospace, Civil Infrastructure, and Transportation XII, page 85. SPIE, mar 2018.

[96] Werner A. Hufenbach, Niels Modler, Anja Winkler, Juergen Ilg, and Stefan J. Rupitsch. Fibre-reinforced composite structures based on thermoplastic matrices with embedded piezoceramic modules. *Smart Materials and Structures*, 23(2):025011, feb 2014.

[97] Stefan J. Rupitsch, Jürgen Ilg, and Reinhard Lerch. Inverse scheme to identify the temperature dependence of electromechanical coupling factors for piezoceramics. In *2013 Joint IEEE International Symposium on Applications of Ferroelectric and Workshop on Piezoresponse Force Microscopy, ISAF/PFM 2013*, number ISAF/PFM 2013, pages 183–186, 2013.

[98] Zhe Yang, Hongdan Peng, Weizhi Wang, and Tianxi Liu. Crystallization behavior of poly(ϵ-caprolactone)/layered double hydroxide nanocomposites. *Journal of Applied Polymer Science*, 116(5):2658–2667, 2010.

[99] Edmon Chehura, Renata Jarzebinska, Elisabete F. R. Da Costa, Alexandros A. Skordos, Stephen W. James, Ivana K. Partridge, and Ralph P. Tatam. Multiplexed fibre optic sensors for monitoring resin infusion, flow, and cure in composite material processing. *Smart Sensor Phenomena, Technology, Networks, and Systems Integration 2013*, 8693(April 2013):86930F, 2013.

[100] Edmon Chehura, Stephen W. James, Stephen Staines, Chris Groenendijk, Denis Cartie, Stephanie Portet, Michael Hugon, and Ralph P. Tatam. Production process monitoring and post-production strain measurement on a full-size carbon-fibre composite aircraft tail cone assembly using embedded optical fibre sensors. *Measurement Science and Technology*, 31(10):105204, oct 2020.

[101] Stephen J. Buggy, Edmon Chehura, Stephen W. James, and Ralph P. Tatam. Fibre gratings for cure monitoring of epoxy resins. *Optics InfoBase Conference Papers*, pages 1–4, 2006.

[102] Stephen J. Buggy, Edmond Chehura, Alexandros A. Skordos, Athanasios Dimopoulos, Stephen W. James, Ivana K. Partridge, and Ralph P. Tatam. Fibre grating refractometer sensors for composite process monitoring. *Optical Measurement Systems for Industrial Inspection V*, 6616(0):661635, 2007.

[103] E. Chehura, A. A. Skordos, C. C. Ye, S. W. James, I. K. Partridge, and R. P. Tatam. Strain development in curing epoxy resin and glass fibre/epoxy composites monitored by fibre Bragg grating sensors in birefringent optical fibre. *Smart Materials and Structures*, 14(2):354–362, 2005.

[104] Edmon Chehura, Chen-chun Ye, Stephen E Staines, Stephen W James, and Ralph P Tatam. Characterisation of the response of fibre Bragg gratings fabricated in stress and geometrically induced high birefringence fibres to temperature and transverse load. *Smart Structures and Materials*, 13(4):888–895, 2004.

[105] Edmon Chehura, Stephen W. James, and Ralph P. Tatam. Simultaneous independent measurement of temperature and strain using a tilted fibre Bragg grating. *Third European Workshop on Optical Fibre Sensors*, 6619(July 2007):66190I, 2007.

[106] Edmon Chehura, Stephen W James, and Ralph P Tatam. Temperature and strain discrimination using a single tilted fibre Bragg grating. *Optics Communications*, 275(2):344–347, 2007.

[107] Ricardo Correia, Edmon Chehura, Stephen W. James, and Ralph P. Tatam. A pressure sensor based upon the transverse loading of a sub-section of an optical fibre Bragg grating. *Measurement Science and Technology*, 18(10):3103–3110, 2007.

[108] Ricardo Correia, Edmon Chehura, Stephen W. James, and Ralph P. Tatam. Transversely loaded fibre Bragg grating for pressure measurements. *Third European Workshop on Optical Fibre Sensors*, 6619:66191A, 2007.

[109] J. Jakobsen, A. Skordos, S. James, R. G. Correia, and M. Jensen. In-situ Curing Strain Monitoring of a Flat Plate Residual Stress Specimen Using a Chopped Stand Mat Glass/Epoxy Composite as Test Material. *Applied Composite Materials*, 22(6):805–822, 2015.

[110] Kazunori Takagaki, Shu Minakuchi, and Nobuo Takeda. Process-induced strain and distortion in curved composites. Part I: Development of fiber-optic strain monitoring technique and analytical methods. *Composites Part A: Applied Science and Manufacturing*, 103:236–251, 2017.

[111] P. J. Schubel, R. J. Crossley, E. K.G. Boateng, and J. R. Hutchinson. Review of structural health and cure monitoring techniques for large wind turbine blades. *Renewable Energy*, 51:113–123, 2013.

[112] Hak Sung Kim, Seong Hwan Yoo, and Seung Hwan Chang. In situ monitoring of the strain evolution and curing reaction of composite laminates to reduce the thermal residual stress using FBG sensor and dielectrometry. *Composites Part B: Engineering*, 44(1):446–452, 2013.

[113] M. Arhant, N. Meek, D. Penumadu, P. Davies, and N. Garg. Residual Strains using Integrated Continuous Fiber Optic Sensing in Thermoplastic Composites and Structural Health Monitoring. *Experimental Mechanics*, 58(1):167–176, 2018.

[114] Shu Minakuchi, Shoma Niwa, Kazunori Takagaki, and Nobuo Takeda. Composite cure simulation scheme fully integrating internal strain measurement. *Composites Part A: Applied Science and Manufacturing*, 84:53–63, 2016.

[115] Takuhei Tsukada, Shin Ichi Takeda, Shu Minakuchi, Yutaka Iwahori, and Nobuo Takeda. Evaluation of the influence of cooling rate on residual strain development in unidirectional carbon fibre/polyphenylenesulfide laminates using embedded fibre Bragg grating sensors. *Journal of Composite Materials*, 51(13):1849–1859, 2017.

[116] Dimitrios Bekas, Zahra Sharif-Khodaei, and M.H. Aliabadi. An Innovative Diagnostic Film for Structural Health Monitoring of Metallic and Composite Structures. *Sensors*, 18(7):2084, jun 2018.

[117] Florian Lambinet and Zahra Sharif Khodaei. Development of Hybrid Piezoelectric-Fibre Optic Composite Patch Repair Solutions. *Sensors*, 21(15):5131, jul 2021.

[118] Ilias N. Giannakeas, Zahra Sharif Khodaei, and M. H. Aliabadi. An up-scaling temperature compensation framework for guided wave–based structural health monitoring in large composite structures. *Structural Health Monitoring*, 0(0):1–22, may 2022.

[119] Nan Yue and M. H. Aliabadi. A scalable data-driven approach to temperature baseline reconstruction for guided wave structural health monitoring of anisotropic carbon-fibre-reinforced polymer structures. *Structural Health Monitoring*, 19(5):1487–1506, 2020.

[120] F. Lambinet and Z. Sharif Khodaei. Damage detection in composite skin stiffener with hybrid PZT-FO SHM system. *Key Engineering Materials*, 754 KEM:367–370, 2017.

[121] Florian Lambinet. *Structural health monitoring of composite patch repair*. PhD thesis, Imperial College London, 2019.

[122] E. Kirkby, R. de Oliveira, V. Michaud, and J. A. Månson. Impact localisation with FBG for a self-healing carbon fibre composite structure. *Composite Structures*, 94(1):8–14, 2011.

[123] Jeannot Frieden, Joël Cugnoni, John Botsis, and Thomas Gmür. Low energy impact damage monitoring of composites using dynamic strain signals from FBG sensors - Part I: Impact detection and localization. *Composite Structures*, 94(2):438–445, 2012.

[124] Byeong Wook Jang, Sang Oh Park, Yeon Gwan Lee, Chun Gon Kim, and Chan Yik Park. Detection of impact damage in composite structures using high speed FBG interrogator. *Advanced Composite Materials*, 21(1):29–44, 2012.

[125] A. Rezayat, B. De Pauw, A. Lamberti, M. El-Kafafy, V. Nassiri, J. Ertveldt, G. Arroud, S. Vanlanduit, and P. Guillaume. Reconstruction of impacts on a composite plate using fiber Bragg gratings (FBG) and inverse methods. *Composite Structures*, 149:1–10, 2016.

[126] Sidney Goossens, Francis Berghmans, Kirsa Muñoz, Miguel Jiménez, Evangelos Karachalios, Diego Saenz-Castillo, and Thomas Geernaert. A global assessment of barely visible impact damage for CFRP sub-components with FBG-based sensors. *Composite Structures*, 272(April):114025, 2021.

[127] Jiang Wensong, Du Liangya, Luo Zai, Yang Li, and Song Hao. Multi-FBG sensor array-based impact localization with an energy eigenvector. *Optical Engineering*, 61(06):1–17, 2022.

[128] Victor Giurgiutiu. Wave Propagation SHM with PWAS Transducers. In *Structural Health Monitoring with Piezoelectric Wafer Active Sensors*, pages 639–706. Elsevier, 2014.

[129] Cheng Xu. *Condition monitoring of composite structure with Fibre Optic Sensors*. PhD thesis, Imperial College London, 2022.

[130] Jung Ryul Lee, Hiroshi Tsuda, and Bon Yong Koo. Single-mode fibre optic Bragg grating sensing on the base of birefringence in surface-mounting and embedding applications. *Optics and Laser Technology*, 39(1):157–164, 2007.

[131] Umesh Sampath, Hyunjin Kim, Dae Gil Kim, Young Chon Kim, and Minho Song. In-situ cure monitoring of wind turbine blades by using fiber bragg grating sensors and fresnel reflection measurement. *Sensors (Switzerland)*, 15(8):18229–18238, 2015.

[132] Ki Joong Kim, Ping Lu, Jeffrey T. Culp, and Paul R. Ohodnicki. Metal-Organic Framework Thin Film Coated Optical Fiber Sensors: A Novel Waveguide-Based Chemical Sensing Platform. *ACS Sensors*, 3(2):386–394, 2018.

[133] Nicholas D. Rees, Stephen W. James, Ralph P. Tatam, and Geoffery J. Ashwell. Optical fiber long-period gratings with Langmuir–Blodgett thin-film overlays. *Optics Letters*, 27(9):686, 2002.

[134] S. M. Topliss, S. W. James, F. Davis, S. P.J. Higson, and R. P. Tatam. Optical fibre long period grating based selective vapour sensing of volatile organic compounds. *Sensors and Actuators, B: Chemical*, 143(2):629–634, 2010.

[135] Stephen W. James and Ralph P. Tatam. Fibre optic sensors with nano-structured coatings. *Journal of Optics A: Pure and Applied Optics*, 8(7):S430–S444, jul 2006.

[136] Stephen W. James, Chun-Yang Wei, Chen-Chung Ye, Ralph P. Tatam, and P. E. Irving. An investigation of the tensile strength of fibre Bragg gratings. In *13th International Conference on Optical Fiber Sensors*, volume 374631, page 108, 1999.

[137] M M B Hasan, Ch Cherif, A B M Foisal, T Onggar, R D Hund, and A Nocke. Development of conductive coated Polyether ether ketone (PEEK) filament for structural health monitoring of composites. *Composites Science and Technology*, 88:76–83, 2013.

[138] Alexander D. Valentine, Travis A. Busbee, John William Boley, Jordan R. Raney, Alex Chortos, Arda Kotikian, John Daniel Berrigan, Michael F. Durstock, and Jennifer A. Lewis. Hybrid 3D Printing of Soft Electronics. *Advanced Materials*, 29(40):1–8, 2017.

[139] Valentin Buchinger, Zahra Sharif-Khodaei, and M.H. Aliabadi. Development of 3D-printed Flexible Devices for Strain Sensing and Damage Detection. In *20th International conference on Fracture and Damage Mechanics FDM 2022*, page (awaiting publication), 2022.

[140] Dimitrios G. Bekas, Zahra Sharif-Khodaei, and Ferri M H Aliabadi. A smart multi-functional printed sensor for monitoring curing and damage of composite repair patch. *Smart Materials and Structures*, 28(8):085029, aug 2019.

[141] F. Lambinet and Z. Sharif Khodaei. Measurement platform for structural health monitoring application of large scale structures. *Measurement: Journal of the International Measurement Confederation*, 190(January):110675, 2022.

[142] FUJIFILM Dimatix Inc. Dimatix Materials Printer and Cartridge, 2019.

[143] I. A. Aponte, B. Esser, Z. C. Shaw, James C. Dickens, John J. Mankowski, and Andreas A. Neuber. Fundamental study of DC and RF breakdown of atmospheric air. *Physics of Plasmas*, 26(12):123512, dec 2019.

[144] Marilyne Philibert, Shuting Chen, Voon Kean Wong, Kui Yao, Constantinos Soutis, and Matthieu Gresil. Direct-Write Piezoelectric Transducers on Carbon-Fiber-Reinforced Polymer Structures for Exciting and Receiving Guided Ultrasonic Waves. *IEEE Transactions on Ultrasonics, Ferroelectrics, and Frequency Control*, 68(8):2733–2740, 2021.

[145] John B. Enns and John K. Gillham. Time–temperature–transformation (TTT) cure diagram: Modeling the cure behavior of thermosets. *Journal of Applied Polymer Science*, 28(8):2567–2591, 1983.

[146] Long Jin, Weigang Zhang, Hao Zhang, Bo Liu, Jian Zhao, Qinchang Tu, Guiyun Kai, and Xiaoyi Dong. An embedded FBG sensor for simultaneous measurement of stress and temperature. *IEEE Photonics Technology Letters*, 18(1):154–156, 2006.

[147] Dirk Havermann, Jinesh Mathew, William N. MacPherson, Robert R.J. Maier, and Duncan P. Hand. Temperature and Strain Measurements With Fiber Bragg Gratings Embedded in Stainless Steel 316. *Journal of Lightwave Technology*, 33(12):2474–2479, 2015.

[148] Linqing Li, Runjie He, Maria Simone Soares, Svetislav Savovic, Xuehao Hu, Carlos Marques, Rui Min, and Xiaoli Li. Embedded FBG-Based Sensor for Joint Movement Monitoring. *IEEE Sensors Journal*, 21(23):26793–26798, 2021.

[149] Diego Saenz-Castillo, María Isabel Martín, Silvia Calvo, and A Güemes. Real-time monitoring of thermal history of thermoplastic automatic lamination with FBG sensors and process modelling validation. *Smart Materials and Structures*, 29(11):115004, nov 2020.

[150] Jerome I. Mars, Edouard Buchoud, Valeriu D. Vrabie, Amir Ali Khan, Sylvain Blairon, and Guy D'Urso. Source separation and distributed sensing: The key for an efficient monitoring. *2013 5th IEEE International Workshop on Computational Advances in Multi-Sensor Adaptive Processing, CAMSAP 2013*, pages 264–267, 2013.

[151] Qiang Li, Zhi Wang, Zejia Huang, Kaili Guo, and Lanlan Liu. Implementation of blind source separation for optical fiber sensing. *Applied Optics*, 53(9):1832, 2014.

[152] Amir A. Khan, Valeriu Vrabie, Jérôme I. Mars, Alexandre Girard, and Guy D'Urso. A source separation technique for processing of thermometric data from fiber-optic DTS measurements for water leakage identification in dikes. *IEEE Sensors Journal*, 8(7):1118–1129, 2008.

[153] Valentin Buchinger and Zahra Sharif Khodaei. OFDR-Based Integral Process Monitoring and SHM System for Composites Manufactured by Resin Infusion Under Flexible Tooling. In Piervincenzo Rizzo and Alberto Milazzo, editors, *EWSHM 2022: European Workshop on Structural Health Monitoring*, pages 360–368. Springer International Publishing, Palermo, 2023.

[154] Mauricio Torres. Parameters' monitoring and in-situ instrumentation for resin transfer moulding: A review. *Composites Part A: Applied Science and Manufacturing*, 124(May):105500, 2019.

[155] Alexandra Allue, Paula Corte-León, Koldo Gondra, Valentina Zhukova, Mihail Ipatov, Juan Maria Blanco, Julian Gonzalez, Margarita Churyukanova, Sergey Taskaev, and Arcady Zhukov. Smart composites with embedded magnetic microwire inclusions allowing non-contact stresses and temperature monitoring. *Composites Part A: Applied Science and Manufacturing*, 120(November 2018):12–20, 2019.

[156] Soohyun Eum, Kazuro Kageyama, Hideaki Murayama, Isamu Ohsawa, Kiyoshi Uzawa, Makoto Kanai, and Hirotaka Igawa. Resin flow monitoring in vacuum-assisted resin transfer molding using optical fiber distributed sensor. *Behavior and Mechanics of Multifunctional and Composite Materials 2007*, 6526(April 2007):65262T, 2007.

[157] Edmon Chehura, Stephen W. James, Stephen Staines, Chris Groenendijk, Denis Cartie, Stephanie Portet, Michael Hugon, and Ralph P. Tatam. Production process monitoring and post-production strain measurement on a full-size carbon-fibre composite aircraft tail cone assembly using embedded optical fibre sensors. *Measurement Science and Technology*, 31(10):105204, oct 2020.

[158] Changhao Chen, Qi Wu, Ke Xiong, Hongzhou Zhai, Nobuhiro Yoshikawa, and Rong Wang. Hybrid Temperature and Stress Monitoring of Woven Fabric Thermoplastic Composite Using Fiber Bragg Grating Based Sensing Technique. *Sensors*, 20(11):3081, may 2020.

[159] Y. Ito, S. Minakuchi, T. Mizutani, and N. Takeda. Cure monitoring of carbon-epoxy composites by optical fiber-based distributed strain-temperature sensing system. *Advanced Composite Materials*, 21(3):259–271, 2012.

[160] Y. Ito, T. Obo, S. Minakuchi, and N. Takeda. Cure strain in thick CFRP laminate: Optical-fiber-based distributed measurement and numerical simulation. *Advanced Composite Materials*, 24(4):325–342, 2015.

[161] Joy P. Dunkers, Joseph L. Lenhart, Sylvia R. Kueh, John H. Van Zanten, Suresh G. Advani, and Richard S. Parnas. Fiber optic flow and cure sensing for liquid composite molding. *Optics and Lasers in Engineering*, 35(2):91–104, 2001.

[162] Seong Taek Lim and Woo Il Lee. An analysis of the three-dimensional resin-transfer mold filling process. *Composites Science and Technology*, 60(7):961–975, 2000.

[163] Sylvia R. M. Kueh, Richard S. Parnas, Joy P. Dunkers, Suresh G. Advani, A. Paige C. Furrow, Mark E. Jones, and Timothy A. Bailey. Long-period gratings as flow sensors for liquid-composite molding. *Nondestructive Evaluation of Aging Materials and Composites IV*, 3993(May 2000):240–250, 2000.

[164] Sylvia R.M. Kueh, Richard S. Parnas, and Suresh G. Advani. A methodology for using long-period gratings and mold-filling simulations to minimize the intrusiveness of flow sensors in liquid composite molding. *Composites Science and Technology*, 62(2):311–327, 2002.

[165] P. Wang, J. Molimard, S. Drapier, A. Vautrin, and J. C. Minni. Monitoring the resin infusion manufacturing process under industrial environment using distributed sensors. *Journal of Composite Materials*, 46(6):691–706, 2012.

[166] Daniel Martínez Sánchez, Matthieu Gresil, and Constantinos Soutis. Distributed internal strain measurement during composite manufacturing using optical fibre sensors. *Composites Science and Technology*, 120:49–57, 2015.

[167] Olubukola Rufai, Neha Chandarana, Mayank Gautam, Prasad Potluri, and Matthieu Gresil. Cure monitoring and structural health monitoring of composites using micro-braided distributed optical fibre. *Composite Structures*, 254(August):112861, 2020.

[168] Takashi Yari, Kanehiro Nagai, and Nobuo Takeda. Aircraft structural-health monitoring using optical fiber distributed BOTDR sensors. *Advanced Composite Materials: The Official Journal of the Japan Society of Composite Materials*, 13(1):17–26, 2004.

[169] A. Güemes and B. Soller. Optical fiber distributed sensing: Physical principles and applications. *Structural Health Monitoring 2009: From System Integration to Autonomous Systems - Proceedings of the 7th International Workshop on Structural Health Monitoring, IWSHM 2009*, 1(3):14–20, 2009.

[170] Patricia Fernández Díaz-Maroto. *Structural Health Monitoring in Aeronautical Structures by Means of Distributed Fibre Optic Sensing Networks*. PhD thesis, Polytechnic University of Madrid School, 2018.

[171] Neha Chandarana, Daniel Sanchez, Constantinos Soutis, and Matthieu Gresil. Early Damage Detection in Composites during Fabrication and Mechanical Testing. *Materials*, 10(7):685, jun 2017.

[172] Monica Ciminello, Natalino Daniele Boffa, Antonio Concilio, Vittorio Memmolo, Ernesto Monaco, and Fabrizio Ricci. Stringer debonding edge detection employing fiber optics by combined distributed strain profile and wave scattering approaches for non-model based SHM. *Composite Structures*, 216(February):58–66, 2019.

[173] Md Shamsuddoha, Matthew David, Ebrahim Oromiehie, and B. Gangadhara Prusty. Distributed optical fibre sensor based monitoring of thermoplastic carbon composite cylinders under biaxial loading: Experimental and numerical investigations. *Composite Structures*, 261(October 2020):113277, 2021.

[174] Ricardo N. Correia, Edmon Chehura, Stephen W. James, and Ralph P. Tatam. Locally Pressed Fibre Bragg Grating Pressure Sensor. In *Optical Fiber Sensors*, page TuE3, Washington, D.C., 2006. OSA.

[175] R. Correia, E. Chehura, S. W. James, and R. P. Tatam. A transverse loading technique to enhance the pressure measurement capability of fibre Bragg gratings. *19th International Conference on Optical Fibre Sensors*, 7004(April):70045Q, 2008.

[176] Chen Chun Ye, S. E. Staines, S. W. James, and R. P. Tatam. A polarisation maintaining fibre Bragg grating interrogation system for multi-axis strain sensing. *2002 15th Optical Fiber Sensors Conference Technical Digest, OFS 2002*, pages 179–182, 2002.

[177] François Trochu, Edu Ruiz, Vincent Achim, and Sofiane Soukane. Advanced numerical simulation of liquid composite molding for process analysis and optimization. *Composites Part A: Applied Science and Manufacturing*, 37(6 SPEC. ISS.):890–902, 2006.

[178] W. D. Brouwer, E. C.F.C. Van Herpt, and M. Labordus. Vacuum injection moulding for large structural applications. *Composites Part A: Applied Science and Manufacturing*, 34(6 SPEC.):551–558, 2003.

[179] Chung Hae Park, Aurélie Lebel, Abdelghani Saouab, Joël Bréard, and Woo Il Lee. Modeling and simulation of voids and saturation in liquid composite molding processes. *Composites Part A: Applied Science and Manufacturing*, 42(6):658–668, 2011.

[180] J. Timms, S. Bickerton, and P. A. Kelly. Laminate thickness and resin pressure evolution during axisymmetric liquid composite moulding with flexible tooling. *Composites Part A: Applied Science and Manufacturing*, 43(4):621–630, 2012.

[181] M. Akif Yalcinkaya, E. Murat Sozer, and M. Cengiz Altan. Effect of external pressure and resin flushing on reduction of process-induced voids and enhancement of laminate quality in heated-VARTM. *Composites Part A: Applied Science and Manufacturing*, 121(December 2018):353–364, 2019.

[182] Frank Gommer, Andreas Endruweit, and Andrew C. Long. Influence of the micro-structure on saturated transverse flow in fibre arrays. *Journal of Composite Materials*, 52(18):2463–2475, 2018.

[183] Louise Brown, Mike-matveev, and Georgespackman. louisepb/TexGen: TexGen v3.12.0, 2020.

[184] M. Valkova, D. B. Anthony, A. R.J. Kucernak, M. S.P. Shaffer, and E. S. Greenhalgh. Predicting the compaction of hybrid multilayer woven composite reinforcement stacks. *Composites Part A: Applied Science and Manufacturing*, 133(November 2019):105851, 2020.

[185] B. Cornelissen, B. Rietman, and R. Akkerman. Frictional behaviour of high performance fibrous tows: Friction experiments. *Composites Part A: Applied Science and Manufacturing*, 44(1):95–104, 2013.

[186] L. Montero, S. Allaoui, and G. Hivet. Characterisation of the mesoscopic and macroscopic friction behaviours of glass plain weave reinforcement. *Composites Part A: Applied Science and Manufacturing*, 95:257–266, 2017.

[187] B. R. Gebart. Permeability of Unidirectional Reinforcements for RTM. *Journal of Composite Materials*, 26(8):1100–1133, 1992.

[188] Caroline A Schneider, Wayne S Rasband, and Kevin W Eliceiri. NIH Image to ImageJ: 25 years of image analysis. *Nature Methods*, 9(7):671–675, jul 2012.

[189] BASF Polyurethanes GmbH. Preliminary information for experimental product Elastollan ® EXP B CF 35 A 12 P, 2020.

[190] Irfan Raza, Lorenzo Iannucci, and Paul T. Curtis. Introducing a Multimaterial Printer for the Deposition of Low Melting Point Alloys, Elastomer, and Ultraviolet Curable Resin. *3D Printing and Additive Manufacturing*, 4(2):83–89, 2017.

ELSEVIER LICENSE TERMS AND CONDITIONS

May 25, 2022

This Agreement between Imperial College London -- Valentin Buchinger ("You") and Elsevier ("Elsevier") consists of your license details and the terms and conditions provided by Elsevier and Copyright Clearance Center.

License Number	5315810533709
License date	May 25, 2022
Licensed Content Publisher	Elsevier
Licensed Content Publication	Composites Science and Technology
Licensed Content Title	Graphene coated piezo-resistive fabrics for liquid composite molding process monitoring
Licensed Content Author	Muhammad A. Ali,Rehan Umer,Kamran A. Khan,Yarjan A. Samad,Kin Liao,Wesley Cantwell
Licensed Content Date	Aug 18, 2017
Licensed Content Volume	148
Licensed Content Issue	n/a
Licensed Content Pages	9
Start Page	106
End Page	114
Type of Use	reuse in a thesis/dissertation
Portion	figures/tables/illustrations
Number of figures/tables/illustrations	1
Format	both print and electronic
Are you the author of this Elsevier article?	No
Will you be translating?	No
Title	Life cycle monitoring of composite aircraft components with structural health monitoring technologies
Institution name	Imperial College London
Expected presentation date	Oct 2022
Portions	Fig. 2
Requestor Location	Imperial College London Flat 2, 42 Dealtry Road 40 Putney Hill London, London SW15 6AQ United Kingdom Attn: Imperial College London
Publisher Tax ID	GB 494 6272 12
Billing Type	Invoice
Billing Address	Imperial College London Exhibition Road Department of Aeronautics London, United Kingdom SW7 2AZ Attn: Valentin Buchinger
Total	**0.00 USD**
Terms and Conditions	

INTRODUCTION

1. The publisher for this copyrighted material is Elsevier. By clicking "accept" in connection with completing this licensing transaction, you agree that the following terms and conditions apply to this transaction (along with the Billing and Payment terms and conditions established by Copyright Clearance Center, Inc. ("CCC"), at the time that you opened your Rightslink account and that are available at any time at http://myaccount.copyright.com).

GENERAL TERMS

2. Elsevier hereby grants you permission to reproduce the aforementioned material subject to the terms and conditions indicated.
3. Acknowledgement: If any part of the material to be used (for example, figures) has appeared in our publication with credit or acknowledgement to another source, permission must also be sought from that source. If such permission is not obtained then that material may not be included in your publication/copies. Suitable acknowledgement to the source must be made, either as a footnote or in a reference list at the end of your publication, as follows:
"Reprinted from Publication title, Vol /edition number, Author(s), Title of article / title of chapter, Pages No., Copyright (Year), with permission from Elsevier [OR APPLICABLE SOCIETY COPYRIGHT OWNER]." Also Lancet special credit - "Reprinted from The Lancet, Vol. number, Author(s), Title of article, Pages No., Copyright (Year), with permission from Elsevier."
4. Reproduction of this material is confined to the purpose and/or media for which permission is hereby given.
5. Altering/Modifying Material: Not Permitted. However figures and illustrations may be altered/adapted minimally to serve your work. Any other abbreviations, additions, deletions and/or any other alterations shall be made only with prior written authorization of Elsevier Ltd. (Please contact Elsevier's permissions helpdesk here). No modifications can be made to any Lancet figures/tables and they must be reproduced in full.
6. If the permission fee for the requested use of our material is waived in this instance, please be advised that your future requests for Elsevier materials may attract a fee.
7. Reservation of Rights: Publisher reserves all rights not specifically granted in the combination of (i) the license details provided by you and accepted in the course of this licensing transaction, (ii) these terms and conditions and (iii) CCC's Billing and Payment terms and conditions.
8. License Contingent Upon Payment: While you may exercise the rights licensed immediately upon issuance of the license at the end of the licensing process for the transaction, provided that you have disclosed complete and accurate details of your proposed use, no license is finally effective unless and until full payment is received from you (either by publisher or by CCC) as provided in CCC's Billing and Payment terms and conditions. If full payment is not received on a timely basis, then any license preliminarily granted shall be deemed automatically revoked and shall be void as if never granted. Further, in the event that you breach any of these terms and conditions or any of CCC's Billing and Payment terms and conditions, the license is automatically revoked and shall be void as if never granted. Use of materials as described in a revoked license, as well as any use of the materials beyond the scope of an unrevoked license, may constitute copyright infringement and publisher reserves the right to take any and all action to protect its copyright in the materials.
9. Warranties: Publisher makes no representations or warranties with respect to the licensed material.
10. Indemnity: You hereby indemnify and agree to hold harmless publisher and CCC, and their respective officers, directors, employees and agents, from and against any and all claims arising out of your use of the licensed material other than as specifically authorized pursuant to this license.
11. No Transfer of License: This license is personal to you and may not be sublicensed, assigned, or transferred by you to any other person without publisher's written permission.
12. No Amendment Except in Writing: This license may not be amended except in a writing signed by both parties (or, in the case of publisher, by CCC on publisher's behalf).
13. Objection to Contrary Terms: Publisher hereby objects to any terms contained in any purchase order, acknowledgment, check endorsement or other writing prepared by you, which terms are inconsistent with these terms and conditions or CCC's Billing and Payment terms and conditions. These terms and conditions, together with CCC's Billing and Payment terms and conditions (which are incorporated herein), comprise the entire agreement between you and publisher (and CCC) concerning this licensing transaction. In the event of any conflict between your obligations established by these terms and conditions and those established by CCC's Billing and Payment terms and conditions, these terms and conditions shall control.
14. Revocation: Elsevier or Copyright Clearance Center may deny the permissions described in this License at their sole discretion, for any reason or no reason, with a full refund payable to you. Notice of such denial will be made using the contact information provided by you. Failure to receive such notice will not alter or invalidate the denial. In no event will Elsevier or Copyright Clearance Center be responsible or liable for any costs, expenses or damage incurred by you as a result of a denial of your permission request, other than a refund of the amount(s) paid by you to Elsevier and/or Copyright Clearance Center for denied permissions.

LIMITED LICENSE

The following terms and conditions apply only to specific license types:
15. **Translation**: This permission is granted for non-exclusive world **English** rights only unless your license was granted for translation rights. If you licensed translation rights you may only translate this content into the languages you requested. A professional translator must perform all translations and reproduce the content word for word preserving the integrity of the article.
16. **Posting licensed content on any Website**: The following terms and conditions apply as follows: Licensing material from an Elsevier journal: All content posted to the web site must maintain the copyright information line on the bottom of each image; A hyper-text must be included to the Homepage of the journal from which you are licensing at http://www.sciencedirect.com/science/journal/xxxxx or the Elsevier homepage for books at http://www.elsevier.com; Central Storage: This license does not include permission for a scanned version of the material to be stored in a central repository such as that provided by Heron/XanEdu.

Licensing material from an Elsevier book: A hyper-text link must be included to the Elsevier homepage at http://www.elsevier.com . All content posted to the web site must maintain the copyright information line on the bottom of each image.

Posting licensed content on Electronic reserve: In addition to the above the following clauses are applicable: The web site must be password-protected and made available only to bona fide students registered on a relevant course. This permission is granted for 1 year only. You may obtain a new license for future website posting.
17. **For journal authors:** the following clauses are applicable in addition to the above:
Preprints:
A preprint is an author's own write-up of research results and analysis, it has not been peer-reviewed, nor has it had any other value added to it by a publisher (such as formatting, copyright, technical enhancement etc.).
Authors can share their preprints anywhere at any time. Preprints should not be added to or enhanced in any way in order to appear more like, or to substitute for, the final versions of articles however authors can update their preprints on arXiv or RePEc with their Accepted Author Manuscript (see below).
If accepted for publication, we encourage authors to link from the preprint to their formal publication via its DOI. Millions of researchers have access to the formal publications on ScienceDirect, and so links will help users to find, access, cite and use the best available version. Please note that Cell Press, The Lancet and some society-owned have different preprint policies. Information on these policies is available on the journal homepage.
Accepted Author Manuscripts: An accepted author manuscript is the manuscript of an article that has been accepted for publication and which typically includes author-incorporated changes suggested during submission, peer review and editor-author communications.
Authors can share their accepted author manuscript:

- immediately
    - via their non-commercial person homepage or blog
    - by updating a preprint in arXiv or RePEc with the accepted manuscript
    - via their research institute or institutional repository for internal institutional uses or as part of an invitation-only research collaboration work-group
    - directly by providing copies to their students or to research collaborators for their personal use
    - for private scholarly sharing as part of an invitation-only work group on commercial sites with which Elsevier has an agreement
- After the embargo period
    - via non-commercial hosting platforms such as their institutional repository
    - via commercial sites with which Elsevier has an agreement

In all cases accepted manuscripts should:

- link to the formal publication via its DOI
- bear a CC-BY-NC-ND license - this is easy to do
- if aggregated with other manuscripts, for example in a repository or other site, be shared in alignment with our hosting policy not be added to or enhanced in any way to appear more like, or to substitute for, the published journal article.

Published journal article (JPA): A published journal article (PJA) is the definitive final record of published research that appears or will appear in the journal and embodies all value-adding publishing activities including peer review co-ordination, copy-editing, formatting, (if relevant) pagination and online enrichment.
Policies for sharing publishing journal articles differ for subscription and gold open access articles:
Subscription Articles: If you are an author, please share a link to your article rather than the full-text. Millions of researchers have access to the formal publications on ScienceDirect, and so links will help your users to find, access, cite, and use the best available version.
Theses and dissertations which contain embedded PJAs as part of the formal submission can be posted publicly by the awarding institution with DOI links back to the formal publications on ScienceDirect.
If you are affiliated with a library that subscribes to ScienceDirect you have additional private sharing rights for others' research accessed under that agreement. This includes use for classroom teaching and internal training at the institution (including use in course packs and courseware programs), and inclusion of the article for grant funding purposes.
Gold Open Access Articles: May be shared according to the author-selected end-user license and should contain a CrossMark logo, the end user license, and a DOI link to the formal publication on ScienceDirect.
Please refer to Elsevier's posting policy for further information.
18. **For book authors** the following clauses are applicable in addition to the above: Authors are permitted to place a brief summary of their work online only. You are not allowed to download and post the published electronic version of your chapter, nor may you scan the printed edition to create an electronic version. **Posting to a repository:** Authors are permitted to post a summary of their chapter only in their institution's repository.
19. **Thesis/Dissertation**: If your license is for use in a thesis/dissertation your thesis may be submitted to your institution in either print or electronic form. Should your thesis be published commercially, please reapply for permission. These requirements include permission for the Library and Archives of Canada to supply single copies, on demand, of the complete thesis and include permission for Proquest/UMI to supply single copies, on demand, of the complete thesis. Should your thesis be published commercially, please reapply for permission. Theses and dissertations which contain embedded PJAs as part of the

formal submission can be posted publicly by the awarding institution with DOI links back to the formal publications on ScienceDirect.

Elsevier Open Access Terms and Conditions

You can publish open access with Elsevier in hundreds of open access journals or in nearly 2000 established subscription journals that support open access publishing. Permitted third party re-use of these open access articles is defined by the author's choice of Creative Commons user license. See our open access license policy for more information.

Terms & Conditions applicable to all Open Access articles published with Elsevier:

Any reuse of the article must not represent the author as endorsing the adaptation of the article nor should the article be modified in such a way as to damage the author's honour or reputation. If any changes have been made, such changes must be clearly indicated.

The author(s) must be appropriately credited and we ask that you include the end user license and a DOI link to the formal publication on ScienceDirect.

If any part of the material to be used (for example, figures) has appeared in our publication with credit or acknowledgement to another source it is the responsibility of the user to ensure their reuse complies with the terms and conditions determined by the rights holder.

Additional Terms & Conditions applicable to each Creative Commons user license:

CC BY: The CC-BY license allows users to copy, to create extracts, abstracts and new works from the Article, to alter and revise the Article and to make commercial use of the Article (including reuse and/or resale of the Article by commercial entities), provided the user gives appropriate credit (with a link to the formal publication through the relevant DOI), provides a link to the license, indicates if changes were made and the licensor is not represented as endorsing the use made of the work. The full details of the license are available at http://creativecommons.org/licenses/by/4.0.

CC BY NC SA: The CC BY-NC-SA license allows users to copy, to create extracts, abstracts and new works from the Article, to alter and revise the Article, provided this is not done for commercial purposes, and that the user gives appropriate credit (with a link to the formal publication through the relevant DOI), provides a link to the license, indicates if changes were made and the licensor is not represented as endorsing the use made of the work. Further, any new works must be made available on the same conditions. The full details of the license are available at http://creativecommons.org/licenses/by-nc-sa/4.0.

CC BY NC ND: The CC BY-NC-ND license allows users to copy and distribute the Article, provided this is not done for commercial purposes and further does not permit distribution of the Article if it is changed or edited in any way, and provided the user gives appropriate credit (with a link to the formal publication through the relevant DOI), provides a link to the license, and that the licensor is not represented as endorsing the use made of the work. The full details of the license are available at http://creativecommons.org/licenses/by-nc-nd/4.0. Any commercial reuse of Open Access articles published with a CC BY NC SA or CC BY NC ND license requires permission from Elsevier and will be subject to a fee.

Commercial reuse includes:

- Associating advertising with the full text of the Article
- Charging fees for document delivery or access
- Article aggregation
- Systematic distribution via e-mail lists or share buttons

Posting or linking by commercial companies for use by customers of those companies.

20. **Other Conditions**:

v1.10

Questions? customercare@copyright.com or +1-855-239-3415 (toll free in the US) or +1-978-646-2777.

ELSEVIER LICENSE TERMS AND CONDITIONS

May 25, 2022

This Agreement between Imperial College London -- Valentin Buchinger ("You") and Elsevier ("Elsevier") consists of your license details and the terms and conditions provided by Elsevier and Copyright Clearance Center.

License Number	5315810567181
License date	May 25, 2022
Licensed Content Publisher	Elsevier
Licensed Content Publication	Composite Structures
Licensed Content Title	Quality assessment and damage detection in nanomodified adhesively-bonded composite joints using inkjet-printed interdigital sensors
Licensed Content Author	Dimitrios G. Bekas,Zahra Sharif-Khodaei,Dimitrios Baltzis,M.H. Ferri Aliabadi,Alkiviadis S. Paipetis
Licensed Content Date	Mar 1, 2019
Licensed Content Volume	211
Licensed Content Issue	n/a
Licensed Content Pages	7
Start Page	557
End Page	563
Type of Use	reuse in a thesis/dissertation
Portion	figures/tables/illustrations
Number of figures/tables/illustrations	1
Format	both print and electronic
Are you the author of this Elsevier article?	No
Will you be translating?	No
Title	Life cycle monitoring of composite aircraft components with structural health monitoring technologies
Institution name	Imperial College London
Expected presentation date	Oct 2022
Portions	Fig. 2. (a)
Requestor Location	Imperial College London Flat 2, 42 Dealtry Road 40 Putney Hill London, London SW15 6AQ United Kingdom Attn: Imperial College London
Publisher Tax ID	GB 494 6272 12
Billing Type	Invoice
Billing Address	Imperial College London Exhibition Road Department of Aeronautics London, United Kingdom SW7 2AZ Attn: Valentin Buchinger
Total	**0.00 USD**
Terms and Conditions	

INTRODUCTION

Licensing material from an Elsevier book: A hyper-text link must be included to the Elsevier homepage at http://www.elsevier.com . All content posted to the web site must maintain the copyright information line on the bottom of each image.

Posting licensed content on Electronic reserve: In addition to the above the following clauses are applicable: The web site must be password-protected and made available only to bona fide students registered on a relevant course. This permission is granted for 1 year only. You may obtain a new license for future website posting.
17. **For journal authors:** the following clauses are applicable in addition to the above:
Preprints:
A preprint is an author's own write-up of research results and analysis, it has not been peer-reviewed, nor has it had any other value added to it by a publisher (such as formatting, copyright, technical enhancement etc.).
Authors can share their preprints anywhere at any time. Preprints should not be added to or enhanced in any way in order to appear more like, or to substitute for, the final versions of articles however authors can update their preprints on arXiv or RePEc with their Accepted Author Manuscript (see below).
If accepted for publication, we encourage authors to link from the preprint to their formal publication via its DOI. Millions of researchers have access to the formal publications on ScienceDirect, and so links will help users to find, access, cite and use the best available version. Please note that Cell Press, The Lancet and some society-owned have different preprint policies. Information on these policies is available on the journal homepage.
Accepted Author Manuscripts: An accepted author manuscript is the manuscript of an article that has been accepted for publication and which typically includes author-incorporated changes suggested during submission, peer review and editor-author communications.
Authors can share their accepted author manuscript:

- immediately
  - via their non-commercial person homepage or blog
  - by updating a preprint in arXiv or RePEc with the accepted manuscript
  - via their research institute or institutional repository for internal institutional uses or as part of an invitation-only research collaboration work-group
  - directly by providing copies to their students or to research collaborators for their personal use
  - for private scholarly sharing as part of an invitation-only work group on commercial sites with which Elsevier has an agreement
- After the embargo period
  - via non-commercial hosting platforms such as their institutional repository
  - via commercial sites with which Elsevier has an agreement

In all cases accepted manuscripts should:

- link to the formal publication via its DOI
- bear a CC-BY-NC-ND license - this is easy to do
- if aggregated with other manuscripts, for example in a repository or other site, be shared in alignment with our hosting policy not be added to or enhanced in any way to appear more like, or to substitute for, the published journal article.

Published journal article (JPA): A published journal article (PJA) is the definitive final record of published research that appears or will appear in the journal and embodies all value-adding publishing activities including peer review co-ordination, copy-editing, formatting, (if relevant) pagination and online enrichment.
Policies for sharing publishing journal articles differ for subscription and gold open access articles:
Subscription Articles: If you are an author, please share a link to your article rather than the full-text. Millions of researchers have access to the formal publications on ScienceDirect, and so links will help your users to find, access, cite, and use the best available version.
Theses and dissertations which contain embedded PJAs as part of the formal submission can be posted publicly by the awarding institution with DOI links back to the formal publications on ScienceDirect.
If you are affiliated with a library that subscribes to ScienceDirect you have additional private sharing rights for others' research accessed under that agreement. This includes use for classroom teaching and internal training at the institution (including use in course packs and courseware programs), and inclusion of the article for grant funding purposes.
Gold Open Access Articles: May be shared according to the author-selected end-user license and should contain a CrossMark logo, the end user license, and a DOI link to the formal publication on ScienceDirect.
Please refer to Elsevier's posting policy for further information.
18. **For book authors** the following clauses are applicable in addition to the above: Authors are permitted to place a brief summary of their work online only. You are not allowed to download and post the published electronic version of your chapter, nor may you scan the printed edition to create an electronic version. **Posting to a repository:** Authors are permitted to post a summary of their chapter only in their institution's repository.
19. **Thesis/Dissertation**: If your license is for use in a thesis/dissertation your thesis may be submitted to your institution in either print or electronic form. Should your thesis be published commercially, please reapply for permission. These requirements include permission for the Library and Archives of Canada to supply single copies, on demand, of the complete thesis and include permission for Proquest/UMI to supply single copies, on demand, of the complete thesis. Should your thesis be published commercially, please reapply for permission. Theses and dissertations which contain embedded PJAs as part of the

Buchinger, Valentin

From:	Flude, Annabel <Annabel.Flude@tandf.co.uk>
Sent:	19 May 2022 15:19
To:	Buchinger, Valentin
Cc:	Flude, Annabel
Subject:	RE: tacm20:Vacuum assisted resin transfer moulding process monitoring by means of distributed fibre-optic sensors: a numerical and experimental study

Dear Author,

Thank you for your correspondence requesting permission to reproduce the above content from our Journal in your thesis to be posted on your University's repository.

We will be pleased to grant permission to reproduce your '**Accepted/Original Manuscript'** (please check the embargo: Open access cost finder - Author Services (taylorandfrancis.com) on the sole condition that you acknowledge the original source of publication.

This is an '**Accepted/Original Manuscript'** of an article published by Taylor & Francis Group in [JOURNAL TITLE] on [DATE], available online: https://wwww.tandfonline.com/[Article DOI]."

This permission does not cover any third party copyrighted work which may appear in the material requested. Please ensure you have checked all original source details for the rights holder.

Further permission will be required if your thesis is published. (Please see information for sharing your work https://authorservices.taylorandfrancis.com/sharing-your-work/)

Thank you for your interest in our Journal.

With best wishes,

Annabel
Annabel Flude| Permissions Administrator
Journals, Taylor & Francis Group
Permissions e-mail: permissionrequest@tandf.co.uk
Web: www.tandfonline.com

4 Park Square, Milton Park, Abingdon, OX14 4RN
+44 (0)20 8052 0659

From: Valentin Buchinger <vb17@ic.ac.uk>
Sent: 19 May 2022 13:44
To: Academic UK Non Rightslink <permissionrequest@tandf.co.uk>
Subject: tacm20:Vacuum assisted resin transfer moulding process monitoring by means of distributed fibre-optic sensors: a numerical and experimental study

Permissions Request

Type of use: Academic
Article title: Vacuum assisted resin transfer moulding process monitoring by means of distributed fibre-optic sensors: a numerical and experimental study
Article DOI: 10.1080/09243046.2021.2001910
Author name: Valentin Buchinger & Zahra Sharif Khodaei
Journal title: Advanced Composite Materials
Volume number: *
Issue number: *
Year of publication: *
Name: Valentin Buchinger
Street address: Exhibition Road, Department of Aeronautics
Town: London
Postcode/ZIP code: SW7 2AZ
Country: United Kingdom
Email: vb17@ic.ac.uk
Telephone: 07425586263
Intended use: To be used in your Thesis?
Are you requesting the full article?: Yes
Which University?: Imperial College London
Title of your Thesis?: Life cycle monitoring of composite aircraft components with structural health monitoring technologies
University repository URL: https://spiral.imperial.ac.uk/
Is this a “Closed” or “Open” deposit?: open
Additional comments: Dear all, I am the main author of the paper and seek permission to re-use the content in my thesis. Thank you. Best wishes, Valentin Buchinger

SPRINGER NATURE LICENSE
TERMS AND CONDITIONS

Sep 16, 2022

This Agreement between Imperial College London -- Valentin Buchinger ("You") and Springer Nature ("Springer Nature") consists of your license details and the terms and conditions provided by Springer Nature and Copyright Clearance Center.

License Number	5390861252252
License date	Sep 16, 2022
Licensed Content Publisher	Springer Nature
Licensed Content Publication	Springer eBook
Licensed Content Title	OFDR-Based Integral Process Monitoring and SHM System for Composites Manufactured by Resin Infusion Under Flexible Tooling
Licensed Content Author	Valentin Buchinger, Zahra Sharif Khodaei
Licensed Content Date	Jan 1, 2023
Type of Use	Thesis/Dissertation
Requestor type	academic/university or research institute
Format	print and electronic
Portion	full article/chapter
Will you be translating?	no

Circulation/distribution	1 - 29
Author of this Springer Nature content	yes
Title	Life cycle monitoring of composite aircraft components with structural health monitoring technologies
Institution name	Imperial College London
Expected presentation date	Oct 2022
Requestor Location	Imperial College London Flat 2, 42 Dealtry Road 40 Putney Hill London, London SW15 6AQ United Kingdom Attn: Imperial College London
Total	0.00 USD

Terms and Conditions

Springer Nature Customer Service Centre GmbH
Terms and Conditions

This agreement sets out the terms and conditions of the licence (the **Licence**) between you and **Springer Nature Customer Service Centre GmbH** (the **Licensor**). By clicking 'accept' and completing the transaction for the material (**Licensed Material**), you also confirm your acceptance of these terms and conditions.

1. Grant of License

1. 1. The Licensor grants you a personal, non-exclusive, non-transferable, world-wide licence to reproduce the Licensed Material for the purpose specified in your order only. Licences are granted for the specific use requested in the order and for no other use, subject to the conditions below.

1. 2. The Licensor warrants that it has, to the best of its knowledge, the rights to license reuse of the Licensed Material. However, you should ensure that the material you are requesting is original to the Licensor and does not carry the copyright of another entity (as credited in the published version).

1. 3. If the credit line on any part of the material you have requested indicates that it was reprinted or adapted with permission from another source, then you should also seek permission from that source to reuse the material.

2. Scope of Licence

2. 1. You may only use the Licensed Content in the manner and to the extent permitted by these Ts&Cs and any applicable laws.

2. 2. A separate licence may be required for any additional use of the Licensed Material, e.g. where a licence has been purchased for print only use, separate permission must be obtained for electronic re-use. Similarly, a licence is only valid in the language selected and does not apply for editions in other languages unless additional translation rights have been granted separately in the licence. Any content owned by third parties are expressly excluded from the licence.

2. 3. Similarly, rights for additional components such as custom editions and derivatives require additional permission and may be subject to an additional fee. Please apply to Journalpermissions@springernature.com/bookpermissions@springernature.com for these rights.

2. 4. Where permission has been granted **free of charge** for material in print, permission may also be granted for any electronic version of that work, provided that the material is incidental to your work as a whole and that the electronic version is essentially equivalent to, or substitutes for, the print version.

2. 5. An alternative scope of licence may apply to signatories of the STM Permissions Guidelines, as amended from time to time.

3. Duration of Licence

3. 1. A licence for is valid from the date of purchase ('Licence Date') at the end of the relevant period in the below table:

Scope of Licence	**Duration of Licence**
Post on a website	12 months
Presentations	12 months
Books and journals	Lifetime of the edition in the language purchased

4. Acknowledgement

4. 1. The Licensor's permission must be acknowledged next to the Licenced Material in print. In electronic form, this acknowledgement must be visible at the same time as the figures/tables/illustrations or abstract, and must be hyperlinked to the journal/book's homepage. Our required acknowledgement format is in the Appendix below.

5. Restrictions on use

5. 1. Use of the Licensed Material may be permitted for incidental promotional use and minor editing privileges e.g. minor adaptations of single figures, changes of format, colour and/or style where the adaptation is credited as set out in Appendix 1 below. Any other changes including but not limited to, cropping, adapting, omitting material that affect the meaning, intention or moral rights of the author are strictly prohibited.

5. 2. You must not use any Licensed Material as part of any design or trademark.

5. 3. Licensed Material may be used in Open Access Publications (OAP) before publication by Springer Nature, but any Licensed Material must be removed from OAP sites prior to final publication.

6. Ownership of Rights

6. 1. Licensed Material remains the property of either Licensor or the relevant third party and any rights not explicitly granted herein are expressly reserved.

7. Warranty

IN NO EVENT SHALL LICENSOR BE LIABLE TO YOU OR ANY OTHER PARTY OR ANY OTHER PERSON OR FOR ANY SPECIAL, CONSEQUENTIAL, INCIDENTAL OR INDIRECT DAMAGES, HOWEVER CAUSED, ARISING OUT OF OR IN CONNECTION WITH THE DOWNLOADING, VIEWING OR USE OF THE MATERIALS REGARDLESS OF THE FORM OF ACTION, WHETHER FOR BREACH OF CONTRACT, BREACH OF WARRANTY, TORT, NEGLIGENCE, INFRINGEMENT OR OTHERWISE (INCLUDING, WITHOUT LIMITATION, DAMAGES BASED ON LOSS OF PROFITS, DATA, FILES, USE, BUSINESS OPPORTUNITY OR CLAIMS OF THIRD PARTIES), AND
WHETHER OR NOT THE PARTY HAS BEEN ADVISED OF THE POSSIBILITY OF SUCH DAMAGES. THIS LIMITATION SHALL APPLY NOTWITHSTANDING ANY FAILURE OF ESSENTIAL PURPOSE OF ANY LIMITED REMEDY PROVIDED HEREIN.

8. Limitations

8. 1. ***BOOKS ONLY:***Where **'reuse in a dissertation/thesis'** has been selected the following terms apply: Print rights of the final author's accepted manuscript (for clarity, NOT the published version) for up to 100 copies, electronic rights for use only on a personal website or institutional repository as defined by the Sherpa guideline (www.sherpa.ac.uk/romeo/).

8. 2. For content reuse requests that qualify for permission under the STM Permissions Guidelines, which may be updated from time to time, the STM Permissions Guidelines supersede the terms and conditions contained in this licence.

9. Termination and Cancellation

9. 1. Licences will expire after the period shown in Clause 3 (above).

9. 2. Licensee reserves the right to terminate the Licence in the event that payment is not received in full or if there has been a breach of this agreement by you.

Appendix 1 — Acknowledgements:

For Journal Content:
Reprinted by permission from [**the Licensor**]: [**Journal Publisher** (e.g. Nature/Springer/Palgrave)] [**JOURNAL NAME**] [**REFERENCE CITATION** (Article name, Author(s) Name), [**COPYRIGHT**] (year of publication)

For **Advance Online Publication papers:**
Reprinted by permission from [**the Licensor**]: [**Journal Publisher** (e.g. Nature/Springer/Palgrave)] [**JOURNAL NAME**] [**REFERENCE CITATION** (Article name, Author(s) Name), [**COPYRIGHT**] (year of publication), advance online publication, day month year (doi: 10.1038/sj.[JOURNAL ACRONYM].)

For Adaptations/Translations:
Adapted/Translated by permission from [**the Licensor**]: [**Journal Publisher** (e.g. Nature/Springer/Palgrave)] [**JOURNAL NAME**] [**REFERENCE CITATION** (Article name, Author(s) Name), [**COPYRIGHT**] (year of publication)

Note: For any republication from the British Journal of Cancer, the following credit line style applies:

Reprinted/adapted/translated by permission from [**the Licensor**]: on behalf of Cancer Research UK: : [**Journal Publisher** (e.g. Nature/Springer/Palgrave)] [**JOURNAL NAME**] [**REFERENCE CITATION** (Article name, Author(s) Name), [**COPYRIGHT]** (year of publication)

For **Advance Online Publication** papers:
Reprinted by permission from The [**the Licensor**]: on behalf of Cancer Research UK: [**Journal Publisher** (e.g. Nature/Springer/Palgrave)] [**JOURNAL NAME**] [**REFERENCE CITATION** (Article name, Author(s) Name), [**COPYRIGHT**] (year of publication), advance online publication, day month year (doi: 10.1038/sj. [JOURNAL ACRONYM])

For Book content:
Reprinted/adapted by permission from [**the Licensor**]: [**Book Publisher** (e.g. Palgrave Macmillan, Springer etc) [**Book Title**] by [**Book author**(s)] [**COPYRIGHT**] (year of publication)

Other Conditions:

Version 1.3

Questions? customercare@copyright.com or +1-855-239-3415 (toll free in the US) or +1-978-646-2777.

ELSEVIER LICENSE
TERMS AND CONDITIONS

May 25, 2022

This Agreement between Imperial College London -- Valentin Buchinger ("You") and Elsevier ("Elsevier") consists of your license details and the terms and conditions provided by Elsevier and Copyright Clearance Center.

License Number	5315810403465
License date	May 25, 2022
Licensed Content Publisher	Elsevier
Licensed Content Publication	Composites Part B: Engineering
Licensed Content Title	Investigation of Electrical Time Domain Reflectometry for infusion and cure monitoring in combination with electrically conductive fibers and tooling materials
Licensed Content Author	Christopher Buchmann,Jürgen Filsinger,Elisabeth Ladstätter
Licensed Content Date	Jun 1, 2016
Licensed Content Volume	94
Licensed Content Issue	n/a
Licensed Content Pages	10
Start Page	389
End Page	398
Type of Use	reuse in a thesis/dissertation
Portion	figures/tables/illustrations
Number of figures/tables/illustrations	1
Format	both print and electronic
Are you the author of this Elsevier article?	No
Will you be translating?	No
Title	Life cycle monitoring of composite aircraft components with structural health monitoring technologies
Institution name	Imperial College London
Expected presentation date	Oct 2022
Portions	Fig. 4
Requestor Location	Imperial College London Exhibition Road London London, London SW7 2AZ United Kingdom Attn: Imperial College London
Publisher Tax ID	GB 494 6272 12
Billing Type	Invoice
Billing Address	Imperial College London Exhibition Road Department of Aeronautics London, United Kingdom SW7 2AZ Attn: Valentin Buchinger
Total	**0.00 USD**
Terms and Conditions	

INTRODUCTION

Licensing material from an Elsevier book: A hyper-text link must be included to the Elsevier homepage at http://www.elsevier.com . All content posted to the web site must maintain the copyright information line on the bottom of each image.

Posting licensed content on Electronic reserve: In addition to the above the following clauses are applicable: The web site must be password-protected and made available only to bona fide students registered on a relevant course. This permission is granted for 1 year only. You may obtain a new license for future website posting.
17. **For journal authors:** the following clauses are applicable in addition to the above:
Preprints:
A preprint is an author's own write-up of research results and analysis, it has not been peer-reviewed, nor has it had any other value added to it by a publisher (such as formatting, copyright, technical enhancement etc.).
Authors can share their preprints anywhere at any time. Preprints should not be added to or enhanced in any way in order to appear more like, or to substitute for, the final versions of articles however authors can update their preprints on arXiv or RePEc with their Accepted Author Manuscript (see below).
If accepted for publication, we encourage authors to link from the preprint to their formal publication via its DOI. Millions of researchers have access to the formal publications on ScienceDirect, and so links will help users to find, access, cite and use the best available version. Please note that Cell Press, The Lancet and some society-owned have different preprint policies. Information on these policies is available on the journal homepage.
Accepted Author Manuscripts: An accepted author manuscript is the manuscript of an article that has been accepted for publication and which typically includes author-incorporated changes suggested during submission, peer review and editor-author communications.
Authors can share their accepted author manuscript:

- immediately
  - via their non-commercial person homepage or blog
  - by updating a preprint in arXiv or RePEc with the accepted manuscript
  - via their research institute or institutional repository for internal institutional uses or as part of an invitation-only research collaboration work-group
  - directly by providing copies to their students or to research collaborators for their personal use
  - for private scholarly sharing as part of an invitation-only work group on commercial sites with which Elsevier has an agreement
- After the embargo period
  - via non-commercial hosting platforms such as their institutional repository
  - via commercial sites with which Elsevier has an agreement

In all cases accepted manuscripts should:

- link to the formal publication via its DOI
- bear a CC-BY-NC-ND license - this is easy to do
- if aggregated with other manuscripts, for example in a repository or other site, be shared in alignment with our hosting policy not be added to or enhanced in any way to appear more like, or to substitute for, the published journal article.

Published journal article (JPA): A published journal article (PJA) is the definitive final record of published research that appears or will appear in the journal and embodies all value-adding publishing activities including peer review co-ordination, copy-editing, formatting, (if relevant) pagination and online enrichment.
Policies for sharing publishing journal articles differ for subscription and gold open access articles:
Subscription Articles: If you are an author, please share a link to your article rather than the full-text. Millions of researchers have access to the formal publications on ScienceDirect, and so links will help your users to find, access, cite, and use the best available version.
Theses and dissertations which contain embedded PJAs as part of the formal submission can be posted publicly by the awarding institution with DOI links back to the formal publications on ScienceDirect.
If you are affiliated with a library that subscribes to ScienceDirect you have additional private sharing rights for others' research accessed under that agreement. This includes use for classroom teaching and internal training at the institution (including use in course packs and courseware programs), and inclusion of the article for grant funding purposes.
Gold Open Access Articles: May be shared according to the author-selected end-user license and should contain a CrossMark logo, the end user license, and a DOI link to the formal publication on ScienceDirect.
Please refer to Elsevier's posting policy for further information.
18. **For book authors** the following clauses are applicable in addition to the above: Authors are permitted to place a brief summary of their work online only. You are not allowed to download and post the published electronic version of your chapter, nor may you scan the printed edition to create an electronic version. **Posting to a repository:** Authors are permitted to post a summary of their chapter only in their institution's repository.
19. **Thesis/Dissertation**: If your license is for use in a thesis/dissertation your thesis may be submitted to your institution in either print or electronic form. Should your thesis be published commercially, please reapply for permission. These requirements include permission for the Library and Archives of Canada to supply single copies, on demand, of the complete thesis and include permission for Proquest/UMI to supply single copies, on demand, of the complete thesis. Should your thesis be published commercially, please reapply for permission. Theses and dissertations which contain embedded PJAs as part of the

formal submission can be posted publicly by the awarding institution with DOI links back to the formal publications on ScienceDirect.

CCC Marketplace™

Order Number: 1223030
Order Date: 19 May 2022

Payment Information

Valentin Buchinger
valentin.buchinger17@imperial.ac.uk
Payment method: Invoice

Billing Address:
Valentin Buchinger
Imperial College London
Exhibition Road
Department of Aeronautics
London, Greater London SW7 2AZ
United Kingdom

+44 7425586263
valentin.buchinger17@imperial.ac.uk

Customer Location:
Valentin Buchinger
Imperial College London
Exhibition Road
Department of Aeronautics
London, Greater London SW7 2AZ
United Kingdom

Order Details

1. Smart Materials and Structures

Billing Status: Open

Order License ID	1223030-1	**Type of use**	Republish in a thesis/dissertation
Order detail status	Completed	**Publisher**	IOP Publishing
ISSN	1361-665X	**Portion**	Image/photo/illustration

0.00 USD
Republication Permission

LICENSED CONTENT

Publication Title	Smart Materials and Structures	**Country**	United Kingdom of Great Britain and Northern Ireland
Author/Editor	Institute of Physics (Great Britain)	**Rightsholder**	IOP Publishing, Ltd
Date	01/01/1992	**Publication Type**	e-Journal
Language	English	**URL**	http://iopscience.iop.org/0964-1726

REQUEST DETAILS

Portion Type	Image/photo/illustration	**Distribution**	Worldwide
Number of images / photos / illustrations	1	**Translation**	Original language of publication
Format (select all that apply)	Print,Electronic	**Copies for the disabled?**	No
Who will republish the content?	Academic institution	**Minor editing privileges?**	No

Duration of Use	Life of current edition	**Incidental promotional use?**	No
Lifetime Unit Quantity	Up to 499	**Currency**	USD
Rights Requested	Main product		

NEW WORK DETAILS

Title	Life cycle monitoring of composite aircraft components with structural health monitoring technologies	**Institution name**	Imperial College London
		Expected presentation date	2022-10-28
Instructor name	Valentin Buchinger		

ADDITIONAL DETAILS

The requesting person / organization to appear on the license	Valentin Buchinger

REUSE CONTENT DETAILS

Title, description or numeric reference of the portion(s)	Figure 5	**Title of the article/chapter the portion is from**	Fibre-reinforced composite structures based on thermoplastic matrices with embedded piezoceramic modules
Editor of portion(s)	N/A	**Author of portion(s)**	Institute of Physics (Great Britain)
Volume of serial or monograph	23	**Publication date of portion**	2013-12-23
Page or page range of portion	4		

IOP Publishing, Ltd Terms and Conditions

Total Items: 1

Subtotal: 0.00 USD

Order Total: 0.00 USD

ELSEVIER LICENSE
TERMS AND CONDITIONS

May 25, 2022

This Agreement between Imperial College London -- Valentin Buchinger ("You") and Elsevier ("Elsevier") consists of your license details and the terms and conditions provided by Elsevier and Copyright Clearance Center.

License Number	5315810506184
License date	May 25, 2022
Licensed Content Publisher	Elsevier
Licensed Content Publication	Analytica Chimica Acta
Licensed Content Title	The oscillation frequency of a quartz resonator in contact with liquid
Licensed Content Author	K Keiji Kanazawa,Joseph G Gordon
Licensed Content Date	Jan 1, 1985
Licensed Content Volume	175
Licensed Content Issue	n/a
Licensed Content Pages	7
Start Page	99
End Page	105
Type of Use	reuse in a thesis/dissertation
Portion	figures/tables/illustrations
Number of figures/tables/illustrations	2
Format	both print and electronic
Are you the author of this Elsevier article?	No
Will you be translating?	No
Title	Life cycle monitoring of composite aircraft components with structural health monitoring technologies
Institution name	Imperial College London
Expected presentation date	Oct 2022
Portions	Fig 3 and 4
Requestor Location	Imperial College London Flat 2, 42 Dealtry Road 40 Putney Hill London, London SW15 6AQ United Kingdom Attn: Imperial College London
Publisher Tax ID	GB 494 6272 12
Billing Type	Invoice
Billing Address	Imperial College London Exhibition Road Department of Aeronautics London, United Kingdom SW7 2AZ Attn: Valentin Buchinger
Total	**0.00 USD**
Terms and Conditions	

INTRODUCTION

Licensing material from an Elsevier book: A hyper-text link must be included to the Elsevier homepage at http://www.elsevier.com . All content posted to the web site must maintain the copyright information line on the bottom of each image.

Posting licensed content on Electronic reserve: In addition to the above the following clauses are applicable: The web site must be password-protected and made available only to bona fide students registered on a relevant course. This permission is granted for 1 year only. You may obtain a new license for future website posting.
17. **For journal authors:** the following clauses are applicable in addition to the above:
Preprints:
A preprint is an author's own write-up of research results and analysis, it has not been peer-reviewed, nor has it had any other value added to it by a publisher (such as formatting, copyright, technical enhancement etc.).
Authors can share their preprints anywhere at any time. Preprints should not be added to or enhanced in any way in order to appear more like, or to substitute for, the final versions of articles however authors can update their preprints on arXiv or RePEc with their Accepted Author Manuscript (see below).
If accepted for publication, we encourage authors to link from the preprint to their formal publication via its DOI. Millions of researchers have access to the formal publications on ScienceDirect, and so links will help users to find, access, cite and use the best available version. Please note that Cell Press, The Lancet and some society-owned have different preprint policies. Information on these policies is available on the journal homepage.
Accepted Author Manuscripts: An accepted author manuscript is the manuscript of an article that has been accepted for publication and which typically includes author-incorporated changes suggested during submission, peer review and editor-author communications.
Authors can share their accepted author manuscript:

- immediately
  - via their non-commercial person homepage or blog
  - by updating a preprint in arXiv or RePEc with the accepted manuscript
  - via their research institute or institutional repository for internal institutional uses or as part of an invitation-only research collaboration work-group
  - directly by providing copies to their students or to research collaborators for their personal use
  - for private scholarly sharing as part of an invitation-only work group on commercial sites with which Elsevier has an agreement
- After the embargo period
  - via non-commercial hosting platforms such as their institutional repository
  - via commercial sites with which Elsevier has an agreement

In all cases accepted manuscripts should:

- link to the formal publication via its DOI
- bear a CC-BY-NC-ND license - this is easy to do
- if aggregated with other manuscripts, for example in a repository or other site, be shared in alignment with our hosting policy not be added to or enhanced in any way to appear more like, or to substitute for, the published journal article.

Published journal article (JPA): A published journal article (PJA) is the definitive final record of published research that appears or will appear in the journal and embodies all value-adding publishing activities including peer review co-ordination, copy-editing, formatting, (if relevant) pagination and online enrichment.
Policies for sharing publishing journal articles differ for subscription and gold open access articles:
Subscription Articles: If you are an author, please share a link to your article rather than the full-text. Millions of researchers have access to the formal publications on ScienceDirect, and so links will help your users to find, access, cite, and use the best available version.
Theses and dissertations which contain embedded PJAs as part of the formal submission can be posted publicly by the awarding institution with DOI links back to the formal publications on ScienceDirect.
If you are affiliated with a library that subscribes to ScienceDirect you have additional private sharing rights for others' research accessed under that agreement. This includes use for classroom teaching and internal training at the institution (including use in course packs and courseware programs), and inclusion of the article for grant funding purposes.
Gold Open Access Articles: May be shared according to the author-selected end-user license and should contain a CrossMark logo, the end user license, and a DOI link to the formal publication on ScienceDirect.
Please refer to Elsevier's posting policy for further information.
18. **For book authors** the following clauses are applicable in addition to the above: Authors are permitted to place a brief summary of their work online only. You are not allowed to download and post the published electronic version of your chapter, nor may you scan the printed edition to create an electronic version. **Posting to a repository:** Authors are permitted to post a summary of their chapter only in their institution's repository.
19. **Thesis/Dissertation**: If your license is for use in a thesis/dissertation your thesis may be submitted to your institution in either print or electronic form. Should your thesis be published commercially, please reapply for permission. These requirements include permission for the Library and Archives of Canada to supply single copies, on demand, of the complete thesis and include permission for Proquest/UMI to supply single copies, on demand, of the complete thesis. Should your thesis be published commercially, please reapply for permission. Theses and dissertations which contain embedded PJAs as part of the

formal submission can be posted publicly by the awarding institution with DOI links back to the formal publications on ScienceDirect.

Elsevier Open Access Terms and Conditions

You can publish open access with Elsevier in hundreds of open access journals or in nearly 2000 established subscription journals that support open access publishing. Permitted third party re-use of these open access articles is defined by the author's choice of Creative Commons user license. See our open access license policy for more information.

Terms & Conditions applicable to all Open Access articles published with Elsevier:

Any reuse of the article must not represent the author as endorsing the adaptation of the article nor should the article be modified in such a way as to damage the author's honour or reputation. If any changes have been made, such changes must be clearly indicated.

The author(s) must be appropriately credited and we ask that you include the end user license and a DOI link to the formal publication on ScienceDirect.

If any part of the material to be used (for example, figures) has appeared in our publication with credit or acknowledgement to another source it is the responsibility of the user to ensure their reuse complies with the terms and conditions determined by the rights holder.

Additional Terms & Conditions applicable to each Creative Commons user license:

CC BY: The CC-BY license allows users to copy, to create extracts, abstracts and new works from the Article, to alter and revise the Article and to make commercial use of the Article (including reuse and/or resale of the Article by commercial entities), provided the user gives appropriate credit (with a link to the formal publication through the relevant DOI), provides a link to the license, indicates if changes were made and the licensor is not represented as endorsing the use made of the work. The full details of the license are available at http://creativecommons.org/licenses/by/4.0.

CC BY NC SA: The CC BY-NC-SA license allows users to copy, to create extracts, abstracts and new works from the Article, to alter and revise the Article, provided this is not done for commercial purposes, and that the user gives appropriate credit (with a link to the formal publication through the relevant DOI), provides a link to the license, indicates if changes were made and the licensor is not represented as endorsing the use made of the work. Further, any new works must be made available on the same conditions. The full details of the license are available at http://creativecommons.org/licenses/by-nc-sa/4.0.

CC BY NC ND: The CC BY-NC-ND license allows users to copy and distribute the Article, provided this is not done for commercial purposes and further does not permit distribution of the Article if it is changed or edited in any way, and provided the user gives appropriate credit (with a link to the formal publication through the relevant DOI), provides a link to the license, and that the licensor is not represented as endorsing the use made of the work. The full details of the license are available at http://creativecommons.org/licenses/by-nc-nd/4.0. Any commercial reuse of Open Access articles published with a CC BY NC SA or CC BY NC ND license requires permission from Elsevier and will be subject to a fee.

Commercial reuse includes:

- Associating advertising with the full text of the Article
- Charging fees for document delivery or access
- Article aggregation
- Systematic distribution via e-mail lists or share buttons

Posting or linking by commercial companies for use by customers of those companies.

20. **Other Conditions**:

v1.10

Questions? customercare@copyright.com or +1-855-239-3415 (toll free in the US) or +1-978-646-2777.

Buchinger, Valentin

From: AMRITA KUMAR <akumar@acellent.com>
Sent: 20 May 2022 15:16
To: Buchinger, Valentin
Cc: AMRITA KUMAR; Sales Team
Subject: Re: Request of permission

Hi Valetin,

Thank you for checking.

Please use the following in your figure legend "SMART Layers and embedding in composite: Courtesy Acellent Technologies Inc., www.acellent.com"

Amrita

On May 20, 2022, at 9:59 AM, Buchinger, Valentin <valentin.buchinger17@imperial.ac.uk> wrote:

Dear Dr Kumar,

In line with the below requirements set out by SPIE I would like to request your approval to reproduce the following item in my thesis:

Title and author	Volume, issue, and page numbers	What you would like to reproduce
Kumar A, Qing X, Delay TK, Beard SJ, Walker JL, Russell SS, et al. Monitoring the integrity of filament-wound structures using built-in sensor networks	Smart Structures and Materials 2003: Industrial and Commercial Applications of Smart Structures Technologies. [Online] 2003;5054(August 2003): 222	Figure 5

Thank you very much for your kind consideration.

Best wishes,

Ing. Valentin Buchinger, MSc

PhD Student
Department of Aeronautics
Level 2, City and Guilds Building
South Kensington Campus, London SW7 2AZ

T: +43 664 130 17 27 | M: +44 742 558 62 63
E: valentin.buchinger17@imperial.ac.uk

From: Karleena Burdick <karleenab@spie.org>
Sent: 19 May 2022 19:11
To: Buchinger, Valentin <valentin.buchinger17@imperial.ac.uk>
Subject: RE: Request of permission

Dear Valentin Buchinger,

Thank you for seeking permission from SPIE to reprint material from our publications. Publisher's permission is hereby granted under the following conditions:

(1) you obtain permission of one of the authors;

(2) the material to be used has appeared in our publication without credit or acknowledgment to another source; and

(3) you credit the original SPIE publication. Include the authors' names, title of paper, volume title, SPIE volume number, and year of publication in your credit statement.

Please let me know if I may be of further assistance.

Best,
Karleena Burdick
Editorial Assistant, Publications
SPIE – the international society for optics and photonics
karleenab@spie.org
1 360 685 5515
<image001.jpg>

From: Buchinger, Valentin <valentin.buchinger17@imperial.ac.uk>
Sent: Thursday, May 19, 2022 4:07 AM
To: reprint_permission <reprint_permission@spie.org>
Subject: Request of permission

Dear Madam/Sir,

I request permission to use the following title for my PhD thesis which will be published on Imperial College London's spiral repository:https://spiral.imperial.ac.uk/

The title of my work is: Life cycle monitoring of composite aircraft components with structural health monitoring technologies
The work will be published in print and electronic form.

I would like to reuse the figures from the work indicated below:

Title and author	Volume, issue, and page numbers	What you would like to reproduce
Kumar A, Qing X, Delay TK, Beard SJ, Walker JL, Russell SS, et al. Monitoring the integrity of filament-wound structures using built-in sensor networks	Smart Structures and Materials 2003: Industrial and Commercial Applications of Smart Structures Technologies. [Online] 2003;5054(August 2003): 222	Figure 5

Thank you.

Best regards,

Ing. Valentin Buchinger, MSc

PhD Student
Department of Aeronautics
Level 2, City and Guilds Building
South Kensington Campus, London SW7 2AZ

T: +43 664 130 17 27 | M: +44 742 558 62 63
E: valentin.buchinger17@imperial.ac.uk

____

AMRITA KUMAR Ph.D.
Executive Vice President
Acellent Technologies Inc.

Tel: (408) 307 4189
E-mail: akumar@acellent.com
www.acellent.com

Buchinger, Valentin

From: Flude, Annabel <Annabel.Flude@tandf.co.uk>
Sent: 18 May 2022 09:52
To: Buchinger, Valentin
Cc: Flude, Annabel
Subject: RE: tacm20:Low-cost fabrication of advanced polymeric composites by resin infusion processes

Good Afternoon,

Thank you for your correspondence requesting permission to reproduce content from a Taylor & Francis Group content from our Journal in your thesis to be posted on your University's repository.

We will be pleased to grant the permission without fee on the condition that you acknowledge the original source of publication and insert a reference to the Journal's web site: www.tandfonline.com

This permission does not cover any third party copyrighted work which may appear in the material requested. Please ensure you have checked all original source details for the rights holder.

Please note that this licence **does not allow you to post our content on any third-party websites.**

Thank you for your interest in our Journal.

With best wishes,

Annabel
Annabel Flude – Permissions Administrator, Journals
Taylor & Francis Group
3 Park Square, Milton Park, Abingdon, Oxon, OX14 4RN, UK.
Tel: +4402080520698
Web: www.tandfonline.com
e-mail: annabel.flude@tandf.co.uk

From: Valentin Buchinger <valentin.buchinger17@imperial.ac.uk>
Sent: 17 May 2022 17:35
To: Academic UK Non Rightslink <permissionrequest@tandf.co.uk>
Subject: tacm20:Low-cost fabrication of advanced polymeric composites by resin infusion processes

Permissions Request

Type of use: Academic
Article title: Low-cost fabrication of advanced polymeric composites by resin infusion processes
Article DOI: 10.1163/156855101753396573
Author name: Alfred C. Loos
Journal title: Advanced Composite Materials
Volume number: 10
Issue number: 2-3
Year of publication: 2001
Name: Valentin Buchinger
Street address: Exhibition Road, Department of Aeronautics
Town: London
Postcode/ZIP code: SW7 2AZ

Country: United Kingdom
Email: valentin.buchinger17@imperial.ac.uk
Telephone: 07425586263
Intended use: To be used in your Thesis?
Are you requesting the full article?: No
Extract and number of words: NA
Details of figure/table: Figure 1, Figure 2, Figure 3
Which University?: Imperial College London
Title of your Thesis?: Life cycle monitoring of composite aircraft components with structural health monitoring technologies
University repository URL: https://spiral.imperial.ac.uk/
Is this a “Closed” or “Open” deposit?: open
Additional comments:

Inverse scheme to identify the temperature dependence of electromechanical coupling factors for piezoceramics

Conference Proceedings:
2013 Joint IEEE International Symposium on Applications of Ferroelectric and Workshop on Piezoresponse Force Microscopy (ISAF/PFM)

Author: Stefan J. Rupitsch

Publisher: IEEE

Date: July 2013

Thesis / Dissertation Reuse

The IEEE does not require individuals working on a thesis to obtain a formal reuse license, however, you may print out this statement to be used as a permission grant:

Requirements to be followed when using any portion (e.g., figure, graph, table, or textual material) of an IEEE copyrighted paper in a thesis:

1) In the case of textual material (e.g., using short quotes or referring to the work within these papers) users must give full credit to the original source (author, paper, publication) followed by the IEEE copyright line © 2011 IEEE.
2) In the case of illustrations or tabular material, we require that the copyright line © [Year of original publication] IEEE appear prominently with each reprinted figure and/or table.
3) If a substantial portion of the original paper is to be used, and if you are not the senior author, also obtain the senior author's approval.

Requirements to be followed when using an entire IEEE copyrighted paper in a thesis:

1) The following IEEE copyright/ credit notice should be placed prominently in the references: © [year of original publication] IEEE. Reprinted, with permission, from [author names, paper title, IEEE publication title, and month/year of publication]
2) Only the accepted version of an IEEE copyrighted paper can be used when posting the paper or your thesis on-line.
3) In placing the thesis on the author's university website, please display the following message in a prominent place on the website: In reference to IEEE copyrighted material which is used with permission in this thesis, the IEEE does not endorse any of [university/educational entity's name goes here]'s products or services. Internal or personal use of this material is permitted. If interested in reprinting/republishing IEEE copyrighted material for advertising or promotional purposes or for creating new collective works for resale or redistribution, please go to http://www.ieee.org/publications_standards/publications/rights/rights_link.html to learn how to obtain a License from RightsLink.

If applicable, University Microfilms and/or ProQuest Library, or the Archives of Canada may supply single copies of the dissertation.

BACK CLOSE WINDOW

ELSEVIER LICENSE TERMS AND CONDITIONS

May 25, 2022

This Agreement between Imperial College London -- Valentin Buchinger ("You") and Elsevier ("Elsevier") consists of your license details and the terms and conditions provided by Elsevier and Copyright Clearance Center.

License Number	5315810628095
License date	May 25, 2022
Licensed Content Publisher	Elsevier
Licensed Content Publication	Composites Part A: Applied Science and Manufacturing
Licensed Content Title	The effect of processing temperature and placement rate on the short beam strength of carbon fibre–PEEK manufactured using a laser tape placement process
Licensed Content Author	C.M. Stokes-Griffin,P. Compston
Licensed Content Date	Nov 1, 2015
Licensed Content Volume	78
Licensed Content Issue	n/a
Licensed Content Pages	10
Start Page	274
End Page	283
Type of Use	reuse in a thesis/dissertation
Portion	figures/tables/illustrations
Number of figures/tables/illustrations	1
Format	both print and electronic
Are you the author of this Elsevier article?	No
Will you be translating?	No
Title	Life cycle monitoring of composite aircraft components with structural health monitoring technologies
Institution name	Imperial College London
Expected presentation date	Oct 2022
Portions	Fig. 1
Requestor Location	Imperial College London Flat 2, 42 Dealtry Road 40 Putney Hill London, London SW15 6AQ United Kingdom Attn: Imperial College London
Publisher Tax ID	GB 494 6272 12
Billing Type	Invoice
Billing Address	Imperial College London Exhibition Road Department of Aeronautics London, United Kingdom SW7 2AZ Attn: Valentin Buchinger
Total	**0.00 USD**
Terms and Conditions	

INTRODUCTION

1. The publisher for this copyrighted material is Elsevier. By clicking "accept" in connection with completing this licensing transaction, you agree that the following terms and conditions apply to this transaction (along with the Billing and Payment terms and conditions established by Copyright Clearance Center, Inc. ("CCC"), at the time that you opened your Rightslink account and that are available at any time at http://myaccount.copyright.com).

GENERAL TERMS

2. Elsevier hereby grants you permission to reproduce the aforementioned material subject to the terms and conditions indicated.
3. Acknowledgement: If any part of the material to be used (for example, figures) has appeared in our publication with credit or acknowledgement to another source, permission must also be sought from that source. If such permission is not obtained then that material may not be included in your publication/copies. Suitable acknowledgement to the source must be made, either as a footnote or in a reference list at the end of your publication, as follows:
"Reprinted from Publication title, Vol /edition number, Author(s), Title of article / title of chapter, Pages No., Copyright (Year), with permission from Elsevier [OR APPLICABLE SOCIETY COPYRIGHT OWNER]." Also Lancet special credit - "Reprinted from The Lancet, Vol. number, Author(s), Title of article, Pages No., Copyright (Year), with permission from Elsevier."
4. Reproduction of this material is confined to the purpose and/or media for which permission is hereby given.
5. Altering/Modifying Material: Not Permitted. However figures and illustrations may be altered/adapted minimally to serve your work. Any other abbreviations, additions, deletions and/or any other alterations shall be made only with prior written authorization of Elsevier Ltd. (Please contact Elsevier’s permissions helpdesk here). No modifications can be made to any Lancet figures/tables and they must be reproduced in full.
6. If the permission fee for the requested use of our material is waived in this instance, please be advised that your future requests for Elsevier materials may attract a fee.
7. Reservation of Rights: Publisher reserves all rights not specifically granted in the combination of (i) the license details provided by you and accepted in the course of this licensing transaction, (ii) these terms and conditions and (iii) CCC's Billing and Payment terms and conditions.
8. License Contingent Upon Payment: While you may exercise the rights licensed immediately upon issuance of the license at the end of the licensing process for the transaction, provided that you have disclosed complete and accurate details of your proposed use, no license is finally effective unless and until full payment is received from you (either by publisher or by CCC) as provided in CCC's Billing and Payment terms and conditions. If full payment is not received on a timely basis, then any license preliminarily granted shall be deemed automatically revoked and shall be void as if never granted. Further, in the event that you breach any of these terms and conditions or any of CCC's Billing and Payment terms and conditions, the license is automatically revoked and shall be void as if never granted. Use of materials as described in a revoked license, as well as any use of the materials beyond the scope of an unrevoked license, may constitute copyright infringement and publisher reserves the right to take any and all action to protect its copyright in the materials.
9. Warranties: Publisher makes no representations or warranties with respect to the licensed material.
10. Indemnity: You hereby indemnify and agree to hold harmless publisher and CCC, and their respective officers, directors, employees and agents, from and against any and all claims arising out of your use of the licensed material other than as specifically authorized pursuant to this license.
11. No Transfer of License: This license is personal to you and may not be sublicensed, assigned, or transferred by you to any other person without publisher's written permission.
12. No Amendment Except in Writing: This license may not be amended except in a writing signed by both parties (or, in the case of publisher, by CCC on publisher's behalf).
13. Objection to Contrary Terms: Publisher hereby objects to any terms contained in any purchase order, acknowledgment, check endorsement or other writing prepared by you, which terms are inconsistent with these terms and conditions or CCC's Billing and Payment terms and conditions. These terms and conditions, together with CCC's Billing and Payment terms and conditions (which are incorporated herein), comprise the entire agreement between you and publisher (and CCC) concerning this licensing transaction. In the event of any conflict between your obligations established by these terms and conditions and those established by CCC's Billing and Payment terms and conditions, these terms and conditions shall control.
14. Revocation: Elsevier or Copyright Clearance Center may deny the permissions described in this License at their sole discretion, for any reason or no reason, with a full refund payable to you. Notice of such denial will be made using the contact information provided by you. Failure to receive such notice will not alter or invalidate the denial. In no event will Elsevier or Copyright Clearance Center be responsible or liable for any costs, expenses or damage incurred by you as a result of a denial of your permission request, other than a refund of the amount(s) paid by you to Elsevier and/or Copyright Clearance Center for denied permissions.

LIMITED LICENSE

The following terms and conditions apply only to specific license types:
15. **Translation**: This permission is granted for non-exclusive world **English** rights only unless your license was granted for translation rights. If you licensed translation rights you may only translate this content into the languages you requested. A professional translator must perform all translations and reproduce the content word for word preserving the integrity of the article.
16. **Posting licensed content on any Website**: The following terms and conditions apply as follows: Licensing material from an Elsevier journal: All content posted to the web site must maintain the copyright information line on the bottom of each image; A hyper-text must be included to the Homepage of the journal from which you are licensing at http://www.sciencedirect.com/science/journal/xxxxx or the Elsevier homepage for books at http://www.elsevier.com; Central Storage: This license does not include permission for a scanned version of the material to be stored in a central repository such as that provided by Heron/XanEdu.

Licensing material from an Elsevier book: A hyper-text link must be included to the Elsevier homepage at http://www.elsevier.com . All content posted to the web site must maintain the copyright information line on the bottom of each image.

Posting licensed content on Electronic reserve: In addition to the above the following clauses are applicable: The web site must be password-protected and made available only to bona fide students registered on a relevant course. This permission is granted for 1 year only. You may obtain a new license for future website posting.
17. **For journal authors:** the following clauses are applicable in addition to the above:
Preprints:
A preprint is an author's own write-up of research results and analysis, it has not been peer-reviewed, nor has it had any other value added to it by a publisher (such as formatting, copyright, technical enhancement etc.).
Authors can share their preprints anywhere at any time. Preprints should not be added to or enhanced in any way in order to appear more like, or to substitute for, the final versions of articles however authors can update their preprints on arXiv or RePEc with their Accepted Author Manuscript (see below).
If accepted for publication, we encourage authors to link from the preprint to their formal publication via its DOI. Millions of researchers have access to the formal publications on ScienceDirect, and so links will help users to find, access, cite and use the best available version. Please note that Cell Press, The Lancet and some society-owned have different preprint policies. Information on these policies is available on the journal homepage.
Accepted Author Manuscripts: An accepted author manuscript is the manuscript of an article that has been accepted for publication and which typically includes author-incorporated changes suggested during submission, peer review and editor-author communications.
Authors can share their accepted author manuscript:

- immediately
    - via their non-commercial person homepage or blog
    - by updating a preprint in arXiv or RePEc with the accepted manuscript
    - via their research institute or institutional repository for internal institutional uses or as part of an invitation-only research collaboration work-group
    - directly by providing copies to their students or to research collaborators for their personal use
    - for private scholarly sharing as part of an invitation-only work group on commercial sites with which Elsevier has an agreement
- After the embargo period
    - via non-commercial hosting platforms such as their institutional repository
    - via commercial sites with which Elsevier has an agreement

In all cases accepted manuscripts should:

- link to the formal publication via its DOI
- bear a CC-BY-NC-ND license - this is easy to do
- if aggregated with other manuscripts, for example in a repository or other site, be shared in alignment with our hosting policy not be added to or enhanced in any way to appear more like, or to substitute for, the published journal article.

Published journal article (JPA): A published journal article (PJA) is the definitive final record of published research that appears or will appear in the journal and embodies all value-adding publishing activities including peer review co-ordination, copy-editing, formatting, (if relevant) pagination and online enrichment.
Policies for sharing publishing journal articles differ for subscription and gold open access articles:
Subscription Articles: If you are an author, please share a link to your article rather than the full-text. Millions of researchers have access to the formal publications on ScienceDirect, and so links will help your users to find, access, cite, and use the best available version.
Theses and dissertations which contain embedded PJAs as part of the formal submission can be posted publicly by the awarding institution with DOI links back to the formal publications on ScienceDirect.
If you are affiliated with a library that subscribes to ScienceDirect you have additional private sharing rights for others' research accessed under that agreement. This includes use for classroom teaching and internal training at the institution (including use in course packs and courseware programs), and inclusion of the article for grant funding purposes.
Gold Open Access Articles: May be shared according to the author-selected end-user license and should contain a CrossMark logo, the end user license, and a DOI link to the formal publication on ScienceDirect.
Please refer to Elsevier's posting policy for further information.
18. **For book authors** the following clauses are applicable in addition to the above: Authors are permitted to place a brief summary of their work online only. You are not allowed to download and post the published electronic version of your chapter, nor may you scan the printed edition to create an electronic version. **Posting to a repository:** Authors are permitted to post a summary of their chapter only in their institution's repository.
19. **Thesis/Dissertation**: If your license is for use in a thesis/dissertation your thesis may be submitted to your institution in either print or electronic form. Should your thesis be published commercially, please reapply for permission. These requirements include permission for the Library and Archives of Canada to supply single copies, on demand, of the complete thesis and include permission for Proquest/UMI to supply single copies, on demand, of the complete thesis. Should your thesis be published commercially, please reapply for permission. Theses and dissertations which contain embedded PJAs as part of the

formal submission can be posted publicly by the awarding institution with DOI links back to the formal publications on ScienceDirect.

Elsevier Open Access Terms and Conditions

You can publish open access with Elsevier in hundreds of open access journals or in nearly 2000 established subscription journals that support open access publishing. Permitted third party re-use of these open access articles is defined by the author's choice of Creative Commons user license. See our open access license policy for more information.

Terms & Conditions applicable to all Open Access articles published with Elsevier:

Any reuse of the article must not represent the author as endorsing the adaptation of the article nor should the article be modified in such a way as to damage the author's honour or reputation. If any changes have been made, such changes must be clearly indicated.

The author(s) must be appropriately credited and we ask that you include the end user license and a DOI link to the formal publication on ScienceDirect.

If any part of the material to be used (for example, figures) has appeared in our publication with credit or acknowledgement to another source it is the responsibility of the user to ensure their reuse complies with the terms and conditions determined by the rights holder.

Additional Terms & Conditions applicable to each Creative Commons user license:

CC BY: The CC-BY license allows users to copy, to create extracts, abstracts and new works from the Article, to alter and revise the Article and to make commercial use of the Article (including reuse and/or resale of the Article by commercial entities), provided the user gives appropriate credit (with a link to the formal publication through the relevant DOI), provides a link to the license, indicates if changes were made and the licensor is not represented as endorsing the use made of the work. The full details of the license are available at http://creativecommons.org/licenses/by/4.0.

CC BY NC SA: The CC BY-NC-SA license allows users to copy, to create extracts, abstracts and new works from the Article, to alter and revise the Article, provided this is not done for commercial purposes, and that the user gives appropriate credit (with a link to the formal publication through the relevant DOI), provides a link to the license, indicates if changes were made and the licensor is not represented as endorsing the use made of the work. Further, any new works must be made available on the same conditions. The full details of the license are available at http://creativecommons.org/licenses/by-nc-sa/4.0.

CC BY NC ND: The CC BY-NC-ND license allows users to copy and distribute the Article, provided this is not done for commercial purposes and further does not permit distribution of the Article if it is changed or edited in any way, and provided the user gives appropriate credit (with a link to the formal publication through the relevant DOI), provides a link to the license, and that the licensor is not represented as endorsing the use made of the work. The full details of the license are available at http://creativecommons.org/licenses/by-nc-nd/4.0. Any commercial reuse of Open Access articles published with a CC BY NC SA or CC BY NC ND license requires permission from Elsevier and will be subject to a fee.

Commercial reuse includes:

- Associating advertising with the full text of the Article
- Charging fees for document delivery or access
- Article aggregation
- Systematic distribution via e-mail lists or share buttons

Posting or linking by commercial companies for use by customers of those companies.

20. **Other Conditions**:

v1.10

Questions? customercare@copyright.com or +1-855-239-3415 (toll free in the US) or +1-978-646-2777.

ELSEVIER LICENSE
TERMS AND CONDITIONS

May 25, 2022

This Agreement between Imperial College London -- Valentin Buchinger ("You") and Elsevier ("Elsevier") consists of your license details and the terms and conditions provided by Elsevier and Copyright Clearance Center.

License Number	5315810472504
License date	May 25, 2022
Licensed Content Publisher	Elsevier
Licensed Content Publication	Composites Part A: Applied Science and Manufacturing
Licensed Content Title	Process-induced strain and distortion in curved composites. Part I: Development of fiber-optic strain monitoring technique and analytical methods
Licensed Content Author	Kazunori Takagaki,Shu Minakuchi,Nobuo Takeda
Licensed Content Date	Dec 1, 2017
Licensed Content Volume	103
Licensed Content Issue	n/a
Licensed Content Pages	16
Start Page	236
End Page	251
Type of Use	reuse in a thesis/dissertation
Portion	figures/tables/illustrations
Number of figures/tables/illustrations	2
Format	both print and electronic
Are you the author of this Elsevier article?	No
Will you be translating?	No
Title	Life cycle monitoring of composite aircraft components with structural health monitoring technologies
Institution name	Imperial College London
Expected presentation date	Oct 2022
Portions	Fig 13 and 14
Requestor Location	Imperial College London Flat 2, 42 Dealtry Road 40 Putney Hill London, London SW15 6AQ United Kingdom Attn: Imperial College London
Publisher Tax ID	GB 494 6272 12
Billing Type	Invoice
Billing Address	Imperial College London Exhibition Road Department of Aeronautics London, United Kingdom SW7 2AZ Attn: Valentin Buchinger
Total	**0.00 USD**
Terms and Conditions	

INTRODUCTION

1. The publisher for this copyrighted material is Elsevier. By clicking "accept" in connection with completing this licensing transaction, you agree that the following terms and conditions apply to this transaction (along with the Billing and Payment terms and conditions established by Copyright Clearance Center, Inc. ("CCC"), at the time that you opened your Rightslink account and that are available at any time at http://myaccount.copyright.com).

GENERAL TERMS

2. Elsevier hereby grants you permission to reproduce the aforementioned material subject to the terms and conditions indicated.
3. Acknowledgement: If any part of the material to be used (for example, figures) has appeared in our publication with credit or acknowledgement to another source, permission must also be sought from that source. If such permission is not obtained then that material may not be included in your publication/copies. Suitable acknowledgement to the source must be made, either as a footnote or in a reference list at the end of your publication, as follows:
"Reprinted from Publication title, Vol /edition number, Author(s), Title of article / title of chapter, Pages No., Copyright (Year), with permission from Elsevier [OR APPLICABLE SOCIETY COPYRIGHT OWNER]." Also Lancet special credit - "Reprinted from The Lancet, Vol. number, Author(s), Title of article, Pages No., Copyright (Year), with permission from Elsevier."
4. Reproduction of this material is confined to the purpose and/or media for which permission is hereby given.
5. Altering/Modifying Material: Not Permitted. However figures and illustrations may be altered/adapted minimally to serve your work. Any other abbreviations, additions, deletions and/or any other alterations shall be made only with prior written authorization of Elsevier Ltd. (Please contact Elsevier’s permissions helpdesk here). No modifications can be made to any Lancet figures/tables and they must be reproduced in full.
6. If the permission fee for the requested use of our material is waived in this instance, please be advised that your future requests for Elsevier materials may attract a fee.
7. Reservation of Rights: Publisher reserves all rights not specifically granted in the combination of (i) the license details provided by you and accepted in the course of this licensing transaction, (ii) these terms and conditions and (iii) CCC's Billing and Payment terms and conditions.
8. License Contingent Upon Payment: While you may exercise the rights licensed immediately upon issuance of the license at the end of the licensing process for the transaction, provided that you have disclosed complete and accurate details of your proposed use, no license is finally effective unless and until full payment is received from you (either by publisher or by CCC) as provided in CCC's Billing and Payment terms and conditions. If full payment is not received on a timely basis, then any license preliminarily granted shall be deemed automatically revoked and shall be void as if never granted. Further, in the event that you breach any of these terms and conditions or any of CCC's Billing and Payment terms and conditions, the license is automatically revoked and shall be void as if never granted. Use of materials as described in a revoked license, as well as any use of the materials beyond the scope of an unrevoked license, may constitute copyright infringement and publisher reserves the right to take any and all action to protect its copyright in the materials.
9. Warranties: Publisher makes no representations or warranties with respect to the licensed material.
10. Indemnity: You hereby indemnify and agree to hold harmless publisher and CCC, and their respective officers, directors, employees and agents, from and against any and all claims arising out of your use of the licensed material other than as specifically authorized pursuant to this license.
11. No Transfer of License: This license is personal to you and may not be sublicensed, assigned, or transferred by you to any other person without publisher's written permission.
12. No Amendment Except in Writing: This license may not be amended except in a writing signed by both parties (or, in the case of publisher, by CCC on publisher's behalf).
13. Objection to Contrary Terms: Publisher hereby objects to any terms contained in any purchase order, acknowledgment, check endorsement or other writing prepared by you, which terms are inconsistent with these terms and conditions or CCC's Billing and Payment terms and conditions. These terms and conditions, together with CCC's Billing and Payment terms and conditions (which are incorporated herein), comprise the entire agreement between you and publisher (and CCC) concerning this licensing transaction. In the event of any conflict between your obligations established by these terms and conditions and those established by CCC's Billing and Payment terms and conditions, these terms and conditions shall control.
14. Revocation: Elsevier or Copyright Clearance Center may deny the permissions described in this License at their sole discretion, for any reason or no reason, with a full refund payable to you. Notice of such denial will be made using the contact information provided by you. Failure to receive such notice will not alter or invalidate the denial. In no event will Elsevier or Copyright Clearance Center be responsible or liable for any costs, expenses or damage incurred by you as a result of a denial of your permission request, other than a refund of the amount(s) paid by you to Elsevier and/or Copyright Clearance Center for denied permissions.

LIMITED LICENSE

The following terms and conditions apply only to specific license types:
15. **Translation**: This permission is granted for non-exclusive world **English** rights only unless your license was granted for translation rights. If you licensed translation rights you may only translate this content into the languages you requested. A professional translator must perform all translations and reproduce the content word for word preserving the integrity of the article.
16. **Posting licensed content on any Website**: The following terms and conditions apply as follows: Licensing material from an Elsevier journal: All content posted to the web site must maintain the copyright information line on the bottom of each image; A hyper-text must be included to the Homepage of the journal from which you are licensing at http://www.sciencedirect.com/science/journal/xxxxx or the Elsevier homepage for books at http://www.elsevier.com; Central Storage: This license does not include permission for a scanned version of the material to be stored in a central repository such as that provided by Heron/XanEdu.

Licensing material from an Elsevier book: A hyper-text link must be included to the Elsevier homepage at http://www.elsevier.com . All content posted to the web site must maintain the copyright information line on the bottom of each image.

Posting licensed content on Electronic reserve: In addition to the above the following clauses are applicable: The web site must be password-protected and made available only to bona fide students registered on a relevant course. This permission is granted for 1 year only. You may obtain a new license for future website posting.
17. **For journal authors:** the following clauses are applicable in addition to the above:
Preprints:
A preprint is an author's own write-up of research results and analysis, it has not been peer-reviewed, nor has it had any other value added to it by a publisher (such as formatting, copyright, technical enhancement etc.).
Authors can share their preprints anywhere at any time. Preprints should not be added to or enhanced in any way in order to appear more like, or to substitute for, the final versions of articles however authors can update their preprints on arXiv or RePEc with their Accepted Author Manuscript (see below).
If accepted for publication, we encourage authors to link from the preprint to their formal publication via its DOI. Millions of researchers have access to the formal publications on ScienceDirect, and so links will help users to find, access, cite and use the best available version. Please note that Cell Press, The Lancet and some society-owned have different preprint policies. Information on these policies is available on the journal homepage.
Accepted Author Manuscripts: An accepted author manuscript is the manuscript of an article that has been accepted for publication and which typically includes author-incorporated changes suggested during submission, peer review and editor-author communications.
Authors can share their accepted author manuscript:

- immediately
    - via their non-commercial person homepage or blog
    - by updating a preprint in arXiv or RePEc with the accepted manuscript
    - via their research institute or institutional repository for internal institutional uses or as part of an invitation-only research collaboration work-group
    - directly by providing copies to their students or to research collaborators for their personal use
    - for private scholarly sharing as part of an invitation-only work group on commercial sites with which Elsevier has an agreement
- After the embargo period
    - via non-commercial hosting platforms such as their institutional repository
    - via commercial sites with which Elsevier has an agreement

In all cases accepted manuscripts should:

- link to the formal publication via its DOI
- bear a CC-BY-NC-ND license - this is easy to do
- if aggregated with other manuscripts, for example in a repository or other site, be shared in alignment with our hosting policy not be added to or enhanced in any way to appear more like, or to substitute for, the published journal article.

Published journal article (JPA): A published journal article (PJA) is the definitive final record of published research that appears or will appear in the journal and embodies all value-adding publishing activities including peer review co-ordination, copy-editing, formatting, (if relevant) pagination and online enrichment.
Policies for sharing publishing journal articles differ for subscription and gold open access articles:
Subscription Articles: If you are an author, please share a link to your article rather than the full-text. Millions of researchers have access to the formal publications on ScienceDirect, and so links will help your users to find, access, cite, and use the best available version.
Theses and dissertations which contain embedded PJAs as part of the formal submission can be posted publicly by the awarding institution with DOI links back to the formal publications on ScienceDirect.
If you are affiliated with a library that subscribes to ScienceDirect you have additional private sharing rights for others' research accessed under that agreement. This includes use for classroom teaching and internal training at the institution (including use in course packs and courseware programs), and inclusion of the article for grant funding purposes.
Gold Open Access Articles: May be shared according to the author-selected end-user license and should contain a CrossMark logo, the end user license, and a DOI link to the formal publication on ScienceDirect.
Please refer to Elsevier's posting policy for further information.
18. **For book authors** the following clauses are applicable in addition to the above: Authors are permitted to place a brief summary of their work online only. You are not allowed to download and post the published electronic version of your chapter, nor may you scan the printed edition to create an electronic version. **Posting to a repository:** Authors are permitted to post a summary of their chapter only in their institution's repository.
19. **Thesis/Dissertation**: If your license is for use in a thesis/dissertation your thesis may be submitted to your institution in either print or electronic form. Should your thesis be published commercially, please reapply for permission. These requirements include permission for the Library and Archives of Canada to supply single copies, on demand, of the complete thesis and include permission for Proquest/UMI to supply single copies, on demand, of the complete thesis. Should your thesis be published commercially, please reapply for permission. Theses and dissertations which contain embedded PJAs as part of the

formal submission can be posted publicly by the awarding institution with DOI links back to the formal publications on ScienceDirect.

Elsevier Open Access Terms and Conditions

You can publish open access with Elsevier in hundreds of open access journals or in nearly 2000 established subscription journals that support open access publishing. Permitted third party re-use of these open access articles is defined by the author's choice of Creative Commons user license. See our open access license policy for more information.

Terms & Conditions applicable to all Open Access articles published with Elsevier:

Any reuse of the article must not represent the author as endorsing the adaptation of the article nor should the article be modified in such a way as to damage the author's honour or reputation. If any changes have been made, such changes must be clearly indicated.

The author(s) must be appropriately credited and we ask that you include the end user license and a DOI link to the formal publication on ScienceDirect.

If any part of the material to be used (for example, figures) has appeared in our publication with credit or acknowledgement to another source it is the responsibility of the user to ensure their reuse complies with the terms and conditions determined by the rights holder.

Additional Terms & Conditions applicable to each Creative Commons user license:

CC BY: The CC-BY license allows users to copy, to create extracts, abstracts and new works from the Article, to alter and revise the Article and to make commercial use of the Article (including reuse and/or resale of the Article by commercial entities), provided the user gives appropriate credit (with a link to the formal publication through the relevant DOI), provides a link to the license, indicates if changes were made and the licensor is not represented as endorsing the use made of the work. The full details of the license are available at http://creativecommons.org/licenses/by/4.0.

CC BY NC SA: The CC BY-NC-SA license allows users to copy, to create extracts, abstracts and new works from the Article, to alter and revise the Article, provided this is not done for commercial purposes, and that the user gives appropriate credit (with a link to the formal publication through the relevant DOI), provides a link to the license, indicates if changes were made and the licensor is not represented as endorsing the use made of the work. Further, any new works must be made available on the same conditions. The full details of the license are available at http://creativecommons.org/licenses/by-nc-sa/4.0.

CC BY NC ND: The CC BY-NC-ND license allows users to copy and distribute the Article, provided this is not done for commercial purposes and further does not permit distribution of the Article if it is changed or edited in any way, and provided the user gives appropriate credit (with a link to the formal publication through the relevant DOI), provides a link to the license, and that the licensor is not represented as endorsing the use made of the work. The full details of the license are available at http://creativecommons.org/licenses/by-nc-nd/4.0. Any commercial reuse of Open Access articles published with a CC BY NC SA or CC BY NC ND license requires permission from Elsevier and will be subject to a fee.

Commercial reuse includes:

- Associating advertising with the full text of the Article
- Charging fees for document delivery or access
- Article aggregation
- Systematic distribution via e-mail lists or share buttons

Posting or linking by commercial companies for use by customers of those companies.

20. **Other Conditions**:

v1.10

Questions? customercare@copyright.com or +1-855-239-3415 (toll free in the US) or +1-978-646-2777.

Resin Directional Flow and Degree of Cure Sensing Using Chirped Optical Fiber Long Period Gratings

Author: Rebecca Y. N. Wong

Publication: IEEE Sensors Journal

Publisher: IEEE

Date: 15 October 2017

Thesis / Dissertation Reuse

The IEEE does not require individuals working on a thesis to obtain a formal reuse license, however, you may print out this statement to be used as a permission grant:

Requirements to be followed when using any portion (e.g., figure, graph, table, or textual material) of an IEEE copyrighted paper in a thesis:

1) In the case of textual material (e.g., using short quotes or referring to the work within these papers) users must give full credit to the original source (author, paper, publication) followed by the IEEE copyright line © 2011 IEEE.
2) In the case of illustrations or tabular material, we require that the copyright line © [Year of original publication] IEEE appear prominently with each reprinted figure and/or table.
3) If a substantial portion of the original paper is to be used, and if you are not the senior author, also obtain the senior author's approval.

Requirements to be followed when using an entire IEEE copyrighted paper in a thesis:

1) The following IEEE copyright/ credit notice should be placed prominently in the references: © [year of original publication] IEEE. Reprinted, with permission, from [author names, paper title, IEEE publication title, and month/year of publication]
2) Only the accepted version of an IEEE copyrighted paper can be used when posting the paper or your thesis on-line.
3) In placing the thesis on the author's university website, please display the following message in a prominent place on the website: In reference to IEEE copyrighted material which is used with permission in this thesis, the IEEE does not endorse any of [university/educational entity's name goes here]'s products or services. Internal or personal use of this material is permitted. If interested in reprinting/republishing IEEE copyrighted material for advertising or promotional purposes or for creating new collective works for resale or redistribution, please go to http://www.ieee.org/publications_standards/publications/rights/rights_link.html to learn how to obtain a License from RightsLink.

If applicable, University Microfilms and/or ProQuest Library, or the Archives of Canada may supply single copies of the dissertation.

BACK CLOSE WINDOW

JOHN WILEY AND SONS LICENSE TERMS AND CONDITIONS

May 25, 2022

This Agreement between Imperial College London -- Valentin Buchinger ("You") and John Wiley and Sons ("John Wiley and Sons") consists of your license details and the terms and conditions provided by John Wiley and Sons and Copyright Clearance Center.

License Number	5315810594531
License date	May 25, 2022
Licensed Content Publisher	John Wiley and Sons
Licensed Content Publication	Polymer Composites
Licensed Content Title	Process–structure–property relationships of thermoformed woven carbon-fiber-reinforced polyether-ether-ketone composites
Licensed Content Author	Dequn Li, Huamin Zhou, Zhigao Huang, et al
Licensed Content Date	Feb 19, 2019
Licensed Content Volume	40
Licensed Content Issue	10
Licensed Content Pages	12
Type of Use	Dissertation/Thesis
Requestor type	University/Academic
Format	Print and electronic
Portion	Figure/table
Number of figures/tables	1
Will you be translating?	No
Title	Life cycle monitoring of composite aircraft components with structural health monitoring technologies
Institution name	Imperial College London
Expected presentation date	Oct 2022
Portions	Figure 8
Requestor Location	Imperial College London Flat 2, 42 Dealtry Road 40 Putney Hill London, London SW15 6AQ United Kingdom Attn: Imperial College London
Publisher Tax ID	EU826007151
Billing Type	Invoice
Billing Address	Imperial College London Exhibition Road Department of Aeronautics London, United Kingdom SW7 2AZ Attn: Valentin Buchinger
Total	**0.00 USD**
Terms and Conditions	

TERMS AND CONDITIONS

This copyrighted material is owned by or exclusively licensed to John Wiley & Sons, Inc. or one of its group companies (each a"Wiley Company") or handled on behalf of a society with which a Wiley Company has exclusive publishing rights in relation to a particular work (collectively "WILEY"). By clicking "accept" in connection with completing this licensing transaction, you agree that the following terms and conditions apply to this transaction (along with the billing and payment terms and conditions established by the Copyright Clearance Center Inc., ("CCC's Billing and Payment terms and conditions"), at the time that you opened your RightsLink account (these are available at any time at http://myaccount.copyright.com).

Terms and Conditions

- The materials you have requested permission to reproduce or reuse (the "Wiley Materials") are protected by copyright.

- You are hereby granted a personal, non-exclusive, non-sub licensable (on a stand-alone basis), non-transferable, worldwide, limited license to reproduce the Wiley Materials for the purpose specified in the licensing process. This license, **and any CONTENT (PDF or image file) purchased as part of your order,** is for a one-time use only and limited to any maximum distribution number specified in the license. The first instance of republication or reuse granted by this license must be completed within two years of the date of the grant of this license (although copies prepared before the end date may be distributed thereafter). The Wiley Materials shall not be used in any other manner or for any other purpose, beyond what is granted in the license. Permission is granted subject to an appropriate acknowledgement given to the author, title of the material/book/journal and the publisher. You shall also duplicate the copyright notice that appears in the Wiley publication in your use of the Wiley Material. Permission is also granted on the understanding that nowhere in the text is a previously published source acknowledged for all or part of this Wiley Material. Any third party content is expressly excluded from this permission.

- With respect to the Wiley Materials, all rights are reserved. Except as expressly granted by the terms of the license, no part of the Wiley Materials may be copied, modified, adapted (except for minor reformatting required by the new Publication), translated, reproduced, transferred or distributed, in any form or by any means, and no derivative works may be made based on the Wiley Materials without the prior permission of the respective copyright owner.**For STM Signatory Publishers clearing permission under the terms of the STM Permissions Guidelines only, the terms of the license are extended to include subsequent editions and for editions in other languages, provided such editions are for the work as a whole in situ and does not involve the separate exploitation of the permitted figures or extracts,** You may not alter, remove or suppress in any manner any copyright, trademark or other notices displayed by the Wiley Materials. You may not license, rent, sell, loan, lease, pledge, offer as security, transfer or assign the Wiley Materials on a stand-alone basis, or any of the rights granted to you hereunder to any other person.

- The Wiley Materials and all of the intellectual property rights therein shall at all times remain the exclusive property of John Wiley & Sons Inc, the Wiley Companies, or their respective licensors, and your interest therein is only that of having possession of and the right to reproduce the Wiley Materials pursuant to Section 2 herein during the continuance of this Agreement. You agree that you own no right, title or interest in or to the Wiley Materials or any of the intellectual property rights therein. You shall have no rights hereunder other than the license as provided for above in Section 2. No right, license or interest to any trademark, trade name, service mark or other branding ("Marks") of WILEY or its licensors is granted hereunder, and you agree that you shall not assert any such right, license or interest with respect thereto

- NEITHER WILEY NOR ITS LICENSORS MAKES ANY WARRANTY OR REPRESENTATION OF ANY KIND TO YOU OR ANY THIRD PARTY, EXPRESS, IMPLIED OR STATUTORY, WITH RESPECT TO THE MATERIALS OR THE ACCURACY OF ANY INFORMATION CONTAINED IN THE MATERIALS, INCLUDING, WITHOUT LIMITATION, ANY IMPLIED WARRANTY OF MERCHANTABILITY, ACCURACY, SATISFACTORY QUALITY, FITNESS FOR A PARTICULAR PURPOSE, USABILITY, INTEGRATION OR NON-INFRINGEMENT AND ALL SUCH WARRANTIES ARE HEREBY EXCLUDED BY WILEY AND ITS LICENSORS AND WAIVED BY YOU.

- WILEY shall have the right to terminate this Agreement immediately upon breach of this Agreement by you.

- You shall indemnify, defend and hold harmless WILEY, its Licensors and their respective directors, officers, agents and employees, from and against any actual or threatened claims, demands, causes of action or proceedings arising from any breach of this Agreement by you.

- IN NO EVENT SHALL WILEY OR ITS LICENSORS BE LIABLE TO YOU OR ANY OTHER PARTY OR ANY OTHER PERSON OR ENTITY FOR ANY SPECIAL, CONSEQUENTIAL, INCIDENTAL, INDIRECT, EXEMPLARY OR PUNITIVE DAMAGES, HOWEVER CAUSED, ARISING OUT OF OR IN CONNECTION WITH THE DOWNLOADING, PROVISIONING, VIEWING OR USE OF THE MATERIALS REGARDLESS OF THE FORM OF ACTION, WHETHER FOR BREACH OF CONTRACT, BREACH OF WARRANTY, TORT, NEGLIGENCE, INFRINGEMENT OR OTHERWISE (INCLUDING, WITHOUT LIMITATION, DAMAGES BASED ON LOSS OF PROFITS, DATA, FILES, USE, BUSINESS OPPORTUNITY OR CLAIMS OF THIRD PARTIES), AND WHETHER OR NOT THE PARTY HAS BEEN ADVISED OF THE POSSIBILITY OF SUCH DAMAGES. THIS LIMITATION SHALL APPLY NOTWITHSTANDING ANY FAILURE OF ESSENTIAL PURPOSE OF ANY LIMITED REMEDY PROVIDED HEREIN.

- Should any provision of this Agreement be held by a court of competent jurisdiction to be illegal, invalid, or unenforceable, that provision shall be deemed amended to achieve as nearly as possible the same economic effect as the original provision, and the legality, validity and enforceability of the remaining provisions of this Agreement shall not be affected or impaired thereby.

- The failure of either party to enforce any term or condition of this Agreement shall not constitute a waiver of either party's right to enforce each and every term and condition of this Agreement. No breach under this agreement shall be deemed waived or excused by either party unless such waiver or consent is in writing signed by the party granting such waiver or consent. The waiver by or consent of a party to a breach of any provision of this Agreement shall not operate or be construed as a waiver of or consent to any other or subsequent breach by such other party.

- This Agreement may not be assigned (including by operation of law or otherwise) by you without WILEY's prior written consent.

- Any fee required for this permission shall be non-refundable after thirty (30) days from receipt by the CCC.

- These terms and conditions together with CCC's Billing and Payment terms and conditions (which are incorporated herein) form the entire agreement between you and WILEY concerning this licensing transaction and (in the absence of fraud) supersedes all prior agreements and representations of the parties, oral or written. This Agreement may not be amended except in writing signed by both parties. This Agreement shall be binding upon and inure to the benefit of the parties' successors, legal representatives, and authorized assigns.

- In the event of any conflict between your obligations established by these terms and conditions and those established by CCC's Billing and Payment terms and conditions, these terms and conditions shall prevail.

- WILEY expressly reserves all rights not specifically granted in the combination of (i) the license details provided by you and accepted in the course of this licensing transaction, (ii) these terms and conditions and (iii) CCC's Billing and Payment terms and conditions.

- This Agreement will be void if the Type of Use, Format, Circulation, or Requestor Type was misrepresented during the licensing process.

- This Agreement shall be governed by and construed in accordance with the laws of the State of New York, USA, without regards to such state's conflict of law rules. Any legal action, suit or proceeding arising out of or relating to these Terms and Conditions or the breach thereof shall be instituted in a court of competent jurisdiction in New York County in the State of New York in the United States of America and each party hereby consents and submits to the personal jurisdiction of such court, waives any objection to venue in such court and consents to service of process by registered or certified mail, return receipt requested, at the last known address of such party.

WILEY OPEN ACCESS TERMS AND CONDITIONS
Wiley Publishes Open Access Articles in fully Open Access Journals and in Subscription journals offering Online Open. Although most of the fully Open Access journals publish open access articles under the terms of the Creative Commons Attribution (CC BY) License only, the subscription journals and a few of the Open Access Journals offer a choice of Creative Commons Licenses. The license type is clearly identified on the article.
The Creative Commons Attribution License
The Creative Commons Attribution License (CC-BY) allows users to copy, distribute and transmit an article, adapt the article and make commercial use of the article. The CC-BY license permits commercial and non-
Creative Commons Attribution Non-Commercial License
The Creative Commons Attribution Non-Commercial (CC-BY-NC)License permits use, distribution and reproduction in any medium, provided the original work is properly cited and is not used for commercial purposes.(see below)

Creative Commons Attribution-Non-Commercial-NoDerivs License
The Creative Commons Attribution Non-Commercial-NoDerivs License (CC-BY-NC-ND) permits use, distribution and reproduction in any medium, provided the original work is properly cited, is not used for commercial purposes and no modifications or adaptations are made. (see below)
Use by commercial "for-profit" organizations
Use of Wiley Open Access articles for commercial, promotional, or marketing purposes requires further explicit permission from Wiley and will be subject to a fee.
Further details can be found on Wiley Online Library http://olabout.wiley.com/WileyCDA/Section/id-410895.html

Other Terms and Conditions:

v1.10 Last updated September 2015

Questions? customercare@copyright.com or +1-855-239-3415 (toll free in the US) or +1-978-646-2777.